



Riggio, Alessandra I. (2017) *The role of Runx1 in genetic models of breast cancer*. PhD thesis.

<https://theses.gla.ac.uk/9103/>

Copyright and moral rights for this work are retained by the author

A copy can be downloaded for personal non-commercial research or study, without prior permission or charge

This work cannot be reproduced or quoted extensively from without first obtaining permission in writing from the author

The content must not be changed in any way or sold commercially in any format or medium without the formal permission of the author

When referring to this work, full bibliographic details including the author, title, awarding institution and date of the thesis must be given

Enlighten: Theses

<https://theses.gla.ac.uk/>
research-enlighten@glasgow.ac.uk

The role of *Runx1* in genetic models of breast cancer

Alessandra I. Riggio

Submitted in fulfillment of the requirements for the degree
of Doctor of Philosophy

Cancer Research UK Beatson Institute
College of Medical, Veterinary and Life Sciences
University of Glasgow
Glasgow, UK

October, 2017

Abstract

Whilst tremendous progress has been made in breast cancer research, substantial gaps still remain which require urgent attention. Behind the majority of them lies the general lack of understanding of the biology underlying the disease. For this reason, it is imperative to interrogate all players involved in the initiation, maintenance and progression of breast tumourigenesis.

For a long time, the *RUNX* family of genes has been linked to different types of human cancers, with the more recent appreciation of a role in breast cancer. Following the discovery of genetic alterations affecting *RUNX1* and its binding partner *CBF β* in biopsies of breast cancer patients, studying the function played by the *RUNX*-*CBF β* transcription factor complex in breast tumourigenesis has become extremely important.

In the present thesis, the use of different experimental *in vivo* and *ex vivo* systems has been exploited in an endeavour to investigate the putative tumour suppressive and/or pro-oncogenic properties of the *Runx1* gene in the context of breast cancer. This has been achieved through characterization of the effects of *Runx1* deletion in the *MMTV-PyMT* breast cancer mouse model, followed by a thorough analysis of how *Runx1* loss affects a novel Wnt/ β -catenin-driven model of mammary tumourigenesis. In the latter, the role of the *Runx2* gene was also interrogated, highlighting the tantalizing interplay existing between the two homologous transcription factors in controlling cell fate decisions and differentiation potential of mammary epithelial cells.

Based on the obtained results, a working model of the putative role played by *RUNX1* and *RUNX2* upon the mammary epithelial cell hierarchy is discussed. This is intended to emphasize how changes affecting the function of the *RUNX* family of transcription factors could lead to loss of mammary tissue homeostasis and eventually breast cancer.

Table of Contents

The role of <i>Runx1</i> in genetic models of breast cancer	1
Abstract	2
Table of Contents.....	3
List of Figures	7
List of Tables	11
List of Publications	12
Author’s Declaration	13
Acknowledgements.....	15
Abbreviations.....	17
Summary	24
1 Introduction	25
1.1 Cancer and its “players”	25
1.1.1 The <i>RUNX1</i> “hill” in the genomic landscape of female-related cancers.....	26
1.2 The ontogeny of the mammary gland	29
1.2.1 The murine mammary gland	29
1.2.2 The developmental stages: embryonic, pubertal, and reproductive	31
1.2.3 Temporal and spatial expression of the <i>Runx</i> genes in the murine mammary gland	35
1.3 The endocrine regulation of the mammary gland	35
1.3.1 Oestrogens and progesterone in regulating mammary development	36
1.3.2 The effects of hormonal paracrine circuits on ductal morphogenesis	37
1.3.3 The mammary interplay between RUNX1 and oestrogens	41
1.4 Mammary epithelial stem cells	43
1.4.1 The discovery of mammary repopulating units.....	43
1.4.2 Phenotypic and functional characterization of mammary stem cells	45
1.5 The hormonal milieu of the stem cell niche.....	49
1.5.1 A “stemness” role for progesterone	49
1.5.2 The link between ovarian hormones and breast cancer	51
1.6 The mammary epithelial cell hierarchy	52
1.6.1 The heterogeneity of the stem cell compartment.....	52
1.6.2 The distinctive features of progenitor cells	54
1.6.3 The different subsets of luminal cells	55
1.7 Breast cancer.....	59

1.7.1	Risk factors and prevention	59
1.7.2	Breast cancer's heterogeneity	61
1.7.3	Clinical management of the disease	67
1.7.4	RUNX1 in breast cancer	70
1.7.5	The "cell-of-origin" of breast cancer.....	73
1.8	Experimental models of breast cancer	76
1.8.1	<i>In vitro</i> and <i>ex vivo</i> culture systems	76
1.8.2	<i>In vivo</i> animal models.....	78
1.9	Aims of the thesis	82
2	Materials and Methods	84
2.1	Animal procedures.....	84
2.1.1	Mouse lines and generation of cohorts	84
2.1.2	Staging of the oestrous cycle	85
2.1.3	Survival analysis	85
2.1.4	Transplants of mouse-derived tumour fragments.....	86
2.1.5	Imaging analysis of RFP expression	86
2.1.6	Virgin analysis of pre-neoplastic lesions	86
2.2	Immunohistochemistry.....	87
2.3	BrdU quantification	88
2.4	Mouse mammary epithelial cell extraction	90
2.5	Flow cytometric analysis	90
2.6	Fluorescence activated cell sorting.....	93
2.7	Mammary gland whole mounts	93
2.8	Tumoursphere assay.....	94
2.9	Colony forming cell assay	95
2.10	RNA extraction	95
2.10.1	Reverse transcription.....	96
2.10.2	Quantitative polymerase chain reaction.....	97
2.11	Statistical analysis	97
3	Investigating the role of <i>Runx1</i> in the <i>MMTV-PyMT</i> mouse model of breast cancer.....	99
3.1	Introduction	99
3.1.1	The PyMT breast cancer mouse model	99
3.2	Experimental procedures.....	102
3.2.1	Generation of a <i>Runx1</i> conditional knock-out breast cancer mouse model.....	102
3.3	Results	103

3.3.1	Deletion of <i>Runx1</i> accelerates PyMT-driven breast tumourigenesis without affecting overall survival	103
3.3.2	Deletion of one or two copies of <i>Runx1</i> does not affect tumour burden of MMTV-PyMT mice	106
3.3.3	RFP imaging analysis of clinical end point MMTV-PyMT mice	108
3.3.4	<i>Ex vivo</i> characterization of MMTV-PyMT derived mammary epithelial cells through the use of the RFP reporter gene	112
3.3.5	Histopathological analysis of PyMT mammary tumour lesions	118
3.4	Discussion	124
4	Investigating the role of <i>Runx1</i> and <i>Runx2</i> in a Wnt/β-catenin mouse model of breast cancer	128
4.1	Introduction	128
4.1.1	Canonical Wnt/ β -catenin signalling.....	128
4.1.2	Wnt signalling, mammary stemness and the <i>Runx</i> genes	129
4.2	Experimental procedures.....	131
4.2.1	Generation of a novel Wnt/ β -catenin-driven breast cancer mouse model.....	131
4.3	Results	133
4.3.1	Deletion of <i>Runx1</i> , and <i>Runx2</i> , accelerates Wnt/ β -catenin mammary tumourigenesis without affecting survival of mice	133
4.3.2	Combined deletion of <i>Runx1</i> and <i>Runx2</i> results in a remarkable acceleration of Wnt/ β -catenin-driven mammary tumourigenesis	140
4.3.3	Characterization of <i>Runx</i> -deficient breast cancer cohorts of mice carrying an activating mutation of β -catenin.....	148
4.3.4	Activation of the Wnt/ β -catenin signalling pathway leads to the formation of adenosquamous mammary lesions.....	156
4.3.5	Investigating the tumourigenic potential of Wnt/ β -catenin-driven mammary lesions upon loss of the <i>Runx</i> genes	158
4.4	Discussion	163
5	Dissecting the role played by <i>Runx1</i> and <i>Runx2</i> in the early stages of Wnt/β-catenin driven breast tumourigenesis	167
5.1	Introduction	167
5.2	Results	168
5.2.1	Activation of Wnt/ β -catenin signalling alters mammary development in the absence of <i>Runx1</i> and <i>Runx2</i>	168
5.2.2	Investigating the tumour suppressive mechanisms exerted by RUNX1 and RUNX2	183
5.2.3	Histopathological characterization of Wnt/ β -catenin preneoplastic lesions in the absence of the <i>Runx</i> genes	189
5.2.4	Expression analysis of Wnt/ β -catenin target genes upon loss of <i>Runx</i> genes.....	196

5.3	Discussion	198
6	Characterization of Wnt/β-catenin activated mammary epithelial cells upon <i>Runx</i> deletion	201
6.1	Introduction	201
6.2	Experimental procedures.....	201
6.3	Results	203
6.3.1	Investigating how loss of <i>Runx1</i> and <i>Runx2</i> impinges on Wnt/ β -catenin-driven mammary stemness	203
6.3.2	Loss of <i>Runx1</i> favours the expansion of a basal subpopulation of mammary cells upon activated Wnt/ β -catenin signalling.....	206
6.3.3	Phenotypic characterization of Wnt/ β -catenin-driven mammary epithelial cells.....	211
6.4	Discussion	223
7	Conclusions.....	232
	Bibliography	240

List of Figures

Figure 1. 1 Frequency of <i>RUNX1</i> genetic alterations across all cancer types.....	28
Figure 1. 2 The bi-layered epithelial structure of the murine mammary gland..	30
Figure 1. 3 Pubertal mammary gland development in wild-type female mice. ...	33
Figure 1. 4 Reproductive mammary gland development in wild-type female mice.	34
Figure 1. 5 Model of the paracrine circuits engaged by oestrogen and progesterone.	40
Figure 1. 6 The <i>RUNX1</i> -ER α interplay.....	42
Figure 1. 7 The mammary epithelial cell hierarchy.	58
Figure 2. 1 Quantification of BrdU-positive cells through the HALO software. ..	89
Figure 2. 2 Flow cytometric analysis of mouse mammary epithelial cells.	92
Figure 3. 1 Deletion of <i>Runx1</i> accelerates PyMT-driven breast tumourigenesis, yet it does not affect survival of the mice.	105
Figure 3. 2 Deletion of one or two copies of <i>Runx1</i> does not affect tumour burden of MMTV-PyMT mice.	107
Figure 3. 3 Imaging analysis of the RFP reporter gene in <i>Runx1</i> -proficient MMTV- PyMT mice.	109
Figure 3. 4 Imaging analysis of the RFP reporter gene in <i>Runx1</i> -deficient MMTV- PyMT mice.	110
Figure 3. 5 Imaging analysis of the RFP reporter gene in MMTV-PyMT mice carrying only one deleted copy of the <i>Runx1</i> gene.....	111
Figure 3. 6 Pipeline for the extraction and <i>ex vivo</i> characterization of RFP+ and RFP- MMECs from MMTV-PyMT mice.	113
Figure 3. 7 Characterization of RFP+ and RFP- cells from <i>Runx1</i> -deficient MMTV- PyMT mice.	116
Figure 3. 8 Characterization of RFP+ and RFP- cells from <i>Runx1</i> -proficient MMTV- PyMT mice.	117
Figure 3. 9 H&Es and Ki67 protein expression analysis of MMTV-PyMT mammary tumours.	120
Figure 3. 10 RFP and <i>RUNX1</i> expression analysis of MMTV-PyMT mammary tumours.	121
Figure 3. 11 <i>RUNX1</i> expression analysis of <i>Runx1</i> -deficient MMTV-PyMT mice. .	122
Figure 3. 12 <i>RUNX2</i> expression analysis of MMTV-PyMT in the presence or absence of <i>Runx1</i>	123
Figure 4. 1 <i>Runx1</i> deletion accelerates Wnt/ β -catenin-driven mammary tumourigenesis, yet it does not affect survival of the mice.	134
Figure 4. 2 Heterozygous deletion of <i>Runx2</i> accelerates Wnt/ β -catenin-driven mammary tumourigenesis, yet it does not affect survival of the mice.	136
Figure 4. 3 Wnt/ β -catenin-driven mammary tumourigenesis, in the absence of <i>Runx1</i> , is not influenced by parity.	138
Figure 4. 4 Deletion of <i>Runx2</i> , in the absence of parity, delays the appearance of BLG-Cre driven Wnt/ β -catenin-activated mammary lesions.	139
Figure 4. 5 Heterozygous deletion of <i>Runx2</i> significantly accelerates Wnt/ β - catenin-driven mammary tumourigenesis in a <i>Runx1</i> -null background.....	141
Figure 4. 6 The effect of parity on heterozygous loss of <i>Runx2</i> upon Wnt/ β - catenin-driven mammary tumourigenesis in a <i>Runx1</i> -null background.....	143

Figure 4. 7 Co-deletion of <i>Runx1</i> and <i>Runx2</i> significantly accelerates Wnt/ β -catenin-driven oncogenic transformation of the mammary epithelium.	145
Figure 4. 8 Survival analysis of <i>Runx</i> -deficient cohorts of multiparous mice carrying an activated mutation of β -catenin.	146
Figure 4. 9 Survival analysis of <i>Runx</i> -deficient cohorts of nulliparous mice carrying an activated mutation of β -catenin.	147
Figure 4. 10 Effect of <i>Runx1</i> loss on body weight, tumour burden and number of tumour burdened mammary glands in Wnt/ β -catenin activated mutant mice at clinical end point.	149
Figure 4. 11 Effect of <i>Runx2</i> loss on body weight, tumour burden and number of tumour burdened mammary glands in Wnt/ β -catenin activated mutant mice at clinical end point.	150
Figure 4. 12 Effect of combined <i>Runx1</i> and <i>Runx2</i> loss on body weight, tumour burden and number of tumour burdened mammary glands in Wnt/ β -catenin activated mutant mice at clinical end point.	152
Figure 4. 13 Characterization of <i>Runx</i> -deficient multiparous cohorts of mice carrying a mammary-specific activating mutation of β -catenin.	153
Figure 4. 14 Characterization of <i>Runx</i> -deficient nulliparous cohorts of mice carrying a mammary-specific activating mutation of β -catenin.	154
Figure 4. 15 Gross appearance of the phenotypical changes affecting the mammary glands of Wnt/ β -catenin-activated mutant mice upon loss of the <i>Runx</i> genes.	155
Figure 4. 16 Histopathological analysis of Wnt/ β -catenin driven adenosquamous lesions.	157
Figure 4. 17 Overview of the transplantation assay.	160
Figure 4. 18 Investigating the tumourigenic potential of Wnt/ β -catenin driven mammary tumours in the absence of the <i>Runx</i> genes.	161
Figure 4. 19 Summary of the tumourigenic potential of Wnt/ β -catenin driven mammary tumours in the absence of the <i>Runx</i> genes.	162
Figure 5. 1 Effect of mammary specific <i>Runx1</i> and <i>Runx2</i> loss on body weight and cumulative mammary gland weight in 9 week old Wnt/ β -catenin mutant and wild type mice.	170
Figure 5. 2 Combined loss of <i>Runx1</i> and <i>Runx2</i> results in a dramatic impairment of ductal morphogenesis upon activation of the Wnt/ β -catenin signalling in late puberty.	171
Figure 5. 3 Mammary-specific deletion of <i>Runx1</i> and <i>Runx2</i> does not affect ductal morphogenesis of Wnt/ β -catenin wild type mice in late puberty.	172
Figure 5. 4 Effect of <i>Runx1</i> and <i>Runx2</i> loss on mammary ductal elongation in 9 weeks old Wnt/ β -catenin activated mutant and wild type mice.	173
Figure 5. 5 Effect of mammary specific <i>Runx1</i> and <i>Runx2</i> loss on body weight and cumulative mammary gland weight in 6 week old Wnt/ β -catenin mutant and wild type mice.	175
Figure 5. 6 Combined loss of <i>Runx1</i> and <i>Runx2</i> results in a dramatic impairment of ductal morphogenesis upon activation of the Wnt/ β -catenin signalling pathway in mid puberty.	176
Figure 5. 7 Mammary-specific deletion of <i>Runx1</i> and <i>Runx2</i> does not affect ductal morphogenesis of Wnt/ β -catenin wild type mice in mid puberty.	177
Figure 5. 8 Effect of <i>Runx1</i> and <i>Runx2</i> loss on mammary ductal elongation in 6 week old Wnt/ β -catenin activated mutant and wild type mice.	178

Figure 5. 9 Effect of mammary specific <i>Runx1</i> and <i>Runx2</i> loss on body weight and cumulative mammary gland weight in 3 week old Wnt/ β -catenin mutant and wild type mice.	180
Figure 5. 10 Individual or combined loss of <i>Runx1</i> and <i>Runx2</i> severely compromise the morphology of the mammary anlage in the presence of activated Wnt/ β -catenin signalling.	181
Figure 5. 11 Mammary-specific deletion of <i>Runx1</i> and <i>Runx2</i> does not affect the morphology of the anlage of Wnt/ β -catenin wild type mice.	182
Figure 5. 12 Perturbation of pubertal mammary epithelium upon activation of the Wnt/ β -catenin pathway in the absence of <i>Runx1</i> and <i>Runx2</i>	185
Figure 5. 13 Quantification of the proliferative density of pubertal mammary epithelium upon activation of the Wnt/ β -catenin pathway in the absence of <i>Runx1</i> and <i>Runx2</i>	186
Figure 5. 14 Normalized proliferative density of pubertal mammary epithelium upon activation of the Wnt/ β -catenin pathway in the absence of <i>Runx1</i> and <i>Runx2</i>	187
Figure 5. 15 Immunohistochemistry for BrdU on pre-neoplastic Wnt/ β -catenin mammary lesions upon loss of <i>Runx1</i> and <i>Runx2</i>	188
Figure 5. 16 Histopathological analysis of Wnt/ β -catenin driven pre-neoplastic lesions.	191
Figure 5. 17 Histopathological analysis of Wnt/ β -catenin driven lesions upon <i>Runx1</i> loss.	192
Figure 5. 18 Histopathological analysis of Wnt/ β -catenin driven lesions upon <i>Runx2</i> loss.	193
Figure 5. 19 Histopathological analysis of Wnt/ β -catenin lesions upon loss of <i>Runx</i> genes.	194
Figure 5. 20 RUNX1 and RUNX2 analysis of Wnt/ β -catenin driven adenosquamous lesions.	195
Figure 5. 21 Expression analysis of Wnt/ β -catenin target genes upon loss of <i>Runx1</i> and <i>Runx2</i>	197
Figure 6. 1 Pipeline for the extraction and characterization of mammary epithelial cells.	202
Figure 6. 2 Primary tumoursphere growth of Wnt/ β -catenin activated mammary epithelial cells in the absence of <i>Runx1</i> and/or <i>Runx2</i>	204
Figure 6. 3 Secondary tumoursphere growth of Wnt/ β -catenin activated mammary epithelial cells in the absence of <i>Runx1</i> and/or <i>Runx2</i>	205
Figure 6. 4 Deletion of <i>Runx1</i> favours the formation of basal colonies on a Wnt/ β -catenin activated background.	207
Figure 6. 5 Size of acinar and solid colonies formed by Wnt/ β -catenin activated mammary epithelial cells upon loss of <i>Runx1</i> and <i>Runx2</i>	208
Figure 6. 6 Morphological heterogeneity displayed by Wnt/ β -catenin activated solid colonies upon loss of <i>Runx1</i> and <i>Runx2</i>	210
Figure 6. 7 Effects of <i>Runx1</i> and <i>Runx2</i> deletion on mammary epithelial and stromal cells in a Wnt/ β -catenin activated and wild type setting.	213
Figure 6. 8 Effects of <i>Runx1</i> and <i>Runx2</i> deletion on luminal and basal mammary epithelial cells in a Wnt/ β -catenin activated and wild type setting.	215
Figure 6. 9 Expression profiles of luminal and basal mammary epithelial cells upon deletion of <i>Runx1</i> and <i>Runx2</i> in a Wnt/ β -catenin activated mutant background.	216

Figure 6. 10 Expression profiles of luminal and basal mammary epithelial cells upon deletion of <i>Runx1</i> and <i>Runx2</i> in a Wnt/ β -catenin wild type background. .	217
Figure 6. 11 Effects of <i>Runx1</i> and <i>Runx2</i> deletion on the expression profile of Sca-1 luminal mammary cells in a Wnt/ β -catenin activated mutant and wild type setting.....	220
Figure 6. 12 Effects of <i>Runx1</i> and <i>Runx2</i> deletion on the expression profile of Sca-1 basal mammary cells in a Wnt/ β -catenin activated mutant and wild type setting.....	221
Figure 6. 13 Sca-1 expression profile of basal mouse mammary epithelial cells upon loss of <i>Runx1</i> and <i>Runx2</i> deletion in a Wnt/ β -catenin activated background.	222
Figure 6. 14 Working model.....	227

List of Tables

Table 1. 1 Summary of the 10 Integrative Clusters of breast cancer.	66
Table 1. 2 Summary of RUNX1 dysregulation in breast cancer.	71
Table 6. 1 BLG-Cre mediated effects of <i>Runx1</i> and <i>Runx2</i> loss in the mammary epithelium.	231

List of Publications

1. Ferrari, N., **Riggio, A.I.**, Mason, S., McDonald, L., King, A., Higgins, T., Rosewell, I., Neil, J.C., Smalley, M.J., Sansom, O.J., Morris, J., Cameron, E.R., and K. Blyth. 2015. *Runx2* contributes to the regenerative potential of the mammary epithelium. *Scientific Reports*. 5:15658.
2. Rooney, N., **Riggio, A.I.**, Mendoza-Villanueva, D., Shore, P., Cameron, E.P., and K. Blyth. 2017. *Runx* genes in breast cancer and the mammary lineage. *Advances in Experimental Medicine and Biology*. 962:353-368.
3. **Riggio, A.I.**, and K. Blyth. 2017. The enigmatic role of RUNX1 in female-related cancers - current knowledge and future perspectives. *The FEBS Journal*. 284(15):2345-2362.

Author's Declaration

I hereby declare that all the work presented in this thesis is my own, unless otherwise stated.

I certify that no part of this thesis has been submitted previously for the award of a degree to any other Institution.

All text and figures are original and not published elsewhere, except extracts taken from the following publication (review), for which formal grant of license from Wiley (FEBS Journal publisher) through RightsLink Copyright Clearance Centre has been obtained.

Riggio, A.I. and K. Blyth. 2017. The enigmatic role of RUNX1 in female-related cancers - current knowledge and future perspectives. The FEBS Journal. 284(15):2345-2362.

All sources of information used in the preparation of this thesis are indicated by references.

Alessandra I. Riggio

October, 2017

Bearing in mind the minuscule effort each scientist can make in respect to the immense vastness of mammary gland and tumour biology, it is hoped that this piece of work might improve the understanding of breast cancer, as a small drop, together with many others, will eventually fill up the ocean.

Alessandra I. Riggio

October, 2017

Acknowledgements

The studies described in this thesis were carried out at the Beatson Institute for Cancer Research (Glasgow), with the support of Cancer Research UK funding. Albeit driving the project with curiosity, effort and passion, none of this work would have been possible without the help and support provided by all the people I have met during my PhD studentship.

First and foremost, I am extremely grateful to my supervisor Karen Blyth: your commitment and passion to work inspired me since the first day I arrived; your meticulousness sometimes puzzled me, but many others made me realize how similar we are; your way of analysing scientific data taught me that science is never black and white, but it is full of shades and our job is to light them up with all means in our power. Thanks for giving me the great opportunity to work with you and for letting me study the changes affecting the mammary gland, an organ which I literally felt in love with! I am also particularly indebted to Ewan Cameron for his excellent supervision, for the time he always dedicated to me and for the precious advice he provided me. I have always admired his immense knowledge and felt “illuminated” after each scientific conversation we had! My sincere gratitude also goes to my advisor Laura Machesky for the helpful oversight and input given to me throughout my PhD project.

Special thanks are reserved to “Y35”, with its past and present members, who have always “tolerated” me, laughed with me and made my life in the lab extremely pleasant. Thanks to the former PhD student Nicola Ferrari for allowing me to continue a very exciting project; for teaching me all animal and lab techniques from scratch; for the patience he always showed me (even when overloaded with tons of questions); and for the “lucky box” he gave me. Thanks to Susan Mason for always being so helpful and for cheering me up all times (especially on a Monday morning!). Thanks to Dimitris Athineos for the expert advice provided to me on numerous occasions and for his kindness in explaining to me different sorts of molecular biology and statistical issues. Thanks to Sandeep Dhayade and Nicholas Rooney for all their help and support, and for counterbalancing “my loud Italian behaviour”; and thanks to Kirsteen Campbell, for useful and valuable discussions!

I would also like to express my appreciation to all Biological Services people operating at the Beatson Institute for their excellent support to the animal and lab work carried out during my PhD studentship. Special thanks go to Colin Nixon, for the much appreciated histological help; Tom Gilbey, for expert advice on flow cytometry analysis; Barry Gusterson and Josh Leach, for sharing their valuable pathological knowledge and discussion. Throughout the course of my studies, I have also had the fortune of having met wonderful colleagues, including Dominika, Jennifer and Tiziana, who made my life in Glasgow so enjoyable; and to Rene Jackstadt, for believing in me, encouraging me and “feeding” me with wonderful cakes!

I am also particularly grateful to my previous mentors Dr. Melchiorre Cervello, at the National Cancer Institute of Palermo, and Dr. Alberto Bardelli, at the Candiolo Cancer Institute of Turin, for guiding me throughout my career and for making me discover my passion for Science. Special thanks also go to all people I have met in Turin, starting off with my working colleague Mariangela Russo, for the wonderful teaching and support provided to me; to Alice Lallo, for always believing in me and for our enduring friendship; to the unforgettable Adriano Trombetta, for being my inspirational “guide” and for encouraging me to move to Glasgow; and to all my ever-lasting friends Carla and “I Duri” (Grazia, Lia, Eleonora, Betta, Elisa, Paparella and Salvo). Special appreciation also goes to my flatmate Slater, for “tolerating” me over the past three months and to my friend “Mango”, for coming up to Glasgow and saving my life during the last period of my thesis writing. Next, I would like to express my sincere gratitude to all the people who have always supported me from my home town Palermo, including Stellix, Smemy, Smartis, Gabriele, Peppe, Giovanni, Ignazio, Cristina, Francesca, Chiara e “Le Giulie”. Thanks for accompanying me throughout my journey, for always believing in me and for our invaluable friendships!

Finally, the biggest THANK YOU above all goes to my beloved FAMILY: my dad Giuseppe, my mum Patrizia, my sister “Sis”, my twin brother “Ciccio” and my grandfather “Nonno”. I truly believe that none of my achievements would have ever been possible without all the LOVE and SUPPORT you have always given me.

THANK YOU!

Abbreviations

A	area
ACD	asymmetric cell division
AE	abnormal epithelium
AML	acute myeloid leukaemia
aMaSC	adult mammary stem cell
APC	adenomatous polyposis coli
AREG	amphiregulin
α -SMA	α smooth muscle actin
BLG	beta-lactoglobulin
BP	basal progenitor
BrdU	bromodeoxyuridine
CBF β	core binding factor β
CD	cell division
CDK(s)	cyclin-dependent kinase(s)
cDNA	complementary deoxyribonucleic acid
CFC	colony forming cell
CK	cytokeratin
CNA	copy number aberration

CNV	copy number variation
CSC	cancer stem cell
DAPI	4',6-diamidino-2-phenylindole
DBD	DNA binding domain
DNA	deoxyribonucleic acid
E	embryonic
E2	17- β -estradiol
EGF	epidermal growth factor
EGFP	enhanced green fluorescent protein
EGFR	epidermal growth factor receptor
Elf-5	E74-like factor 5 transcription factor
ER	oestrogen receptor
ERE	oestrogen response element
ETOH	ethanol
FACS	fluorescence-activated cell sorting
FBS	foetal bovine serum
FGF(s)	fibroblast growth factor(s)
FGFR2	fibroblast growth factor receptor 2
fMaSC	foetal mammary stem cell

fl	floxed
FSC	forward scatter
FZ	frizzled
g	gram
GEMM	genetically engineered mouse model
GFP	green fluorescent protein
GH	growth hormone
GHR	growth hormone receptor
GSK3 β	glycogen synthase kinase 3 β
H	height
HER2	human epidermal growth factor receptor type 2
H&E	haematoxylin and eosin
HR	hormone receptor
HSC	haematopoietic stem cell
IGF1	insulin-like growth factor 1
IGFR1	insulin-like growth factor 1 receptor
IHC	immunohistochemistry
kDa	kilodalton
LEF	lymphoid enhancer-binding factor

Lgr5	leucine-rich repeat-containing G-protein-coupled receptor 5
Lin	lineage
Lob	lobule
LP	luminal progenitor
LPR	low-density lipoprotein-related protein
LTR	long terminal repeat
M	molar
Ma-CFC	mammary colony forming cell
MaSC	mammary stem cell
MDTF	mouse-derived tumour fragment
MEC	mammary epithelial cell
MG	mammary gland
ml	millilitre
mM	millimolar
MMEC	mouse mammary epithelial cell
MMTV	mouse mammary tumour virus
µg	microgram
µl	microliter
µM	micromolar

μm	micrometer
MP	multiparous
mRNA	messenger ribonucleic acid
MRU	mammary repopulating unit
MYO	myoepithelial
NE	normal epithelium
ng	nanogram
NGS	next generation sequencing
nm	nanometer
NP	nulliparous
PBS	phosphate buffered saline
PDTX	patient-derived tumour xenograft
PI3K	phosphoinositide 3'-kinase
PR	progesterone receptor
ProcR	protein C receptor
PSQ	penicillin/streptomycin/L-glutamine
PyMT	polyoma virus middle T antigen
PyV	polyoma virus
qPCR	quantitative polymerase chain reaction

RANK	receptor activator of nuclear factor k-B
RANKL	receptor activator of nuclear factor k-B ligand
RFP	red fluorescent protein
RNA	ribonucleic acid
RT	reverse transcription
RT-qPCR	reverse transcription quantitative polymerase chain reaction
RUNX1	runt-related transcription factor 1
RUNX2	runt-related transcription factor 2
RUNX3	runt-related transcription factor 3
SC	stem cell
Sca-1	stem cell antigen 1
SCD	symmetric cell division
SD	standard deviation
SL	synthetic lethality
SNP	single nucleotide polymorphism
SNV	single nucleotide variant
SSC	side scatter
TBST	Tris-buffered saline Tween
TCF	T-cell factor

TDLU	terminal ductal lobular unit
tdRFP	tandem dimer red fluorescent protein
TE	total epithelium
TEB	terminal end bud
TIC	tumour initiating cell
TME	tumour microenvironment
TN	triple negative
U	unit
wt	wild type

Summary

Given the recent discovery of *RUNX1* somatic mutations in biopsies of breast cancer patients, the overall purpose of the present thesis consists of using different *in vivo* and *ex vivo* experimental systems in the attempt to answer two main questions: firstly, if the *Runx1* gene plays any causative role in the context of breast cancer; and secondly, if its putative function is symptomatic of a tumour suppressor gene and/or of a pro-oncogene.

By characterizing the effects of *Runx1* deletion in two different breast cancer mouse models (i.e. the *MMTV-PyMT* and the Wnt/ β -catenin-driven models of mammary tumourigenesis), this thesis provides the first *in vivo* evidence of a dualistic role played by the gene in the context of breast cancer. *Runx1* would in fact appear to act as a tumour suppressor at early stages of the disease, whilst as a pro-oncogene at later stages of mammary tumourigenesis.

To fully comprehend the significance of these major findings, the introduction will first provide a brief description on the *RUNX* family of genes, as well as on the state-of-the-art knowledge of *RUNX1*'s role in both mammary gland and breast cancer biology. As such, particular attention will then be given not only to the ontogeny, endocrine regulation and composition of the murine mammary gland, yet also to the high degree of heterogeneity, the putative "cell-of-origin(s)" and the different experimental models commonly used to study breast cancer.

Through the aforementioned rationale, it is hoped that the introduction will serve as a platform which may hold the key for unveiling the controversial role played by *RUNX1* in the context of breast cancer.

1 Introduction

Cancer has historically been given several different names. Starting with the Greek word *karkinos* (i.e. crab), Hippocrates first described a tumour with its vessels as a '*crab dug in the sand with its legs spread in a circle*', as early as 400 BC. Afterwards, even the term *oknos* (i.e. load, mass) has been used to describe the disease with its connotations as a '*burden carried by the body*'. But what do all these terms have in common? The idea that cancer was a terrible unspoken malignancy, whose cause(s) was unknown and for which there was no cure. What was unclear to our ancestors was the fact that cancer originated from the uncontrolled growth of cells, a process which was only described in the 20th century by the German researcher Rudolf Virchow with the word *neoplasia* (Siddhartha, 2010).

1.1 Cancer and its “players”

[For this section, the text has been adapted from Riggio and Blyth (2017)].

Generally regarded as a genetic disease, cancer arises from the dysregulation of normal gene expression, which is mainly caused by the sequential accumulation of deoxyribonucleic acid (DNA) alterations (mostly somatic mutations) affecting tumour suppressors, oncogenes and stability genes (Vogelstein and Kinzler, 2004). Aided by the advent of next-generation sequencing (NGS), the identification of many novel cancer players and the determination of their genetic alterations have become possible, thus leading towards a more comprehensive picture of the cancer genome. The genomic landscape of most common cancers has been eloquently described as composed of a few 'mountains', which represent the frequently mutated genes, and many 'hills', being the less frequently altered genes (Wood et al., 2007). Nevertheless, while the causative link between highly mutated genes (e.g. *TP53* and *KRAS*) and cancer is well documented, discovering the relationship between infrequently mutated genes and tumourigenesis still remains a big endeavour (Vogelstein et al., 2013). But why should we care about these 'hills'? Firstly, although substantial progress has been made over the past decade to decrease cancer morbidity, the incidence of many cancers still remains high (Torre et al., 2016). Secondly, the presence of these less frequently altered genes numerically

dominates the landscape of most tumours (Wood et al., 2007), thus strengthening the pressing need to investigate their putative function. However, given that the majority of the reported genetic abnormalities may be incidental to the neoplastic process, how do we know which ‘hills’ take an active part in the transformation of a benign cell into an incipient malignant one? The answer comes from the “driver-versus-passenger” concept whereby only driver genes are capable of conferring a selective growth advantage to the insulted cells (Greenman et al., 2007). As such, coupling NGS data with structural analysis to look at the pattern and pathogenicity of the detected mutations in cancer (rather than just at their frequencies), a list of driver genes including 74 tumour suppressors and 64 oncogenes has been compiled (Vogelstein et al., 2013). One of these reported driver genes, *RUNX1*, which is found to be altered in 9.2% of all tumours (Vogelstein et al., 2013), is of particular interest to our lab and forms the basis of this thesis.

1.1.1 The *RUNX1* “hill” in the genomic landscape of female-related cancers

[For this section, the text has been adapted from Riggio and Blyth (2017)].

The Runt-related transcription factor 1 gene (*RUNX1*) belongs to an evolutionary conserved family of three related genes (*RUNX1*, *RUNX2* and *RUNX3*) (Ito et al., 2015), which encode transcription factors that bind to DNA in partnership with the core binding factor β (CBF β) (Kamachi et al., 1990), itself responsible for enhancing DNA-binding activity (Ogawa et al., 1993) and stability (Huang et al., 2001) of the RUNX proteins. These transcription factors are involved in the regulation of cell fate determination and lineage differentiation during development, as well as cancer (Ito et al., 2015), with *RUNX1* being absolutely required for definitive haematopoiesis (Okuda et al., 1996).

For a long time *RUNX1* has been intensively studied in haematological cancers, where it gathered attention as a tumour suppressor, being the most common *locus* of numerous chromosomal translocations (Blyth et al., 2005). With the advent of NGS technologies and the generation of conditional knockout mouse models, *RUNX1* has been found to have a more widespread role in cancer than previously thought. Indeed, *RUNX1* downregulation has been reported in gastric

cancer (Sakakura et al., 2005) and hepatocellular carcinoma (Miyagawa et al., 2006), while *RUNX1* single nucleotide polymorphisms (SNPs) have been associated with colorectal (Slattery et al., 2011), as well as prostate cancer (Huang et al., 2011). Additionally, *RUNX1* appeared to be a factor essential for the initiation and maintenance of skin and oral squamous cell carcinoma (Hoi et al., 2010) and highly focal *RUNX1* deletions were observed in almost 15% of oesophageal cancers (Dulak et al., 2012).

To date, *RUNX1* genetic alterations are reported in almost 50% of all cancer genomic studies listed in cBioPortal (Figure 1. 1). Albeit, as expected, haematological cancers are at the top of the list, a plethora of epithelial cancers also appear. Among the latter, is striking the preponderance of *RUNX1* genetic alterations in hormone-associated cancers, where the majority of female-related studies (including breast, ovarian and uterine cancers) are among the top 20 hits (Figure 1. 1). Whilst male-specific cancers (e.g. prostate and testicular) also feature in this list, most of those are grouped with tumours showing less frequent *RUNX1* genetic perturbations, with the exception of a rare and aggressive form of prostate cancer, termed neuroendocrine prostate cancer (Parimi et al., 2014), in which *RUNX1* is frequently altered (Figure 1. 1). But what role does the *RUNX1* ‘hill’ play on the genomic landscape of female-related cancers? Several pieces of evidence suggest that *RUNX1* contributes to ovarian and uterine cancer (Riggio and Blyth, 2017), as well as having an important role in breast cancer.

To elucidate the function of *RUNX1* in the genomic landscape of breast cancer, it would be useful to take a step back. If Farber’s sixth sense was true, that is in order to study leukaemia one should first understand how normal blood cells are generated (Siddharta, 2010), then equally to study breast cancer, one should figure out how mammary cells are formed in the first place. Thus applying the concept of confronting breast cancer “in reverse”, it is important to delve into the deeper understanding of a specific organ: the murine mammary gland.

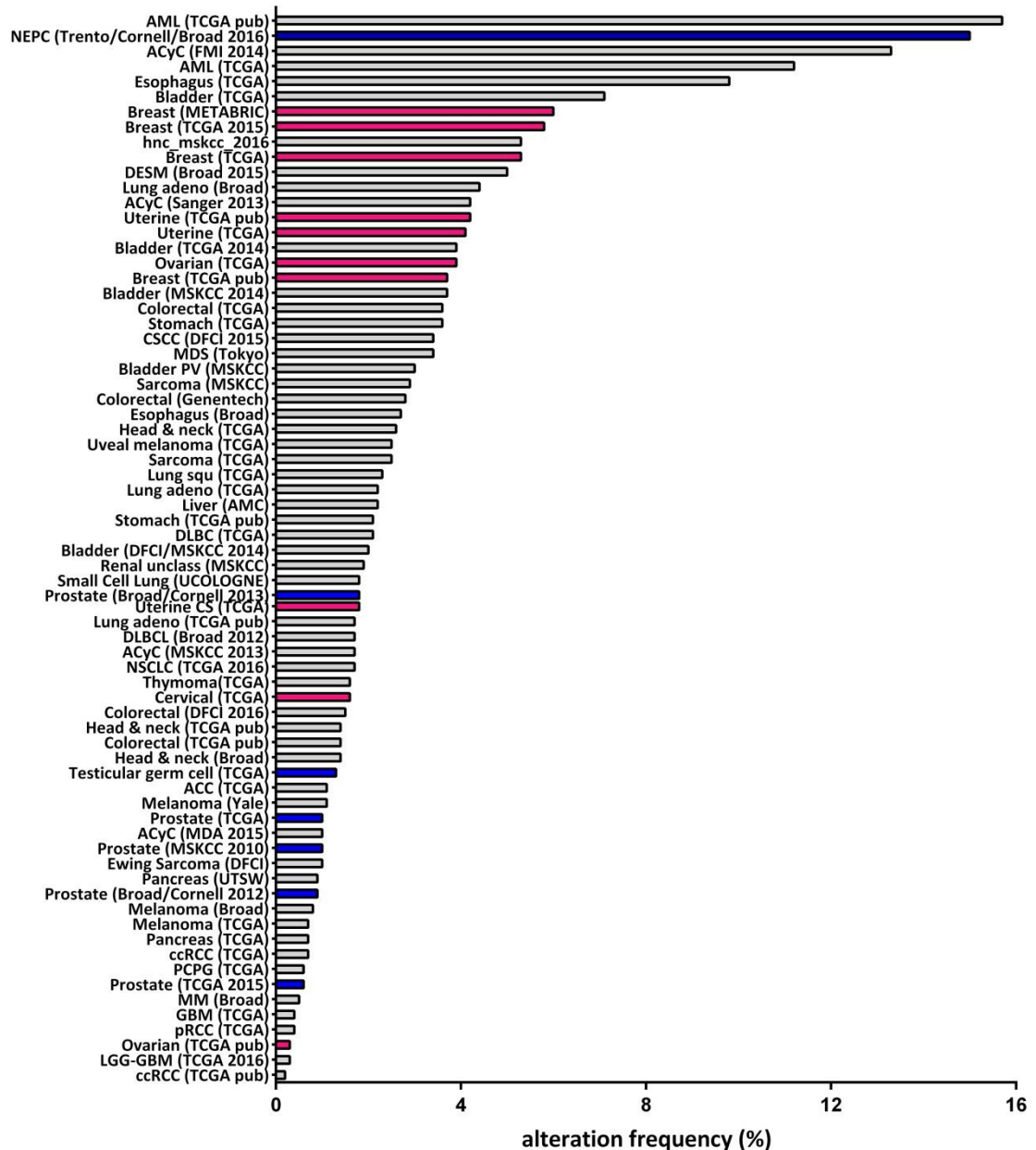


Figure 1. 1 Frequency of *RUNX1* genetic alterations across all cancer types.

Depicted is the frequency of *RUNX1* genetic alterations in 71 out of 144 cancer genomic studies. No *RUNX1* genetic perturbations were detected in 73 cancer studies (data not shown). Female-related cancers of the breast, ovary, uterus and cervix are shaded in pink and generally appear high on the list. Male-related cancers of the prostate and testis are shaded in blue and also appear, but with less frequent percentages with the exception of a very rare, aggressive form of prostate cancer. Data obtained through cBioportal for Cancer Genomics, <http://www.cbioportal.org/> (Cerami et al., 2012; Gao et al., 2013). ACC, Adrenocortical Carcinoma; ACyC, Adenoid Cystic Carcinoma; AML, Acute Myeloid Leukemia; ccRCC, Kidney Renal Clear Cell Carcinoma; CSCC, Cutaneous Squamous Cell Carcinoma; DESM, Desmoplastic Melanoma; DLBC, Lymphoid Neoplasm Diffuse Large B-cell Lymphoma; hnc_mskcc, recurrent and metastatic head and neck cancer; GBM, Glioblastoma Multiforme; LGG-GBM, Merged Cohort of Low-Grade Glioma and Glioblastoma Multiforme; MDS, Myelodysplasia; MM, Multiple Myeloma; NEPC, Neuroendocrine Prostate Cancer; NSCLC, Pan-Lung Cancer; PCPG, Pheochromocytoma and Paraganglioma; pRCC, Kidney Renal Papillary Cell Carcinoma. Taken from Riggio and Blyth (2017).

1.2 The ontogeny of the mammary gland

During evolution, the appearance of mammary glands has profoundly distinguished the class of Mammalia from other animals, by giving them the opportunity to nourish their offspring through the production and secretion of milk. As such, it should not be surprising that the anatomical and morphological features of this organ, as well as the highly regulated endocrine system which controls it, are all devoted to the sole physiological function of lactation (Medina, 1996).

1.2.1 The murine mammary gland

Due to the high level of similarities between mice and humans, the murine mammary gland represents an attractive experimental system to study, as its uniqueness relies on several factors. Firstly, it is the only organ of the mouse whose development mainly takes place postnatally, a precious advantage for biologists to “watch” and study the growth of the organ in “real-time” (Medina, 1996). Secondly, it allows performing orthotopic experiments without the confounding presence of the endogenous tissue, which can be easily removed from 3 weeks old recipient mice in a process known as depithelized (cleared) mammary fat pad (DeOme et al., 1959). Thirdly, being situated just underneath the skin, it is very easily accessible and amenable to different sorts of experimental manipulations (Brisken and O'Malley, 2010). Lastly, it is very abundant in mice, which are characterized by five pairs of mammary glands, located in the neck region (1st), the chest wall (2nd and 3rd), the abdominal wall (4th) and the inguinal region (5th) (Figure 1. 2), thus providing ample tissue for research analysis (Cardiff and Wellings, 1999). However, it is important to mention that morphological and structural differences exist between the murine mammary gland and the human breast. Firstly, humans only have one pair of mammary glands located on the anterior chest wall, which anatomically would correspond to the 3rd pair of murine mammary glands. Secondly, the human stroma, or parenchyma, is constituted by more fibrous connective tissue and less adipose tissue as compared to the murine mammary fat pad (Cardiff and Wellings, 1999). Thirdly, the ramified network of human ducts ends in small clusters of ductules, which are usually referred to as terminal ductal lobular units (TDLUs). Similar to terminal end buds (TEBs), TDLUs undergo dynamic

morphological changes during development, passing from undifferentiated lobules (Lob1) characteristic of virgin glands, through differentiated structures with more ductules (Lob2 and Lob3) and secretory acinar types (Lob4) seen during pregnancy, to then return to less differentiated ones (Lob 1 or Lob2) after lactation (Russo et al., 2005). The murine mammary gland is a very heterogeneous organ made up of two compartments: the stroma, better known as fat pad, formed by adipocyte, fibroblast, vascular and immune cells; and the epithelium, a bilayered structure comprised of luminal and basal cells (Hennighausen and Robinson, 2005). The luminal compartment of the mammary epithelium is composed of tightly connected apically oriented luminal cells of the ductal and alveolar subtypes, the latter of which produce milk during lactation. The basal compartment, lying between the luminal layer and the basement membrane, is made up of highly elongated contractile myoepithelial (MYO) cells, which help luminal cells in milk ejection and circulation throughout the ductal tree (Macias and Hinck, 2012). Of note, while luminal cells can be identified by expression of cytokeratin (CK) 8 and CK18, basal cells can be distinguished for the presence of CK5, CK14 and α smooth muscle actin (α SMA) (Inman et al., 2015) (Figure 1. 2).

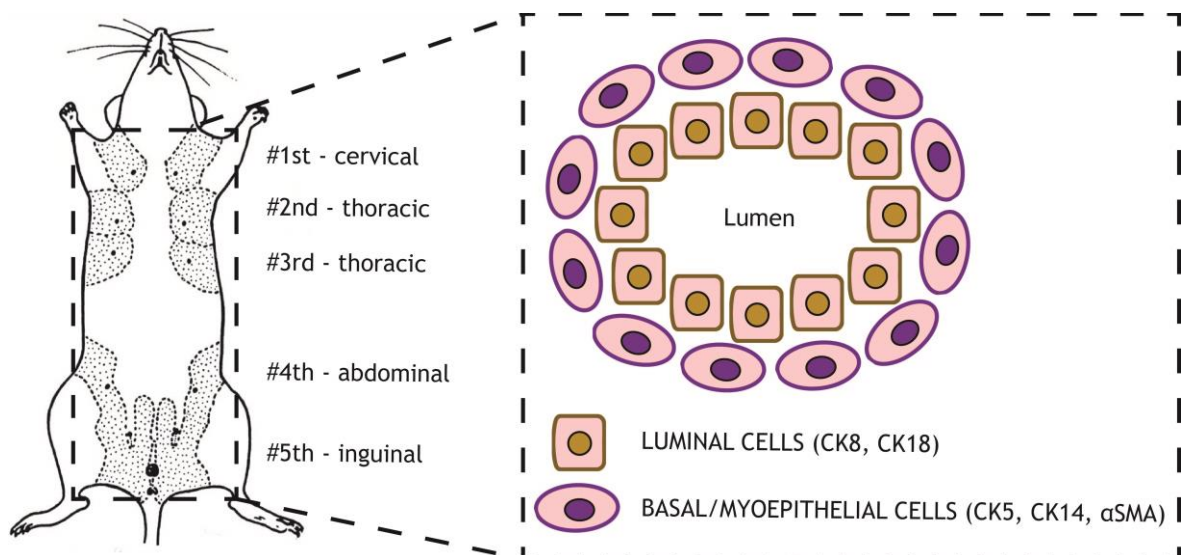


Figure 1. 2 The bi-layered epithelial structure of the murine mammary gland.

Schematic representation of the five different pairs of murine mammary glands, each one consisting of a bi-layered structure of luminal and basal/myoepithelial cells. Luminal cells are characterized by the presence of CK8 and CK18, whilst basal/myoepithelial cells can be distinguished for the expression of CK5, CK14 and α SMA. α SMA, α smooth muscle actin; CK, cytokeratin.

1.2.2 The developmental stages: embryonic, pubertal, and reproductive

The growth of the murine mammary gland, a derivative of the ectoderm, is multistage and encompasses three main developmental phases: embryonic, pubertal, and reproductive. The embryonic development of the mammary gland starts at embryonic (E) day 10 with the formation of bilateral milk lines composed of multi-layered ectoderm. By day E11.5, these give rise (asynchronously, yet at specific locations) to five pairs of placodes constituted by a thickened plate of ectoderm made up of columnar-shaped cells. By E14, placodes expand forming a ball of cells which infiltrates the underlying mesenchyme. By E16, this leads to the appearance of a rudimentary tree-like structure, known as the anlage, which remains quiescent until puberty. By E18, the nipple is formed and a ductal lumen becomes apparent, as a result of autophagy, apoptosis and cellular remodelling (Macias and Hinck, 2012).

Because of the absence of any overt phenotype shown by several hormone receptors (HRs)-deficient mice, the isometric growth of the anlage from birth to puberty is believed to be hormone-independent (Figure 1. 3A) (Briskin and O'Malley, 2010), although HRs are expressed beforehand, prior to maturation of the ovaries (Shyamala et al., 2002; Stumpf et al., 1980). At the onset of puberty, the anlage starts to proliferate expansively, as its growth becomes totally dependent on ovarian and growth hormones (GHs), which define the so-called hormone-dependent phase (Figure 1. 3C, D, E, F) (Briskin and O'Malley, 2010). Major players of this stage are TEBs: spoon-shaped structures located at the tips of growing ducts and representing the hormone-sensitive engines of the pubertal mammary tree. Following the release of hormones, these motile buds start invading the empty mammary fat pad, allowing the elongation of the ducts and the simultaneous formation of the forked architecture typical of the mammary gland. With TEBs regression occurring at the end of puberty, the mammary epithelial tree is thought to have filled up to 60-80% of the stroma (Figure 1. 3) (Hinck and Silberstein, 2005). Importantly, from puberty onwards, the mammary gland undergoes subtle morphological changes in response to the oestrous cycle, which is made up of four different phases: proestrous, oestrus, metestrous and diestrus (Caligioni, 2009). Diestrus, for example, is characterized by the

formation of progesterone-driven short tertiary side branches, which are necessary to prepare the mammary gland for a putative pregnancy (Figure 1. 3).

During the reproductive stage, with the arrival of pregnancy hormones, primarily progesterone and prolactin, alveologenesis takes place, leading to the formation of small alveoli which culminate in the production of milk during lactation. When the demand from new-borns ceases, the mammary gland undergoes an involution phase, characterized by extensive apoptosis and tissue remodelling, in order to return to a virgin-like resting state (Figure 1. 4) (Macias and Hinck, 2012).

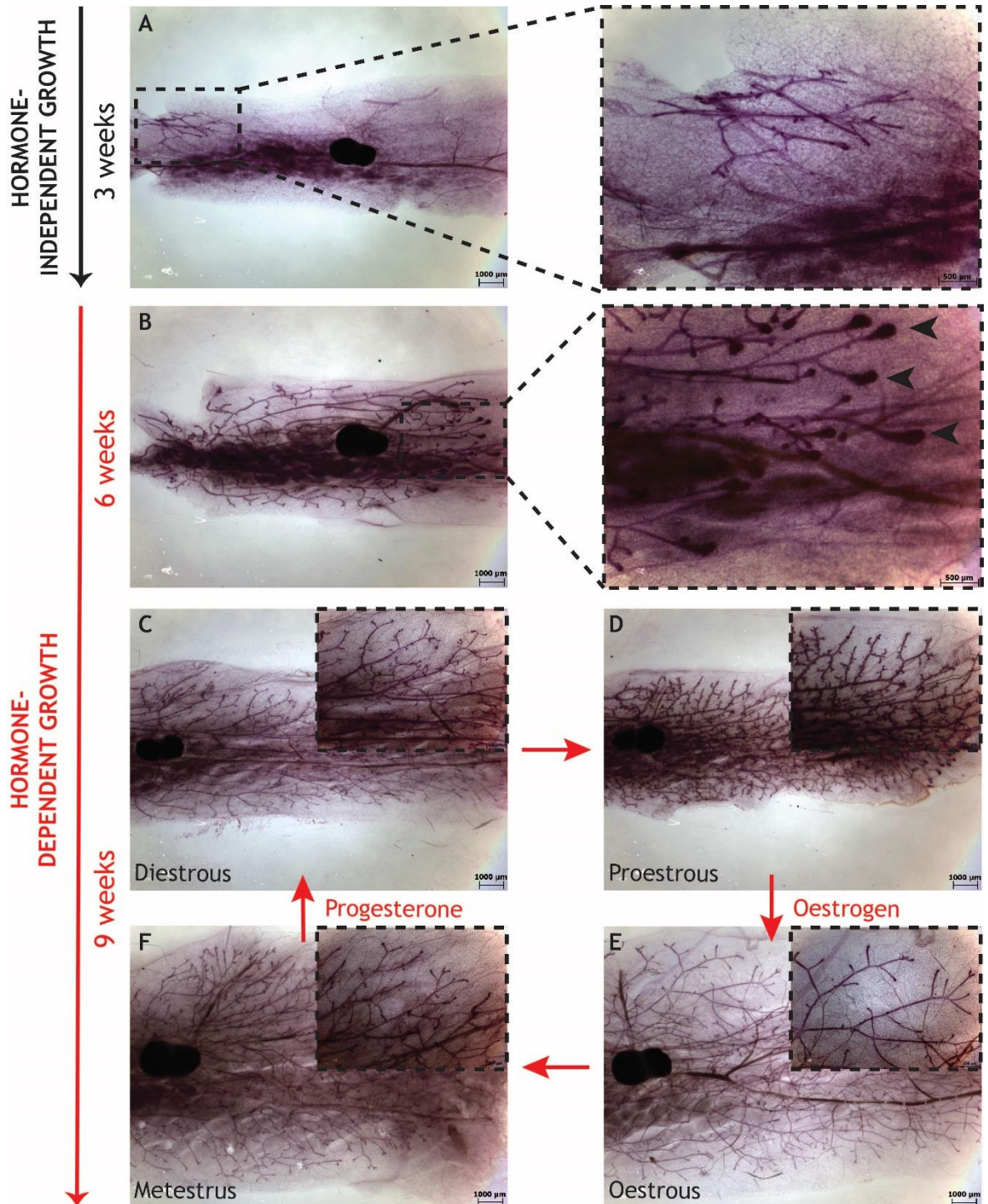


Figure 1. 3 Pubertal mammary gland development in wild-type female mice.

Whole-mounts of #4 mammary glands from wild type females at 3, 6 and 9 weeks of age. Scale bar, 1000 μm . (A) From birth to early puberty (3 weeks), the rudimentary epithelial tree (anlage) grows in the absence of hormones (hormone-independent phase). Right hand side - Higher magnification of the anlage. Scale bar, 500 μm . (B) At 6 weeks, the growth of the mammary gland becomes dependent on oestrogens and progesterone (hormone-dependent phase), responsible for ductal elongation, bifurcation and side branching. Right-hand side - Higher magnification of TEBs (see arrowheads). Scale bar, 500 μm . (C, D, E, F) By 9 weeks, the mammary gland has formed a ramified ductal structure which undergoes subtle morphological changes at each oestrous cycle. Diestrus-staged (c), proestrus-staged (d), oestrous-staged (e) and metestrus-staged (F) mammary glands. Scale bar of inserts, 500 μm . TEB, terminal end bud.

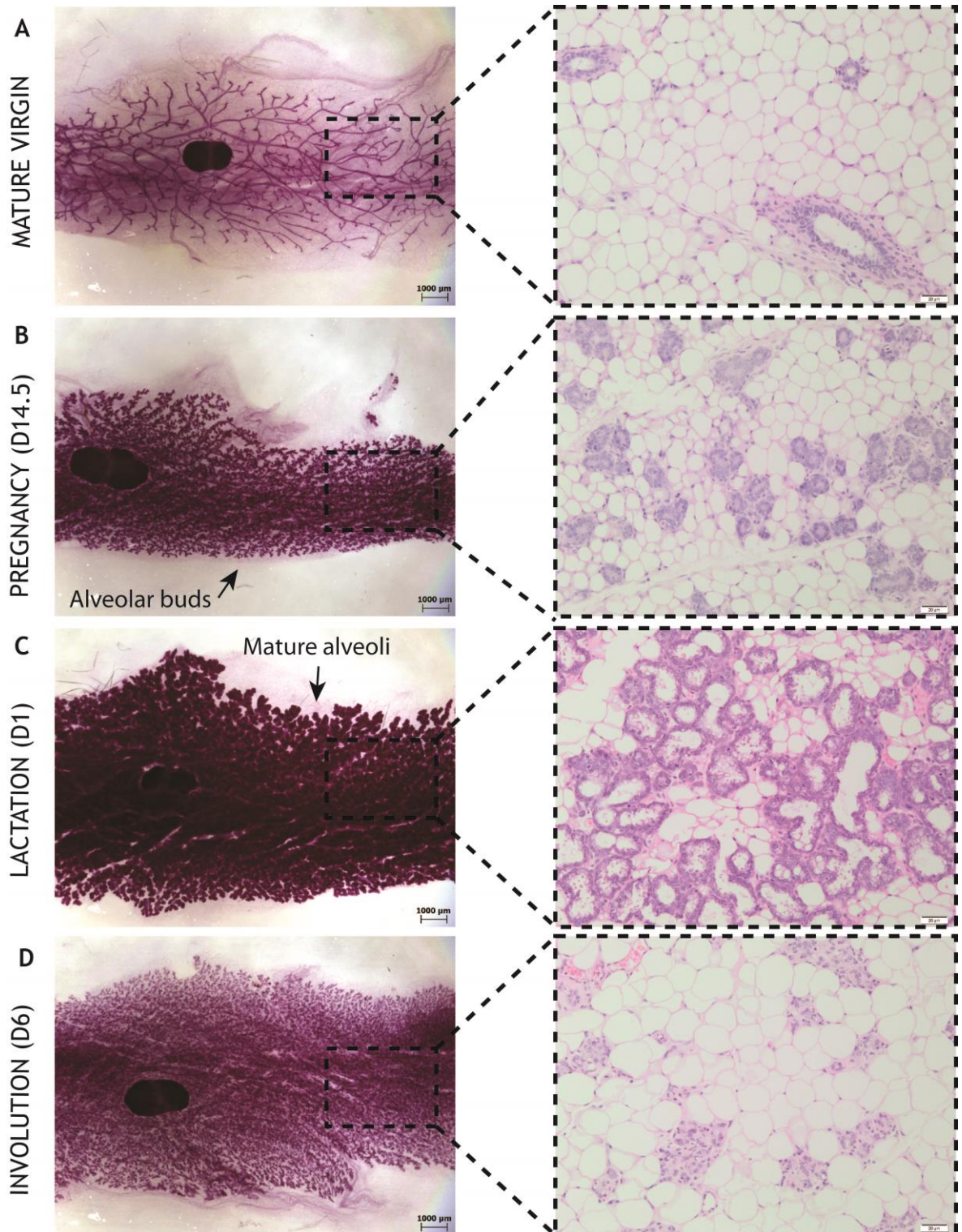


Figure 1. 4 Reproductive mammary gland development in wild-type female mice.

Whole-mounts of #4 mammary glands (left column) and corresponding H&Es (right column) from mature virgin (A), D8 pregnancy (B), D7 lactation (C) and D4 involution (D) wild type females. Scale bar of whole-mounts, 1000 μm . Scale bar of H&Es, 500 μm . (A) In mature virgin, the mammary tree presents with a forked network of primary and secondary ducts. (B) During pregnancy, the release of prolactin and progesterone causes an increase in cell proliferation accompanied by the formation of alveolar buds (see arrow). (C) At lactation, mature alveoli (see arrow) synthesize and secrete milk components into the lumen. (D) During involution, when pups are weaned, an extensive remodelling programme of the mammary gland restores the epithelial ductal tree seen in mature virgin. H&E, haematoxylin and eosin.

1.2.3 Temporal and spatial expression of the *Runx* genes in the murine mammary gland

[For this section, the text has been taken from Riggio and Blyth (2017)].

Runx1 has been shown to be the most abundantly expressed among all *Runx* genes in murine mammary epithelial cells (MMECs) (Blyth et al., 2010). Within the latter, its mRNA was found to be more elevated in the basal as compared to the luminal compartment (McDonald et al., 2014; van Bragt et al., 2014), whilst its protein was detected in both lineages of the murine gland (van Bragt et al., 2014) and the human breast epithelium (<http://www.proteinatlas.org/>). Nevertheless, RUNX1 expression seems to be very dynamic throughout the development of the organ, reaching a peak at virgin and involution, whilst decreasing at mid-gestation and lactation, when it seems lost by alveolar luminal cells, yet retained by MYO cells (van Bragt et al., 2014). Akin to *Runx1*, expression of *Runx2* fluctuates during different physiological stages of the murine mammary gland (Blyth et al., 2010) and is enriched in the basal compartment, albeit at a lower extent than *Runx1* (McDonald et al., 2014; van Bragt et al., 2014). Indeed, RUNX2 seems to have a central role during development of the organ, as suggested by its function in mammary stem cells (Ferrari et al., 2013; Ferrari et al., 2015) and the impaired growth of the mammary epithelial tree shown by *Runx2* deletion and overexpression mouse models (McDonald et al., 2014; Owens et al., 2014). However, the picture is not quite so clear for RUNX3 with one school of thought documenting lack of expression in isolated MMECs (Kendrick et al., 2008; McDonald et al., 2014; van Bragt et al., 2014), while others reporting protein expression in human breast tissue (Chen et al., 2007) and downregulation during breast tumorigenesis (Bai et al., 2013; Hwang et al., 2007; Jiang et al., 2008).

1.3 The endocrine regulation of the mammary gland

The importance of hormonal regulation and its impact on mammary gland development traces back to the 19th century with G. T. Beatson, who first identified the important role of endocrine ablation in breast cancer management (Beatson, 1896). Fascinated by the topic of lactation, Beatson realized that the elevated mammary epithelial cells' proliferation taking place at this stage

closely resembled the one occurring during breast cancer. In addition, he learned a very basic principle known to all farmers, whereby removal of the ovaries in cows after calving allowed indefinite production of milk. This suggested an intimate relationship between two fairly distant organs: the ovaries and the mammary glands. Thus, if removal of the ovaries was halting cow's mammary glands in a lactation-stage, then oophorectomy (removal of the ovaries) in breast cancers' patients might have stopped tumour's growth. Indeed, Beatson became the first surgeon who started performing oophorectomy in women with advanced breast cancers, laying the foundation for a new way of managing the disease (Beatson, 1896). It was only in the 20th century that steroid hormones were discovered and that the mechanisms underpinning their tissue-specificity revealed to be based on the presence of nuclear receptors (Shyamala et al., 2002).

1.3.1 Oestrogens and progesterone in regulating mammary development

Hormonal regulation of the mammary gland occurs via binding of ovarian hormones 17- β -estradiol (E2) and progesterone to their cognate nuclear HRs, oestrogen receptor α (ER α) and β (ER β) (Jensen, 1984; Saji et al., 2000) and progesterone receptor A (PR_A) and B (PR_B) (Giangrande and McDonnell, 1999; Mulac-Jericevic et al., 2003), respectively. However, mounting evidence suggests that only ER α and PR_B isoforms represent the main players in the mammary epithelium (Macias and Hinck, 2012; Mallepell et al., 2006). As such, both ER α and PR_B are predominantly present in the luminal compartment, wherein their patterns of expression fluctuates during mammary gland development, increasing from birth to puberty, remaining elevated in virgin, decreasing during pregnancy and lactation, and returning to basal levels at involution (Shyamala et al., 2002). The reason behind this fluctuation was unveiled when ovariectomized mice displayed high levels of ER expression and low levels of PR expression, while the opposite effect was seen upon E2 administration. These findings highlighted an intricate role exerted by E2 (yet not by progesterone), whereby the hormone would act as a negative regulator of ER and a positive regulator of PR expression, without altering the total percentage of positive cells (Shyamala et al., 2002).

As demonstrated by the absence of mammary gland development beyond a rudimentary ductal tree in $ER\alpha^{-/-}$ mice (Mallepell et al., 2006), E2 is the first mitogenic stimulus of the hormone-dependent phase, responsible for the tremendous surge in ductal elongation and bifurcation occurring in pubertal mammary glands. Importantly, whilst achieving these aims, E2 is also responsible for inducing the expression of PR, a process known as oestrogen priming (Haslam and Shyamala, 1981). This sets the stage for progesterone, which instead represents the major proliferative stimulus of the adult mammary gland. As shown by $PR^{-/-}$ mice (Lydon et al., 1995), the hormone appears to stimulate extensive ductal side branching and alveologensis, which are necessary to prepare a lactation-competent mammary gland (Brisken et al., 1998). In conjunction with the latter, prolactin signalling is required to complete alveologensis at mid-pregnancy and drive lactational differentiation during lactation (Brisken and O'Malley, 2010).

In summary, endocrine regulation of the mammary gland appears to be a highly controlled process whereby hormones act in a sequential order on the mammary epithelium, thus ensuring that specific morphological steps occur in a tightly organized manner. However, one should always bear in mind that, albeit at different concentrations, hormones are all simultaneously present both systemically and locally, highlighting the high level of complexity and synergy existing among them. In line with the latter, several experiments done in ovariectomized mice have repeatedly shown that it is only with the combinatorial administration of E2 and progesterone that a biological effect is achieved (Asselin-Labat et al., 2010; Beleut et al., 2010; Joshi et al., 2010).

1.3.2 The effects of hormonal paracrine circuits on ductal morphogenesis

What is fascinating about the endocrine regulation of the mammary gland is the fact that only a subset (50%) of luminal cells is believed to 'sensor' circulating hormones through expression of $ER\alpha$ and PR_B (Shyamala et al., 2002). A similar scenario appears to hold true for the human breast, wherein 'sensor' luminal cells (7-15%) were found to be surrounded by a larger proportion of HR-negative cells, known as the 'effectors' (Clarke et al., 1997). Additionally, a plethora of both murine and human studies have demonstrated that the vast majority of

proliferation seems to occur in effector, rather than in sensor cells (Clarke et al., 1997; Mallepell et al., 2006). Thus, how can hormonal proliferative signals be conveyed from sensor to effector cells? The answer relies on the presence of paracrine circuits acting within each epithelial layer, between the luminal and basal layers, and between the epithelial and stromal compartments of the mammary gland (Briskin and O'Malley, 2010; Macias and Hinck, 2012).

At the onset of puberty, circulating oestrogens bind to ER α ⁺ sensor cells, stimulating proliferation of neighbouring ER α ⁻ effector cells (Figure 1. 5) (Mallapel et al., 2006). This regulated process is elicited through the release of paracrine molecules, primarily amphiregulin (AREG), a transmembrane protein of the epidermal growth factor (EGF) family, that gets cleaved and released by the metalloproteinase ADAM17/TACE (Ciarloni et al., 2007; Sternlicht et al., 2005). Following this event, AREG travels through the MYO layer and the basement membrane to reach the stromal compartment, where it binds to the EGF receptor (EGFR) expressed on fibroblasts (Schroeder and Lee, 1998; Wiesen et al., 1999). This leads to the subsequent production and release of fibroblast growth factor molecules (FGFs), including FGF7 and FGF10, which bind to FGF receptor 2 expressed by luminal cells (Briskin and O'Malley, 2010). In parallel, GH release from the pituitary gland and the binding to its receptor GHR stimulates insulin-like growth factor 1 (IGF1) production both systemically, in the liver; and locally, in the mammary gland. The binding of IGF1 to IGF 1 receptor (IGF1R) expressed on luminal cells then act in concert with E2, culminating in ductal elongation and bifurcation (Figure 1. 5) (Macias and Hinck, 2012). Through similar paracrine mechanisms, circulating progesterone binds to PR_B⁺ sensor cells (Briskin et al., 1998), leading to the transcription of several target genes, including the tumour necrosis factor member receptor activator of nuclear kB ligand (RANKL) (Figure 1. 5) (Beleut et al., 2010; Mulac-Jericevic et al., 2003). Importantly, the same scenario holds true for humans, wherein a correlation between high levels of RANKL and high levels of progesterone in the blood was found (Tanos et al., 2012). As a pivotal progesterone-induced paracrine mediator, RANKL travel to the basal compartment of the mammary gland to bind to its cognate receptor RANK. By means of yet unknown mechanisms, this axis impinges on luminal PR-negative effector cells, triggering their proliferation and culminating in the formation of short side branches in

virgin mice and alveoli during pregnancy (Figure 1. 5) (Mukjerjee et al., 2010). It is important to mention, however, that progesterone also induces proliferation of a subset of PR_B⁺ cells via a cell-autonomous mechanism involving Cyclin D1. Thus, it is tempting to speculate that these PR_B⁺ proliferating cells might represent stem or progenitor cells (Beleut et al., 2010).

Such coordinated mode of paracrine action has two very important consequences: firstly, it does not require high amount of hormones, as the proliferating signal gets amplified at each sequential step; and secondly, it regulates mammary gland development by fine-tuning the proliferation of different MMECs at a specific time and space (Briskin et al., 2010). As such, through the use of paracrine circuits, HRs are able to convey systemic signals into fine-tuned local ones, thus achieving a tight control upon ductal morphogenesis. Interestingly, more than 90% of breast tumours appear to be ductal in origin (Russo et al., 2005). Given that many pathways observed during breast cancer progression mirror the physiological ones, a deep understanding of the biology underlying ductal morphogenesis might also offer insights into the fascinating, yet not fully explained biology of breast tumourigenesis.

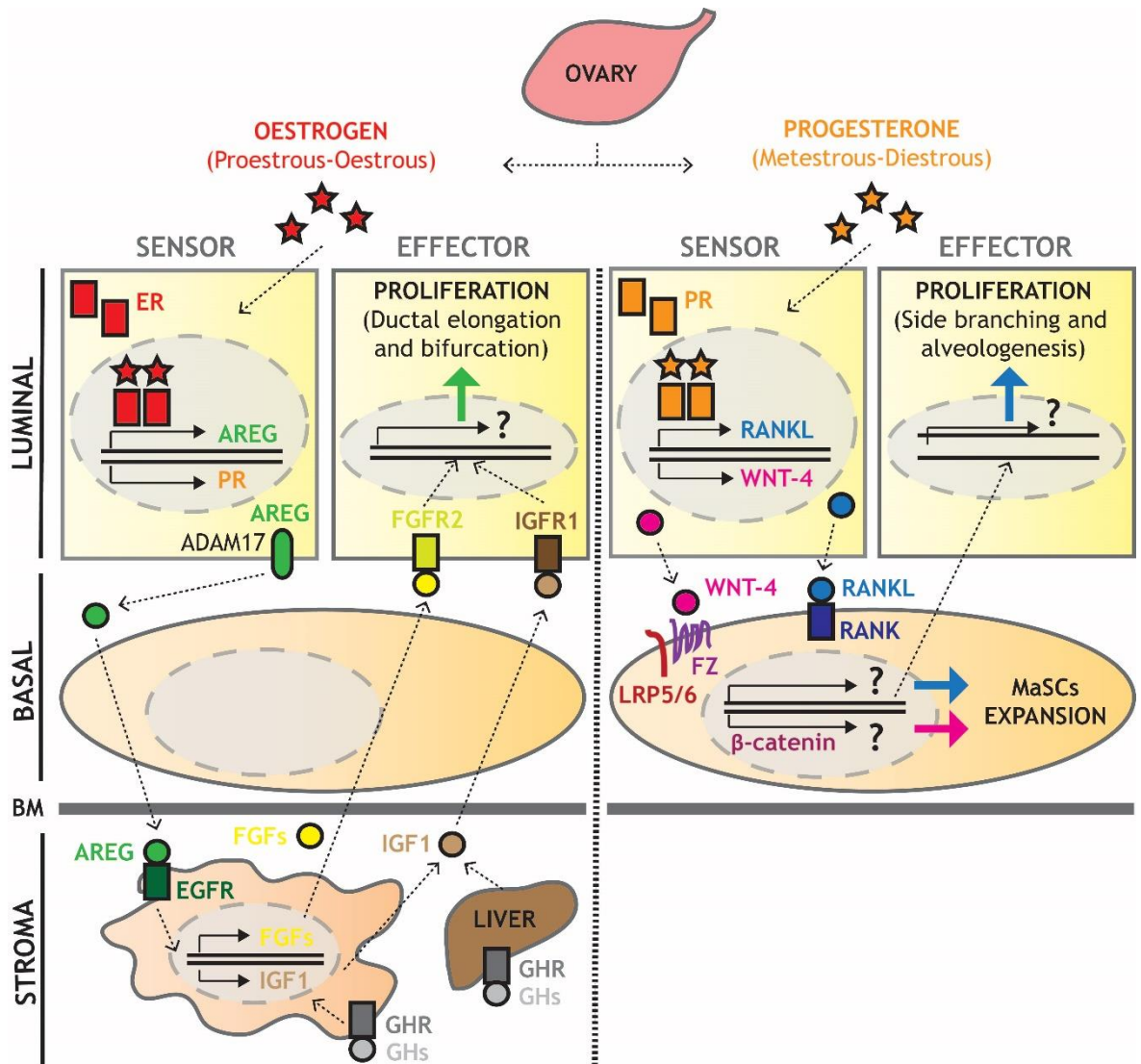


Figure 1. 5 Model of the paracrine circuits engaged by oestrogen and progesterone.

The release of ovarian oestrogen at pro-oestrus and oestrus allows the hormone to engage with ER expressed by luminal sensor cells. This results in the production of AREG, which translocates to the cell membrane where it gets cleaved by ADAM17. Soluble AREG travels through the basal compartment to bind to EGFR expressed by stromal cells. This leads to the production and release of FGFs, which signal back to luminal compartment via binding to FGFR2. In concert with the latter, binding of GHs (released from the pituitary gland) to GHR present in the liver and in stromal cells of the MG triggers the production and release of IGF1, which binds to IGF1R in the luminal compartment. Altogether, these two axes foster the proliferation of luminal ER- (effector) cells, resulting in ductal elongation and bifurcation at puberty. Please note that oestrogen would also stimulate the transcription of PR (oestrogen priming). The release of ovarian progesterone at metestrus and diestrus allows the hormone to engage with PR expressed by luminal sensor cells. This leads to the production of two main paracrine molecules, RANKL and WNT-4, whose binding to RANK and FZ/LRP5/6 co-receptors present on basal cells drive MaSCs expansion during diestrus and pregnancy. In addition, the RANKL/RANK axis generates a signalling cascade which feeds back to the luminal layer, stimulating the proliferation of luminal PR- (effector) cells, resulting in side branching at puberty and alveologenes during pregnancy. AREG, amphiregulin; BM, basement membrane; EGFR, epidermal growth factor receptor; ER, oestrogen receptor; FGF, fibroblast growth factor; FGFR2, fibroblast growth factor receptor 2; FZ, frizzled; LRP5/6, low-density lipoprotein-related protein; MG, mammary gland; GH, growth hormone; GHR, growth hormone receptor; IGF1, insulin-like growth factor 1; IGF1R, insulin-like growth factor 1 receptor; PR, progesterone receptor; RANK, receptor activator of nuclear factor k-B; RANKL, receptor activator of nuclear factor k-B ligand.

1.3.3 The mammary interplay between RUNX1 and oestrogens

[For this section, the text has been adapted from Riggio and Blyth (2017)].

According to the classical paradigm, diffusion of steroid hormones through the plasma and nuclear membranes results in the formation of activated oestrogen-ER complexes that directly bind to consensus oestrogen response elements (EREs) of hormone-responsive genes (Hewitt et al., 2003). However, since the initial discovery of this direct DNA binding (ERE-dependent) model, alternative mechanisms of oestrogen function have become apparent. These include an ERE-independent pathway involving ‘tethering’ of ligand-activated-receptor complexes by transcription factors already bound to the DNA through their respective response elements (Kushner et al., 2000; Safe and Kim, 2008).

With the discovery of RUNX among the top five most enriched motifs in ER α tethering sites of breast cancer cell lines, a “non-classical” interplay between RUNX1 and the oestrogen/ER signalling pathway has been unveiled (Stender et al., 2010). In line with this, co-immunoprecipitation studies demonstrated the presence of a basal interaction between RUNX1 and ER α , which was further enhanced upon oestrogen stimulation. Given the connection between RUNX1 and chromatin modifier enzymes (Yamagata et al., 2005), and its occupancy of ER α tethered binding sites even prior to oestrogen stimulation, RUNX1 might facilitate the recruitment of ER α to permissive remodelled chromatin loci (Figure 1. 6), thereby mediating the transcriptional regulation of specific oestrogen-responsive genes (Stender et al., 2010). Albeit insufficient to direct a full hormonal response in mice, the ERE-independent tethering mechanism appears to regulate up to 25% of ER α -responsive genes, thus perhaps acting complementary to the classical oestrogen signalling (Ahlbory-Dieker et al., 2009; Hewitt et al., 2016).

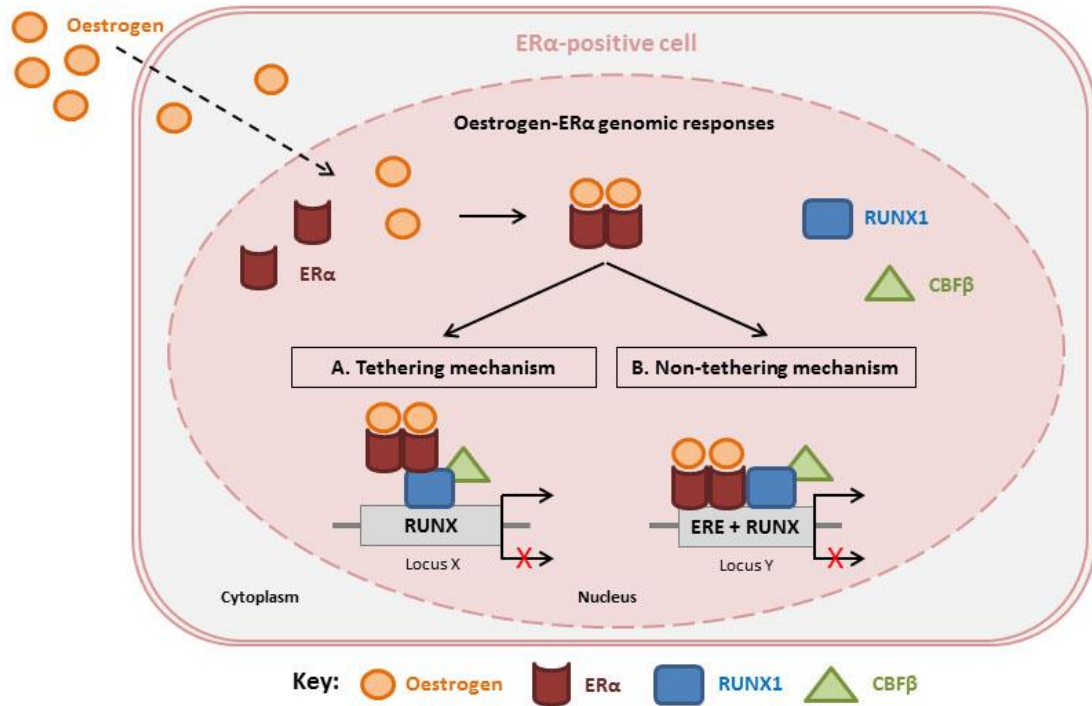


Figure 1. 6 The RUNX1-ERα interplay.

Model showing two possible mechanisms by which RUNX1 might act as a fine-tuning orchestrator of oestrogen-ERα genomic responses in ERα-positive cells. (A) Tethering mechanism: RUNX1 (together with CBFβ) binds to its respective RUNX motif on the DNA and acts as a tethering factor for the oestrogen-ERα complex to modulate transcription of Locus X. (B) Non-tethering mechanism: RUNX1 (together with CBFβ) binds to its RUNX motif on the DNA and interacts with the oestrogen-ERα complex, bound to an ERE site, to modulate transcription of Locus Y. Further details and references can be found in the text. Taken from Riggio and Blyth (2017).

1.4 Mammary epithelial stem cells

Unlike any other cells in the body, stem cells (SCs) are devoted to three main biological processes: organ development, tissue homeostasis and tissue repair (Reya and Clevers, 2005). This unique capability arises from the fact that SCs are defined by two main properties, self-renewal and multi-potency (or multi-lineage differentiation), which in turn depend on the instructive signals present in the surrounding “SC niche” (Lin, 2002). The first one refers to the ability of SCs to replenish themselves, while the second one to SCs’ differentiation into terminally mature cells through intermediate progenitors (Chen et al., 2017). Of note, these two key features are intimately linked to SCs capability of undergoing different types of cell division (CD), i.e. symmetric (SCD) or asymmetric (ACD). During SCD, a SC would divide equally to generate two identical daughter cells, namely two SCs (self-renewal). In ACD, instead, a SC would divide unequally to generate two daughter cells with different fates, that is a SC and a committed progenitor or transient amplifying cell, which will then give rise to a differentiated cell (multi-potency) (Knoblich, 2010; Smith, 2005). Of note, this has been shown to depend on the partitioning of the molecular components of the cell. Additionally, a SC could also generate two different daughter cells through SCD if, following mitosis, these are differentially placed in the surrounding environment (extrinsic ACD) (Ballard et al., 2015). Importantly, the interplay between Wnt/ β -catenin, Notch and Hedgehog signalling pathways, coupled with the activation of key transcription factor genes including *Myc*, *Slug* and *Sox9*, have been shown to be critical for the maintenance of the stemness phenotype (Chen et al., 2017; Guo et al., 2012).

1.4.1 The discovery of mammary repopulating units

The remarkable outgrowth of the mammary epithelium at puberty and its extensive remodelling capability of undergoing multiple cycles of proliferation, differentiation and apoptosis hinted at the presence of SCs in the mammary gland, the so-called mammary SCs (MaSCs) (Macias and Hinck, 2012). It was only in the 1960’s that this hypothesis could be tested when injection of pieces of mammary tissue into cleared fat pads of recipient mice resulted in outgrowth of complete epithelial ductal trees (DeOme et al., 1959; Faulkin and DeOme, 1960; Hoshino et al., 1964). A decade later, the existence of a “*growth-regulating*

system”, as it was called hitherto, was further confirmed through serial engraftments of mammary epithelium for up to seven generations, after which time senescence occurred, probably due to the exhaustion of MaSC(s) contained in the original fragment (Daniel et al., 1968). Of note, the innate regenerative capacity of the engrafted mammary tissue did not seem to depend on the regional location of the original tissue, nor by the age, hormonal status and reproductive history of donor mice (DeOme et al., 1959). When the same experiments were repeated by retrovirally tagging mammary epithelial fragments with mouse mammary tumour virus (MMTV), it was realized that this ‘*growth-regulating ability*’ could be inferred to a single epithelial cell, which (if transplanted *in vivo*) was able to reconstitute an entire functional ductal tree comprised of its progeny (Kordon and Smith, 1998).

Collectively, these data indicated that repopulating cells, inferred to be MaSCs, were indeed present in the mammary gland, scattered throughout the epithelial tree and capable not only of multi-lineage differentiation but also of a remarkable, yet limited self-renewing potential. Undoubtedly, these findings represented a breakthrough in the mammary SC field, as corroborated by the fact that the gold standard assay to detect MaSCs still consists in the ability of a single cell to reconstitute a fully competent mammary tree upon serial transplantations *in vivo* (Visvader, 2009). Overtime, however, criticism has significantly arisen when trying to extrapolate the biological significance of the aforementioned results. In fact, by mimicking a forced regenerative state, it has been argued that transplantation assays could have led to misleading findings, whereby the regenerative potential shown by transplanted cells might not have necessarily been the same to the one owned by the same cells under physiological conditions (Blanpain and Fuchs, 2014). For this reason, scientists reckoned a more appropriate term to refer to these cells would be as mammary repopulating units (MRUs) (Shackleton et al., 2006; Stingl et al., 2006). Nevertheless, to avoid further confusion, in the present text MRUs will mostly be referred to as MaSCs.

1.4.2 Phenotypic and functional characterization of mammary stem cells

With the advent of single-cell based methods, such as flow cytometry and fluorescence-activated cell sorting (FACS), MMECs started to be molecularly characterized for the first time by the presence of two distinct cell surface markers: CD24 (heat stable antigen) and either CD49f ($\alpha 6$ -integrin) or CD29 ($\beta 1$ -integrin). By doing so, the CD24⁺CD29^{low}CD49f^{low} population was found to be enriched in luminal cells, based on the high prevalence of K18⁺ cells, whereas the CD24⁺CD29^{high}CD49f^{high} were predominantly in basal cells, based on the high prevalence of K14⁺ cells (Asselin-Labat et al., 2010; Shackleton et al., 2006; Stingl et al., 2006).

1.4.2.1 Insights from FACS-based studies

When transplantation assays were carried out at limiting dilutions to test the reconstitution efficiency of different sorted MMEC populations, the vast majority of MaSCs was found to lie within the CD24⁺CD49f^{high}/CD29^{high} subset (Shackleton et al., 2006; Sleeman et al., 2007). Furthermore, when primary outgrowths were dissociated and their cells re-transplanted in limiting dilutions, secondary outgrowths appeared, further confirming the self-renewal potential of MaSCs (Shackleton et al., 2006; Stingl et al., 2006). Lastly, when the same assay was repeated on sorted foetal MaSCs (fMaSCs), isolated at E18.5 from the anlage, they showed a higher regenerative potential compared to adult MaSCs (aMaSCs) (Spike et al., 2012). Collectively, these data led to two important conclusions: firstly, that MaSCs with multi-lineage and self-renewal potential could be isolated from both foetal mammary rudiments and adult mammary glands; and secondly, that, based on their molecular profile which clustered them together with basal cells, MaSCs were thought to reside in the basal layer of the mammary gland. However, due to the low prevalence of MaSCs in sorted CD24⁺CD49f^{high}/CD29^{high} cells and the degree of heterogeneity shown by this cluster, which also contains MYO cells and putative basal progenitor intermediates; efforts have been put into refining the molecular identification and subsequent isolation of MaSCs.

Stem cell antigen 1 (Sca-1), routinely used as a cell surface marker for enrichment strategies of haematopoietic stem cells (HSCs) (Goodell et al., 1996; Spangrude et al., 1988), did not appear to be enriched in the CD24⁺CD49f^{high}Sca-1⁺ subset when tested, and shows a lack of reconstitution when Sca-1-expressing cells are transplanted *in vivo* (Shackleton et al., 2006; Stingl et al., 2006). Therefore, perhaps counterintuitively, Sca-1 negativity has been used as a marker to enrich for MaSCs. Another breakthrough arrived with the discovery of the Wnt3a target protein C receptor (ProcR) (Wang et al., 2015). Generation of a knock-in allele for ProcR found the protein to be expressed in the basal epithelium of the mammary gland, with positive cells present in an actively cycling state and characterized by low levels of K5 and K14. More importantly, when their stem-like features were tested both *in vitro* and *in vivo*, CD24⁺CD29^{high}ProcR⁺ displayed increased colony forming cell (CFC) ability and a remarkable reconstitution capacity, respectively (Wang et al., 2015). Given the well-known role played by the Wnt/ β -catenin signalling pathway in SCs (Reya and Clevers, 2005), other scientists started using the leucine-rich repeat-containing G-protein-coupled receptor 5 (Lgr5) as a marker for MaSCs. Known to be a key Wnt/ β -catenin target gene expressed by cycling SCs of several epithelial tissues (Barker et al., 2013), Lgr5 was also found to be present in the mammary gland, particularly in the basal layer. Yet, its use yielded inconsistent data. On one side, CD24⁺CD49f^{high}Lgr5⁺ cells showed an outstanding repopulating activity upon serial transplantations compared to their parental population (de Visser et al., 2012; Plaks et al., 2013), yet on the other, Lgr5⁺ cells were found to fall within the basal ProcR⁻ subset characterized by very low regenerative potential (Wang et al., 2015). Lastly, a very recent study demonstrated that, albeit Lgr5 can be found in both fMaSCs and aMaSCs, its expression appears to be dispensable for SC activity (Trejo et al., 2017). In conclusion, despite some contrasting findings, these studies have led to a significant refinement of the molecular profile displayed by MaSCs, which appear to be enriched within the CD24⁺CD49f^{high}/CD29^{high}ProcR⁺Sca-1⁻ subset of MMECs.

1.4.2.2 Insights from lineage-tracing studies

Notwithstanding the progress achieved by FACS-based approaches, these are not without caveats. Firstly, they allow the molecular characterization of cells *ex vivo* that is freshly extracted from the primary tissue, yet not in their

physiological context. Secondly, as the properties displayed by MRUs might differ from the properties of MaSCs *in vivo* (Blanpain and Fuchs, 2014), these methods have not been able to assess the natural multi-lineage potential of MaSCs. For these reasons, the use of lineage-tracing studies, coupled with genetically engineered mouse models (GEMMs), offered a better way to interrogate the physiological regenerative potential of MaSCs. This technique is primarily based on the *in situ* labelling of a putative SC, with either a fluorescent or a histochemical reporter, and on the possibility to track its fate and ascertain its relative contribution to mammary gland development. As such, being that the label permanently expressed by the targeted cell, it is possible to assess its uni- or bi-potential depending on whether its progeny is made up of lineage-restricted clones or of both basal and luminal cells, respectively (Lloyd-Lewis et al., 2017).

On one side, according to some of the first lineage-tracing experiments, the growth of the mammary gland from embryonic to early pubertal stage was shown to depend on the presence of multipotent embryonic K14⁺ SCs, able to differentiate into the basal and luminal lineage. However, the extensive postnatal mammary gland development occurring during puberty, as well as the homeostatic control of the organ during adulthood, was found to be governed by lineage-restricted K14⁺ and K8⁺ progenitors, which were only capable of generating either basal or luminal progeny, respectively (Van Keymeulen et al., 2011). Similar results have recently been reported for Lgr5, whose expression appeared to mark bipotent fMaSCs, while becoming restricted to basal unipotent progenitors during adulthood (Trejo et al., 2017). Additionally, evidence for the presence of restricted progenitors in the adult mammary gland holds true for the E74-like factor 5 (Elf5) transcription factor, which has been shown to label a subset of luminal cells found to contribute to ductal morphogenesis in puberty, mammary gland maintenance in virgin and alveologenesis during pregnancy (Rios et al., 2014). On the other side, more recent studies tracing the fate of K5-expressing cells, highly abundant in TEBs, as well as in basal and luminal cells of terminal ducts, supported the presence of bipotent SCs in pubertal mammary glands. Additionally, the presence of K5⁺ biclonal patches found in the adult organ indicated that long-lived K5⁺ bipotent basal MaSCs were also actively involved in ductal morphogenesis and homeostasis during adulthood. Notably, similar results were also obtained when tracing K14- and Lgr5-expressing cells

(Rios et al., 2014), albeit in contrast to what previously reported (Trejo et al., 2017; Van Keymeulen et al., 2011). Ultimately, bipotent ProcR⁺ MaSCs (K5-low, K14-low) were also shown to be able to self-renew through SCD and differentiate through ACD, giving rise to committed progenitors of the luminal and basal lineage (Wang et al., 2015).

Notwithstanding the potential of lineage-tracing techniques, these have led to a high degree of discrepancies between studies, even when the same promoter was selected. In this regards, however, it is worth mentioning that part of these inconsistencies may arise from technical differences in the experimental settings. These include the type and dose of induction agents used, the type of promoter and reporter gene employed, as well as the chosen labelling times. Also, both knock-in and transgenic mice have been shown to be differently prone to insertion-sites effects, which could alter gene expression from the selected promoter leading to misleading results (Rios et al., 2016). Additionally, when dealing with heterogeneous population of cells wherein SCs only represent a tiny fraction, one should bear in mind that the most prevalent cell type will tend to have the highest chance to be labelled. As such, in the case of the mammary gland, these could be represented by unipotent progenitors (Visvader and Stingl, 2014). In summary, whilst there is no doubt on the existence of bipotent fMaSCs responsible for the formation of the anlage, confusion has concerned so far the presence of bipotent SCs in the postnatal mammary gland. Based on the results accumulated hitherto, there is evidence for both long-lived bipotent SCs and unipotent progenitors in the adult organ, where they seem to play an active role in governing pubertal development and organ homeostasis (Rios et al., 2014). Of note, the distinct properties of these two cell types are intimately linked to their ACD, which in the case of bipotent MaSCs will give rise to cells with different self-renewal in different cell lineage, whereas in the case of unipotent progenitors will give rise to daughter cells of the same cell lineage, yet with different self-renewal potential (Ballard et al., 2015). By confirming the presence of bipotent MaSCs in the adult organ, these findings have also mitigated some of the criticisms over transplantation assay. Furthermore, as no MRUs were found to be enriched in the luminal population, likewise no bipotent MaSCs were seen to reside in the luminal layer of the mammary gland, yet only in the basal layer (Visvader and Stingl, 2014).

1.5 The hormonal milieu of the stem cell niche

Albeit deemed to reside in the basal compartment of the mammary gland (Shackleton et al., 2006; Stingl et al., 2006), mounting evidence suggests that MaSCs might be sensitive to ovarian hormones. Support of this hypothesis dates back to transplantation experiments, when older hosts did not allow the growth of transplanted mammary fragments as compared to young hosts; a phenotype attributed to an impairment of their endocrine system (Young et al., 1971). Additionally, although ovariectomy was shown to reduce the number of luminal cells, yet not of MaSCs, the latter subpopulation displayed a marked decrease in its regenerative ability when transplanted *in vivo* (Asselin-Labat et al., 2010). MaSCs were shown to lack ER and PR expression in both mice and humans (Asselin-Labat et al., 2006; Lim et al., 2009) and also are generally thought to lie in the mammary epithelium in a resting-quiescent state, unless activated during puberty and pregnancy (Shackleton et al., 2006; Stingl et al., 2006). Therefore, it may be counterintuitive that HR-negative MaSCs should be so exquisitely influenced by ovarian hormones.

1.5.1 A “stemness” role for progesterone

Given the similarity between the murine oestrous cycle and the human menstrual cycle, studying changes occurring in the murine mammary gland upon hormonal exposure has been instrumental to investigate the hormonal regulation of MaSCs. In fact, as the surge in circulating oestrogens during the human follicular phase is mirrored by the murine pro-oestrus/oestrous phase, the rise in progesterone levels typical of the human luteal phase is reflected by the murine diestrus phase (Caligioni, 2009). Evidence gathered from both mice and humans points towards progesterone as the main regulator of MaSCs and cellular turnover in the mammary gland. In mice, a high proliferative and apoptotic index, coupled with a pronounced side branching morphology of mammary whole-mounts, were shown to characterize diestrus-staged mammary glands compared with other oestrous phases (Joshi et al., 2010). In addition, serial engraftments of mammary epithelial fragments from *PR*^{-/-} mice were found to result in an impairment of their regenerative potential at the 3rd generation of passages (Rajaram et al., 2015). In humans, breast proliferation in parous women was shown to be significantly higher during the luteal as compared to the

follicular phase of the menstrual cycle (Masters et al., 1977). Moreover, mounting evidence has reported a role for progesterone in inducing alveologenesis during pregnancy, a process which is known to require a marked yet temporary expansion of MaSCs (Asselin-Labat et al., 2010). As mentioned above, progesterone action strictly relies on the presence of paracrine molecules, primarily RANKL and Wnt-4 (Fernandez-Valdivia and Lydon, 2012). On one hand, both luminal RANKL and basal RANK mRNAs were shown to reach very high levels during pregnancy, consistent with the well-known expansion of MaSCs and the extensive alveologenesis occurring at this reproductive stage (Asselin-Labat et al., 2010). On the other hand, when pieces of virgin mammary epithelium from *Rankl*^{-/-} mice were serially engrafted in the cleared fat pad of recipient mice, these showed the same regenerative potential as the wild type counterpart, albeit with a lessened degree of side branching. On the contrary, *Wnt4*^{-/-} embryonic epithelial buds displayed a significant impairment in their ability to engraft. Indeed, WNT-4 ligand was recently shown to be critical for the activation of canonical Wnt/ β -catenin signalling in the MYO (Rajaram et al., 2015). Therefore, progesterone might hijack specific paracrine signals to drive MaSCs expansion at different developmental stages of the mammary gland. As such, the hormone would preferentially engage the RANKL-RANK axis to drive alveologenesis during pregnancy, while it would depend on WNT-4 when controlling MaSCs expansion during ductal morphogenesis and possibly mammary gland homeostasis.

Importantly, whichever way progesterone acts, it certainly does not do it on its own. In fact, when ovariectomized mice were treated with E2, progesterone or E2 and progesterone, an expansion of basal and luminal cells, as well as luminal increase in the levels of both *RANKL* and *Wnt-4*, could only be observed when the combination of both hormones was used (Asselin-Labat et al., 2010; Joshi et al., 2010). This data would suggest that the action of progesterone in the adult mammary gland would mainly rely on the presence of E2, which in fact appears to be a potent inducer of PR expression (Beleut et al., 2010; Haslam and Shyamala, 1981; Shyamala et al., 2002). A model might then be envisioned in which E2 would induce PR expression on luminal sensor cells, so that progesterone could bind to its receptor, in order to trigger the production and release of its paracrine target Wnt4. The latter would then travel to the MYO

layer to activate canonical Wnt/ β -catenin signalling, which would result in a transient, yet profound expansion of MaSCs in postnatal mammary glands, at both diestrus and reproductive stage (Rajaram et al., 2015) (Figure 1. 5).

1.5.2 The link between ovarian hormones and breast cancer

The endocrine regulation of MaSCs becomes of crucial importance if we think that the hormones that control mammary gland postnatal development and homeostasis, i.e. E2 and progesterone, are also the same which influence breast tumourigenesis. In line with the latter, it is generally believed that a women's risk of developing breast cancer is tightly linked with her lifetime hormonal exposure and reproductive history (Brisken and O'Malley, 2010). On the other side, as firstly shown by G.T. Beatson (1896), ovarian ablation has a protective effect against the disease. If at each diestrus cycle, as well as at each pregnancy, progesterone induces the expansion of MaSCs, would not the latter accumulate over time and be susceptible to oncogenic transformation? In a physiological setting the answer appears to be no, in line with the fact that the increased proliferative index observed in diestrus-staged mammary glands is also accompanied by a high degree of apoptosis (Joshi et al., 2010). Similarly, the expansion of the MaSCs pool occurring during pregnancy is followed by the increased apoptotic rate seen in involution (Inman et al., 2015). Therefore, by means of compensatory mechanisms, mammary gland homeostasis is always been at the end of each estrous and reproductive cycle. Nevertheless, if the homeostatic regulation of the mammary gland gets impaired, one could envision the possibility of MaSCs accumulating overtime, and becoming more susceptible to additional hits, eventually leading to tumourigenesis. In this regard, pregnancy has been shown to be one of the strongest risk factor for breast cancer. According to one of the current hypotheses, the long-term protective effect conferred by an early pregnancy (before the age of 20) could be due to a reduction in the number and activity of MaSCs (Meier-Abt et al., 2013). Nevertheless, in view of the tendency of modern women to delay childbirth, the incidence of pregnancy-associated breast cancer, that is breast cancer occurring during or post-partum, is unfortunately expected to increase (Lyons et al., 2009). Collectively, these results highlight the importance of understanding the paracrine mechanisms of hormonal regulation and how they impinge on the

activity of MaSCs. This might then shed light on how dysregulation of the system underpins breast cancer initiation, progression and possibly relapse.

1.6 The mammary epithelial cell hierarchy

Along with the discovery of a “*growth-regulating system*” within the mammary gland (Faulkin and DeOme, 1960) came the hypothesis that a differentiation hierarchy, analogous to the one found in the haematopoietic system, might also exist in this organ (Visvader, 2009). This idea was further corroborated by the remarkable degree of heterogeneity characterizing the gland, made up by two epithelial lineages (basal and luminal) present at different differentiation stages (stem, progenitor and differentiated cells). In view of their ability to differentiate into basal and luminal cells through a series of intermediate progenitors, bipotent MaSCs were placed on the top of the mammary epithelial cell hierarchy (Chen et al., 2017). Nevertheless, if what depicted could hold true for the formation of the anlage by bipotent fMaSCs, the same picture could not fully explain mammary gland pubertal development or its homeostasis during adulthood. With the advent of FACS-based and lineage-tracing studies, a further level of complexity was added to the mammary epithelial cell hierarchy, starting to shed light on the profound cellular heterogeneity existing within each compartment of the mammary gland (Visvader and Stingl, 2014).

1.6.1 The heterogeneity of the stem cell compartment

Although all believed to be enriched within the CD24⁺CD29^{high}/CD49f^{high} subset of MMECs, there are phenotypic and functional disparities within MaSCs. One of the most striking differences is between foetal and adult MaSCs (Visvader and Stingl, 2014). Firstly, fMaSCs are found in the embryonic bud and in the anlage of the mammary gland, whereas aMaSCs are present in the adult organ. Secondly, while fMaSCs are believed to be responsible for the formation of the mammary rudiment, aMaSCs would be devoted to mammary gland pubertal development and tissue homeostasis during adulthood. Thirdly, although they both display a basal-like gene signature characterized by lack of HRs expression, fMaSCs have also been shown to express a few genes specific of the luminal lineage (e.g. *Elf5*). Fourthly, when challenged in transplantation assays, fMaSCs exhibited a significantly higher regenerative ability compared to the adult counterpart

(Spike et al., 2012). For the above reasons, fMaSCs were proposed to lay the foundation of the mammary epithelial cell hierarchy, whereas aMaSCs are likely derivatives of the former (Figure 1. 7A). Whether fMaSCs would also persist in the adult organ is still a matter of debate. However, due to the embryonic SC-like gene signature shown by certain types of undifferentiated and aggressive breast cancers, it is tempting to speculate that fMaSCs, or alternatively any cell which would revert to an embryonic SC-like state, might be putative targets for oncogenic transformation (Ben-Porath et al., 2008).

An additional layer of MaSC heterogeneity refers to their proliferative status. As mentioned above, there are specific developmental stages of the mammary gland (e.g. ductal morphogenesis and alveologenesi s) which require the presence of active pools of MaSCs (Asselin-Labat et al., 2010). Indeed, via the use of the s-SHIP marker, cycling MaSCs were found in the cap layer of TEBs (Bai and Rohrschneider, 2010). Likewise, when following the fate of proliferating K5+ MaSCs, these appeared to give rise to luminal body cells of TEBs (Rios et al., 2014). However, despite being the most proliferative units of the mammary gland, TEBs are not the only place where actively cycling MaSCs were found. In recent years, lineage-tracing studies have reported the presence of proliferative bipotent MaSCs both in TEBs and terminal ducts of pubertal and adult mammary glands (Visvader and Stingl, 2014). An active population of MaSCs has also been identified during pregnancy, where it appears to govern the process of alveologenesi s. Yet, when challenged in serial transplantation assays, “pregnant” MaSCs showed a lower regenerative and self-renewal potential compared to “virgin” MaSCs. As such, they have been proposed to represent an active, yet short-term repopulating pool of MaSCs, which could even be responsible for the transient increase in breast cancer risk associated with pregnancy (Visvader and Stingl, 2014). Unless activated during puberty or pregnancy, MaSCs are believed to reside in the mammary gland in a resting, slow-cycling state. Several studies using label-retention approaches support the hypothesis that MaSCs, due to their slow rate of proliferation and apoptosis, would have had a higher chance to retain the label as compared to actively cycling cells. Accordingly, the MaSC population has often appeared to be enriched for label-retaining cells (Shackleton et al., 2006; Welm et al., 2002). In addition to quiescent MaSCs, there also seems to be a category of MaSCs, which

remain dormant during mammary development, while retaining its regenerative potential upon forced regenerative conditions or even cancer. To distinguish them from the previously discussed “professional MaSCs”, these cells were referred to as potential or facultative MaSCs (Visvader and Stingl, 2014), as they potentially bear all MaSCs properties, albeit they do not generally display them in physiological conditions (Lloyd-Lewis et al., 2017). Due to the low prevalence of MaSCs and the lack of consensus regarding their molecular profile, studying the cycling status of MaSCs does not represent an easy task to accomplish. There is evidence for the presence of both quiescent and actively cycling aMaSCs in postnatal mammary glands. However, while, by definition, quiescent SCs are all long-lived cells, not all actively cycling MaSCs bear the same self-renewal potential, thus encompassing both short and long-term repopulating cells (Visvader and Stingl, 2014).

1.6.2 The distinctive features of progenitor cells

In addition to the presence of MaSCs, the mammary gland contains several types of progenitor cells, namely daughter cells originating from the ACD of MaSCs and usually characterized by a lower regenerative potential and restricted cell fate (Knoblich, 2010; Smith, 2005). In support of the parent-progeny relationship between MaSCs and progenitor cells, *in vitro* assays have represented extremely valuable tools (Smalley et al., 1998). Of note, depending on the cultivation system used, stem/progenitor cells have been ascribed different names, being labelled as mammospheres, owing to their ability to form spheres in suspension or as mammary colony forming cells (Ma-CFCs), in view of their ability to form colonies in 3D (Stingl et al., 2006). The discovery that multipotent undifferentiated neural SCs could be cultured in suspension as neurospheres (Reynolds and Weiss, 1992) had a huge impact on the cultivation of human and mouse MECs. Hitherto, culture of primary cells on solid surfaces appeared to induce their differentiation and subsequent senescence. The use of non-adherent conditions was instead found to privilege the survival of undifferentiated stem/progenitors, whilst causing the death of differentiated cells through a process known as “*anoikis*” (Frisch and Francis, 1994; Streuli and Gilmore, 1999). In reminiscence of neurospheres, the colonies formed by surviving MMECs were called mammospheres, if originating from non-transformed cells, or tumourspheres, if originating from transformed cells. In line with the

undifferentiated status of the cells was the ability of primary-derived spheres to: 1) generate mixed colonies (composed of MYO, ductal and alveolar cells), if plated on a collagen substratum in the presence of serum; 2) form complex functional structures, if grown in matrigel; and 3) give rise to secondary spheres with multi-lineage differentiation potential, if re-plated in suspension. This led to the hypothesis that spheres stemmed from the ability of MaSCs to undergo a few SCDs versus several ACDs: through the former, MaSCs were able to maintain their self-renewal potential and generate secondary spheres; through the latter, they could give rise to progenitor cells with multipotent differentiation potential (Dontu et al., 2003). With the concomitant transplantation of MMECs *in vivo* and cultivation *in vitro*, resulting in both outgrowth of mammary trees and discrete colonies, respectively, a link between MaSCs/MRUs and Ma-CFCs was found (Smith et al., 1996). Albeit arising from the division of MaSCs, Ma-CFCs have been shown to display a distinct molecular phenotype, being enriched in the luminal (CD24⁺CD49f^{low}) versus the basal (CD24⁺CD49f^{high}) subpopulation. This was corroborated by transcriptomic analysis which confirmed the enrichment of luminal CK8, CK18 and CK19 transcripts in Ma-CFCs, versus basal CK5, ck14 and α SMA transcripts in MRUs and MYO subpopulations. Furthermore, when challenged in a 3D CFC assay, Ma-CFCs and MRUs displayed different morphological types of colonies, that is more spherical acinar-like in the first case, while more irregular solid-like in the second (Stingl et al., 2006). What emerged from these studies was the presence of an additional layer of heterogeneity affecting the mammary epithelial cell hierarchy. What remained to be assessed was the regenerative potential of these cells. Using lineage-tracing, two different pools of unipotent cells appeared to populate both the pubertal and the adult mammary gland: basal progenitors (BPs) and luminal progenitors (LPs). These lineage-restricted pools of progenitors have proven to be fundamental for the maintenance and replenishment of differentiated MMECs (Figure 1. 7B).

1.6.3 The different subsets of luminal cells

Akin to the MaSC and progenitor compartment, the luminal layer of the mammary gland has also been shown to display a remarkable degree of heterogeneity (Visvader and Stingl, 2014). Whilst all luminal cells are characterized by the CD24⁺CD29^{low}/CD49f^{low} phenotype, this cluster is believed

to contain different types of LPs and differentiated luminal cells (Figure 1. 7B, C). Luminal cells are generally subdivided into the ductal and alveolar subtypes, as well as in the ER⁺/PR⁺ (sensor) or ER⁻/PR⁻ (effector) subsets. For a long time, the majority of HR⁺ cells were believed to be mature cells, as it was postulated that only ER⁻ cells were able to proliferate upon the release of ovarian hormones (Clarke et al., 1997; Russo et al., 1999). Nonetheless, other studies have argued against this hypothesis, claiming that rare ER⁺ luminal cells were also found to proliferate *in vivo* (Beleut et al., 2010; Booth and Smith, 2006) and display clonogenic potential *in vitro* (Shehata et al., 2012; Sleeman et al., 2007). The heterogeneity of the luminal compartment was corroborated by the presence of multiple cell surface markers found to be expressed by these cells, including CD61 (Asselin-Labat et al., 2007), c-kit (Asselin-Labat et al., 2011), Sca-1 and CD49b (Shehata et al., 2012). As such, CD61 (β 3-integrin) was shown to label a larger proportion of ER⁻ LPs (Asselin-Labat et al., 2007; Sleeman et al., 2007), whereas Sca-1 expression appeared to be present in a more differentiated subset of LPs, characterized by high levels of ER expression (Shehata et al., 2012). Luminal Sca-1⁺ cells were found to incorporate bromodeoxyuridine (BrdU) during pregnancy and adulthood, albeit not to the same extent of their negative counterpart (Van Keymeulen et al., 2017). The c-kit and CD49b (α 2-integrin) markers, instead, were found to be present in a common LP, being expressed by both Sca-1⁺ and Sca-1⁻ cells (Regan et al., 2012), whereas the combinatorial use of Sca-1 and CD49b appeared to better discriminate between ER⁻ and ER⁺ LPs. While the Sca-1⁻CD49b⁺ subset was found to be enriched in ER⁻ LPs, the Sca-1⁺CD49b⁺ subpopulation was deemed to mark a small fraction of ER⁺ LPs (9%). Notwithstanding the higher clonogenic ability displayed by Sca-1⁻CD49b⁺ cells (40%), the Sca-1⁺CD49b⁺ subset was also shown to be characterized by a moderate degree of CFC ability *in vitro* (25%). Major differences, however, were related to their transcriptomic profiles, whereby Sca-1⁺CD49b⁺ displayed high levels of luminal specific genes (e.g. *Esr-1*, *FoxoA1*, *Gata3*, *CK8* and *CK18*), whereas the Sca-1⁻CD49b⁺ subset was characterized by an intermediate levels of expression of both luminal and basal genes, thus placing the latter population in between basal MaSCs and more differentiated ER⁺ LPs (Shehata et al., 2012) (Figure 1. 7B, C).

Whilst these data were supportive of profound molecular and functional differences between ER⁻ and ER⁺ LPs, it was unclear whether the maintenance of the corresponding mature luminal cells within the adult mammary gland could be ascribed to both cell types or not. Through the use of lineage tracing studies, where acidic protein-tagged ER⁻ luminal cells during a first pregnancy were shown to generate ER⁻ cells during the following pregnancy (Chang et al., 2014), as Notch1- and Sox9-labelled ER⁻ luminal cells were found to give rise to ER⁻ ductal and alveolar cells only (Rodilla et al., 2015; Wang et al., 2017). Likewise, ER⁺ cells were shown to originate exclusively via the presence of ER⁺ LPs, yet not ER⁻ LPs. Thus, during mammary gland pubertal development and tissue homeostasis, mature luminal ER⁻ and ER⁺ cells would be maintained via the presence of lineage-restricted ER⁻ and ER⁺ LPs (Figure 1. 7B, C) (Van Keymeulen et al., 2017). The moderate, yet significant proliferation reported in ER⁺ LPs is of particular interest in view of the increased number of proliferating ER⁺ cells found to occur in the human breast of older women (particularly after menopause), where they often appear in contiguous patches of positive cells (Shoker et al., 1999). This observation has led to hypothesize that dysregulation of the ER α signalling pathway may occur with ageing, thus leading to the clonal expansion of a putative ER⁺ LP population, which was also reported to be the least sensitive to hormone deprivation (Shehata et al., 2012). Likewise, proliferation of ER⁺ cells has also been found in HR⁺ tumours (Clarke et al., 1997), a subtype of breast cancer particularly abundant in older versus younger women (Gradishar et al., 1998). Thus, these data emphasize the urgent need to study the mechanisms underpinning the tight control over ER⁺ cell proliferation, as well as its tantalizing link with ageing.

Altogether, these findings have remarkably refined our understanding of the mammary epithelial cell hierarchy, wherein the luminal layer of the mammary gland is more heterogeneous than initially perceived, being comprised of multiple LPs as well as different mature luminal cells. In view of the belief that the majority of human breast cancers are thought to originate within this compartment (see below), the identification of new cell-surface markers as well as a greater knowledge of the distinctive features of each of these luminal subpopulations might help unveil the cell-of-origin of many breast tumours.

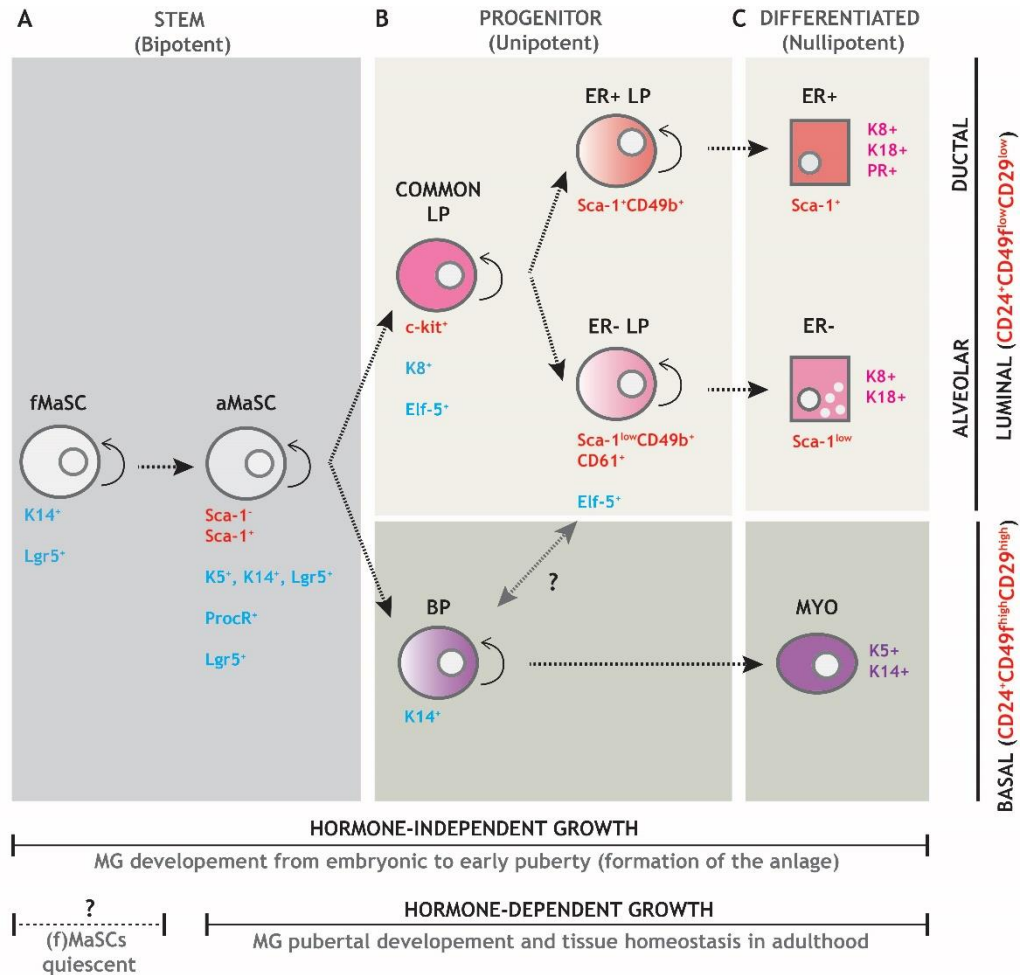


Figure 1. 7 The mammary epithelial cell hierarchy.

Working model depicting the distribution and parent-progeny relationships between MMECs, subdivided into three main developmental stages (stem, progenitor and differentiated) across two epithelial compartments (basal and luminal). (A) Bipotent MaSCs are at the origin of the mammary epithelial cell hierarchy and comprise fMaSCs, found in the embryonic bud and responsible for the formation of the anlage (hormone-independent growth), and aMaSCs, found within the virgin organ onwards and responsible for MG pubertal development and homeostasis (hormone-dependent growth). (B) Unipotent BPs and common LPs arise from MaSCs asymmetric cell division. BPs lie in the basal compartment, while common LPs are in the luminal layer, where they divide into distinct ER+ and ER- LPs. (C) Nullipotent MYO cells (expressing high levels of CK5 and CK14) arise from the differentiation of BPs, while nullipotent ER+ ductal and ER-alveolar cells (expressing high levels of CK8 and CK18) come from the differentiation of ER+ and ER- LPs, respectively. In red are indicated the cell-surface markers used by FACS studies, in blue those by lineage tracing. Curved arrow indicates self-renewal. Straight dotted arrow indicates differentiation. BP, basal progenitor; FACS, fluorescence activated cell sorting; LP, luminal progenitor; MaSC, mammary stem cell; aMaSC, adult MaSC; fMaSC, foetal MaSCs; MG, mammary gland; MMEC, mouse mammary epithelial cells; MYO, myoepithelial.

1.7 Breast cancer

Whilst being an essential organ of food supply, due to its evolutionary ability to produce milk to nourish the offspring, the mammary gland is also an important site of diseases, first and foremost breast cancer (Cardiff and Wellings, 1999). As a human illness, breast cancer was first recorded in a papyrus of the 17th century BC (itself a transcription of a manuscript dated 2500 BC) attributed to the Egyptian physician Imhotep, who described a case of “*bulging masses in the breast*”, with no therapeutic cure. Two millennia after this (440 BC) the historian Herodotus in his *Histories* reported that the queen of Persia Atossa suddenly noticed “*a bleeding lump in her breast*” (Siddharta, 2010). Nowadays, breast cancer represents the most commonly diagnosed cancer in women worldwide and the most frequent cause of cancer-related female deaths in both developed and developing world (Torre et al., 2016).

1.7.1 Risk factors and prevention

Different breast cancer risk factors have been identified, including genetic and epigenetic causes, as well as the hormonal and reproductive status of a woman. Among the genetic causes, several known breast cancer genes (*BRCA1*, *BRCA2*, *TP53*, *PTEN*, *CDH1*, etc.) are thought to be responsible for 25-30% of the heritability, together with SNPs and copy number variants (CNVs) (28%) (Eccles et al., 2013). Epigenetic factors have also been recognized as important biomarkers for breast cancer risk. As such, epigenetic alterations might be hijacked by hormonal signalling to drive breast tumourigenesis. Indeed, *in utero* exposure to diethylstilbestrol has been shown to increase the risk of breast cancer perhaps through alteration of the epigenome (Hoover et al., 2011). Recent studies suggested the possibility to evaluate DNA methylation levels of white blood cells (Brennan et al., 2012) and circulating tumour DNA (Han et al., 2017) in peripheral blood, as a diagnostic and perhaps prognostic indicator of the disease. Breast cancer risk is intimately linked to the endocrine system of a woman, as well as to all the conditions affecting the latter, including age, menopausal status and reproductive history. Early and late menarches, nulliparities or late pregnancies are all among the strongest risk factors for breast cancer development (Veronesi et al., 2005). Conversely, women who give birth at young ages are believed to have a decreased risk of the disease, which

appears to be further improved with subsequent pregnancies, due to the long-term protective effects of the latter (Russo et al., 2005). Lastly, although not incorporated into the current risk prediction models, it is believed that mammographic density represents a very strong breast cancer risk factor (McCormack and dos Santos Silva, 2006), in which changes might potentially be used as a biomarker for patient response to preventive treatment, albeit it does not seem to be linked with any molecular subtypes (Eriksson et al., 2012).

As for many other types of cancer, detecting breast cancer at early stages significantly increases patients' chances of being cured. However, the major challenges faced by the preventive field are: firstly, to precisely identify those individuals who have a high likelihood of developing the disease; and secondly, to tailor the most appropriate preventive method for each of these high-risk people (Eccles et al., 2013). Mammography represents a commonly used diagnostic technique which allows early detection of abnormal masses or micro-calcification within the breast tissue via the use of low-energy X-rays (Sree et al., 2011). According to the current "work-up" process, women would usually face three sequential steps: screening mammography, diagnostic mammography and biopsy. If areas of concerns appear during the first screening mammography, women are called back (diagnostic mammography) to better monitor the results. If the cause of the concern is not believed to be benign, a core biopsy with local anaesthetic is then highly recommended in order to microscopically examine the abnormal tissue. Of note, mammography screening is currently offered to women between 50-70 years old, every one, two or three years, depending on the country. As such, the small yet significant increase in breast cancer risk induced by radiation exposure and the 10% rate of false-positive results, often due to the presence of dense tissue and leading to unnecessary treatment and psychological distress, have rendered the potential use of universal mammography screening a matter of huge debate (Defrank and Brewer, 2010). Additionally, chemopreventive agents including selective oestrogen receptor modulators, such as tamoxifen and raloxifene, have been shown to reduce breast cancer in high-risk women during the five years of treatment and up to five years afterwards. Nevertheless, the fact that their efficacy is often accompanied by toxic side-effects means that none of them have been approved by the Food and Drug Administration as preventive agents as yet. Whilst nothing is currently

available for the prevention of ER-negative disease (Cuzick et al., 2013), prophylactic mastectomy represents instead the method of choice to reduce breast cancer risk in women with a *BRCA1/2* mutations (Heemskerk-Gerritsen et al., 2007). Last but not least, caloric restriction, reduction in alcohol intake and physical exercise are all believed to have beneficial effects on disease prevention, even though their underlying mechanisms of action are still unclear (Eccles et al., 2013).

1.7.2 Breast cancer's heterogeneity

Our lack of knowledge of the exact cause(s) of breast cancer, together with the development of disease in women with no apparent risk factors, clearly reflects a poor understanding of the underlying biology of the disease. As for many other tumours, breast cancer is not just one disease, but rather it comprises several different malignancies displaying a very high degree of heterogeneity. This is reflected by the existence of different levels of breast cancer classifications.

1.7.2.1 Histopathological classification

Traditional methods for the histopathological assessment of breast cancer take into account different parameters, including histological type, tumour size and grade, and axillary lymph-node involvement (Dawson et al., 2013). Histologically, breast cancer can be broadly classified in two categories: *in situ* carcinoma or invasive carcinoma. *In situ* carcinoma is composed of both the ductal or lobular subtypes. Ductal *in situ* carcinoma, commonly known as DCIS, is more frequent than lobular *in situ* carcinoma (LCIS) and comprises at least five different subgroups (Comedo, Cribiform, Micropapillary, Papillary and Solid). Invasive carcinoma represents instead a very heterogeneous class of breast tumours, of which ductal, lobular, ductal/lobular, mucinous, medullary and tubular represent the major subtypes (Malhotra et al., 2010). Tumour size gives an indication of the dimension of a tumour at diagnosis, while tumour grade refers to the proliferative and differentiation indexes of the cancer (Rakha et al., 2010). Last but not least, the axillary lymph-node involvement informs on the extent of the disease, depending on whether cancer cells have left or not the primary site to reach surrounding lymph nodes (Jatoi et al., 1999). Whilst informative of the type and extent of the disease, no clinician could ever select

the appropriate treatment for a breast cancer patient if based solely on the aforementioned parameters. Remarkable improvements in this regard were achieved following the discovery of the molecular mechanisms underpinning the endocrine regulation of the mammary gland and the existence of similar parallels in certain breast tumours. Thereafter, immunohistochemistry (IHC) and fluorescence *in situ* hybridization became commonly used techniques to assess the expression levels of ER, PR, as well as amplification and/or overexpression of the Human epidermal growth factor receptor type 2 (HER2), respectively. Routinely used in the clinic since 1970s in the case for ER and PR (Osborne et al., 1980), and for more than a decade in the case of HER2 (Ross et al., 2009), these three markers represent the most important indicators of patients' subtypes of breast cancer and predictors of clinical response (Norum et al., 2014). In fact, on the basis of the receptor status of the tumour, breast cancer patients are currently treated with different therapeutic regimens. ER-positive and/or PR-positive breast cancers, representing the majority of cases (75-80%), usually rely on hormone-based therapies (e.g. tamoxifen and aromatase inhibitors); HER2-positive patients (10-15%) are generally administered anti-HER2 molecularly based therapies (e.g. Trastuzumab or Herceptin), with half of those cases co-expressing one or both HRs receiving a combination of both compounds. For the remaining patients (10-15%), referred to as triple negative (TN) due to lack of ER, PR and HER2 expression, standard-of-care is currently the only line of therapeutic option available. For this reason, TN breast cancer patients represent the most aggressive subgroup above all (Gu et al., 2016). Although additional predictive markers have been recently identified, none of these have been implemented into clinical practice yet. Thus, ER, PR and HER2 remain the only three biomarkers which set the stage for breast cancer patients' diagnosis and prognosis (Dawson et al., 2013).

1.7.2.2 Transcriptomic classification

As proposed by Perou and Sorlie (Perou et al., 2000; Sorlie et al., 2001), the phenotypic heterogeneity shown by breast cancers is linked to a corresponding diversity in their gene expression patterns. With the use of DNA microarray, coupled to hierarchical clustering to group samples according to similarity in their gene expression patterns, the very first "molecular portrait" of human breast cancer was proposed. This was comprised of five different groups, namely

luminal A, luminal B, basal-like, HER2+ and normal-like, whose major determinants were the presence or absence of ER, PR expression and HER2 amplification and/or overexpression (Visvader, 2009). Accordingly, luminal tumours display a gene expression profile similar to luminal epithelial cells, being characterized by high levels of K8/18 and low HER2 expression. The luminal A subtype, however, includes low-grade tumours characterized by the highest levels of ER and GATA3 expression and a moderate proliferation rate, whereas luminal B tumours include high-grade malignancies with moderate to low levels of ER expression and a high proliferative index (Inic et al., 2014). By clustering together with basal epithelial cells, basal-like tumours show positive expression for K5/6 and 17, while lack of ER, PR and HER2. As implied by the name, HER2+ tumours are characterized by amplification and expression of the *HER2* gene, together with expression of genes present within the same amplicon. In addition, HER2+ breast tumours display low levels of ER expression, a feature which places them closer to basal-like tumours. Lastly, normal-like tumours show a gene expression profile similar to basal (rather than luminal) epithelial cells, as well as to adipose and other non-epithelial tissues (Perou et al., 2000; Sorlie et al., 2001). In addition to the latter, more recent unsupervised analysis of both mouse and human data led to the identification of a potentially new subtype of breast cancer, referred to as “claudin-low”. As implied by the name, this subset appeared to be characterized by low levels of tight junction and cell-cell adhesion proteins (e.g. Claudins 3, 4 and 7, Occludin and E-cadherin). Besides the absence of ER expression, these tumours showed low levels of luminal genes and inconsistent expression of basal markers (Herschkowitz et al., 2007). By unveiling the molecular mechanisms underpinning the inter-tumoural heterogeneity, these studies paved the way for a new method of classifying breast tumours. Moreover, each of these newly identified intrinsic molecular subtypes of breast cancer, characterized by a surprising degree of stability and homogeneity, should be treated as a distinct biological entity accompanied by unique clinical features (Perou et al., 2000). Significant differences in relapse-free (as time to distant metastasis) and overall survival could now be attributed more robustly to specific breast cancer subtypes. Univariate Kaplan-Meier analysis reported HER2+ and basal-like tumours with the shortest relapse-free and the worst overall survival, a finding proposed to be linked to the higher frequency of *TP53* mutations found in both subgroups (Sorlie et al., 2001).

Likewise, the tendency of *BRCA1* tumours to fall within the basal-like subtype of the disease was also noted, highlighting how different breast cancer susceptibility genes may preferentially predispose to specific subtypes of the disease (Sorlie et al., 2003). Patients with luminal A like tumours displayed the longest relapse-free and the most favourable overall survival, whereas luminal B tumours showed an intermediate outcome (Sorlie et al., 2001; Sorlie et al., 2003). Of note, a slightly different finding emerged in a study involving 1,000 women followed for a period of 20 years, wherein reduced overall survival was displayed by HER2+ and luminal B patients, rather than basal-like breast cancer women which showed intermediate survival times (Haque et al., 2012). Notwithstanding its favourable prognosis, it is important to highlight that luminal A tumours, representing the vast majority of breast cancers (40%), display the highest level of molecular heterogeneity. This is also reflected in the clinical setting, as some luminal A patients are often over-treated unnecessarily, whereas some others will face the highest risk of local and/or distant relapse in the long-term (over a 20 years follow-up period) as compared to other subtypes (Haque et al., 2012). A more recent analysis was able to split the luminal A subtype of breast cancer into two different cohorts on the basis of a differentially expressed 71 microRNA signature. When the prognostic value of each signature was investigated using different breast cancer datasets, the two luminal A clusters showed clinically distinct behaviours in terms of overall survival and freedom from any recurrence (Aure et al., 2017).

1.7.2.3 Integrated classification

With the emergence and widespread use of high-throughput technologies, it became possible to dissect tumours not only at their histopathological and transcriptomic levels, but also at their genetic level. By characterizing the mutational landscape of breast cancer, these studies emphasized the importance of inherited genetic variation, including the SNPs and CNVs discussed earlier, as well as of acquired genomic aberrations, such as single-nucleotide variants (SNVs) and copy number aberrations (CNAs), as being equally involved in the initiation, maintenance and progression of carcinomas (Dawson et al., 2013). On one side, this allowed the identification of new breast cancer-associated genes, but on the other the discovery that the majority of alterations in these putative players were relatively infrequent. With the realization that CNAs could have a

huge impact on gene expression by acting either in *cis* (on genes in close proximity to the aberration) or in *trans* (on genes in distant sites), distinct cellular pathways began to be linked to specific patterns of genomic aberration, rather than to alterations in individual genes. Thus, when it was realized that genomic aberrations could inform on the tumour phenotype and its underlying biology, the intrinsic transcriptomic classification was further refined to provide a more comprehensive profiling of breast cancer, which could also capture the genomic landscape of the disease. By integrating both transcriptomic and genomic data of 2,000 breast tumours included in the METABRIC (Molecular Taxonomy of Breast Cancer International Consortium) study (Curtis et al., 2012), a novel breast cancer classification composed of ten integrative clusters (IntClust 1-10) was proposed (Dawson et al., 2013). A very concise look at each one of these clusters, characterized by distinct gene expression profiles and CNAs, is summarized in (Table 1. 1). Some of the most profound refinements emerging from this analysis referred to luminal A and HER2+ tumours. While luminal A tumours could be split into multiple groups, characterized by either worst disease-free survival (IntCluster2), or favourable prognosis (IntCluster3, 7 and 8), HER2+ tumours, partly represented by the HER2+ intrinsic subtype, were now grouped together. The significance of such refinement could potentially lead to some luminal A patients (those with good prognosis) being spared from unnecessary systemic chemotherapy, while more HER2+ individuals benefit from the use of HER2-targeted therapies in the future (Curtis et al., 2012; Dawson et al., 2013). By turning the spotlight on new putative breast cancer drivers and emphasizing the clinical features of each IntCluster, this new classification has improved our understanding of the aetiology of breast cancer. Nonetheless, biology is not as simple as it seems and, besides the inter-tumoural heterogeneity highlighted above, there is a more subtle level of diversity within each individual neoplasm referred to as intra-tumoural heterogeneity. In essence, this means that “one size” does not “fit all” and perhaps treating each IntCluster as a biologically and clinically different entity might not be the solution. With this in mind, clinical management of breast cancer has slowly started to embrace the concept of personalized medicine, whereby each individual patient represents a biologically and clinically distinct entity which requires custom-tailored treatment.

Table 1. 1 Summary of the 10 Integrative Clusters of breast cancer.

IntCluster	Intrinsic subtype2	IHC group	Clinical features	Prognosis (10-year DFS)	Molecular features
IntCluster 1	Luminal B	ER+ve	High grade	Intermediate	Amplification of the 17q23 locus; overexpression of cis-adjacent genes (RPS6KB1, PPM1D, PTRH2 and APPBP2) Highest prevalence of GATA3 mutations
IntCluster 2	Luminal A	ER+ve	-	Worst of all ER+ve (50%)	Amplification of the 11q13/14 locus (CCND1, EMSY and PAK1)
	Luminal B				Enrichment of genes involved in cell-cycle regulation (G1/S transition)
IntCluster 3	Luminal A		Low grade	Best (90%)	Highest frequency of PIK3CA, CDH1 and RUNX1 mutations
			No LN involmnet		Low prevalence of TP53 mutations
IntCluster 4	Luminal-A	ER+ve	Low grade	Good (80%)	CAN-devoid
	Basal-like	ER-ve	High immune response		Deletions at the T-cell receptor (TCR) loci (20%)
IntCluster 5	ERBB2+ve	ERBB2+ve/ER+ve (42%)	High grade	Worst (45%)	Amplification of the 17q12 locus (ERBB2)
		ERBB2+ve/ER-ve (58%)	LN involvement		High propoirtin of TP53 mutations (>60%)
			Younger age		
IntCluster 6	Luminal A	ER+ve	-	Intermediate (60%)	Amplification of the 8p12 locus
	Luminal B				Lowest prevalence of PIK3CA mutations across all ER+ve tumours
IntCluster 7	Luminal A	ER+ve/PR+ve	Low grade (Well-differentiated)	Good (80%)	Amplification of the 8q locus, 16p gain, 16q loss
					Highest frequency of MAP3K1 and CTCF mutations
IntCluster 8	Luminal A	ER+ve	Low grade (Well-differentiated)	Good (80%)	1qgain/16qloss (common unbalanced translocation event)
					High levels of PIK3CA, GATA3 and MAP2K4 mutations
IntCluster 9	Luminal B	ER+ve	High grade	Intermediate (60%)	8q cis-acting alterations and 20q amplification
					Highest levels of TP53 mutations among the ER+ve subgroup
IntCluster 10	Basal-like	TN	High grade (Poorly differentiated)	Bad in the first 5 yrs	8q, 10p and 12p gain
			Younger age	Good after the first 5 yrs	Deletion of the 5q locus
					Highest rate of TP53 mutations

ER+ patients did not receive chemotherapy; All ER- patients received chemotherapy; None of the HER2+ patients received Trastuzumab. ER, oestrogen receptor; HER2, human epidermal growth factor receptor type 2; PR, progesterone receptor, TN, triple negative. Adapted from Dawson et al., 2013.

1.7.3 Clinical management of the disease

Current clinical therapies for breast cancer encompass surgery, radiotherapy or systemic therapy, the latter of which encompasses chemotherapy and molecularly targeted therapy (Caley and Jones, 2012). Importantly, the type of therapy, the order of administration, the ideal timing and the optimal duration are all factors decided by a multidisciplinary team of experts on an individual basis, depending on several variables including patient's age, tumour grade, stage and subtype of the disease (Eccles et al., 2013).

1.7.3.1 Surgery and radiotherapy

As for all other solid tumours, surgery is the mainstream treatment of localized breast cancers, aiming at removing all malignant cells via mastectomy or breast conservation surgery (plus whole breast radiotherapy to reduce the risk for local recurrence). Importantly, the operation is carried out together with sentinel node biopsy, a widespread procedure which identifies and removes what it is thought to be the first nearby lymph node to which cancer cells might have spread. By checking for the presence of any axillary metastasis, this technique helps define the stage and extent of the disease (Eccles et al., 2013). Additionally, early-stage tumours can be further reduced preoperatively using neoadjuvant therapies (including chemo, hormonal and targeted therapies), with the beneficial effects of improving the rate for breast conservation, assessing drug efficacy and safely delaying the timing of surgery in specific circumstances. However, not all breast cancer patients might benefit from neoadjuvant therapies, highlighting the need to carefully assess its use on a case by case basis (Chatterjee and Erban, 2017). It should be noted, however, that surgery is usually only applied to early-stage patients, 80-99% of which are estimated to survive up to five years (<https://www.cancerresearchuk.org/>).

1.7.3.2 Chemotherapy and molecularly targeted therapies

The idea of using a “cocktails of chemical drugs” to cure cancer dates back to 1947, when Dr. Sidney Farber started treating leukaemic patients with aminopterin (an antifolate), dreaming about the possibility to eradicate such an aggressive systemic disease with a “medicine” (Siddharta, 2010). What was unknown to Farber was the principle behind the mechanism of action of these

cytotoxic agents, which strictly rely on the cell division properties owned by normal and cancer. Indeed, by interfering with DNA synthesis or with key proteins of the cell cycle, chemotherapy aims at specifically targeting highly proliferative tumour cells by inducing their cell death (Caley and Jones, 2012). This is usually achieved via a combination of more than one cytotoxic agent (e.g. cisplatin, gemcitabine, 5-fluorouracil), depending on several factors, including the subtype of breast cancer, the likelihood of its relapse and the presence of other medical conditions. Unfortunately, however, the cytotoxic effects exerted by chemotherapy can often target normal dividing cells, particularly those characterized by a high turnover rate (e.g. lymphocytes) (Caley and Jones, 2012). Thus, to maximize its efficacy whilst minimizing its side effects, chemotherapy is usually administered in period of 3 to 4 weeks, also known as cycles, in order to give patients' body enough time to repair and replenish all pools of disrupted normal cells. Furthermore, according to the current clinical management of breast cancer, this treatment is usually given either before or after surgery. In the first case, chemotherapy, better known as neo adjuvant therapy, is used with the aim of reducing locally advanced diseases, whilst in the second (adjuvant therapy), to prevent the relapse of aggressive forms of breast cancer in case cancer cells might have disseminated away from the primary site. Of note, given the fundamental role played by immune cells in fighting infections and diseases, the combinatorial use of immunotherapy (aiming at reinforcing the body's immune system) with chemotherapy has been recently considered as a valuable option in cancer treatment (www.cancerresearchuk.org).

Targeted therapies refer instead to the use of molecular agents (monoclonal antibodies and small molecule inhibitors), which often rely on the concept of oncogene addiction (Torti and Trusolino, 2011). First described in 2002 by Bernard Weinstein, oncogene addiction states that, despite the "multi-hit" nature of cancer, some tumours rely on the function of a single dominant oncogene to proliferate and survive. Hence, by identifying such oncogene and preventing their function, tumour stabilization and/or regression could, at least in principle, be achieved (Weinstein, 2002). In breast cancer, the dependency shown by certain tumour subtypes towards ER, PR and HER2 signalling pathways laid the foundation for the design of molecularly targeted therapies towards

these targets. TN patients, however, currently lack any targeted treatment options and rely on standard-of-care (e.g. surgery, radiotherapy and chemotherapy) intervention. Recently, new evidence has shown promising results for the treatment of rare forms of TN tumours via the use of cyclin-dependent kinase 4/6 (CDK4/6) inhibitors (e.g. Palpociclib) (Asghar et al., 2017). It was shown, in fact, that sensitivity of TN tumours to CDK4/6 inhibitors is inversely correlated to the level of CDK2 after mitosis. Thus, cells which exit mitosis with low levels of CDK2 (quiescent cells) would strictly depend upon CDK4/6 function to re-enter the cell cycle, whereas cells which exit mitosis with high levels of CDK2 (proliferating cells) would by-pass the requirement for CDK4/6 activity. Importantly, this study heralds new possibilities for the treatment of this disease subtype, which commonly affect 7,500 women (the majority of which present at young ages) each year in the UK (www.cancerresearchuk.org). It is worthwhile mentioning that the development of other targeted therapies for the treatment of inherited forms of breast cancer has exploited a slightly different version of the concept of oncogene addiction. Synthetic lethality (SL) refers to the notion that while the loss of one gene is compatible with life, the simultaneous loss of another gene (thought to be in a synthetic lethal relationship with the first one), results in death (Kaelin, 2005). However, since in cancer SL genes are often in their wild-type form, SL is often referred to as “non-oncogene addiction” (Torti and Trusolino, 2011). One of the best examples is represented by poly-ADP-ribose-polymerase inhibitors, the first drugs based on the concept of SL which have been approved for the clinical treatment of *BRCA1* and *BRCA2* mutated breast cancers (Lord and Ashworth, 2008). Nonetheless, a common issue that spans across all clinical breast cancer therapies is overtreatment. In addition, there is also a significant proportion of women who experience the opposite problem, being often undertreated. Regardless of the case, this reflects the inadequate tailoring of clinical therapies on an individual basis, thus often culminating in more harmful effects than actual benefits (Eccles et al., 2013). Thus, despite the remarkable impact that breast cancer stratification has had in refining therapeutic treatments, the response of patients to either conventional or targeted therapies still remain dramatically unpredictable. This could be mainly attributed to the high degree of heterogeneity characterizing the disease. But what has remained unappreciated is the fact this heterogeneity is due not only to the genetic and

molecular mutational landscape of a patient's tumour per se, but also to its "cell of origin" (Visvader and Stingl, 2014).

1.7.4 RUNX1 in breast cancer

[For this section, the text has been adapted from Riggio and Blyth (2017)].

It was only with the switch from classic Sanger sequencing, which focused on small cohorts of samples and lacked adequate sensitivity, to the advent of multiplexed NGS, targeting larger data sets, that *RUNX1* was revealed as one of the most significantly altered genes in breast cancer (Banerji et al., 2012; Cancer Genome Atlas, 2012; Cornen et al., 2014; Ellis et al., 2012). Of note, three main observations emerged from these studies: firstly, the presence of somatic mutations (including point mutations and deep deletions) mainly affecting the gene; secondly, the fact that they seem to cluster with hormone receptor positive (ER+/PR+) breast cancers (Table 1. 2); thirdly, the prediction that these would result in loss-of-function of the protein (Li et al., 2003; van Bragt et al., 2014). Additionally, the gene encoding RUNX1's DNA-binding partner *CBFβ* was also found to be frequently mutated in breast cancer (Banerji et al., 2012; Ellis et al., 2012), heightening the putative tumour suppressive function played by the RUNX1/*CBFβ* complex in this disease, especially in the ER+/PR+ subtypes. Indeed, RUNX1 mRNA downregulation was found to be part of a 17-gene signature associated with breast cancer metastasis (Ramaswamy et al., 2003) and RUNX1 protein expression was reduced in high-grade compared to low/mid-grade breast tumours (Kadota et al., 2010), consistent with the transcription factor's ability to act as a positive regulator of E-cadherin (Liu et al., 2005). Moreover, RUNX1 knockdown was found to cause hyper-proliferation and abnormal morphogenesis of MCF10A breast epithelial cells (Wang et al., 2011), while RUNX1 SNPs were strongly associated with breast cancer risk in a Moroccan study (Marouf et al., 2016). On the other hand, an increasing amount of evidence is indicative of a pro-oncogenic role played by the *RUNX1* gene in breast cancer, intriguingly associated with the ER- and TN subtypes (Table 1. 2). Accordingly, different transcriptome studies have reported *RUNX1* mRNA upregulation in the TN group (Karn et al., 2011; Rody et al., 2011), while *RUNX1* was found to be associated with super-enhancer elements, linked to oncogenes and/or genes associated with cancer pathogenesis, specifically in an ER- breast

cancer cell line (Hnisz et al., 2013). Expression of RUNX1 also increased with disease progression in patient samples, as well as in a mouse model of breast cancer (Browne et al., 2015). Lastly, in a tissue microarray study carried out in our lab (Ferrari et al., 2014), a strong positive correlation between RUNX1 expression and poor overall survival in ER- and TN breast cancer patients was shown. Altogether, these studies revealed opposing and context-dependent roles for RUNX1 in breast cancer, culminating with recent high-throughput analyses which listed *RUNX1* and *CBFβ* among the candidate driver genes relevant to breast cancer pathogenesis (Nik-Zainal et al., 2016; Pereira et al., 2016).

Table 1. 2 Summary of RUNX1 dysregulation in breast cancer.

RUNX1 dysregulation	Subtype/Stage of Tumour	References
mRNA downregulation	Metastasis	Ramaswamy et al., 2003
mRNA downregulation	High grade	Kadota et al., 2010
mRNA upregulation	Triple negative	Karn et al., 2011
		Rody et al., 2011
Homozygous deletions	-	Banerji et al., 2012
Missense mutations	Luminal -B (ER-positive)	Ellis et al., 2012
Truncating & Missense mutations	Luminal-A & B (ER-positive)	Cancer Genome Atlas Network, 2012
	& HER2-enriched	
CNAs (deletion) & Mutations	Luminal-A & B (ER-positive)	Cornen et al., 2014
Protein expression (high)	ER-negative & Triple negative	Ferrari et al., 2014
Protein upregulation	Invasive Ductal Carcinoma	Browne et al., 2015
Single nucleotide polymorphisms	-	Marouf et al., 2016
Mutations (driver)	ER-positive & ER-negative	Nik-Zainal et al., 2016
Mutations (driver)	ER-positive & ER-negative	Pereira et al., 2016
	ER-negative	
CNAs (deletion & amplification)		

CNA, copy number alteration; ER, oestrogen receptor. Adapted from Riggio and Blyth (2017).

1.7.4.1 RUNX1 in hormone-dependent tumours

[For this section, the text has been adapted from (Riggio and Blyth, 2017)].

As corroborated by the reduction in ER⁺ cells seen upon MMTV-driven deletion of *Runx1* (van Bragt et al., 2014), expression of the gene appears fundamental to the survival and maintenance of E2-responsive cells. Indeed, as a master regulator of cell fate decision, RUNX1 was shown to be critical in promoting the ER program whilst inhibiting the alveolar one. With this in mind, it is perhaps surprising to find RUNX1 somatic mutations in ER⁺ breast cancer (Banerji et al., 2012; Cancer Genome Atlas, 2012; Ellis et al., 2012), a subtype of the disease thought to originate from luminal ER⁺ cells. Given an enrichment of the p53 signature in *Runx1*-deleted luminal cells (van Bragt et al., 2014) and the frequent co-association between *TP53* and *RUNX1* dysregulation in human luminal B tumours (Ellis et al., 2012), perhaps loss of *RUNX1*-dysregulated luminal cells can only be rescued by the presence of additional mutations (e.g. *TP53*). To render the interplay between RUNX1 and ER α even more intriguing, the two transcription factors were recently shown to co-occupy a regulatory region of *AXIN1* (Chimge et al., 2016), a tumour suppressor gene encoding a crucial component of the β -catenin destruction complex. Yet, the two proteins appeared to act as antagonists since shRNA-mediated RUNX1 suppression resulted in *AXIN1* downregulation and increased ER α -mediated proliferation. This provided mechanistic evidence for a putative tumour suppressive function mediated by RUNX1, which was specific for ER⁺ and not ER⁻ breast cell lines. One could then speculate that *RUNX1* dysregulation in ER⁺ breast cancer would facilitate oestrogen/ER α -mediated *AXIN1* suppression, leading to aberrant WNT/ β -catenin signalling pathway. Nevertheless, the fact that the local interaction between RUNX1 and ER α at the *AXIN1* locus seemed to occur through a non-tethering mechanism (Figure 1. 6) and that RUNX1 transcriptional regulation is generally not dependent on oestrogen's activity led to the speculation that perhaps the gene could acquire an oestrogen/ER α -dependent tumour suppressive activity only at a few critical regulatory loci. In this way, one could envision RUNX1 as a fine-tuning orchestrator of ER α -dependent transcription (Figure 1. 6). Intriguingly, this is in line with very recent findings depicting RUNX1 as an architectural genome regulator of local (rather than

global) chromatin interactions that might become dysregulated in cancer (Barutcu et al., 2016).

It is important to note, however, that this is not the first time the *RUNX* genes have been associated with the oestrogen/ER signalling, where an antagonist relationship with *RUNX2* (Chimge et al., 2012; Chimge and Frenkel, 2013) and *RUNX3* (Huang et al., 2012) has been proposed. Given the putative tumour suppressive function exerted by *RUNX1* in ER+ breast cancers, how can the low percentage of reported somatic mutations in the gene be explained? It is important to take into account that *RUNX1* dysregulation could also arise from other types of alteration (epigenetic and/or post-translational), but also that it could be mirrored by dysregulation of its binding partner *CBF β* (Banerji et al., 2012; Cancer Genome Atlas, 2012; Ellis et al., 2012; Nik-Zainal et al., 2016; Pereira et al., 2016).

1.7.5 The “cell-of-origin” of breast cancer

Three main hypotheses have been proposed to explain the origin of breast cancer. According to the first one, breast tumours would arise from a common cell-of-origin; according to the second one, each type of breast cancer would originate from a different cell-of-origin; according to the third one, breast cancer would be the result of both processes (Stingl and Caldas, 2007).

1.7.5.1 The cancer stem cell theory

The cancer SC (CSC) theory refers to the belief that cancer arises from the dysregulation of a common cell-of-origin that is a SC. This theory is strictly based on the main properties characterizing the latter, such as the ability to self-renew and expand the pool of SCs through SCDs, as well as to give rise to progenitors, or transient amplifying cells, via ACDs (Chen et al., 2017; Lin, 2002). Altogether, these unique features, ascribed among the world-famous cancer hallmarks (Hanahan and Weinberg, 2011), are believed to render SCs highly vulnerable targets for neoplastic transformation more than any other cell type of the body (Dontu et al., 2003). Thus, occurrence of genetic alterations in SCs would rapidly result in their conversion into CSCs, whose division would then give rise to self-renewing cells devoted to the expansion and maintenance of the

CSCs pool, in addition to rapidly dividing cells responsible for the proliferation of the bulk of the tumour (Macias and Hinck, 2012).

As mentioned above, the use of transplantation experiments has been instrumental to the identification and phenotypic characterization of MaSCs, Hitherto, however, whether MaSCs were able to initiate cancer when exposed to carcinogenic agents was still unknown. One of the first evidences arrived when exposure of young rats to the potent carcinogen 7,12-dimethylbenz(a)anthracene resulted in the formation of mammary lesions in TEBs, the most proliferating units of pubertal mammary gland found to contain a high number of MaSCs (Russo et al., 1983). Along with the efforts to refine the molecular profile of MaSCs came the discovery that transplants of CD44⁺CD24^{low} cells was able to give rise to heterogeneous tumours (Al-Hajj et al., 2003). When expression of ProCR, a putative marker of bipotent MaSCs (Wang et al., 2015), was recently reported in CD44⁺ cells, it was hypothesized that this subset could have represented a likely MaSC target population for oncogenic transformation (Shipitsin et al., 2007). In addition, the finding of an embryonic SC-like gene signature characterizing certain types of undifferentiated and aggressive breast cancers emphasized the intriguing parallels between tumourigenesis and embryonic SCs (Spike et al., 2012). Thus, fMaSCs, or alternatively any cell which could have reverted to an embryonic SC-like state, were also hypothesized as putative targets for oncogenic transformation (Ben-Porath et al., 2008).

Nevertheless, proving that MaSCs are the cell-of-origin of breast cancers, or of at least some subtypes of the disease, still remains a big endeavour. This is due not only to their low prevalence or slow-cycling state, but mainly to the absence of specific markers that could univocally identify their presence (Chen et al., 2017). For this reason, it has been recently argued that CSCs, or tumour-initiating cells, do not arise from the transformation of normal MaSCs, since they appeared to reside in the luminal layer of the mammary gland. This observation led scientists to postulate a “plasticity tumour model”, whereby transit-amplifying cells, rather than MaSCs, would represent the most probable cell-of-origin of tumours. As such, neoplastic transformation of progenitor cells would induce their de-differentiation and conversion into tumour initiating cells, whose

proliferation would then culminate in tumour formation (Chaffer and Weinberg, 2015).

1.7.5.2 Progenitor cells as tumour-initiating sources

The idea of different subtypes of breast cancers originating from the transformation of a single epithelial cell type has been revisited recently. Given the slow-cycling state of MaSCs as compared to the proliferative ability of progenitor cells, LPs were proposed to give rise to luminal tumours, whereas BPs would yield to basal-like tumours. This hypothesis was corroborated by gene expression analyses which were often clustering luminal-like tumours with luminal cells and basal-like-tumours with basal cells (Koren and Bentires-Alj, 2015; Perou et al., 2000). However, when more precise studies started to compare the five intrinsic molecular subtypes of the disease with the different MMEC subpopulations constituting the mammary epithelial cell hierarchy, results pointed towards a different direction. Accordingly, MaSCs/BPs/basal cells appeared closer to the claudin-low and normal-like subtypes of breast cancer (rather than to the basal-like one), whereas LPs/luminal cells aligned to the basal-like subtype of the disease (rather than to the luminal-like one) (Prat et al., 2010; Visvader and Stingl, 2014). Of note, the second scenario, supported not only by human evidences (Lim et al., 2009), but also by GEMMs (Molyneux et al., 2010), was revealed to be particularly true for *BRCA1*-driven breast cancers, found to originate from the re-programming of LPs towards a basal-like phenotype upon specific initiating genetic alterations (Chen et al., 2017; Visvader and Stingl, 2014).

Altogether, these data led to three important conclusions. The first one was that the different subtypes of breast cancer were likely to originate from different cells-of-origin. The second one that LPs, more than other epithelial cell types of the mammary gland, were a likely target for oncogenic transformation; and the third one that, when transformed, LPs gave rise to very aggressive and heterogeneous tumours, such as basal-like breast cancers. What remained unclear was whether this higher susceptibility and degree of tumour heterogeneity stemmed from the intrinsic plasticity shown by LPs upon transformation or, instead, from the oncogenic targeting of different luminal populations of the mammary gland, i.e. ER⁺ or ER⁻ (Van Keymeulen et al.,

2017). As discussed above, the highest degree of proliferation seen in the luminal compartment has thus far been attributed to ER⁻ cells (the effectors), which would react to the presence of paracrine signals released by ER⁺ cells (the sensors) in response to hormones. However, recent evidences for proliferation of ER α ⁺ cells have also been found. Accordingly, the number of double positive ER/Ki67 cells increases in the breast of older women, correlating with the higher percentage of HR⁺ tumours affecting the latter. But if ER α ⁺ cells' main role is to sensor E2 to convey its proliferative message to neighbouring ER α ⁻ cells, it would be surprising for ER α ⁺ cells to be TICs? It has been suggested that perhaps, through upregulation of both ER α and AREG, a self-propagating feeding loop might be generated, thus eventually fostering proliferation and oncogenic transformation of this otherwise quiescent cell type (Macias and Hinck, 2012).

1.8 Experimental models of breast cancer

Over time, different methods have been employed to study breast cancer, beginning with the establishment of human breast cancer cell lines and continuing with the generation of animal tumour models. Herein, pros and cons for each experimental model system will briefly be discussed.

1.8.1 *In vitro* and *ex vivo* culture systems

Since the establishment of the first human cancer cell line, the world famous HeLa cells coming from a patient (Henrietta Lacks) with cervical carcinoma (Gey et al., 1952), the use of cultured tumour cells became “viral” in the research field, thus significantly improving our understanding of the biology of cancer and of its well-described hallmarks (Hanahan and Weinberg, 2011). This discovery reached the breast cancer field in 1958, with the establishment of the BT-20 cell line (Lasfargues and Ozzello, 1958), to then continue with the commonly used MDA-MB series of cells (Cailleau et al., 1978) and the popular MCF-7 cell line (Soule et al., 1973). Since then, beside one of latest accomplishments referred to as the SUM series of breast cancer cells (Ethier et al., 1993), not much improvement has been made, partly due to the difficulty in maintaining an homogeneous population of cells *in vitro*, partly due to the tight regulation

regarding the research use of human tissues (<https://www.hta.gov.uk/>) (Holliday and Speirs, 2011). Furthermore, notwithstanding the possibility to perform experiments in a standardised format and the ease to get fast biological readouts, cell culture system is not devoid of caveats. First and foremost, established breast cancer cell lines do not represent the high degree of heterogeneity shown by breast cancer, thus hindering the study of certain subtypes of the disease. Secondly, the majority of established breast cancer cell lines come from metastatic or pleural effusions, leading to an over representation of late-stage tumours without covering the early-stages of breast tumourigenesis. Thirdly, 2D culture systems do not recapitulate the physiological environment surrounding cancer cells *in vivo*, not only because of the use of plastic dishes, but also because of the lack of the correct tumour microenvironment (TME). Lastly, due to the different culture methods used worldwide, originally identical breast cancer cell lines might have differently adapted overtime, thus losing their molecular and phenotypic integrity to acquire changes which have rendered experimental results across different labs not equally comparable or reproducible (Bruna et al., 2016).

To overcome some of the aforementioned shortcomings, it is always advisable to use an expanded panel of cancer cell lines in order to have a better representation of the heterogeneity of the disease. Cell lines should also be passaged in culture for a minimal length of time to maintain their integrity and avoid any issue related to contamination. Heterotypic co-culture systems using cancer and host stromal cells (such as fibroblasts and immune cells) should be utilized more, in order to study the intimate relationships between the tumour and its TME. Whenever possible, cell lines (and their hosts) should be cultured in 3D, either in solid-based matrixes (matrigel, collagen, etc..) as organoids or in suspension as spheres, thus closely mimicking their physiological behaviour. Nonetheless, whilst the development of more sophisticated *in vitro* systems remains a pressing need, a fairly remarkable level of success has been lately achieved in establishing the optimal conditions for “primary” culture, namely directly from the primary source (i.e. a patient or an animal). In brief, by harvesting cells from core biopsies or from the blood, scientist have been able to culture primary murine and human cancer cells, either in 3D or in suspension, whilst maintaining their integrity as close as possible to the physiological setting.

For this reason, *ex vivo* systems are currently deemed to provide the best condition to characterize the behaviour of cancer cells and predict their response to therapy. This is particularly exciting for breast cancer research, especially in view of the under-representation shown by HR+ breast cancer models and the difficulty to study the endocrine regulation of the mammary gland *in vitro*. In regards to the first point, culture of circulating tumour cells from ER+ breast cancers has now become possible, thus allowing characterization of their mutational landscape and discovery of the most effective drug therapy that could predict patients' response (Yu et al., 2014). In regards to the second point, albeit ER+ breast cancer cell lines (e.g. MCF-7 or T47D) have been instrumental for understanding the molecular mechanisms of E2 and progesterone signalling, target genes modulated by the latter are often different from the ones induced *in vivo* (Fernandez-Valdivia et al., 2008). Limitations are also encountered when primary human breast epithelial cells are cultured *in vitro*, as they either seem to lose expression of steroid HRs in 2D or show a different transcriptional profile in response to progesterone in 3D, without induction of Wnt-4 or RANKL (Graham et al., 2009). As such, based on the knowledge that hormone signalling strictly relies on paracrine mechanisms, an *ex vivo* system based on fresh explants of intact breast "tissue microstructures" was recently developed, enabling to maintain the physiological integrity of the human breast (Tanos et al., 2012).

1.8.2 *In vivo* animal models

In the lookout for experimental systems which could be more relevant to the human scenario, since the early 1900s scientists have turned their head towards the development and implementation of the so-called *in vivo* cancer models. Herein, two of the most commonly used animal models in the cancer field will be discussed, highlighting their pros and cons particularly in relation to breast cancer research.

1.8.2.1 Transplantation-based models

Cancer transplantation models generally refer to the injection of tumour cells in living model organisms, most commonly mice. Importantly, the injection of these cells, of murine (allotransplantation) or human (xenotransplantation)

origin, can occur either in the anatomical site of tumour formation (orthotopic graft) or in a different site (allotopic grafts), such as the subcutaneous compartment of the skin. So far, breast cancer orthotopic grafts have been usually generated through injection of cancer cells in the fat pad of the mammary gland, albeit some laboratories have successfully attempted to perform the injection in the ductal compartment of the gland (Richard et al., 2016; Sflomos et al., 2016). Such technique has proven to be a valuable tool to assess the function of a gene on tumour's growth, survival and progression (often even to a metastatic stage). However, due to the intrinsic nature of the system which involves inoculation of already established cancer cells, the use of transplantation models does not allow investigation into how genes and their encoded proteins affect the early-stages of tumourigenesis. Furthermore, by often employing the use of cultured cell lines, they carry most of the *in vitro* caveats outlined above. In addition, to avoid rejection of the inoculated cells, transplantation models mainly rely on the use of immune-deficient mice (but for allotransplantation), hindering the study of the crosstalk between the immune system and cancer (Holen et al., 2017).

A remarkable improvement has been achieved with the direct inoculation of human cancer cells freshly extracted from patients into mice, the so-called patient-derived tumour xenografts (PDXs), which allowed functional characterization of the properties of human primary tumours in a physiological setting while preserving histological and molecular heterogeneity (Hidalgo et al., 2014). One of the first attempts to create breast cancer PDXs occurred with work led by (DeRose et al., 2013), who started grafting human breast tumours into the fat pad of the murine mammary glands, showing the predictive nature of such system which could inform on patient's clinical outcomes. More recently, the biggest breast cancer biobank comprising 83 PDXs was generated (Bruna et al., 2016). Albeit the majority of PDXs were from ER+ tumours, a huge variability in terms of proliferative rate upon initial engraftment and subsequent passages was reported, with ER-negative tumours displaying the fastest take and growth rate. Importantly, through a comprehensive molecular analysis, established PDXs were shown to fall within the same IntCluster of the original tumour (Curtis et al., 2012) and to retain the same histopathological features through serial passaging, confirming the reliability of such system. Lastly, PDXs

represent a robust platform to perform pre-clinical drug screening in the attempt to predict patient's response (Bruna et al., 2016). In the near future, the implementation of a new generation of PDTXs, known as "Mouse Avatars", might allow the identification of a personalized therapeutic regimen in "real-time" that is while the patient is still alive (Malaney et al., 2014).

Whilst heralding a new era of breast cancer research and setting the stage for precision cancer medicine, PDTXs are not devoid of shortcomings. One of the main ones refers to the presence of over-represented TN and under-represented ER+ PDTXs, due to the intrinsic take and growth rate differences of these subtypes (Landis et al., 2013). Furthermore, there is increasing evidences reporting discrepancies in the metastatic pattern of tumour cells seen in PDTXs as compared to the one observed in the patient (Holen et al., 2017). Lastly, like for all transplantation-based models, PDTXs rely on the use of immune-deficient mice, although lately there has been a great interest in generating more humanized mice through the engraftment of CD34+ haematopoietic stem and precursor cells into immune-deficient animals (Holzapfel et al., 2015). Of note, humanized PDXs have been recently made available by the Jackson Laboratories which presented them as "*the next big thing in cancer modelling*" (www.jax.org/news-and-insights). To conclude, even though transplantation-based models represent the most common system used in the preclinical setting to rapidly validate new cancer drug targets as well as optimise dosing and treatment regimens, there has been a need for more relevant *in vivo* models of breast cancer.

1.8.2.2 Genetically engineered mouse models

The origin of GEMMs traces back to the 1980s when the first oncogene was cloned into the mouse genome, giving birth to the so-then-called "oncomice" (Hanahan et al., 2007). With the advent of gene targeting technology, it was then the turn of tumour suppressor genes to be targeted, leading to the generation of the first knockout mice (Jacks, 1996). By targeting the expression of an oncogene or the inactivation of a tumour suppressor to all cells of the body, first-generation GEMMs did not truly recapitulate the origin of sporadic human tumours (Kersten et al., 2017). It was only with the introduction of the Cre-loxP system, which enabled targeted genetic events to occur specifically in

the organs of interest, that conditional GEMMs could be created (Jonkers and Berns, 2002). This step represented a milestone in the cancer field as it allowed studying “naturally occurring” cancers by targeting clinically relevant genetic abnormalities (e.g. *BRCA1* mutations or HER2 overexpression) in the correct anatomical location of immune-proficient mice. However, being the Cre recombinase constitutively expressed by tissue-specific promoters, conditional GEMMs did not allow any temporal control over the targeted genetic event. Consequently, in the presence of multiple “hits”, the latter would have likely occurred simultaneously without mimicking the sequential multistep progression of human cancer (Kersten et al., 2017). Over recent years, more sophisticated GEMMs implemented by high-throughput genetic approaches (e.g. CRISPR/Cas9 gene editing system) have been generated, thus significantly improving our understanding of the molecular mechanisms underpinning cancer biology. Nowadays, GEMMs represent extremely valuable tools for preclinical research, as they allow the evaluation of new therapies, the refinement of treatment strategies and the study of drug resistance (Kersten et al., 2017). There are of course pitfalls with this model system. Firstly, creation of GEMMs can be very laborious and their husbandry not cost-effective. In addition, some GEMMs are characterized by long tumour latency, which render their use very time-consuming. Secondly, GEMMs do not cover the wide heterogeneity shown by breast cancer, thus hampering the study of certain subtypes of the disease (Holen et al., 2017). Thirdly, not all GEMMs will progress to the metastatic stage, which represents the major cause of breast cancer morbidity, affecting almost 40% of patients in the whole UK (<http://breastcancer.org/>). Moreover, even when they do metastasize, secondary tumour sites do not always occur at clinically relevant organs, and almost never represent the cause of primary death due to tight government regulations. Lastly, given their short life-span, very few GEMMs would enable the study of long-term tumour dormancy, a recurring issue responsible for the majority of patients’ relapse (Kersten et al., 2017). Overall, this urges the development of novel mouse model strategies in order to better recapitulate the heterogeneity of breast cancer, improve our knowledge on the biology of this enduring disease and hopefully accelerate the *in vivo* validation of new drug targets. In summary, if all the advantages and disadvantages of *in vitro*, *ex vivo* and *in vivo* models were to be considered, there is no perfect model system to study breast cancer.

1.9 Aims of the thesis

Breast cancer currently remains the leading cause of cancer-related death among women worldwide. As for all other types of tumour, this genetic disease arises from the interplay between highly mutated genes (more commonly known) and infrequently altered ones (less commonly known). With the advent of NGS, the identity of the vast majority of these less commonly altered players has been finally unveiled. What remains to be elucidated, however, is the putative role played by these “uncommon” genes in the initiation, maintenance and progression of the disease. In this regards, following the discovery of *RUNX1* genetic alterations in biopsies of breast cancer patients, it became imperative to turn the spotlight on the function owned by this new pawn in the chess game of breast cancer.

Thus far, the state-of-the-art knowledge of *RUNX1* depicted the gene as a crucial regulator of cell fate determination and lineage-specific differentiation, particularly in the context of the haematopoietic system. As such, *RUNX1* has been renowned as one of the most common site of chromosomal translocations in haematological malignancies. Over time, however, the cumulative discovery of *RUNX1* genetic alterations in several solid tumours, including breast cancer, has led to the realization that the function owned by the gene in tumourigenesis was more widespread than previously thought. Further to that, what appeared to be rather surprising was the fact that *RUNX1* could act as a tumour suppressor or as an oncogene depending on the specific context.

Therefore, on the basis of what has been previously discussed and of the evidence gathered so far, the overall aim of the present thesis is to unveil what role could the *Runx1* gene possibly play in the context of breast cancer. In an endeavour to do so, the first experimental approach to be outlined consists in the characterization of the effects following *Runx1* deletion in the *MMTV-PyMT* breast cancer mouse model. In the latter, expression of *RUNX1* interestingly appears to be restricted to early-stage mammary lesions, whilst lost in established tumours. Intriguingly, this finding may provide mechanistic insights into why *Runx1* loss results in an accelerated onset of breast tumourigenesis, without affecting the overall survival of *MMTV-PyMT* mice.

Given the presence of a putative interplay between the RUNX and β -catenin transcription factors, the second experimental approach investigates how deletion of *Runx1* and *Runx2* may impinge on a novel Wnt/ β -catenin-driven model of breast tumourigenesis. Herein, *Runx1* loss results in a similar decrease of the time from birth to tumour onset, without again affecting the overall survival of Wnt/ β -catenin-driven mice. This time, however, a remarkable acceleration of pre-neoplastic mammary lesions is seen upon concomitant deletion of *Runx2*, as confirmed by the profound disruption of mammary anlagen, as well as by the dramatic increase in tumour burden. These latter results offer the rationale for further challenging the stemness capability of *Runx1*- and *Runx2*-deficient Wnt/ β -catenin-driven mammary lesions through the use of transplantation- based models.

Finally, the third experimental approach comprises of a variety of *ex vivo* experimental techniques implemented to delve into the molecular roots of the tumour suppressive functions shown by the *Runx* genes at early stages of breast tumourigenesis. Thus, through the use of colony-forming cell assays and flow cytometry analysis, the *Runx* genes unveil their identity as guardians of the mammary epithelial cell hierarchy.

Altogether, the results presented in this thesis are intended to shed light on the crucial role played by the *Runx* “hills” in the genomic landscape of breast cancer. By highlighting the detrimental consequences of *Runx1* and *Runx2* loss, resulting in an impairment of mammary tissue homeostasis and eventually tumour development, this work wishes to improve the poor understanding of both mammary gland and breast cancer biology

2 Materials and Methods

2.1 Animal procedures

All animal works were performed with ethical approval from University of Glasgow under the revised Animal (Scientific Procedures) Act 1986 and the EU Directive 2010 (PPL 70/8645). All mice were housed in a pathogen-free animal facility within appropriate ventilated cages. Mouse health check was carried out at least two times a week. General husbandry (food, water and housing) and mouse ear notching were carried out by the Biological Services Unit at the Beatson Institute for Cancer Research. Genotyping was performed through ear-notching by Transnetyx, Inc. (Cordova, TN, USA). Animals were euthanized by carbon dioxide asphyxiation.

2.1.1 Mouse lines and generation of cohorts

The MMTV-Cre line was kindly provided by the laboratory of WJ Muller (Andrechek et al., 2000), as was the MMTV-PyMT line (Guy et al., 1992); the betalactoglobulin (BLG)-Cre line was obtained from AR Clarke (Selbert et al., 1998); the K14-Cre line (Dassule et al., 2000) was bought in from The Jackson Laboratory (USA); the stabilized β -catenin line (*Catnb*^{wt/lox(ex3)}) was kindly provided by OJ Sansom (Harada et al., 1999); the tandem dimer red fluorescent protein (tdRFP) line (Gt(ROSA)26Sor^{tm1Hjf}) was obtained from the EMMA archive and was generated as previously described (Luche et al., 2007); the *Runx1* line (*Runx1*^{fl/fl}) was generated in the lab of Professor Nancy Speck (Growney et al., 2005) and kindly given to us by Marella De Bruijn, Oxford; and the *Runx2* line (*Runx2*^{fl/fl}) was created by Theresa Higgins and Ian Rosewell in the lab of Professor Mike Owen (ICRF labs, London). To study the effect of *Runx1* deletion using the MMTV-PyMT model, MMTV-PyMT mice were crossed onto MMTV-Cre;*Runx1*^{fl/fl} mice. To use a reporter gene as a surrogate marker for MMTV-Cre expression and *Runx1* recombination, MMTV-PyMT;MMTV-Cre;*Runx1*^{fl/fl} mice were crossed onto tdRFP mice. All mice were backcrossed for up to 10 generations onto a pure FVB background. To study the effect of *Runx1* and *Runx2* deletion in the context of activated Wnt/ β -catenin signalling, BLG-

Cre;Catnb^{wt/lox(ex3)} mice were crossed with *Runx1^{fl/fl}* and *Runx2^{fl/fl}* conditional knock-out mice. All mice were maintained on a mixed background. For subcutaneous transplantation experiments, all CD1 nude and athymic nude mice used were obtained from Charles River Research Models & Services (UK).

2.1.2 Staging of the oestrous cycle

To stage the oestrous cycle of the mice, animals were euthanized and their vagina gently flushed three to five times using a plastic pipette filled with phosphate buffered saline (PBS). The collected flush (vaginal smear) was spread onto a glass slide [VWR, UK] to dry and slides were then subjected to H&E stain using the ST5020 Leica Autostainer. The specific stage of the oestrous cycle was determined based on the proportion of three different cell types: epithelial cells, cornified cells and leukocytes. When there was a higher abundance of nucleated cells, mice were staged at pro-oestrus; when there was a higher abundance of cornified cells, mice were staged at oestrus; when there was an abundance of all three cell types, mice were staged at metestrous; and when there was an abundance of leukocytes, mice were staged at diestrous (Caligioni, 2009).

2.1.3 Survival analysis

For survival analysis, mice were kept under enhanced monitoring in order to assess for the formation of mammary tumour lesions by palpation. Once a lesion was noticed, its size was recorded and the tumour measured twice a week with the use of a caliper. Mice were sacrificed when a tumour lesion reached clinical end point, that is when its length or width equalled 15 mm or if the tumour ulcerated. The body weight of the mouse was then recorded and all mammary glands dissected out and weighed to calculate tumour burden (expressed as a percentage of mammary gland weight divided by the body weight of the mouse). Mammary tumours were then formalin-fixed paraffin-embedded for histological analysis and frozen down at -80°C for molecular analysis. For survival analysis, data were plotted using Kaplan-Meiers curves. Importantly, mice culled due to other pathologies (including gasping, runty mice or animals with cystic tumours) were censored and marked on the respective curves.

2.1.4 Transplants of mouse-derived tumour fragments

Clinical end-point mice of the *BLG-Cre;Catnb^{wt/lox(ex3)}* cohorts were euthanized and their tumours removed. From the biggest lesion, five mouse-derived tumour fragments of 2 mm by 2 mm were generated. Each fragment was transplanted subcutaneously into the right flank of immunocompromised (CD1 nude and athymic nude) mice. Tumour growth was monitored over time by measuring tumour volume [(length x width x width)/2, with length>width] with the use of calipers. Recipient mice were euthanized when clinical end point was reached. Tumours were then dissected out and divided in two parts: one was frozen down at -80°C for molecular analysis, while the other was formalin-fixed paraffin embedded for immunostaining analysis.

2.1.5 Imaging analysis of RFP expression

Clinical end point mice of the MMTV-PyMT cohorts were euthanized, opened up to allow visualization of all ten murine mammary glands and imaged for red fluorescent protein (RFP) expression through the IVIS Spectrum *in vivo* imaging system (PerkinElmer). Mice were illuminated via the 554 nm excitation filter, whereas fluorescence was detected with the 581 nm emission filter.

2.1.6 Virgin analysis of pre-neoplastic lesions

To look for the presence of pre-neoplastic lesions, virgin mice were sacrificed at 3, 6 and 9 weeks of age, prior to the development of palpable mammary tumours in some genotypes. Right-hand side mammary glands were excised for whole-mount analysis, whereas left-hand side mammary tissues were either formalin-fixed paraffin-embedded for histological analysis or frozen down at -80°C for molecular analysis. To assess the proliferative ability of pre-neoplastic lesions, *in vivo* intraperitoneal BrdU (GE Healthcare, VWR) injection (200 µl/25 g body weight) was performed. Animals were euthanized two hours after injection and all ten mammary glands harvested and paraffin-embedded formalin-fixed for immunohistochemical analysis.

2.2 Immunohistochemistry

Dissected mammary glands were formalin-fixed undergoing appropriate tissue processing and paraffin-embedded to preserve tissue architecture. Tissue blocks were sectioned at 4 μm on a microtome and blanks were mounted onto adhesive glass slides [VWR, UK]. Routine haematoxylin eosin (H&E) staining (as processed by the Beatson Histology Service) was carried out to check the quality of the sample. IHC staining was performed as followed. Slides were de-waxed through repetitive (3X) xylene washes and re-hydrated in decreasing concentration of ethanol (ETOH), i.e. 100%, 100% and 70%. Heat-induced antigen retrieval was performed at 95°C for 30 minutes using the Dako Target Retrieval Solution, Citrate pH 6 [Dako, S236984-2], followed by a cooling down period of 30 minutes. Slides were then rinsed (2X) for 5 minutes in Tris-Buffered Saline with 0.05% Tween (TBST) at low shaking. Sections were then blocked for 5 minutes using the Dako Peroxidase Block [Dako, UK] to avoid endogenous peroxidase activity. Following rinsing (2X), slides were blocked for 30 minutes using 5% Rabbit Serum [Dako, X090210-8] in PBS to avoid secondary antibody non-specific binding. Slides were then incubated with primary antibodies either overnight at 4°C for anti-ER α 1:200 [Santa Cruz, SC-542] and anti-PR 1:200 [Santa Cruz, SC-539], for 1 hour at room temperature for anti-CK5 1:500 [Cambridge, PRB-16OP-100], anti-CK8/18 1:250 [Fitzgerald, 20R-CP004] and anti-CK14 1:100 [abcam, ab7800], or for 2 hours at room temperature for anti- β -catenin 1:50 [BD Transduction Laboratories, 610154]. Following rinsing with TBST (2X), sections were incubated for 1 hour at room temperature with horseradish peroxidase-conjugated anti-rabbit secondary antibodies, except for CK8/18 and β -catenin for which anti-guinea pig or anti-mouse secondary antibodies were used, respectively [Dako, UK]. All antibodies were diluted in Dako REAL Antibody Diluent [Dako, UK]. Following rinsing with TBST (2X), the reaction was visualized with the DAB Chromogen + DAB Substrate Buffer, according to manufacturer's instructions [Dako, UK]. After immersion in distilled H₂O to stop the reaction, slides were counterstained and mounted by the Beatson Histology Service.

The anti-RUNX1 1:75 [Cell Signalling, 8529], anti-RUNX2 1:300 [Cell Signalling, 8486], anti-BrdU 1:150 [BD Biosciences, 347580], anti-Ki67 1:100 [Thermo, RM-9106], anti-RFP 1:100 [Tebu, 600-401-379], anti- α SMA 1:25,000 [Sigma, A2547]

IHC staining were carried out by Colin Nixon and the Beatson Histology Service using the Dako Autostainer link48. Sections were dewaxed as previously described and subject to heat induced antigen retrieval using the Dako Pre-Treatment module. The sections underwent antigen retrieval for 25 minutes at 98°C using 10 mM pH6 Citrate retrieval buffer (Thermo, TA-250-PM1X). After washing in TBST, sections were placed onto the Dako Autostainer link48. Dako peroxidase block was applied for 5 minutes before rinsing with TBST. The primary antibody was applied to the sections at previously described dilutions for 35 minutes at room temperature. Slides were rinsed with TBST before application of appropriate rabbit or mouse secondary antibody (Dako, K4001; K4003) and rinsed again with TBST before application of 3,3 diaminobenzidine tetrahydrochloride (Dako, K3468) to allow visualisation of the antigen-antibody interaction. The sections were then removed from the autostainer, counterstained with haematoxylin z (CellPath, RBA-4201-00A), washed with water, differentiated in 2 dips 1% acid alcohol, washed with water then the nuclei blue'd in Scotts tap water substitute. The sections were again washed in water before dehydration through graded alcohols, cleared in xylene and mounted with a glass coverslip using DPX mountant for microscopy (CellPath, SEA-1300-00A). Images were captured using an Olympus CKX41 microscope.

2.3 BrdU quantification

Mammary glands of BrdU-injected mice were harvested, formalin-fixed paraffin-embedded and stained with anti-BrdU antibody (see above). Three to six mice per genotype were analysed. Quantification of BrdU staining was achieved using the HALO software. Firstly, the total mammary gland area (TA) of each slide was measured by drawing a (thick) line around each tissue section via the pen annotation tool. In doing so, any empty area within the gland was carefully marked with a dotted line and excluded using the exclusion drawing tool (Figure 2. 1A). Secondly, all epithelial ducts within the TA were encircled via the pen annotation tool, whilst their lumen (if present) excluded via the exclusion drawing tool (Figure 2. 1B). This allowed quantifying the total epithelium (TE) area as a percentage of TA. Within TE, a distinction between normal epithelium (NE) and abnormal epithelium (AE) was achieved through the creation of different color-coded layers (Figure 2. 1C). This allowed quantifying total NE and AE areas percentages of TE area. Once the HALO software was trained to

recognize a cell and distinguish between a BrdU-positive and -negative one (Figure 2. 1D), the proliferative density of each NE and AE layer was calculated by dividing the number of BrdU-positive cells by the area of the corresponding layer. The calculated proliferative indexes were then normalized by multiplying their values by the percentage of each corresponding layer.

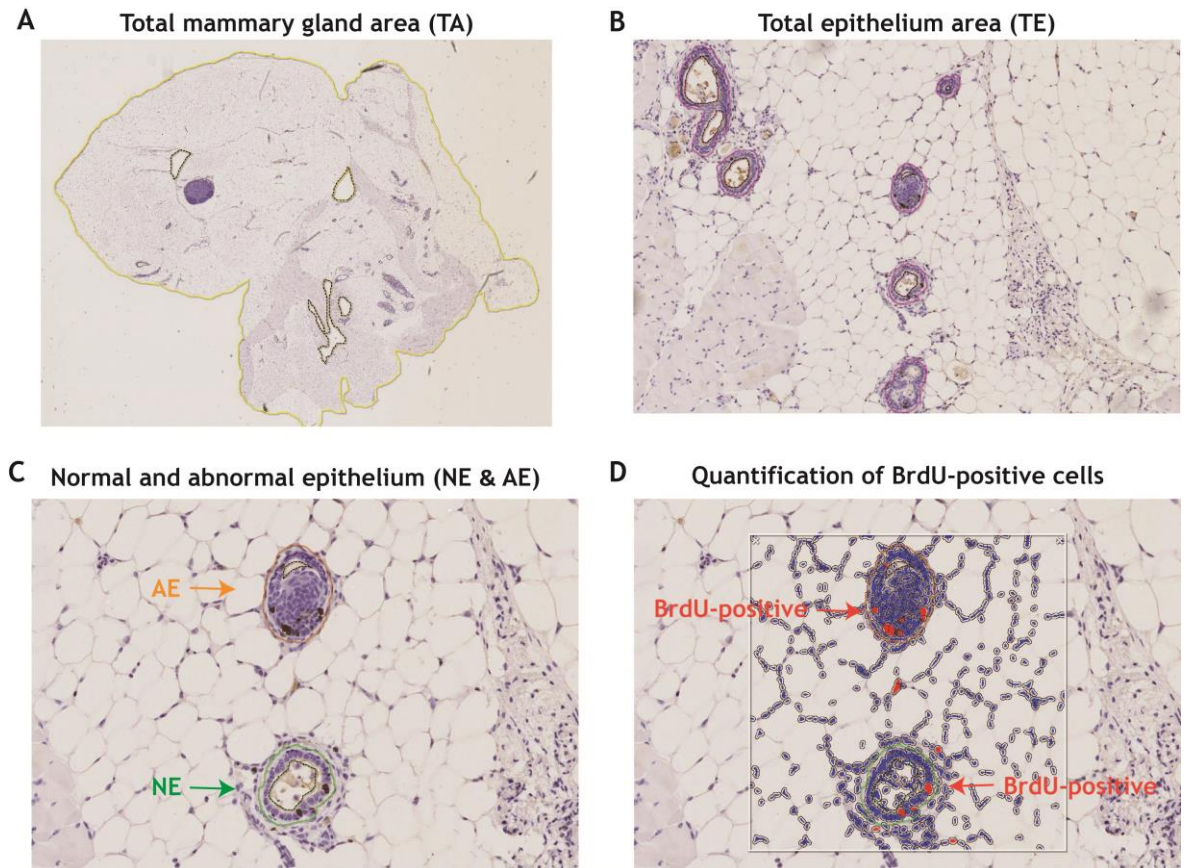


Figure 2. 1 Quantification of BrdU-positive cells through the HALO software.

Representative screenshots of the different steps needed to quantify the proliferative index characterizing the mammary gland tissues of each *BLG-Cre;Catnb^{wt/lox(ex3)}* cohort of mice upon loss of *Runx1* and/or *Runx2*. Quantification of (A) total mammary gland area within each slide; (B) total epithelium area within each tissue section; (C) total normal and abnormal epithelia area within each tissue section; and (D) BrdU-positive cells within normal and abnormal epithelia areas.

2.4 Mouse mammary epithelial cell extraction

All ten mammary gland from pubertal and clinical end-point mice were dissected out, after removal of lymph nodes and avoidance of surrounding muscles, and placed in a 50 ml falcon tube containing 10 ml serum-free working solution - F12 Nutrient Mixture (Ham) (1X), 1% Penicillin-Streptomycin and L-Glutamine 200 mM (100X) (PSQ) [Life Technologies]. After finely mincing glands with the McIlwain tissue chopper [Mickle Lab, UK], tissue pastes were placed in a 50 ml falcon tube containing 15 ml serum-free digestion solution - F12 Nutrient Mixture (Ham) (1X), 1% PSQ, 10% Collagenase/Hyaluronidase [300 units (U)/ml Sigma, C9891; 100 U/ml Sigma, H3506] - and incubated for 1.5 hours at 37°C in a shaking incubator at 100 rpm. Primary epithelial organoids were then collected through differential centrifugation by spinning tubes down (2X) at 350g for 5 minutes. Pellets were re-suspended in 1.5 ml NH₄Cl (0.8%) and kept at room temperature for 5 minutes for red blood cells lysis. Once the reaction was stopped in working medium and tubes were spun down at 350g for 5 minutes, pellets were re-suspended in 1 ml TEG dissociation solution - 1X PBS, 0.25% Trypsin 2.5% (10X) [Life Technologies] and 1mM EGTA - plus 0.1 mg/ml DNase I recombinant, RNase-free 10000 U [Roche, 04716728001] and incubated at 37°C for 10 minutes in the water bath to obtain a single cell suspension. After the addition of 10% foetal bovine serum (FBS) supplemented working solution to stop trypsinization, MMECs were purified through filtration with 70 µm cell strainers [Greiner Bio One] and centrifugation at 350g for 5 minutes. Lastly, MMECs were diluted 1:2 with Trypan Blue Stain 0.4% [Life Technologies, T10282] and live cells were counted based on dye exclusion with the haemocytometer and used for further analysis.

2.5 Flow cytometric analysis

A maximum number of 5×10^6 MMECs were blocked with the Fc receptor antibody [Biolegend, 101319 - anti-mouse CD16/32 antibody] for 15 minutes at room temperature, by diluting it 1:100 in FACS buffer - 1X PBS, 2mM EDTA pH 8 and 1% FBS. Tubes were washed with 1ml FACS buffer, spun down at 350g for 5 minutes and supernatant was removed. MMECs were then labelled with a master mix containing the following antibodies at a 1:200 dilution in FACS buffer: Allophycocyanin (APC) anti-mouse CD31 [BD Pharmingen, 551262], APC anti-mouse CD45 [BD Pharmingen, 559864], APC anti-mouse Ter119 [BD Pharmingen,

557909], Phycoerythrin (PE) anti-mouse CD24 [BD Pharmingen, 553262], PerCP-eFluor710 anti-human/mouse CD49f [eBioscience, 46-0495], Alexa Fluor 488 anti-mouse Ly-6A/E (Sca-1) [Biolegend, 108115]. Labelled MMECs were then incubated on ice in the dark for 30 minutes. Afterwards, tubes were washed with 1ml FACS buffer, spun down at 350g for 5 minutes and supernatant was removed. Lastly, MMECs were labelled with 1mg/ml 4',6-diamidino-2-phenylindole (DAPI) [Life Technologies, D1306], incubated on ice in the dark for 5 minutes and analysed via the Attune NxT Flow Cytometer [Life Technologies]. For Single labelled colour controls were done for each independent experiment by using UltraComp eBeads Compensation Beads [eBioscience/ThermoFisher Scientific, 01-2222-42], which were washed and re-suspended in Flow Cytometry Staining Buffer [eBioscience, 00-4222-57]. Gates were set using fluorescence minus one controls. Data was analysed with the FlowJo V10.2 software. MMECs profiling (Figure 2. 2) was achieved by following a series of sequential steps. These consisted in the elimination of cell debris (SSC-A vs FSC-A) (A), exclusion of doublets (FSC-H vs FSC-A and SSC-A vs SSC-H) (B, C), removal of dead cells (DAPI positive) (D) and exclusion of haematopoietic (CD45⁺/Ter119⁺) and endothelial (CD31⁺) cells, collectively called lineage positive (Lin⁺) cells (E). The remaining subset of Lin⁻ cells was then analysed for CD24 and CD49f expression, in order to discriminate between the luminal (Lin⁻CD24⁺CD49f^{low}) and basal/MYO (Lin⁻CD24⁺CD49f^{high}) subpopulations of MMECs (F). Within each subset of MMECs, the percentage of Sca-1⁺ and Sca-1⁻ was finally calculated.

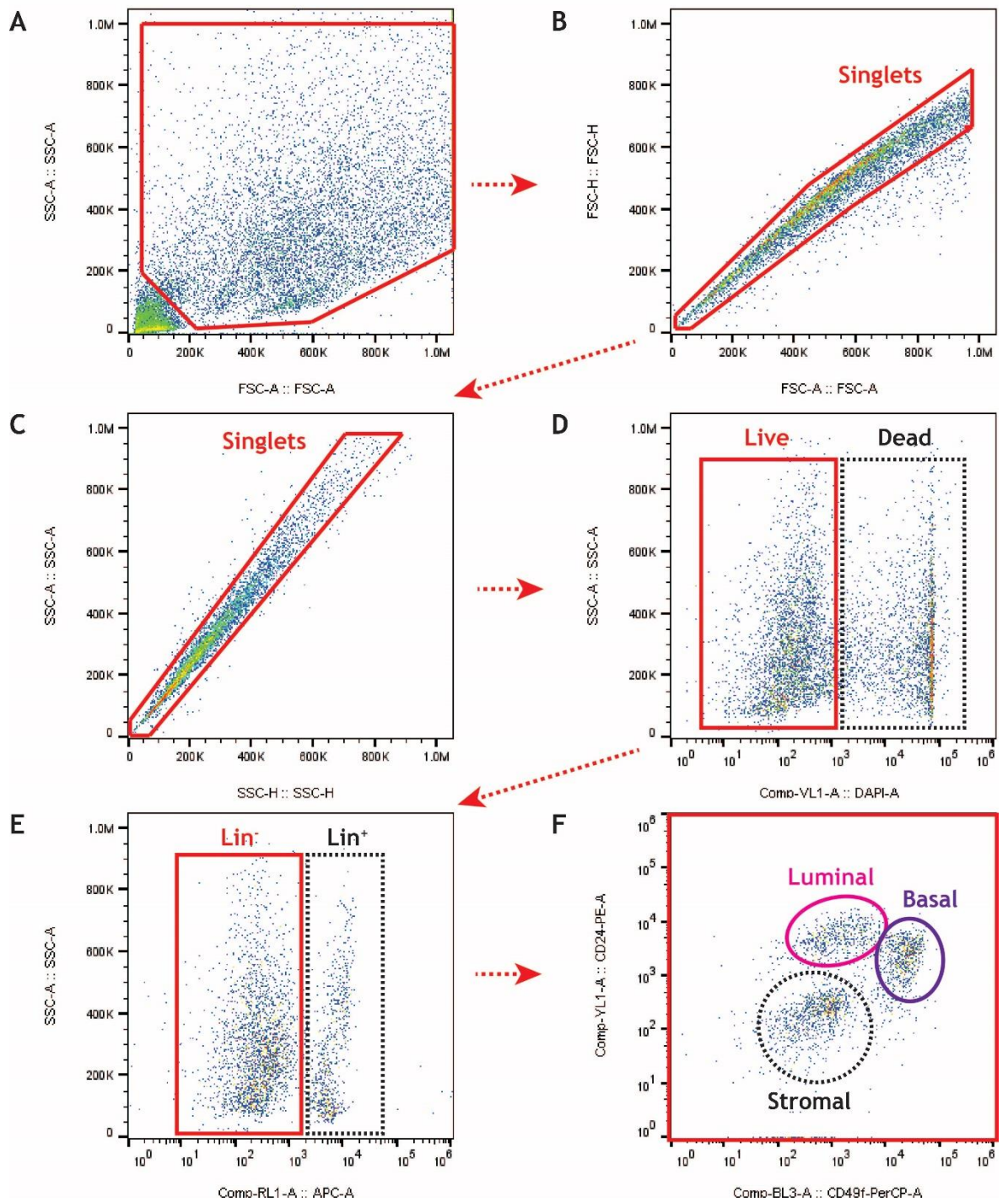


Figure 2. 2 Flow cytometric analysis of mouse mammary epithelial cells.

Gating strategy utilized for flow cytometric analysis of MMECs. Representative dot plots showing (A) the exclusion of debris and inclusion of all cells, (B, C) the exclusion of doublets and inclusion of singlets, (D) the exclusion of dead cells (DAPI positive) and inclusion of live cells (DAPI negative), (E) the exclusion of haematopoietic and endothelial (Lin⁺) cells (CD31⁺CD45⁺Ter119⁺) and inclusion of epithelial cells (Lin⁻), (F) the exclusion of stromal cells and inclusion of luminal (CD24⁺CD49f^{low}) and basal (CD24⁺CD49f^{high}) cells. MMEC, mouse mammary epithelial cells; Lin, lineage. A, area; FSC, forward scatter; H, height; SSC, side scatter.

2.6 Fluorescence activated cell sorting

To perform FACS of RFP⁺ and RFP⁻ cells from the *MMTV-PyMT* cohorts of mice, animals were euthanized when clinical end point was reached. Mammary glands were dissected out and processed as described above until a single cell suspension was obtained. Cells were then labelled with 1mg/ml DAPI [Life Technologies, D1306], incubated on ice in the dark for 5 minutes and run through the FACSARIA Z6001 [BD Bioscience]. Through elimination of cell debris (SSC-A vs FSC-A), exclusion of doublets (FSC-H vs FSC-A), and removal of dead cells (DAPI positive), live (DAPI negative) cells were sorted in two populations based on positive or negative expression for RFP. The RFP gate was set using an RFP negative *MMTV-PyMT* control female.

2.7 Mammary gland whole mounts

Murine mammary glands #4 were harvested from 3, 6 and 9 week old female, spread onto a glass slide [VWR] and air dried for 10 minutes prior to placement in 50 ml tube containing Carnoy's fixative. Tissues were fixed overnight and washed in decreasing concentrations of EtOH, i.e. 70%, 50%, 25%, for approximately 15 minutes per wash. Mammary glands were then rinsed in distilled H₂O for 10 minutes and stained in Carmine Alum overnight. The following day, tissues were washed in increasing concentration of EtOH, i.e. 70%, 95%, 100%, for approximately 15 minutes per wash, cleared in Xylene overnight and mounted with Pertex Mounting Medium [HistoLab, 00801] the following day. After photographic documentation using a Zeiss stereomicroscope, mammary gland whole-mounts were analysed through ImageJ software. Carnoy's fixative was prepared by mixing 6 parts of EtOH 100%, 3 parts of chloroform (CHCl₃) and 1 part of glacial acetic acid. Carmine Alum stain was prepared by boiling 1g carmine [Sigma, C1022] and 2.5 g aluminium potassium sulphate dodecahydrate [Sigma, 237086] in 500 ml distilled H₂O for 20 minutes. The solution was then filtered and stored in the fridge at 4 °C. To quantify the elongation of the ductal mammary tree, the distance between three longest TEBs and the lymph node (taken as a reference point) was calculated and averaged. Four mice per genotype were used.

2.8 Tumoursphere assay

Freshly extracted MMECs from 7 to 8 weeks old females of the *BLG-Cre;Catnb^{wt/lox(ex3)}* cohorts, and sorted RFP⁺ and RFP⁻ cells from clinical end point *MMTV-PyMT* mice, were plated on ultra-low attachment 24-well plates [VWR, 734-1584] at a density of 10,000 live cells per well in serum-free culture medium - F12 Nutrient Mixture (Ham) (1X) - supplemented with 4 µg/ml Heparin [Sigma, H3149], 20 ng/ml EGF [Sigma, E4127], 20 ng/ml FGF2 [Sigma, SRP4038] and B-27 Supplement without Vitamin A (1X) [Thermo Fisher Scientific, 12587-010]. For each independent experiment, twelve technical replicates (wells) were used per cohort. At Day 3, cells were fed with the addition of fresh EGF and FGF2. At Day 6, the number of primary tumourspheres per well was manually counted using the 4X objective lens of the Olympus CKX41 microscope and one representative picture of each replicate was taken to assess the size of the spheres. This was done by manually measuring the area of all visible spheres present in each representative picture of the 12 technical replicates using the ImageJ software. Measured area values, expressed in µm, were split into three groups (1500-4500, 4500-7500 and 7500-15000) and the frequency of spheres present into each group was then calculated.

For second passage, primary tumourspheres were collected and gently spun down at 350g for 5 minutes. The pellet was enzymatically re-suspended in 100 µl of 0.25% trypsin and incubated at 37°C for 15 minutes. After stopping the reaction with the addition of fresh medium, tubes were spun down at 350g for 5 minutes and cells were counted based on dye exclusion with the haemocytometer. 5,000 live tumoursphere-derived cells per well were plated again on new ultra-low attachment 24-well plates using fresh tumoursphere serum-free medium. For each independent experiment, twelve technical replicates (wells) were used per cohort. At Day 3, cells were fed by the addition of fresh EGF and FGF2. At Day 6, the number of secondary tumourspheres per well was manually counted using the 4X objective lens of the Olympus CKX41 microscope and one representative picture of each replicate was taken to assess the size of the spheres. Secondary tumoursphere area was measured using the ImageJ software. This was done by manually measuring the area of all visible spheres present in each representative picture of the 12 technical replicates using the ImageJ software. Measured area values, expressed in µm, were then

split into three groups (1500-3500; 3500-5500 and 5500-7500) and the frequency of spheres present into each group was then calculated.

2.9 Colony forming cell assay

Freshly extracted MMECs from 7 to 8 weeks old females of the *BLG-Cre;Catnb^{wt/lox(ex3)}* cohorts were plated on 24-well plates [VWR, UK] at a density of 5,000 live cells per well and embedded in a 20 μ l drop of Matrigel [Corning Matrigel Basement Membrane Matrix Growth Factor Reduced, Phenol Red Free, 356231]. Once matrigel had solidified at 37°C in the incubator for almost 10 minutes, 500 μ l of culture medium - F12 Nutrient Mixture (Ham) (1X) [Gibco], 10% FBS [Gibco], 1% PSQ [Gibco], 10 ng/ml EGF [Sigma, E4127], 5 μ g/ml Insulin solution human [Sigma, I9278], 0.25 ng/ml Fungizone [Thermo Fisher Scientific, 15290-018], 5 ng/ml Cholera Toxin [Sigma, C8052], 50 μ g/ml Gentamicin [Sigma, G1272] - was added to each well. For each independent experiment, twelve technical replicates (wells) were used per cohort. At Day 3, cells were fed with the addition of 500 μ l of fresh culture medium. At Day 6, the number of acinar and solid colonies per well was manually counted using the 4X objective lens of the Olympus CKX41 microscope and one representative picture of each replicate was taken to assess the size of the colonies. This was done by manually measuring the diameter of all visible acinar and solid colonies present in each representative picture of the 12 technical replicates using the ImageJ software. Measured diameter values, expressed in μ m, were split into three groups (0-200, 200-400 and 400-600) in the case of acinar colonies and four groups (0-100, 100-200, 200-300 and 300-400) in the case of solid colonies. The frequency of colonies present into each group was then calculated.

2.10 RNA extraction

Total ribonucleic acid (RNA) was extracted from MMECs using the RNeasy Mini Kit (QIAGEN), as per manufacturer's instructions. Samples were lysed using the denaturing guanidine-thiocyanate RLT buffer, containing β -mercaptoethanol to prevent RNases activity and degradation of RNA. Lysed samples were homogenized through the use of QIAshredder Spin Columns, which were spun down for 2 minutes at 14680 rpm via a standard microcentrifuge. Homogenized samples were mixed with 70% ETOH and added onto RNeasy Mini Spin Columns,

where total RNA could be isolated through specific binding to silica-based membranes. Following sequential washing steps in the presence of supplied RW1 and RPE Buffers, contaminants and residual ETOH were removed. Total bound RNA was eluted with the addition of 40 μ l of supplied RNase-Free Water into 1.5 ml collection tubes. Purified RNA was either stored at -80°C or used for the next application. The DNA-free DNA removal kit [Thermo Fisher Scientific] was used to treat the RNA prior to reverse transcription polymerase chain reaction (RT-PCR) to eliminate genomic DNA contamination, according to the manufacturer's instructions (standard treatment protocol). To assess the yield and purity of RNA samples and calculate the amount of material needed for cDNA synthesis, eluted RNA was quantified using the NanoDrop 2000c spectrophotometer [Thermo Fisher Scientific]. The concentration of RNA was determined by measuring its absorbance at 260 nm (A_{260}), given that an absorbance of 1 unit corresponds to approximately 44 μg of RNA per ml (if the pH solution is neutral). To estimate the purity of the RNA, a ratio of the readings at 260 nm and 280 nm was calculated (A_{260}/A_{280}), since the majority of contaminants including proteins absorb at 280 nm.

2.10.1 Reverse transcription

Quantified RNA was reversed transcribed using the Superscript III Kit [Thermo Fisher Scientific], as per manufacturer's protocol. 1 μg of RNA was mixed with a master mix containing 1 μ l of 50 μM oligo(dT)₂₀ [Invitrogen], 1 μ l of 50 μM random hexamers (Invitrogen-Applied Biosystems), 1 μ l of dNTP mix (10 mM each) and RNase-free water to reach a total volume of 13 μ l. Samples were incubated at 65°C for 5 minutes using a Thermal Cycler (Bio-Rad DNA Engine) and quickly chilled on ice for approximately 1 minute. A master mix of 7 μ l, containing 4 μ l of 5X first-strand buffer, 1 μ l of 0.1 M DTT, 1 μ l of RNase inhibitor (40 U/ μ l) and 1 μ l of Superscript III, was added to each sample. Samples were then incubated at 25°C for 5 minutes, 50°C for 60 minutes and 70°C for 15 minutes. Newly synthesized complementary (c)DNA was diluted 1:10 with the addition of RNase-Free Water and either stored at -20°C or used for the next application.

2.10.2 Quantitative polymerase chain reaction

SYBR Green-based quantitative qPCR was carried out using a 20 μ l reaction containing: 10 μ l of 2X SYBR Green Jumpstart Taq ReadyMix [Sigma, S4438], 0.5 μ M of forward and reverse primers and 5 μ l of diluted cDNA (or 5 μ l of water for the no-template controls). The cycling conditions used were: 94°C for 2 minutes, followed by 40 cycles of cDNA denaturation at 94°C for 15 seconds and primer annealing at 60°C for 60 seconds. To verify the specificity of each amplicon and the presence of primer-dimers, a melting curve analysis was carried out from 70°C to 95°C in 0.3°C intervals. Acquisition of the data was done using CFX96 Real-Time PCR Detection System [BioRad]. Data analysis was performed using the CFX Manager software, version 3.1 [BioRad] and the GenEx Standard software, version 6.1 (MultiD Analyses). The following primers were used for the target genes: *Ccnd1* (GAGAAGTTGTGCATCTACTG; AAATGAACTTCACATCTGTGGC); *Cd44* (CAC ATA TTG CTT CAA TGC CTC AG; CCA TCA CGG TTG ACA ATA GTT ATG); *Lgr5* (GAGTCAACCCAAGCCTTAGTATCC; CATGGGACAAATGCAACTGAAG); *Myc* (CCC AAA TCC TGT ACC TCG TC; TTG CCT CTT CTC CAC AGA CA), and *Ascl2* (GAGCAGGAGCTGCTTGACTT; TCCGGAAGATGGAAGATGTC). *Runx1* and *Runx2* primers were purchased via QIAGEN (QT00100380 and QT00102193, respectively) and reconstituted by the addition of 1.1ml of d H₂O. To normalize the expression of the *Runx1* and *Runx2* genes in sorted RFP⁺ and RFP⁻ MMTV-PyMT cells, *Gapdh* was used as a reference gene. To normalize the expression of *Ccnd1*, *Cd44*, *Lgr5*, *Myc* and *Ascl2*, reference genes were selected from a panel of 10 genes, *Actb*, *B2m*, *Csnk2a2*, *Cyc1*, *Fbxo38*, *Gapdh*, *Htatsf1*, *Mon2*, *Pak1ip1* and *Rpl13a* [PrimerDesign], using the NormFinder method (Andersen et al., 2004). As the analysis identified *Actb* and *Fbxo38* as the best candidates, these genes were used to normalise for differences in RNA input.

RNA extraction, cDNA synthesis and qPCR analysis of Wnt/ β -catenin target genes was performed by Dimitris Athineos.

2.11 Statistical analysis

All statistical tests were performed with GraphPad Prism 6. For *in vivo* survival analysis with Kaplan-Meiers curves, the Log-rank (Mantel-Cox) test was used. For

scatter dot plots of body weight, tumour burden, number of tumour burdened mammary gland and ductal elongation, statistical analysis was performed by the Kruskal-Wallis (nonparametric) test with Dunn's multiple comparisons in GraphPad Prism. For scatter dot plots of tumoursphere area, colonies diameter, the ratio of solid/acinar colonies, the molecular heterogeneity of solid colonies and flow cytometry data, statistical analysis was performed by the two-way ANOVA test with the Dunnett's multiple comparisons to compare all genotypes to the control cohort and/or the Tukey's multiple comparisons to compare all genotypes with each other. Error bars represented the mean with standard deviation (SD). P values were considered significant if $P < 0.05$. In particular, significance was set as: * $P < 0.05$, ** $P < 0.01$, *** $P < 0.001$, **** $P < 0.0001$. For RT-qPCR, relative expression with the ddCq method and statistical analysis were carried out using GenEx. T-test, with Dunn-Bonferroni correction for multiple testing, was used to determine statistical significance of changes.

3 Investigating the role of *Runx1* in the *MMTV-PyMT* mouse model of breast cancer

3.1 Introduction

One of the biggest breakthroughs in breast cancer research is attributed to Timothy Stewart and Phillip Leder, the pioneers of the first transgenic mouse model of breast cancer (Hanahan et al., 2007). Around that time, scientists were aware of the existence of a retrovirus known as mouse mammary tumour virus (MMTV), able to cause mammary tumours in specific strain of mice. In addition, the MMTV long terminal repeat (LTR) was also known to regulate the expression of a fused oncogene in response to steroid hormones in cultured mammalian cells (Huang et al., 1981). So it was in 1984 that the expertise of the Leder molecular biology lab along with the transgenic skills of Stewart led to the generation of the first breast cancer *MMTV-Myc* oncomouse (Stewart et al., 1984). Whilst on one hand this ground breaking finding reinforced the idea of oncogenes as causative agents of cancer, on the other the long temporal latency and the relatively low tumour burden showed by *MMTV-Myc* mice emphasized the “multihit” nature of the disease, which required more than one genetic event to arise (Vogelstein et al., 1983). With this in mind, the first double transgenic *MMTV-v-Ha-Ras/MMTV-Myc* breast cancer mouse model was created, thus proving that the cooperation of two oncogenes significantly accelerated tumourigenesis. Nonetheless, the presence of focal lesions displayed by mice reiterated the necessity of additional hits, perhaps stochastic changes on top of those programmed by the oncogenes (Sinn et al., 1987). With the concomitant advent of gene targeting technology, tumour suppressor genes also started to be targeted, either alone or in combination with already known oncogenes (Jacks, 1996), leading to the generation of a multitude of breast cancer GEMMs.

3.1.1 The *PyMT* breast cancer mouse model

Since its discovery, the MMTV promoter has been extensively used in the GEMM field of breast cancer to drive expression of different oncogenes, including the *HER2/neu* gene, specifically in the mammary gland (Huang et al., 1981).

Nonetheless, beside the discovery of the HER2 tyrosine kinase in driving the development of adenocarcinoma (Muller et al., 1988), another tyrosine kinase was also found to dramatically transform the mammary epithelium. This refers to the Polyomavirus (PyV) middle T antigen (PyMT). The tumourigenic potency of the PyMT and its preferential targeting of the mammary gland emerged when infection of new-borns or nude mice with PyMT caused the formation of several epithelial and mesenchymal tumour types, among which mammary carcinomas appeared to dominate (Dawe et al., 1987; Berekbi et al., 1990). Of note, the oncogenic capability of PyV was ascribed to the presence of the middle T antigen (Israel et al., 1979), able to interact with and activate the tyrosine kinase activity of several proteins, including members of the c-src family (Courtneidge and Heber, 1987). In addition, cellular transformation was also found to stem from PyMT association with the 85-kDa subunit of the phosphoinositide 3'-kinase (PI3K) (Whitman et al., 1985; Courtneidge and Heber, 1987; Talmage et al., 1989). Thus, in an effort to better guide the tumourigenic potency of PyMT exclusively to the mammary gland, expression of the transgene was finally put under the control of the MMTV promoter, giving rise to the MMTV-PyMT breast cancer mouse model (Guy et al., 1992).

Deemed as one of the most common breast cancer GEMMs used worldwide, the MMTV-PyMT model is characterized by several distinctive features. First and foremost, despite some degree of variability depending on the strain (Davie et al., 2007), MMTV-PyMT mice generally displays short tumour latency, with evidence of mammary hyperplasia detected by 4 weeks of age. Secondly, due to the high tumourigenicity of the PyMT oncogene, mammary tumours are shown with 100% penetrance and appear to arise in a multifocal way, affecting all ten murine mammary glands. Thirdly, albeit driven by a hormonally-regulated promoter, females do not require undergoing parity to increase expression of the oncogene. Last, but not least, it allows all stages of breast tumourigenesis to be studied, from the inception of lesions to dissemination of cancer cells to distant organs, due to the high incidence of metastatic disease (Lin et al., 2003). However, this conventional model is not without caveats. One of the first shortcomings refers to the fact that the tumourigenic signalling cascade driven by the PyMT oncogene does not necessarily mirror the one occurring in the human situation. In addition, the multifocal nature of PyMT-driven tumours

contrasts against the clonal features of human breast cancer. In addition, there is also uncertainty regarding the specific lineage wherein the not well-defined regulatory sequences of the MMTV promoter drive expression of the transgene (Holen et al., 2017). Lastly, being lungs the preferential site for PyMT-driven metastatic dissemination, this model does not fully mimic the pattern and seeding properties of human breast cancer metastasis, which also tend to occur in the liver and bones (Weigelt et al., 2005).

In view of the requirement of multiple genetic events for the genesis of tumours (Hanahan et al., 2007), several putative cancer-associated genes have been investigated in the context of PyMT tumourigenesis. Following the elucidation of the genomic landscape of breast cancer, characterized by a few ‘mountains’ (frequently mutated genes) and many ‘hills’ (infrequently mutated genes) (Wood et al., 2007), attention has focused on the putative role played by infrequently mutated genes in the initiation, maintenance or progression of the disease. As *RUNX1* was recently reported among the most significantly altered breast cancer genes (Banerjee et al., 2012; Cancer Genome Atlas, 2012; Ellis et al., 2012; Nik-Zainal et al., 2016; Pereira et al., 2016), whose majority of identified mutations were believed to be *loss-of-function* (Li et al., 2003; van Bragt et al., 2014), investigation of the effect of *Runx1* deletion in the context of PyMT tumourigenesis was undertaken. *RUNX1* has a prominent role in the development of the haematopoietic system, wherein its function is required for the conversion of endothelial cells of the haemogenic endothelium into haematopoietic stem cells (HSCs) (Chen et al., 2009). *RUNX* transcription factors act in partnership with *CBF β* to form a heterodimeric complex (Kamachi et al., 1990). Within the latter, *RUNX* proteins bind directly to specific *RUNX* motifs scattered across the genome via their DNA binding domain (DBD), whereas *CBF β* is responsible for increasing *RUNXs*’ affinity to the DNA (Ogawa et al., 1993) and protecting proteins from proteosomal degradation (Huang et al., 2001). Of note, the DBD was shown to be contained within the so-called Runt domain (RD), a 128-amino acid region (aa 58-178) shared between the *Drosophila* segmentation *Runt* gene and the human *AML1* gene and crucial for mediating genome binding and dimerization with *CBF β* (Kagoshima et al., 1993; Meyers et al., 1993). In view of the latter, disruption of exon 4 of *Runx1*, encoding part of the DBD (aa 143-178), was found to cause lethality of mice at E11.5-E12.5, due to a block in

definitive haematopoiesis and the presence of necrosis and haemorrhages in the central nervous system (Okuda et al., 1996; Wang et al., 1996).

3.2 Experimental procedures

3.2.1 Generation of a *Runx1* conditional knock-out breast cancer mouse model

In an attempt to overcome the embryonic lethal phenotype and study the function played by RUNX1 in the mammary gland, a conditional gene-targeting strategy based on the Cre-loxP technology was employed. This system relies on the function of the Cre recombinase enzyme, a bacteriophage P1-derived integrase able to catalyse a site specific recombination event between two DNA loxP recognition sites. As a result, whenever a portion of the genome is flanked by two loxP sites (floxed), this is efficiently excised in the presence of an active Cre recombinase (Hamilton and Abremski, 1984). Generation of a conditional knock-out *Runx1* transgenic line (*Runx1^{fl/fl}*) was achieved through the insertion of loxP-targeting sites flanking exon 4 of the murine gene (Growney et al., 2005). To achieve conditional deletion of *Runx1* in the mammary epithelium, *Runx1^{fl/fl}* mice were mated with *MMTV-Cre* mice. To then study the impact of *Runx1* loss upon PyMT-driven tumourigenesis, *MMTV-Cre;Runx1^{fl/fl}* mice were crossed with the *MMTV-PyMT* line. It has to be noted, however, that one of the caveats of the generated breast cancer *MMTV-PyMT;MMTV-Cre;Runx1^{fl/fl}* cohort was the fact that PyMT-driven tumourigenicity and Cre-driven recombination of *Runx1* were ascribed to two separate transgenes inserted into the mouse genome. Therefore, albeit both guided by the hormonally-regulated MMTV promoter, these events could have occurred asynchronously and independently. In an effort to better trace *MMTV-Cre* expression, *MMTV-PyMT;MMTV-Cre;Runx1^{fl/fl}* mice were crossed with a transgenic reporter line wherein the gene encoding for the tdRFP was preceded by a stop codon flanked by two loxP-sites (Luche et al., 2007). In this way, only in the presence of an active MMTV-Cre recombinase, recombination of the loxP-stop-loxP codon and visualization of RFP expression could be achieved. Finally, the *MMTV-PyMT;MMTV-Cre;Runx1^{fl/fl};tdRFP* line was backcrossed onto a

pure FVB background for up to ten generations to avoid the variability existing between mouse strains.

3.3 Results

3.3.1 Deletion of *Runx1* accelerates PyMT-driven breast tumourigenesis without affecting overall survival

To investigate if deletion of *Runx1* impinged on PyMT-driven breast tumourigenesis, *MMTV-PyMT;MMTV-Cre;tdRFP;Runx1^{fl/fl}* females were monitored for the formation of palpable mammary lesions. Once a lesion was noticed, its size was recorded and measured twice a week via the use of calipers. When a mammary tumour reached clinical end point, that is when its width or length equalled 15 mm or if the tumour ulcerated, the mouse was euthanized. By doing so, three parameters could be calculated: the time from birth to tumour notice, the time from tumour notice to clinical end point and the time from birth to clinical end point (Figure 3. 1A). Accordingly, deletion of one (*Runx1^{wt/fl}*) or two copies (*Runx1^{fl/fl}*) of *Runx1* appeared to significantly accelerate the formation of palpable mammary lesions (54 and 48 average days, respectively), as compared to *Runx1^{wt/wt}* control mice (64 average days) (Figure 3. 1B). This difference, however, was not reflected by any changes in overall survival, as both *Runx1^{wt/fl}* and *Runx1^{fl/fl}* mice were sacrificed at an average time of 91 and 87 days, respectively, which approached the 92 days displayed by *Runx1^{wt/wt}* mice (Figure 3. 1C). Nevertheless, when the timeframe from tumour notice to tumour end point was calculated, the growth of established PyMT-driven mammary tumours appeared lessened in the absence of *Runx1*. In fact, whilst *Runx1^{wt/wt}* control mice showed an average tumour progression of 26 days, tumours from both the *Runx1^{wt/fl}* and *Runx1^{fl/fl}* cohorts reached clinical end point at an average time of 37 and 33 days, respectively (Figure 3. 1D). In agreement with the recent NGS findings discussed in Chapter 1, these results provided for the first time a compelling evidence for a tumour suppressive function exerted by *Runx1* in a breast cancer mouse model (Figure 3. 1B). In support of its remarkable function, the phenotype displayed by *Runx1^{fl/fl}* mice was also found to be recapitulated by *Runx1^{wt/fl}* mice, which only carried one copy of the recombined allele. Curiously,

however, whilst RUNX1 appears to halt the formation of palpable mammary lesions, deletion of *Runx1* delayed the growth of established PyMT-driven tumours. In this regards, two main hypotheses are proposed. According to the first one, RUNX1 might display a dualistic role, acting as a tumour suppressor at early stages, whilst as a pro-oncogene at later stages of tumourigenesis. Alternatively, a compensatory tumour suppressive mechanism might take place in the absence of *Runx1*. In view of the high degree of homology existing between the *Runx* family of genes (Chuang et al., 2013), it is tempting to speculate that this role might be fulfilled by one of the other *Runx* family members. Importantly, it should be noted that survival analysis of *MMTV-Cre;MMTV-PyMT;tdRFP* was carried out by plotting data obtained only from *tdRFP*⁺ mice, yet not from the negative ones. In this way, as expression of the *tdRFP* transgene might have affected the phenotype of mice, animals from different cohorts could be equally compared. Moreover, the presence of RFP positivity could have been used as a surrogate marker for *MMTV-Cre* expression, yet also to infer recombination of the *Runx1* allele. Lastly, mice whose tumour's size was greater than the 0.7 mm cut-off at date of notice were excluded from the time from birth to tumour notice parameter (Figure 3. 1B). Similarly, mice displaying cystic lesions, namely tumours which reached end point because full of liquid, were censored from the overall survival and tumour progression analysis.

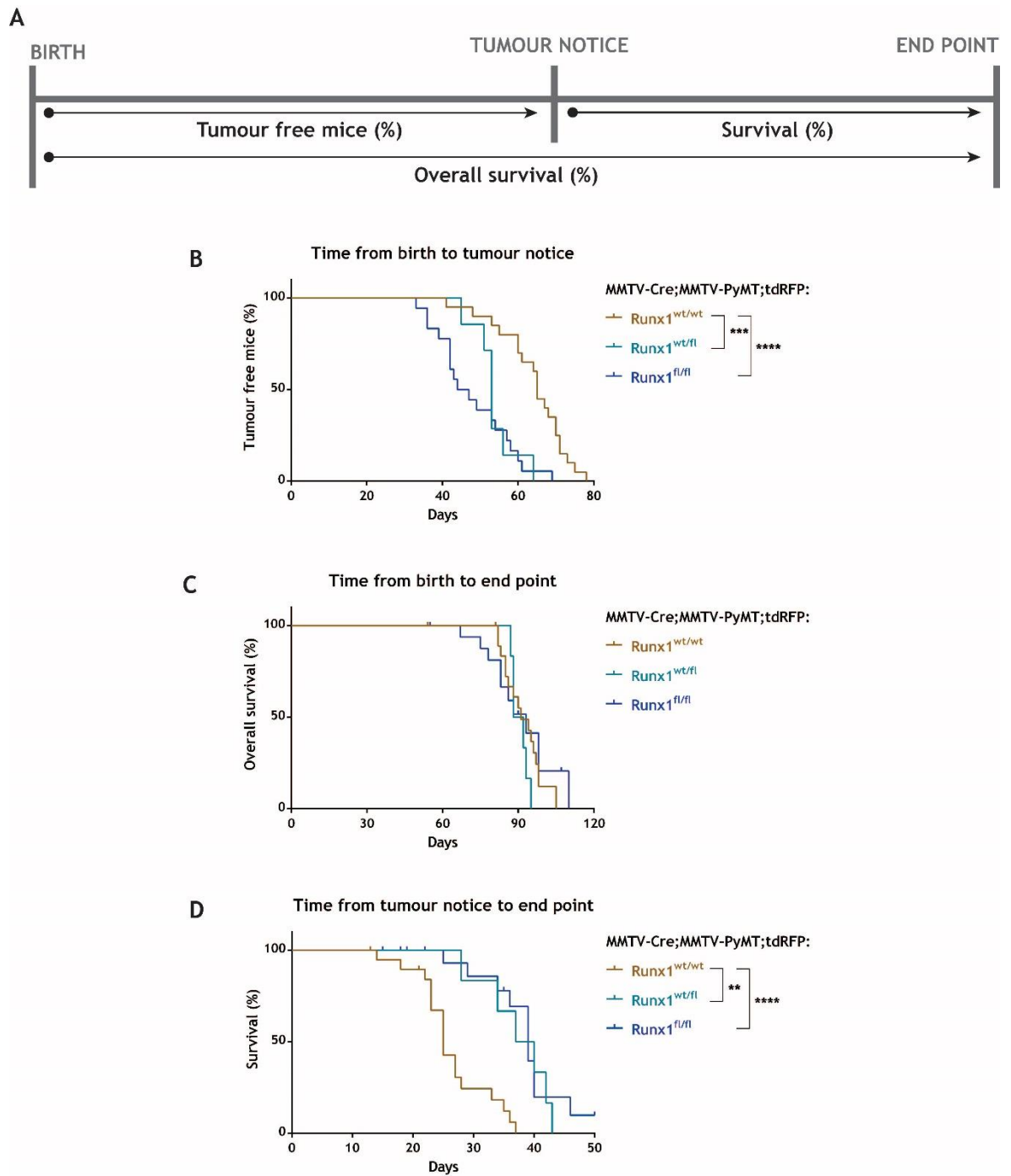


Figure 3. 1 Deletion of *Runx1* accelerates PyMT-driven breast tumourigenesis, yet it does not affect survival of the mice.

(A) Schematic of the three parameters used to assess the impact of *Runx1* deletion upon PyMT-driven tumourigenesis. Cohort females were monitored for the development of palpable mammary tumours. Once a lesion was noticed, its size was recorded and measured twice a week with the use of calipers. When a mammary tumour reached clinical end point, the mouse was sacrificed. (B, C, D) Kaplan-Meier curves of MMTV-Cre;MMTV-PyMT;tdRFP mice of the $Runx1^{wt/wt}$, $Runx1^{wt/fl}$ and $Runx1^{fl/fl}$ cohorts. (B) Time from birth to tumour notice of $Runx1^{wt/wt}$ (n=20), $Runx1^{wt/fl}$ (n=7) and $Runx1^{fl/fl}$ (n=18) mice. (C) Time from birth to end point of $Runx1^{wt/wt}$ (n=20), $Runx1^{wt/fl}$ (n=6), $Runx1^{fl/fl}$ (n=19) mice. (D) Time from tumour notice to end point of $Runx1^{wt/wt}$ (n=20), $Runx1^{wt/fl}$ (n=6), $Runx1^{fl/fl}$ (n=18) mice. Statistical analysis performed using the Log-rank (Mantel-Cox) test in GraphPad Prism. ** $P < 0.01$, *** $P < 0.001$, **** $P < 0.0001$.

3.3.2 Deletion of one or two copies of *Runx1* does not affect tumour burden of MMTV-PyMT mice

When all cohorts of *MMTV-PyMT;MMTV-Cre;tdRFP* mice reached clinical end point, the body weight and the total weight of all tumour-bearing and non-tumour bearing mammary glands were recorded. The combination of these two measures was then used to calculate the tumour burden displayed by each mouse cohort. In doing so, no significant differences emerged in relation to both body weight (Figure 3. 2A), nor tumour burden (Figure 3. 2B) among the *Runx1^{wt/wt}*, *Runx1^{wt/fl}* and *Runx1^{fl/fl}* cohorts. In other words, the accelerated appearance of palpable mammary lesions shown in the absence of *Runx1* did not translate into increased tumour burden or number of tumour burdened mammary glands displayed by *Runx1^{wt/fl}* and *Runx1^{fl/fl}* mice as compared to controls (data not shown). If at a glance counterintuitive, this result further corroborated the delayed tumour progression displayed by established PyMT mammary tumour upon *Runx1* loss. On the other hand, the absence of significant differences in relation to tumour burden could be related to the intrinsic nature of the *MMTV-PyMT;MMTV-Cre;tdRFP;Runx1^{fl/fl}* model. Indeed, considering the presence of two independent transgenes (the *MMTV-PyMT* and the *MMTV-Cre*), the possibility of escaping *Runx1*-proficient tumours in the *Runx1^{fl/fl}* cohort of mice could be envisioned.

Representative pictures of the gross pathological changes characterizing clinical end point *MMTV-PyMT;MMTV-Cre;tdRFP* mice from the *Runx1^{wt/wt}*, *Runx1^{wt/fl}* and *Runx1^{fl/fl}* cohorts are shown in Figure 3. 2C. Note the high tumourigenic potential of the PyMT oncogene, capable of transforming the mammary epithelium of almost all ten murine mammary glands.

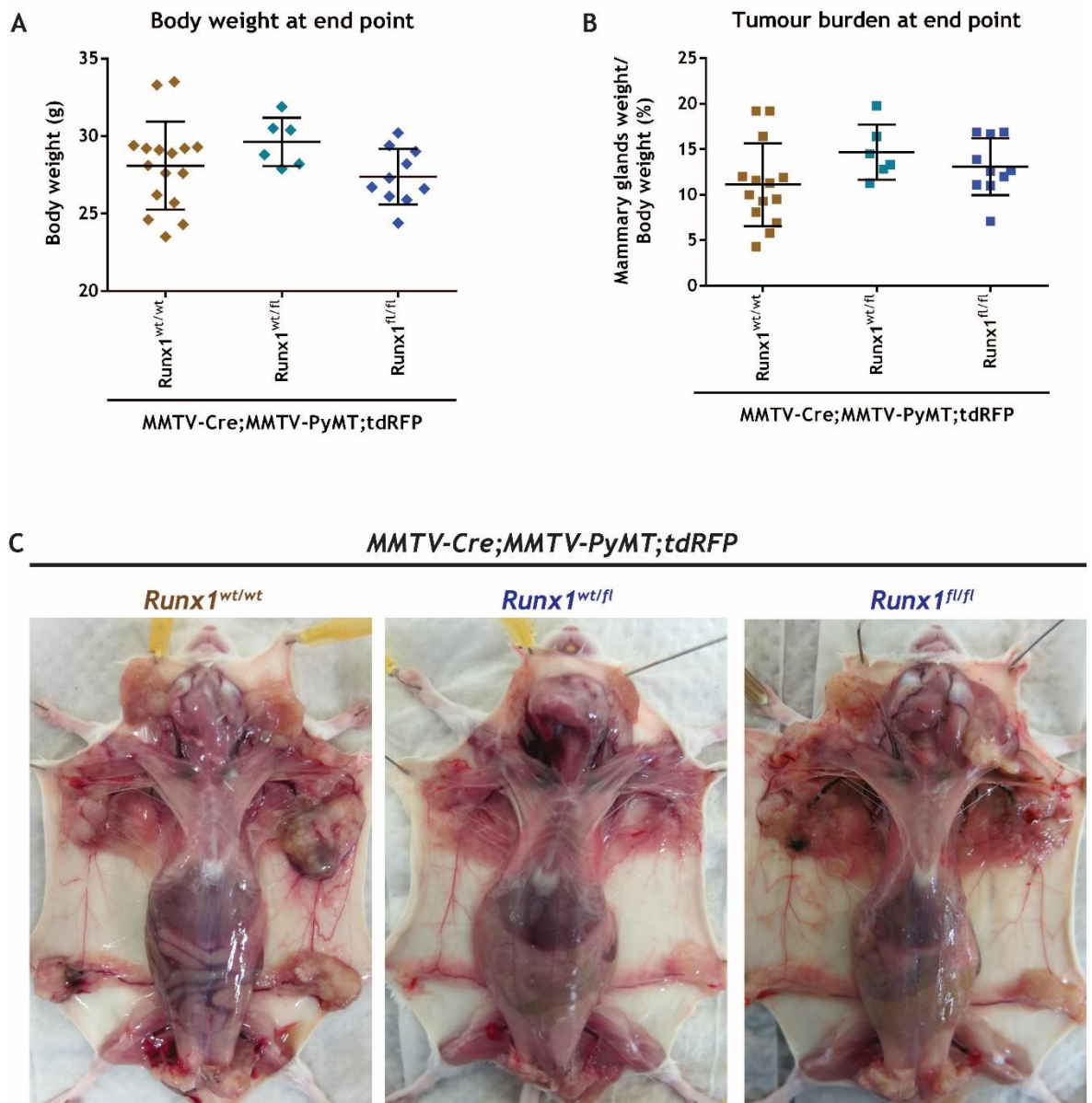


Figure 3. 2 Deletion of one or two copies of *Runx1* does not affect tumour burden of MMTV-PyMT mice.

Scatter dot plots of body weight (A), tumour burden (B) and representative pictures (C) from clinical end point *MMTV-PyMT;MMTV-Cre;tdRFP* mice of the *Runx1*^{wt/wt} (n=20), *Runx1*^{wt/fl} (n=6) and *Runx1*^{fl/fl} (n=19) groups. Cohort females were monitored for the development of palpable mammary lesions. Once a tumour lesion was noticed, its size was recorded and measured twice a week with the use of calipers. When a mammary tumour reached clinical end point, the mouse was sacrificed and both its body weight and tumour burden were recorded. Statistical analysis was performed by the Kruskal-Wallis nonparametric test with Dunn's multiple comparisons in GraphPad Prism. Error bars represent mean with SD (n≥6 per each cohort). For each parameter, no significance was found among cohorts.

3.3.3 RFP imaging analysis of clinical end point MMTV-PyMT mice

In view of the caveats displayed by the *MMTV-PyMT;MMTV-Cre;tdRFP* model, to better monitor the expression and recombination activity of the MMTV-Cre enzyme across all *Runx1* cohorts of mice, RFP imaging was performed. To this end, clinical end point mice from the *Runx1*^{wt/wt}, *Runx1*^{wt/fl} and *Runx1*^{fl/fl} groups were euthanized and imaged for RFP fluorescence via the IVIS Spectrum imaging system. By doing so, imaging analysis of the *Runx1*^{wt/wt} cohort showed a remarkable amount of RFP positivity across specimens, with exception of only a few negative mice (1/9) (Figure 3. 3). Furthermore, due to the multifocal nature of the PyMT-oncogene, expression of RFP could be observed among the majority of murine mammary glands. Therefore, despite the intrinsic pitfalls of the model, these results suggested that PyMT-driven breast tumourigenesis and activity of the MMTV-Cre were likely occurring in the same targeted cell.

A slightly different scenario applied instead to the *Runx1*^{fl/fl} cohort of mice, wherein a higher degree of variability in RFP signal was observed (Figure 3. 4). As such, whilst some mice exhibited comparable levels of RFP positivity to the *Runx1*^{wt/wt} cohort, a higher percentage of animals appeared to be completely negative (5/14). These results could be explained by lack of activity of the MMTV-Cre recombinase or by loss of *Runx1*-deleted (RFP+) cells during PyMT-driven breast tumourigenesis.

When RFP imaging analysis of the *Runx1*^{wt/fl} cohort of mice was performed, mice displayed a pattern of RFP expression similar to the *Runx1*^{wt/wt} control group, rather than to the *Runx1*^{fl/fl} one (Figure 3. 5). It should be noted, however, that this latter cohort of mice was composed of the lowest number of animals.

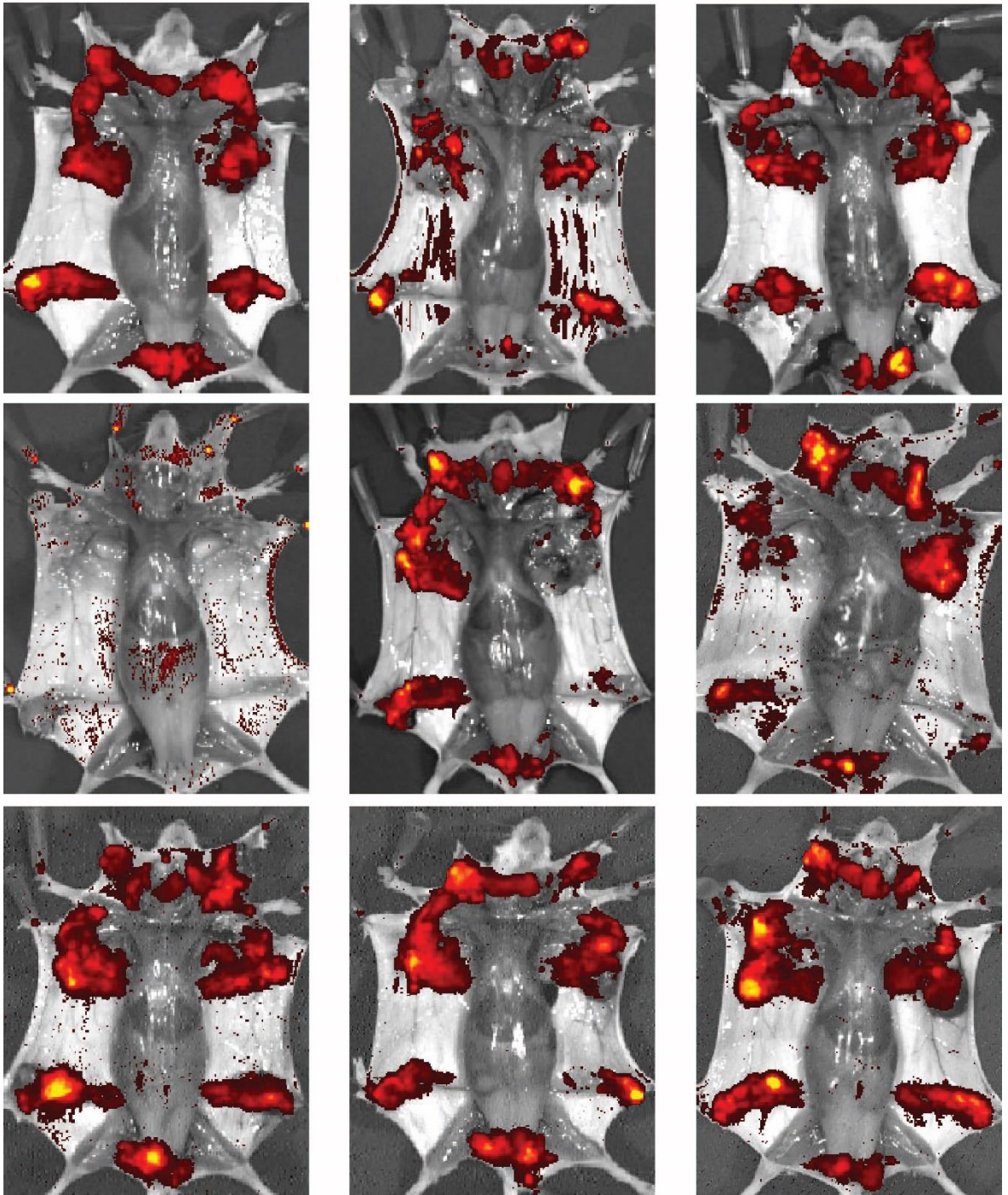


Figure 3.3 Imaging analysis of the RFP reporter gene in *Runx1*-proficient MMTV-PyMT mice.

Representative snapshots of clinical end point *MMTV-PyMT;MMTV-Cre;tdRFP;Runx1^{wt/wt}* mice (n=9) showing expression of the RFP reporter gene as detected via the IVIS Spectrum *in vivo* imaging system. Mice were euthanized, placed on a black cardboard and imaged for RFP fluorescence. Animals were illuminated via the 554 nm excitation filter, whereas fluorescence was detected with the 581 nm emission filter. Images were captured with an Auto exposure time using the small binning and F/Stop 2 settings. RFP, red fluorescent protein.

MMTV-PyMT;MMTV-Cre;tdRFP;Runx1^{fl/fl}

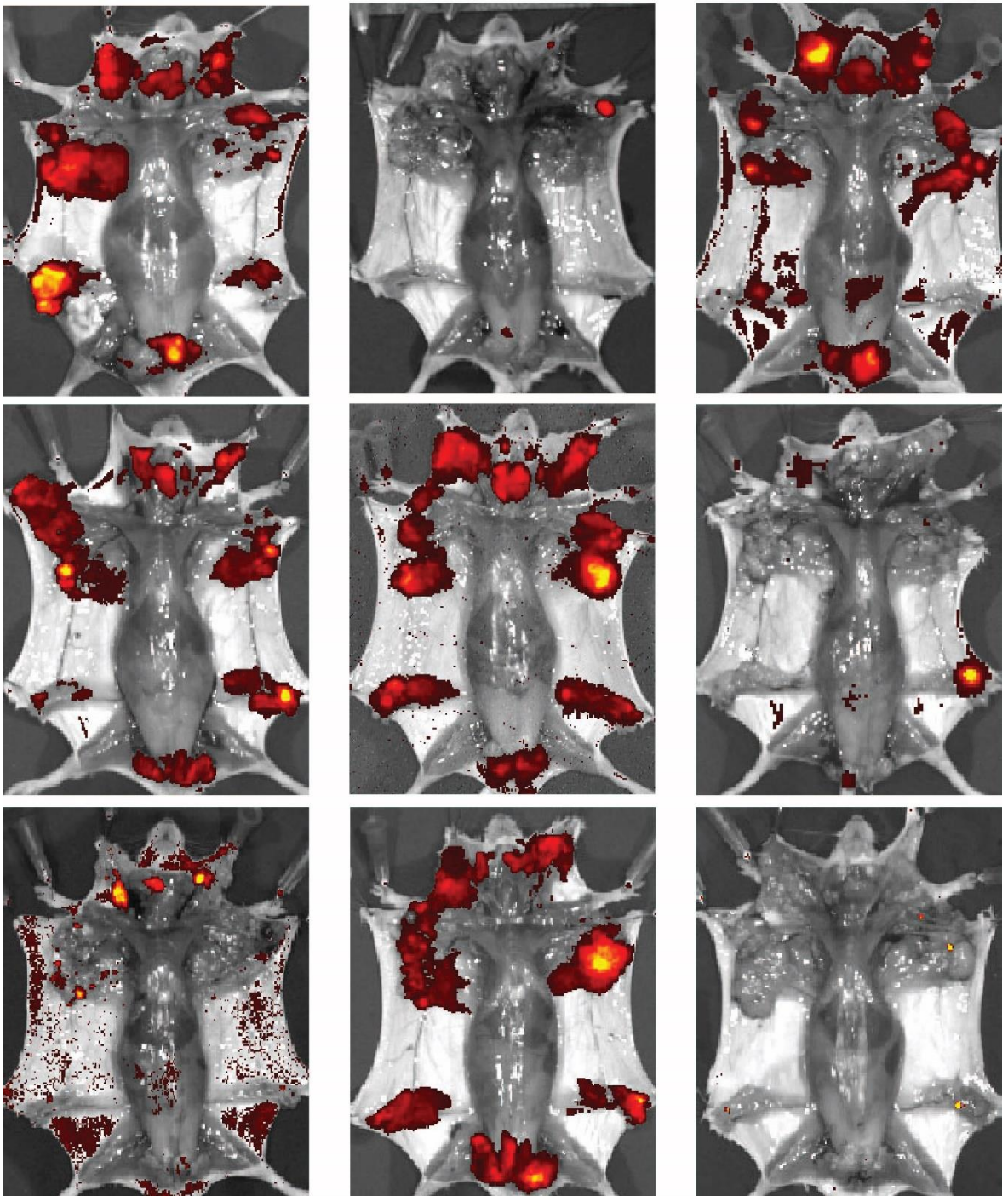


Figure 3. 4 Imaging analysis of the RFP reporter gene in *Runx1*-deficient MMTV-PyMT mice.

Representative snapshots of clinical end point *MMTV-PyMT;MMTV-Cre;tdRFP;Runx1^{fl/fl}* mice (n=14) showing expression of the RFP reporter gene as detected via the IVIS Spectrum *in vivo* imaging system. Mice were euthanized, placed on a black cardboard and imaged for RFP fluorescence. Animals were illuminated via the 554 nm excitation filter, whereas fluorescence was detected with the 581 nm emission filter. Images were captured with an Auto exposure time using the small binning and F/Stop 2 settings. RFP, red fluorescent protein.

MMTV-PyMT;MMTV-Cre;tdRFP;Runx1^{wt/fl}

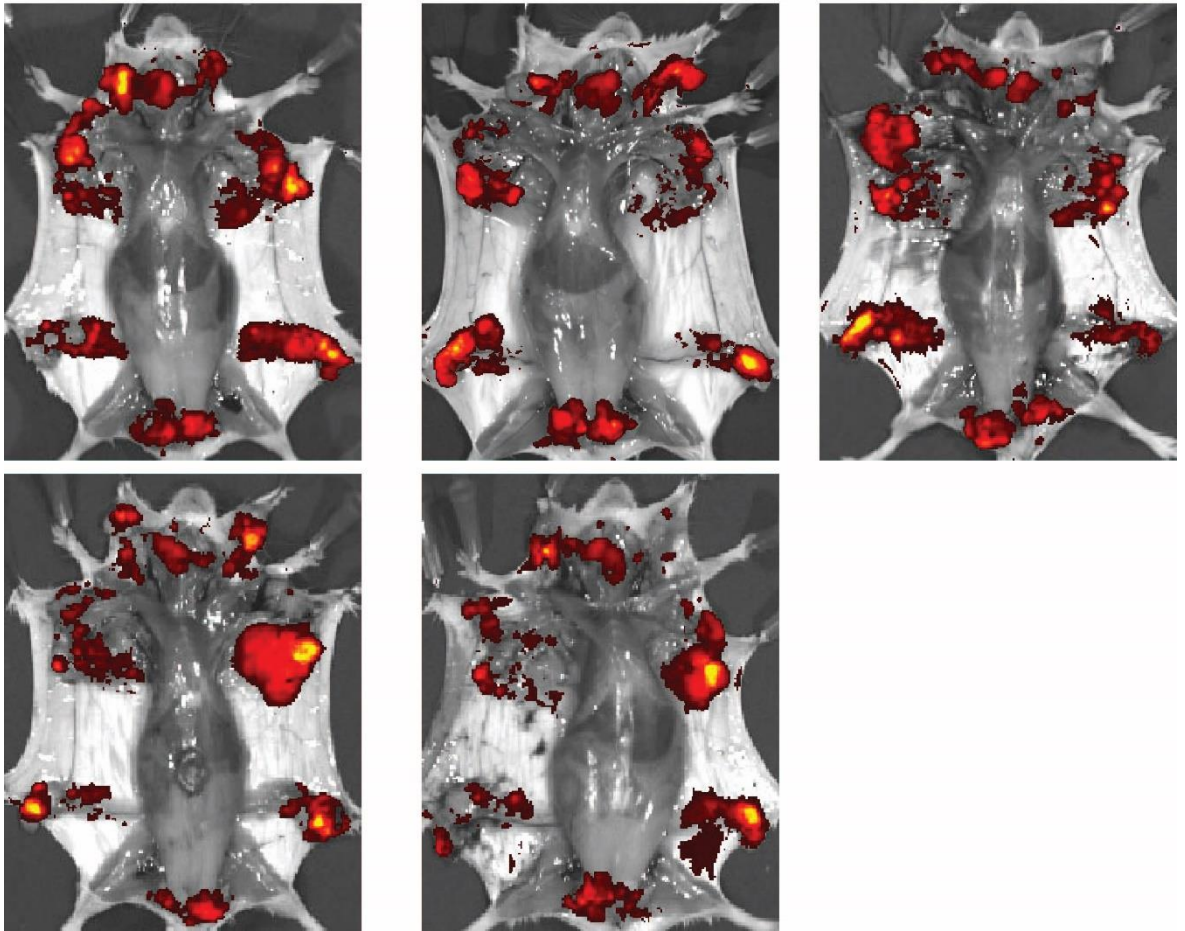


Figure 3. 5 Imaging analysis of the RFP reporter gene in *MMTV-PyMT* mice carrying only one deleted copy of the *Runx1* gene.

Representative snapshots of clinical end point *MMTV-PyMT;MMTV-Cre;tdRFP;Runx1^{wt/fl}* mice (n=5) showing expression of the RFP reporter gene as detected via the IVIS Spectrum *in vivo* imaging system. Mice were euthanized, placed on a black cardboard and imaged for RFP fluorescence. Animals were illuminated via the 554 nm excitation filter, whereas fluorescence was detected with the 581 nm emission filter. Images were captured with an Auto exposure time using the small binning and F/Stop 2 settings. RFP, red fluorescent protein.

3.3.4 *Ex vivo* characterization of MMTV-PyMT derived mammary epithelial cells through the use of the RFP reporter gene

Considering the higher percentage of RFP- animals detected in the *Runx1^{fl/fl}* group of mice in respect to the *Runx1^{wt/wt}* control one (33% versus 11%), *ex vivo* characterization of the properties of RFP+ and RFP- cells was next performed. The presence of RFP positivity could in fact be used not only as a surrogate measure of MMTV-Cre expression, yet also to infer the extent of Cre recombinase activity over recombination of the *Runx1^{fl/fl}* allele. To this end, clinical end point mice from the *Runx1^{fl/fl}* cohort of *MMTV-PyMT;MMTV-Cre;tdRFP* animals were euthanized and all tumour-bearing and non-tumour bearing mammary glands harvested (Figure 3. 6). Through mechanical dissociation of the organs via the use of a tissue chopper and enzymatic digestion of chopped tissues at 37°C in the presence of collagenase and hyaluronidase, a fine mammary tissue paste was collected. Following a series of washes to remove all cell debris and the majority of non-epithelial cells, digested mammary tissue was subjected to red blood cell lysis. After two sequential steps of trypsinization and filtration, a single-cell suspension was finally obtained. At this stage, the cell mixture was labelled with a live/dead marker (DAPI) and run through the fluorescence activated cell sorting (FACS) in order to separately collect live (DAPI-) RFP- and RFP+ MMECs. In an attempt to validate the activity of the MMTV-Cre recombinase and assess transcript levels of *Runx1* by qPCR, RNA was extracted from both RFP- and RFP+ groups. In addition, the levels of *Runx2* transcripts were also evaluated in order to investigate the presence of putative compensatory mechanisms between the two *Runx* genes. In view of the reduction of RFP+ cells observed in the *Runx1^{fl/fl}* cohort of *MMTV-PyMT;MMTV-Cre;tdRFP* mice, it was hypothesized that deletion of *Runx1* could impinge on the survival and/or tumourigenic potential of PyMT cells. To test this hypothesis, RFP- and RFP+ sorted cells were challenged through the tumoursphere assay by plating 10,000 live cells per well in low-adherent plates in the presence of growth factors. Whilst differentiated cells undergo *anoikis* (Frisch et al., 1994), cells with stem/progenitor characteristic are believed to survive and form spheres in suspension (Dontu et al., 2003). After a week, the number of tumourspheres per well was manually counted and collected for RNA and qPCR purposes (Figure 3. 6).

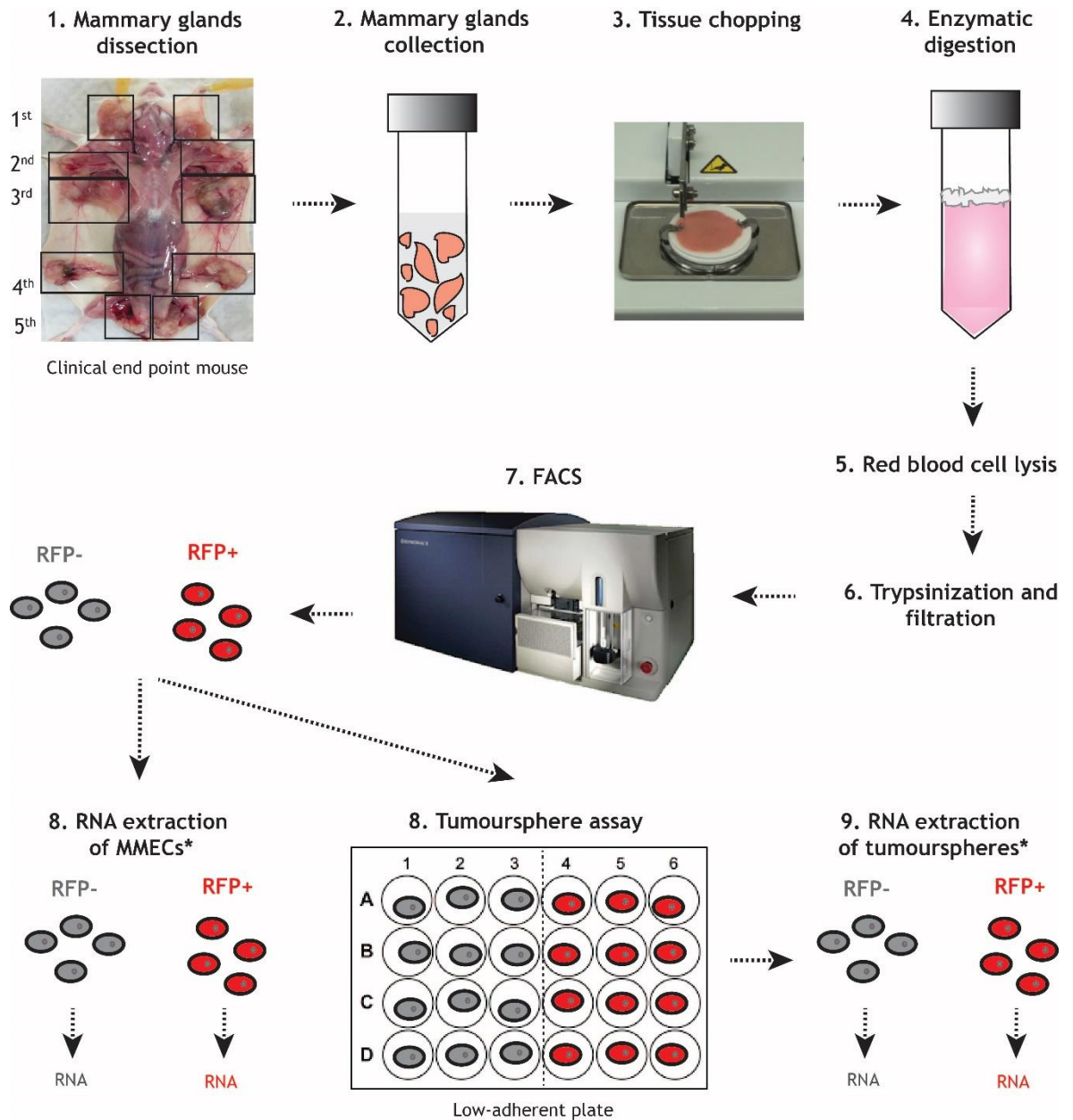


Figure 3. 6 Pipeline for the extraction and *ex vivo* characterization of RFP+ and RFP- MMECs from MMTV-PyMT mice.

Workflow of the nine steps required to extract and characterize the properties of RFP+ and RFP- MMECs extracted from *MMTV-PyMT; MMTV-Cre; tdRFP; Runx1^{fl/fl}* and *Runx1^{wt/wt}* mice. Clinical end point mice are euthanized and (1) all five pairs of tumour-bearing and nontumour-bearing mammary glands are collected and (2) placed in a 50 ml tube with PBS. (3) Mammary glands are mechanically disrupted via a tissue chopper and (4) enzymatically digested at 37°C for 1 hour and a half in the presence of collagenase and hyaluronidase. (5) Digested tissue is treated with NHCl₄ for 5 minutes at room temperature to lyse red blood cells. (6) Lysate is trypsinized for 10 minutes at 37°C and filtered through 70 μm pores. (7) A single cell suspension enriched in MMECs is run through FACS in order to separate live RFP+ and RFP- cells. (8) Sorted RFP+ and RFP- MMECs are utilized for RNA extraction purposes and/or plated at a density of 10,000 live cells per well using low-adherent plates in the presence of EGF and FGF2 (tumoursphere assay). After a week, the number of tumourspheres per well is manually counted and (9) spheres from all 12 technical replicates are collected for RNA extraction purposes. Asterisks indicate that RNA extraction was not always possible due to low amount of sorted MMECs or tumourspheres. FACS, fluorescence-activated cell sorting; MMEC, mouse mammary epithelial cell; RFP, red fluorescent protein.

Following extraction of MMECs from the *Runx1^{fl/fl}* cohort of *MMTV-PyMT;MMTV-Cre;tdRFP* mice, decreased levels of *Runx1* expression were displayed by RFP+ cells as compared to RFP- ones in three independent experiments (Figure 3. 7A). These results confirmed the presence of an active MMTV-Cre, able to recombine both *tdRFP* and *Runx1^{fl/fl}* alleles. Of note, a similar pattern of expression could also be observed for *Runx2*, with exception of sample #3 where no difference was found between groups (Figure 3. 7B). When the tumourigenic ability of RFP- and RFP+ cells was tested in seven independent experiments, five of them showed a significant reduction of tumoursphere formation in the RFP+ group. No significant difference was instead observed in samples #3 and #4 (Figure 3. 7C). In addition, RFP+ derived tumourspheres generally appeared to be smaller in size than the negative counterpart (Figure 3. 7D). Altogether, these results suggested that deletion of *Runx1* was able to decrease the tumourigenic and proliferative ability of PyMT cells. In line with the latter, sample #3 was the only one to display the smallest fold change difference of *Runx1* levels between the RFP- and the RFP+ groups. Interestingly, however, following RNA extraction of RFP- and RFP+ derived tumourspheres, a modest increase in *Runx1* levels was detected in the RFP+ cells of all four samples tested (Figure 3. 7E). As MMTV-Cre-mediated deletion of the *Runx1^{fl/fl}* allele was not 100% efficient, this result was indicative of a survival advantage shown by the few *Runx1*-proficient cells present in the original mixture. Preliminary qPCR analysis of *Runx2* resembled the levels of expression displayed by extracted MMECs, at least for the two samples tested (Figure 3. 7F). This data indicated not only that *Runx2* expression remained unchanged during growth of MMECs in suspension, but more importantly that no compensatory mechanism occurred upon deletion of *Runx1*.

To assess if expression of the tdRFP transgene could impinge upon the molecular and functional properties of MMECs, the same experiments were performed by extracting cells from the *Runx1^{wt/wt}* cohort of *MMTV-PyMT;MMTV-Cre;tdRFP* mice. In doing so, a high degree of variability was found among mice in relation to expression of both *Runx1* and *Runx2* genes. As such, whilst two independent experiments showed comparable *Runx1* levels, RFP+ cells of sample #2 displayed an increased *Runx1* expression as compared to the negative control (Figure 3. 8A). Similarly, a modest increase in *Runx2* levels was reported by RFP+ cells of samples #2 and 3, whereas no change was observed in specimen #4 (Figure 3.

8B). Some inconsistencies were also noticed when RFP- and RFP+ *Runx1*^{wt/wt} cells were challenged in a tumoursphere assay. In fact, whilst an equal tumourigenic potential between RFP+ and RFP- MMECs could be observed in samples #1 and #3, a significantly lower or higher number of tumourspheres was reported by RFP+ cells of specimens #2 and #4 (Figure 3. 8C). No difference, however, was observed when the size of RFP- and RFP+ derived tumourspheres was compared across all four independent experiments (Figure 3. 8D). Lastly, qPCR analysis of *Runx1* levels showed no major changes between the two RFP groups in the three samples tested (Figure 3. 8E). A modest reduction of *Runx2* levels was instead displayed by RFP+ derived spheres from all three independent experiments (Figure 3. 8F). Thus, before drawing any conclusions about the impact the tdRFP transgene might have on the functional and molecular features of MMECs, more experiments will need to be performed. This might in turn help to reduce the level of “noise” and allow a better interpretation of the decreased tumourigenic potential displayed by PyMT cells upon loss of *Runx1*.

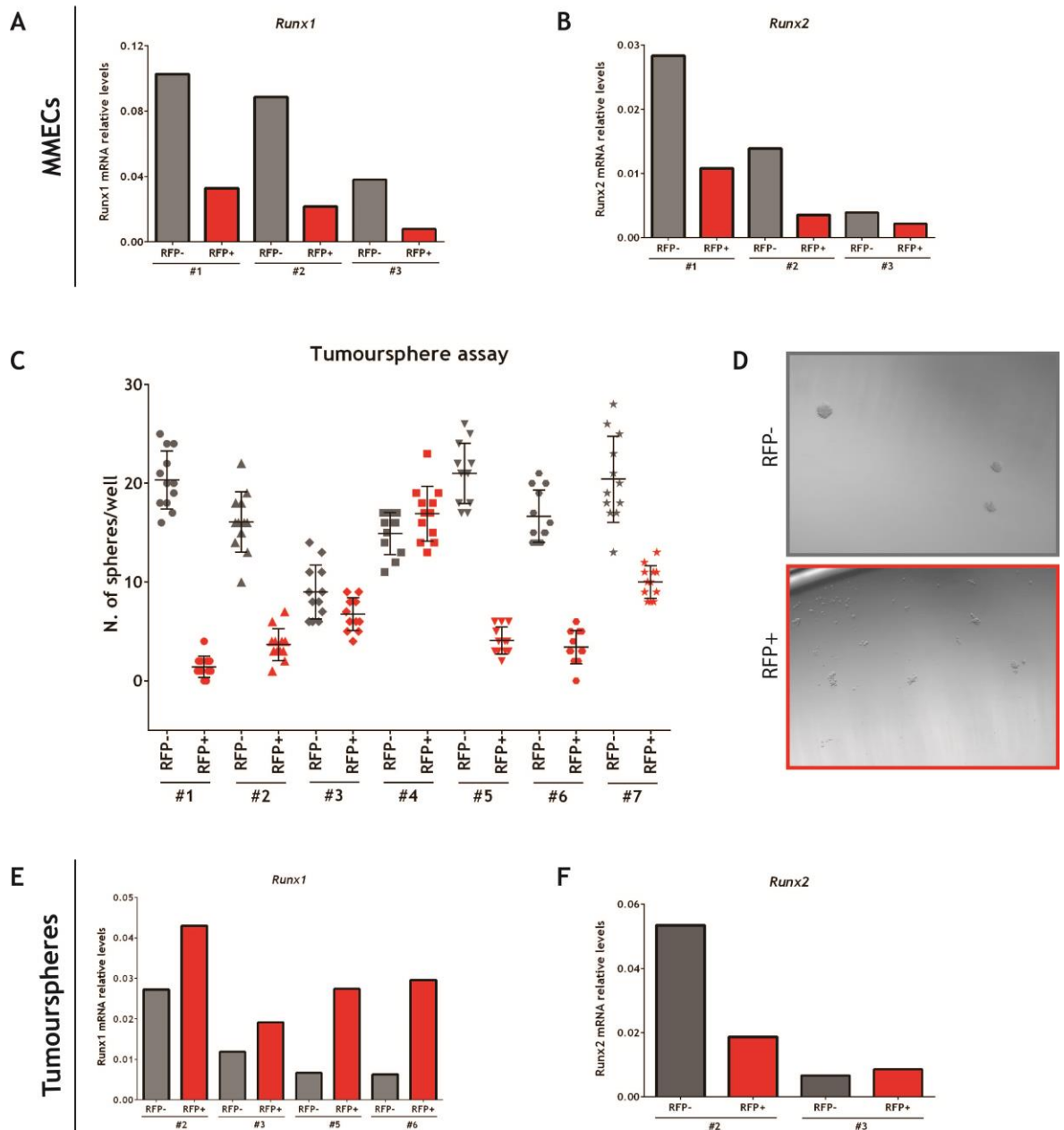


Figure 3. 7 Characterization of RFP+ and RFP- cells from *Runx1*-deficient *MMTV-PyMT* mice.

Bar charts of *Runx1* (A) and *Runx2* (B) transcript levels and tumoursphere assay (C) of RFP- and RFP+ MMECs extracted from *MMTV-PyMT;MMTV-Cre;tdRFP;Runx1^{fl/fl}* mice. (D) Representative pictures of RFP-negative and RFP-positive-derived tumourspheres. One image of n=12 is shown per group. Pictures were taken with the 4x objective lens of the Olympus CKX41 microscope. Bar charts of *Runx1* (E) and *Runx2* (F) transcript levels of RFP- and RFP+ tumourspheres. Clinical end point mice were euthanized, all their mammary glands harvested, digested and sorted for RFP expression. RFP- and RFP+ cells were either used for qPCR analysis or plated in suspension in the presence of growth factors (tumoursphere assay) to test their tumourigenic potential. After a week, the number of tumourspheres per well was manually calculated. Tumourspheres from all 12 technical replicates were then collected in order to extract RNA for qPCR purposes. *Runx1* and *Runx2* mRNA levels are relative to the *Gapdh* reference gene. The number displayed below each graph indicates independent experiments performed by harvesting the mammary glands from individual mice. MMECs, mouse mammary epithelial cell; qPCR, quantitative polymerase chain reaction; RFP, red fluorescent protein.

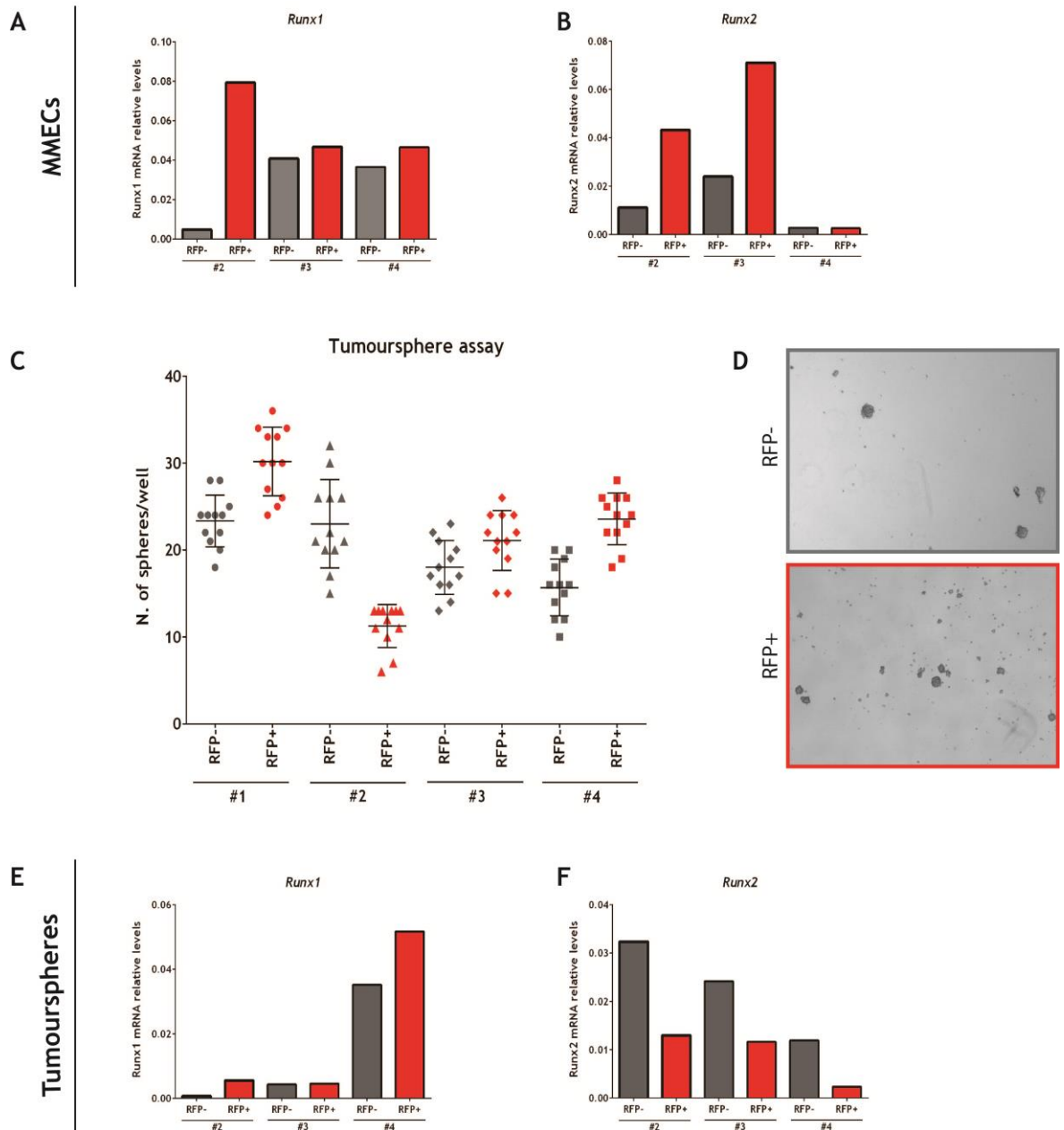


Figure 3. 8 Characterization of RFP+ and RFP- cells from *Runx1*-proficient *MMTV-PyMT* mice.

Bar charts of *Runx1* (A) and *Runx2* (B) transcript levels and tumoursphere assay (C) of RFP- and RFP+ MMECs extracted from *MMTV-PyMT;MMTV-Cre;tdRFP;Runx1^{wt/wt}* mice. (D) Representative images of RFP-negative and RFP-positive-derived tumourspheres. One image of n=12 is shown per group. Pictures were taken with the 4x objective lens of the Olympus CKX41 microscope. Bar charts of *Runx1* (E) and *Runx2* (F) transcript levels of RFP- and RFP+ tumourspheres. Clinical end point mice were euthanized, all their mammary glands harvested, digested and sorted for RFP expression. RFP- and RFP+ cells were either used for qPCR analysis or plated in suspension in the presence of growth factors (tumoursphere assay) to test their tumourigenic potential. After a week, the number of tumourspheres per well was manually calculated. Tumourspheres from all 12 technical replicates were then collected in order to extract RNA for qPCR purposes. *Runx1* and *Runx2* mRNA levels are relative to the *Gapdh* reference gene. The number displayed below each graph indicates independent experiments performed by harvesting the mammary glands from individual mice. MMECs, mouse mammary epithelial cell; qPCR, quantitative polymerase chain reaction; RFP, red fluorescent protein.

3.3.5 Histopathological analysis of PyMT mammary tumour lesions

In view of the delayed tumour progression observed in the *Runx1^{fl/fl}* cohort of mice, it remained to be addressed if deletion of *Runx1* could interfere with the well-described histopathology characterizing the MMTV-PyMT breast cancer mouse model. To this end, clinical end point mammary tumours from the *Runx1^{wt/wt}* and *Runx1^{fl/fl}* cohorts of *MMTV-PyMT;MMTV-Cre;tdRFP* mice were formalin-fixed paraffin-embedded in order to be analysed by H&E and IHC. Upon H&E examination, mammary glands from *Runx1^{wt/wt}* mice displayed the characteristic pattern of PyMT breast tumourigenesis, shown to resemble the multi-stage progression of human breast cancer (Lin et al., 2003). Indeed, besides the remaining presence of a few non-transformed mammary ducts (Figure 3. 9A), the first sign of PyMT transformation could be recognized by hyperplasia, whereby densely packed lobules started protruding from normal ducts (Figure 3. 9B). Hyperplastic lesions were then followed by the formation of adenomas, defined as masses of benign tumours characterized by the disappearance of lumen and the appearance of solid sheets of relatively uniform epithelial cells. In the initial phase of malignant transformation (early carcinomas), greater cytological atypia with increased nuclear pleomorphism could be observed (Figure 3. 9C), at later stages tumours were mainly composed of solid sheets of transformed epithelial cells (Figure 3. 9D). When *Runx1^{wt/wt}* mammary tumours were analysed for Ki67, a nuclear marker of cell proliferation (Gerdes et al., 1983), very few positive cells could be visible in the remaining normal ducts (Figure 3. 9E). On the contrary, a high mitotic index was found to correlate with all stages of PyMT-driven tumourigenesis (Figure 3. 9F, G, H). In line with the well-characterized mosaicism displayed by the MMTV-Cre (Andrecek et al., 2000), RFP staining of *Runx1^{wt/wt}* mammary tumours was found to be scattered over a few MMECs present in normal ducts (Figure 3. 10A). Consequently, a patchy pattern of RFP expression was exhibited at all stages of PyMT tumourigenesis, wherein fully positive lobules were found to be adjacent to completely negative ones (Figure 3. 10B, C, D). Interestingly, however, a different scenario held true for RUNX1 expression. In line with high levels of transcripts reported in virgin mammary glands (Blyth et al., 2010), RUNX1 protein expression was observed in the remaining normal mammary ducts (Figure 3. 10E). Whilst this pattern appeared to be maintained during mammary

hyperplasia (Figure 3. 10F), no staining could be detected in adenomas (Figure 3. 10G) nor late carcinomas (Figure 3. 10H) of *Runx1^{wt/wt}* mice. Collectively, these data further corroborated a tumour suppressive function exerted by RUNX1, present in normal mammary glands, yet absent in incipient and established PyMT tumours. This was supported not only by the expected absence of RUNX1 positivity in RFP+ tumours, yet also by its lack of expression in RFP- ones. When the same analysis was applied to the *Runx1^{fl/fl}* cohort of *MMTV-PyMT; MMTV-Cre; tdRFP* mice, no major differences emerged in terms of histopathology nor mitotic index of mammary tumours. A degree of variability was instead found in regards to RUNX1. As such, whilst some mice showed detectable RUNX1 expression in normal mammary glands, as well as in hyperplastic and late carcinoma lesions (Figure 3. 11A, B), in some others these were found to be completely negative (Figure 3. 11E, F). This variability could be ascribed to differential levels of MMTV-Cre expression and/or activity between mice. Regardless, no RUNX1 expression could be observed in adenomas or late carcinomas (Figure 3. 11C, D, G, H), in line with the pattern showed by *Runx1^{wt/wt}* mice. Lastly, in view of the high degree of homology existing among the *Runx* genes and the possibility to compensate for each other, IHC analysis for RUNX2 was also performed. Differently from RUNX1, RUNX2 expression in normal mammary ducts of *Runx1^{wt/wt}* mice appeared to be very faint in the epithelium, yet more abundant in the stroma (Figure 3. 12A). Whilst some epithelial expression was observed at the adenoma/early carcinoma stage (Figure 3. 12C), RUNX2 was observed in the stroma of late stage PyMT tumours (Figure 3. 12D). When mammary tumours from the *Runx1^{fl/fl}* cohort of mice were analysed, RUNX2 expression was also found to be located in the surrounding stroma of normal ducts (Figure 3. 12E). Yet, this time, expression appeared to be stronger in intensity than in *Runx1^{wt/wt}* mice. Moreover, whilst hyperplastic lesions of *Runx1^{wt/wt}* mice showed no RUNX2 staining (Figure 3. 12B), the gene now appeared to be expressed in the hyperplastic epithelium of *Runx1^{fl/fl}* mice (Figure 3. 12F). Finally, positivity for RUNX2 was shown in both the epithelium and stroma of adenoma and late carcinoma tumours (Figure 3. 12G). Based on the above and in view of the delayed tumour progression of *Runx1^{fl/fl}* mice, it is tempting to speculate a compensatory tumour suppressive role played by RUNX2, able to halt progression of PyMT-driven tumour lesions in the absence of *Runx1*.

MMTV-PyMT;MMTV-Cre;tdRFP;Runx1^{wt/wt}

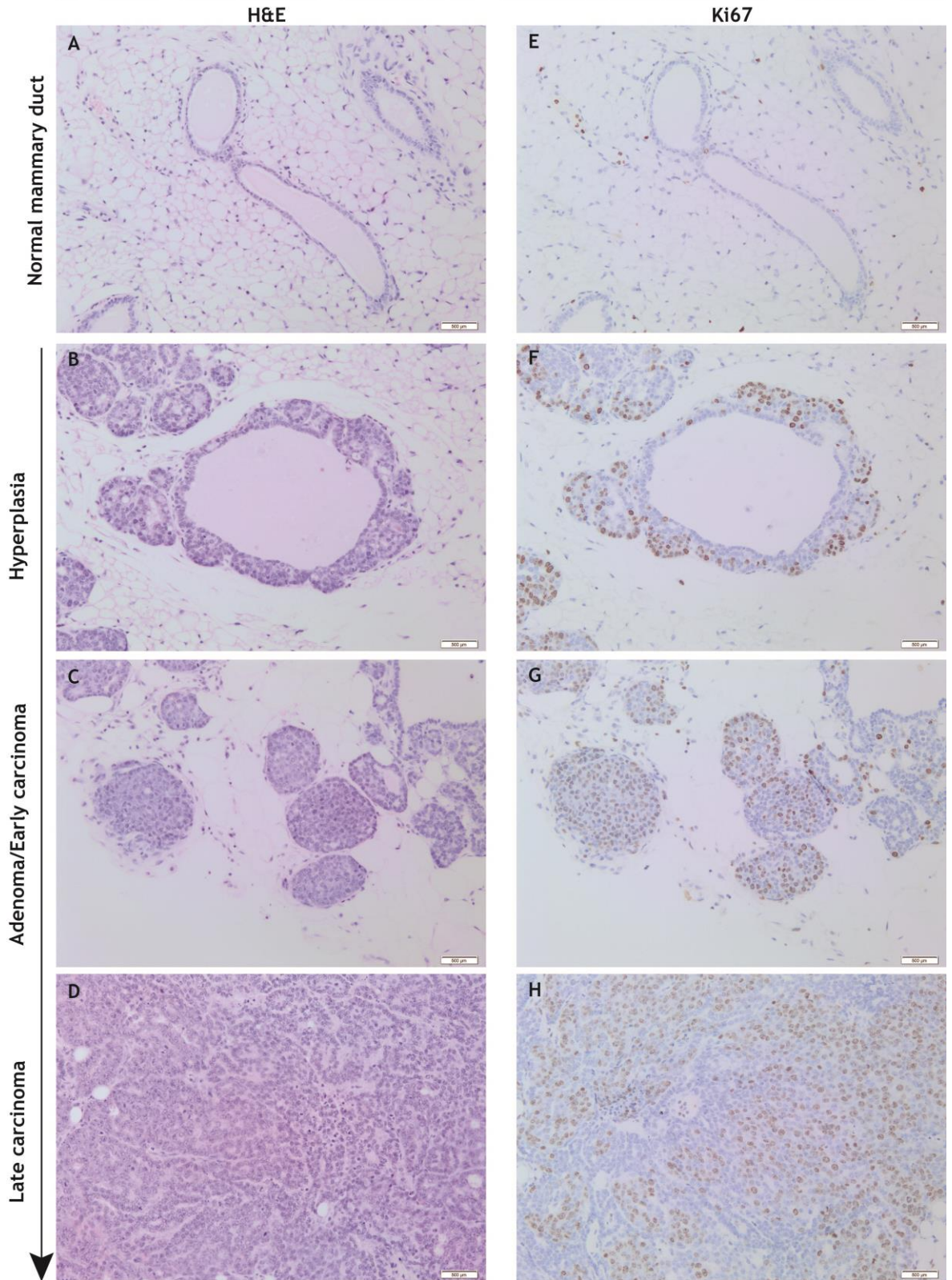


Figure 3. 9 H&Es and Ki67 protein expression analysis of MMTV-PyMT mammary tumours.

Representative images of H&E (A, B, C, D) and Ki67 stainings (E, F, G, H) of mammary tumours from the *MMTV-PyMT;MMTV-Cre;tdRFP;Runx1^{wt/wt}* cohort of mice. One representative image of $n=3$ is shown. Scale bar, 500 μm . The different stages of PyMT-driven breast tumourigenesis are depicted on the left. H&E, haematoxylin eosin.

MMTV-PyMT;MMTV-Cre;tdRFP;Runx1^{wt/wt}

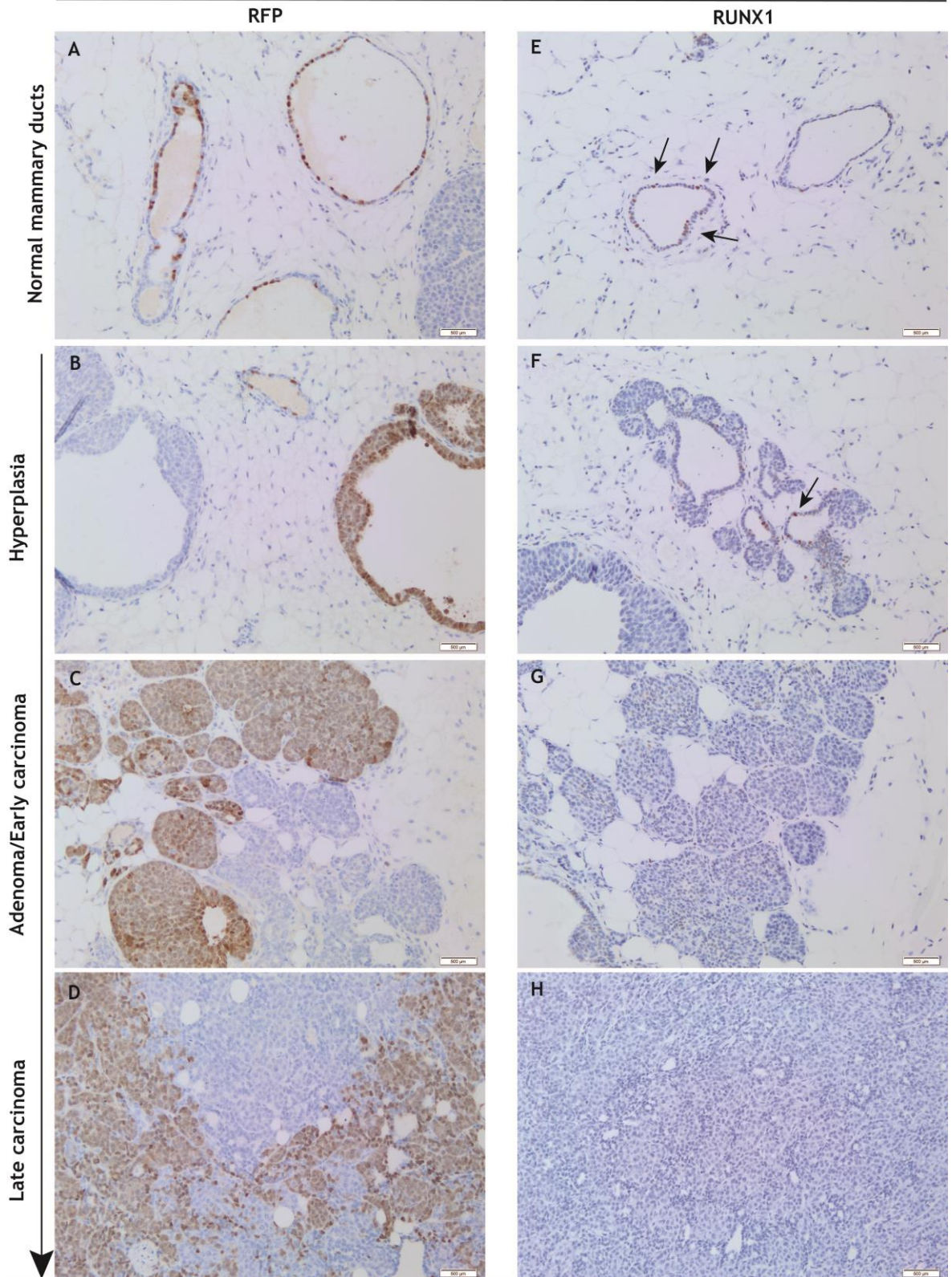


Figure 3. 10 RFP and RUNX1 expression analysis of MMTV-PyMT mammary tumours.

Representative IHC images of RFP (A, B, C, D) and RUNX1 (E, F, G, H) staining of mammary tumours from the *MMTV-PyMT;MMTV-Cre;tdRFP;Runx1^{wt/wt}* cohort of mice. One representative image of $n=3$ is shown. Scale bar, 500 μ m. The different stages of PyMT-driven breast tumourigenesis are depicted on the left. Arrows indicate the location of RUNX1 positive cells in normal mammary ducts and hyperplastic lesions. IHC, immunohistochemistry.

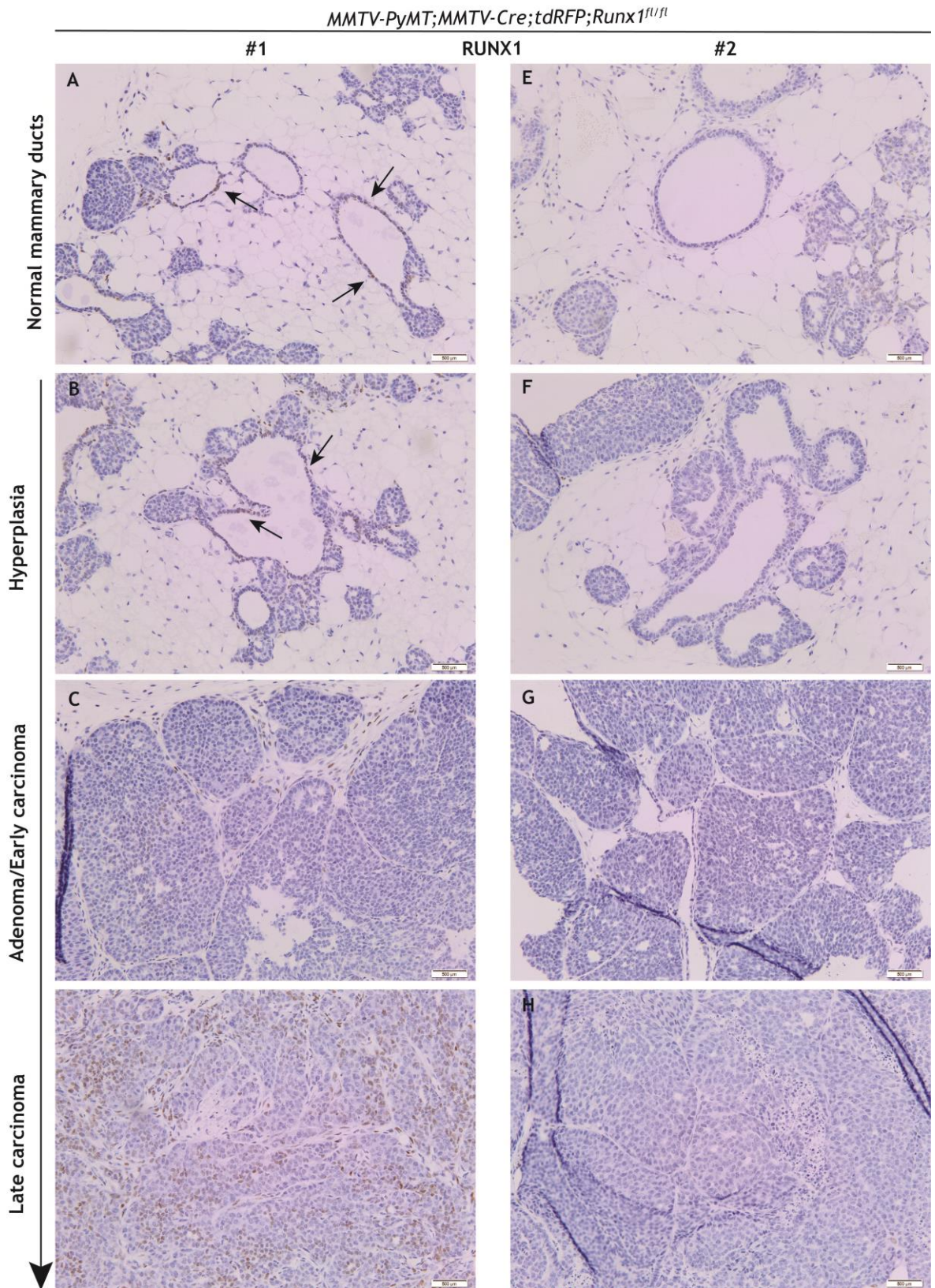


Figure 3. 11 RUNX1 expression analysis of *Runx1*-deficient MMTV-PyMT mice.

Representative IHC images of RUNX1 expression shown by mammary tumour from two independent (#1 and #2) mice of the *MMTV-PyMT;MMTV-Cre;tdRFP;Runx1^{fl/fl}* cohort. One representative image of n=3 is shown. Scale bar, 500 μ m. The different stages of PyMT tumorigenesis are depicted on the left. Arrows indicate RUNX1 positive cells in normal and hyperplastic ducts. IHC, immunohistochemistry.

RUNX2

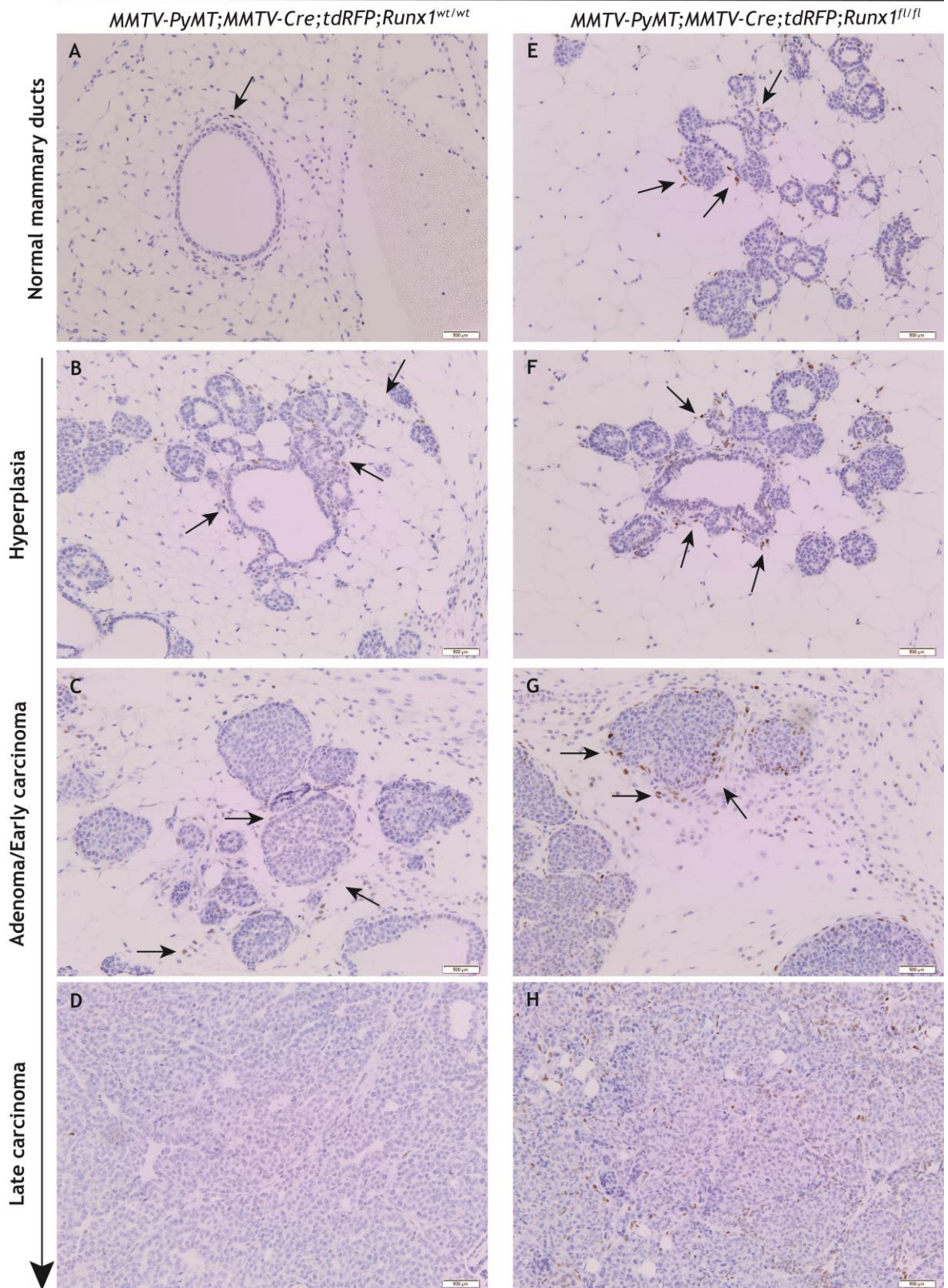


Figure 3. 12 RUNX2 expression analysis of MMTV-PyMT in the presence or absence of *Runx1*.

Representative IHC images of RUNX2 expression shown by mammary tumour from the *MMTV-PyMT;MMTV-Cre;tdRFP;Runx1^{wt/wt}* (A, B, C, D) and *Runx1^{fl/fl}* cohort (E, F, G, H). One representative image of $n=3$ is shown per cohort at each stage. Scale bar, 500 μm . The different stages of PyMT tumourigenesis are depicted on the left. Arrows indicate RUNX2 positive cells. IHC, immunohistochemistry.

3.4 Discussion

Following the characterization of the genomic landscape of human breast cancer, the focus of research attention recently moved onto the putative role played by infrequently mutated genes. Interestingly, *RUNX1* was found to be one of them (Riggio and Blyth, 2017), with somatic mutations reported in biopsies of breast cancer patients and predicted to cause *loss-of-function* of the protein. Due to its widespread use, high penetrance and short tumour latency, the MMTV-PyMT breast cancer GEMM was exploited in the attempt to investigate the function played by *RUNX1* in the initiation, maintenance and progression of breast cancer. As both homozygous and heterozygous deletion of the gene caused a significant acceleration of PyMT-driven palpable tumours formation, *Runx1* was ascribed as a tumour suppressor gene. Surprisingly, however, this acceleration did not result in decreased overall survival of the mice, as growth of established PyMT tumour lesions appeared halted in the absence of the gene. In view of the latter, two possible scenarios could be envisioned. Firstly, *RUNX1* could exert a chameleon-like role, acting as a tumour suppressor at early stages and an oncogene at later stages of the disease. Alternatively, compensatory mechanisms, perhaps exerted by *Runx2*, might take place in the absence of *Runx1*. To test the first hypothesis, an inducible model could be exploited in order to either overexpress or delete *Runx1* in established PyMT-driven tumours. If *RUNX1* is an oncogene at later stages of tumourigenesis, then its overexpression should further accelerate the growth of PyMT mammary lesions, whereas its deletion would delay their progression. To test the second hypothesis, combined deletion of *Runx1* and *Runx2* would need to be performed. If *RUNX2* acted as a tumour suppressor, then its deletion should accelerate the formation of palpable lesions, as well as fostering the growth of established ones on a *Runx1*-null background. Consequently, this should result in decreased overall survival of *Runx1*- and *Runx2*-deficient mice as compared to controls. Of note, the possibility of *Runx2*-independent compensatory mechanisms should also be taken into account. To this end, being *RUNX1* a potent activator and repressor of gene transcription, a molecular analysis of *Runx1* downstream targets might help unveil the causative players of the delayed growth showed by *Runx1*-deficient PyMT mammary tumours.

In line with a tumour suppressive function exerted by RUNX1 were also the observations gathered from IHC analysis of MMTV-PyMT mammary tumours. According to the well-characterized histopathology displayed by this model, four different stages of PyMT-driven tumorigenesis could be discerned: hyperplasia, adenomas, early carcinomas and late carcinomas (Lin et al., 2003). In addition to the latter, the presence of a few non-transformed mammary ducts could also be observed. In this regard, RUNX1 levels appeared to be restricted exclusively to normal mammary ducts and hyperplastic lesions of MMTV-PyMT mice, whereas no staining was seen in adenomas or early and late carcinomas. Interestingly, this pattern of expression did not seem to correlate with RFP positivity, not only because established PyMT lesions displayed a patchy pattern of RFP expression, but also because RFP- PyMT tumours showed lack of RUNX1 levels. In view of above, the decreased tumourigenic potential displayed by *Runx1*-deleted RFP+ cells should perhaps be better ascribed to the function exerted by the gene during the very early stages of PyMT-driven oncogenic transformation of normal epithelium. Collectively, these results suggested the ability of PyMT incipient mammary lesions to originate in RUNX1 negative cells or to downregulate transcription of the *Runx1* gene during oncogenic transformation of the mammary epithelium.

In line with the latter, *RUNX1* mRNA downregulation was reported within a 17-gene signature linked to breast cancer metastasis (Ramaswamy et al., 2003). In addition, RUNX1 protein expression appeared decreased in high-grade breast cancers versus low/mid-grade tumours (Kadota et al., 2010). Consistent with its ability to act as a positive regulator of E-cadherin (Liu et al., 2005), these observations might suggest the need of late-stage/aggressive tumours to down-regulate RUNX1 expression in order to metastasize. If this hypothesis holds true, then loss of *Runx1* should result in increased metastatic burden of MMTV-PyMT mice. Albeit macroscopic examination of lungs of *Runx1^{fl/fl}* mice did not show signs of gross metastasis, serial H&Es of the same organ will next be assessed to evaluate the presence of micro-lesions and compare them with the *Runx1^{wt/wt}* cohort of *MMTV-PyMT;MMTV-Cre* mice.

Interestingly, opposite conclusions were observed by Browne et al. (2015), who proposed an oncogenic role played by *Runx1*, due to the concomitant increase of

RUNX1 expression along with PyMT tumourigenesis. In support of the latter were also complementary *in vitro* studies with *Runx1* knock-down resulting in reduced migratory and invasive ability of cells. Of note, these discrepancies might arise to the use of different RUNX1 antibodies which, in the case of Browne et al. (2015), showed high level of stromal expression and elevated levels of background, indicating some degree of non specificity.

Following the intrinsic molecular classification of human breast cancer (see Chapter 1), several gene expression based studies have been carried out in the attempt to compare the molecular profile of different breast cancer GEMMs against the five intrinsic subtypes of the human disease (Perou et al., 2000; Sorlie et al., 2001). Accordingly, some GEMMs were shown to develop more homogeneous tumours with consistent expression patterns, while some others were found to be characterized by a higher degree of heterogeneity, in terms of expression and histopathological phenotypes. Based on one of these studies (Herschkowitz et al., 2007), GEMMs were clustered into 10 intrinsic groups, including one normal mammary gland group and nine tumour groups, further encompassed within four main categories: normal mammary gland samples and mesenchymal tumours; basal/MYO tumours; luminal tumours; and tumours with mixed characteristics. In this regards, the MMTV-PyMT was among “the homogeneous models” and appeared to fall within the third category of luminal tumours, displaying high levels of CK8/18, as well as Occludin and Tight junction protein 2 and 3. Nonetheless, a level of discrepancy was found to exist between the mouse and human “luminal tumour” profiles. Besides expressing high levels of CK8/18 and GATA3 luminal markers, many of the genes found in the human setting, first and foremost *ESTR-1*, were not observed in murine tumours. Due to the seminal role played by hormone signalling in controlling the transcriptional profiles of the mammary gland, both ER-negativity and the lack of ER-regulated genes (e.g. PR) were proposed to account for the majority of inconsistencies between the two species (Herschkowitz et al., 2007).

An intriguing link between PyMT mammary tumourigenesis and hormone signalling was already reported in ovariectomized mice, which showed decreased PyV-induced tumour burden as compared to controls (Berebbi et al., 1990). This phenotype, however, appeared to stem from an E2-dependency displayed by

incipient PyMT mammary lesions, yet not by more advanced tumours. These results suggested that, whilst the initial stages of PyMT-driven oncogenic transformation of the mammary epithelium relies on hormonal cues, progression of established tumours is independent of the latter. This observation was later confirmed by expression analysis of ER α and PR, which appeared increased in early stages, whilst decreased in the late stages of PyMT tumourigenesis (Lin et al., 2003). In view of the previously discussed tumour-suppressive role exerted by RUNX1 in ER+ cells (see introduction), these findings might hold the key for the accelerated tumourigenesis, yet delayed tumour progression of MMTV-PyMT mice upon *Runx1* loss.

4 Investigating the role of *Runx1* and *Runx2* in a Wnt/ β -catenin mouse model of breast cancer

4.1 Introduction

4.1.1 Canonical Wnt/ β -catenin signalling

The Wnt signalling pathway dates back to the discovery of the segment polarity gene *Wingless* in *Drosophila* and its homolog *Int-1* in mice (Rijsewijk et al., 1987). According to the traditional model, canonical Wnt signalling is initiated when Wnt ligands bind to their cognate receptor complex, composed of a member of the *Frizzled* family of genes encoding for seven-pass transmembrane receptors (Yang-Snyder et al., 1996) and a member of the low-density lipoprotein-related proteins (LPR) 5/6 (Dieckmann et al., 2010). Thus far, almost 16 Wnt ligands and 11 Frizzled receptors have been identified in vertebrates, although the function of some of them still remains elusive (Wodarz and Nusse, 1998; Polakis, 2000). The main player of canonical Wnt signalling is represented by β -catenin, a pleiotropic protein which exerts several functions within the cell. One of the first one to be described refers to its role as a cell-cell adhesion molecule, whereby β -catenin favours cytoskeleton-membrane interactions through binding of E-cadherin and α -catenin (Cowin and Burke, 1996). Additionally, β -catenin behaves as a signal transduction molecule in the nucleus, wherein it regulates gene expression programs essential for mammary gland biology as well as cancer (Gumbiner, 1995). Due to the latter, β -catenin cytoplasmic levels within the cells are tightly regulated by a multiprotein destruction complex wherein the adenomatous polyposis coli (APC) and Axin serve as scaffolds. In the absence of Wnt ligands, two kinases present within the complex, i.e. casein kinase 1 and glycogen synthase kinase 3 β (GSK3 β), act in a sequential manner to phosphorylate key serine and threonine residues located in the amino terminus of bound β -catenin. This represents a footprint which marks β -catenin for ubiquitination and proteosomal degradation (Incassati et al., 2010). The arrival of secreted Wnt ligands and engagement with membrane receptor complex prevents these events through a series of mechanisms which

are still not fully understood. This leads to phosphorylation of Disheveled, which associates with Axin to inhibit GSK β 3 function (Kishida et al., 1999). Thus, unphosphorylated β -catenin can accumulate in the cytoplasm and translocate to the nucleus, wherein it forms a bipartite transcription factor complex together with the T-cell factor (TCF)/lymphoid enhancer factor (LEF) (Eastman et al., 1999). Whilst in the absence of ligands TCF/LEF DNA binding proteins act as transcriptional co-repressor through binding with members of the Groucho/transducing-like Enhancer of split family (Chen et al., 2000), these are displaced upon β -catenin arrival resulting in a transient, yet potent, activation of gene transcription (Daniels and Weis, 2005). Recently, two additional *Drosophila* genes, which appear to be conserved in vertebrates, have been found to take part in the β -catenin transcriptional complex. These are Pygo 2/Pygopus homolog 2, required for the activation of TCF/LEF proteins, and legless/B-cell lymphoma 9, acting as a bridge between Pygopus homolog 2 and TCF-bound β -catenin (Reya and Clevers, 2005). Despite the majority of β -catenin downstream targets being obscure, among the most common mammalian transcriptional candidates are Myc and Cyclin D1, whose levels appear to be intimately linked to activation or reduction of the pathway (Lin et al., 2000). Finally, albeit other effector proteins were found to mediate noncanonical Wnt signalling pathway, the latter plays a seminal role as a potent antagonist of β -catenin through action of Wnt5 and TGF β . Equally, cumulative evidence suggests that β -catenin stabilization can occur via Wnt-independent routes, including the PTEN/Akt and the NF- κ B pathways (Incassati et al., 2010).

4.1.2 Wnt signalling, mammary stemness and the *Runx* genes

The causative link between Wnt signalling and breast cancer traces back to the discovery of *Wnt1*, *Wnt3* and *Wnt10a*, as preferential sites for MMTV insertion. Revealed as potent proto-oncogenes, aberrant expression of these ligands was shown to cause transformation of human primary epithelial cells and induction of mammary tumours (Nusse and Varmua, 1982; Roelink et al., 1990). One of the main reasons behind this phenotype relates to the crucial regulation exerted by Wnt signalling upon MaSC self-renewal and multipotency (Zeng et al., 2010). In line with the latter, this pathway was found to be essential for the specification and morphogenesis of the mammary gland (Cowin and Wysolmerski, 2010), being

detected in both the mammary lines and subsequently in the cells forming placodes (Chu et al., 2004). Through the use of Axin2::LacZ reporter mice, expression of canonical Wnt/ β -catenin signalling was later confirmed at E12.5/13.5, both in the stroma of pubertal mice around TEBs necks, as well as in the MYO layer of the ducts in adult animals (Rajaram et al., 2015). As mentioned previously (Chapter 1), activation of canonical Wnt/ β -catenin signalling is intimately linked to the paracrine mechanisms of action of ovarian hormones. Indeed, through release of RANKL and Wnt-4 by PR_B⁺ luminal cells, progesterone was shown to regulate MaSC basal expansion during ductal morphogenesis and mammary gland homeostasis in adulthood (Asselin-Labat et al., 2010; Rajaram et al., 2015). On the other hand, stabilization of β -catenin in the luminal layer, an event essential for alveologenesis, was instead shown to rely on Wnt-independent mechanisms (Incassati et al., 2010).

The *RUNX* family of genes has been shown to interact with a wide range of signalling cascades, among which the Wnt/ β -catenin pathway is by far one of the most important in terms of both mammary development and neoplasia (Ito et al., 2015). In line with the latter, *Runx2* was found to be specifically upregulated in mouse models of Wnt-driven metaplastic breast tumours (Ferrari et al., 2015), as well as in metaplastic human breast cancer (Hennessy et al., 2010). Alongside, our lab has recently shown the existence of a putative interplay between *Runx* and Wnt/ β -catenin in regulating the regenerative potential of the stem/progenitor cell population present in the mammary gland. Results showed that conditional deletion of *Runx2* in the basal layer of the mammary epithelium severely compromised mammary stemness. Accordingly, addition of the Wnt3a ligand, responsible for fostering MaSC regenerative potential, proved unable to rescue the phenotype of *Runx2*-depleted mammospheres (Ferrari et al., 2015). Although RUNX2, and RUNX1, protein expressions has been reported in both basal and luminal layers of the murine gland and human breast (www.proteinatlas.org), the basal compartment showed the highest levels of transcripts for both genes. Nonetheless, *Runx1* expression in extracted basal MMECs appeared to be significantly higher than *Runx2*, whereas *Runx3* could not be found in either epithelial compartment (McDonald et al., 2014; van Bragt et al., 2014). These observations unleashed the question as to what role could

Runx1 and *Runx2* possibly play in the basal layer of the mammary epithelium and how their expression impinged upon the Wnt/ β -catenin signalling pathway.

4.2 Experimental procedures

4.2.1 Generation of a novel Wnt/ β -catenin-driven breast cancer mouse model

To study the *in vivo* interplay between the *Runx* genes and Wnt/ β -catenin, it was first necessary to generate a GEMM of Wnt/ β -catenin-driven mammary tumourigenesis. To achieve this aim, a line of mice carrying a stabilized form of β -catenin (*Catnb*^{wt/lox(ex3)}) was used (Harada et al., 1999). The latter was characterized by the presence of loxP recombination sites flanking exon 3 of the gene, which contains critical residuals for β -catenin degradation. As such, removal of this exon allows the generation of a stabilized β -catenin protein, thus mimicking constitutive activation of the Wnt/ β -catenin signalling pathway reported by many epithelial cancers (Harada et al., 1999). To allow recombination of the allele specifically in the mammary epithelium, *Catnb*^{wt/lox(ex3)} mice were crossed onto a transgenic line of mice wherein the expression of the Cre DNA-recombinase was under the control of a mammary specific promoter. In view of what was discussed above, the use of a basal promoter (e.g. K14) may have been considered a preferred option. However, when choosing a driver it is imperative to bear in mind not only the specificity of its expression, but also the impact of the recombined genetic events in the targeted tissues. As K14 is ubiquitously expressed across all basal epithelial tissues (Byrne et al., 1994) and given the importance of the Wnt/ β -catenin pathway in the latter compartment, the use of the ovine BLG gene promoter was chosen. Owned to its specific function in the mammary epithelium, wherein it encodes for a milk secreted protein (Selbert et al., 1998), crossing of the BLG-Cre line with *Catnb*^{wt/lox(ex3)} mice allowed conditional activation of the Wnt/ β -catenin signalling specifically in the mammary gland. Importantly, whilst BLG-Cre and *Catnb*^{wt/lox(ex3)} mice have been extensively used worldwide, our lab was the first one to cross these lines together, thus giving rise to a new conditional breast cancer mouse model. In view of the crucial role played by the Wnt/ β -

catenin pathway during mammary gland pubertal and reproductive development (Alexander et al., 2012), as well as the predominant activity of BLG-Cre during lactation (Selbert et al., 1998), all cohort females employed in this study were always carrying one mutant allele of the *Catnb* gene (*Catnb*^{wt/lox(ex3)}).

To investigate if deletion of *Runx1* and *Runx2* impinged on Wnt/ β -catenin driven mammary tumourigenesis, *Runx1*^{fl/fl} and *Runx2*^{fl/fl} mice were crossed onto *BLG-Cre;Catnb*^{wt/lox(ex3)} mice to generate two separate conditional knock-out colonies: the *BLG-Cre;Catnb*^{wt/lox(ex3);Runx1}^{fl/fl} and *BLG-Cre;Catnb*^{wt/lox(ex3);Runx2}^{fl/fl} cohorts of mice. The *Runx1*^{fl/fl} line, previously discussed in Chapter 1, was generated in the lab of Professor Nancy Speck (Growney et al., 2005) and kindly given to us by Marella De Bruijn (Oxford). The *Runx2*^{fl/fl} line was created by Theresa Higgins and Ian Rosewell in the lab of Professor Mike Owen (ICRF labs, London) and characterized by Ferrari et al. (2015). Similarly to *Runx1*, by placing the loxP sites flanking exon 3 of the gene, recombination of *Runx2* excises the DNA binding domain, leading to the formation of a non-functional protein. Of note, all GEMM lines, and therefore all mouse cohorts described in the following chapters, were maintained on a mixed background. Furthermore, in view of the pattern of BLG-Cre expression, low in pubertal and virgin mice, while high during lactation, all females from the *BLG-Cre;Catnb*^{wt/lox(ex3);Runx1}^{wt/wt}; *Runx2*^{wt/wt} and single *BLG-Cre;Catnb*^{wt/lox(ex3);Runx1}^{fl/fl} and *BLG-Cre;Catnb*^{wt/lox(ex3);Runx2}^{fl/fl} conditional knock-out colonies were mated at the age of 12 weeks in order to undergo two rounds of parities. By doing so, expression of BLG-Cre, and therefore recombination of the *Catnb*^{wt/lox(ex3)} and either *Runx1*^{fl/fl} or *Runx2*^{fl/fl} alleles, could be maximized. All pups were standardly culled at day 0 due to lactation deficits in the β -catenin positive glands. After the second round of parity, females were monitored weekly for the formation of mammary tumours. Once a palpable lesion was noticed in any of the five pairs of murine mammary glands, this was recorded and measured twice a week with the use of calipers. When a lesion reached clinical end point, the animal was humanely sacrificed. This experimental procedure allowed the evaluation of three different parameters: the time from birth to tumour notice, the time from birth to clinical end point and the time from tumour notice to end point.

4.3 Results

4.3.1 Deletion of *Runx1*, and *Runx2*, accelerates Wnt/ β -catenin mammary tumourigenesis without affecting survival of mice

When the *Runx1*^{wt/wt}, *Runx1*^{wt/fl} and *Runx1*^{fl/fl} multiparous (MP) cohorts of *BLG-Cre;Catnb*^{wt/lox(ex3)} mice were monitored for tumour formation (Figure 4. 1A), homozygous deletion of *Runx1* resulted in a significant acceleration of palpable tumour formation (258 average days) in respect to control mice (341 average days). The same scenario did not hold true when only one copy of the gene was excised, as heterozygous (*Runx1*^{wt/fl}) mice displayed an average palpable tumour formation at 282 days (Figure 4. 1B). In view of the recent NGS findings reporting the presence of *RUNX1* somatic mutations in human breast biopsies (Banerji et al., 2012; Cancer Genome Atlas, 2012; Cornen et al., 2014; Ellis et al., 2012), this result was indicative of a tumour suppressive role exerted by the gene in a GEMM of mammary tumourigenesis. Nonetheless, no differences were observed in terms of overall survival, as both *Runx1*^{wt/fl} and *Runx1*^{fl/fl} mice showed an average time from birth to clinical end point of 335 and 347 days, respectively, which closely approached the average 370 days displayed by controls (Figure 4. 1C). Accordingly, when the time from tumour notice to clinical end point was assessed, the absence of both copies of *Runx1* resulted in a significantly extended survival (90 average days from tumour notice), compared to *Runx1*^{wt/fl} and *Runx1*^{wt/wt} mice (56 and average 53 days, respectively) (Figure 4. 1D). Two different hypotheses could be proposed to explain the intriguing pattern of Wnt/ β -catenin-driven tumourigenesis upon loss of *Runx1*. According to the first one, the gene might have a dualistic role during mammary tumourigenesis, acting as a tumour suppressor at early stages, yet as an oncogene at later stages. This is synonymous with reports showing a chameleon-like role for *RUNX1* in different tissues, as well as in different tissue-contexts (see Chapter 1). Alternatively, the delay of established Wnt/ β -catenin-driven lesions could be instead ascribed to the presence of *RUNX2*. On multiple occasions, in fact, the two genes have been shown to compensate for each other (Chuang et al., 2013), thus envisioning a scenario whereby *Runx2*, in the absence of *Runx1*, might exert a tumour suppressive role.

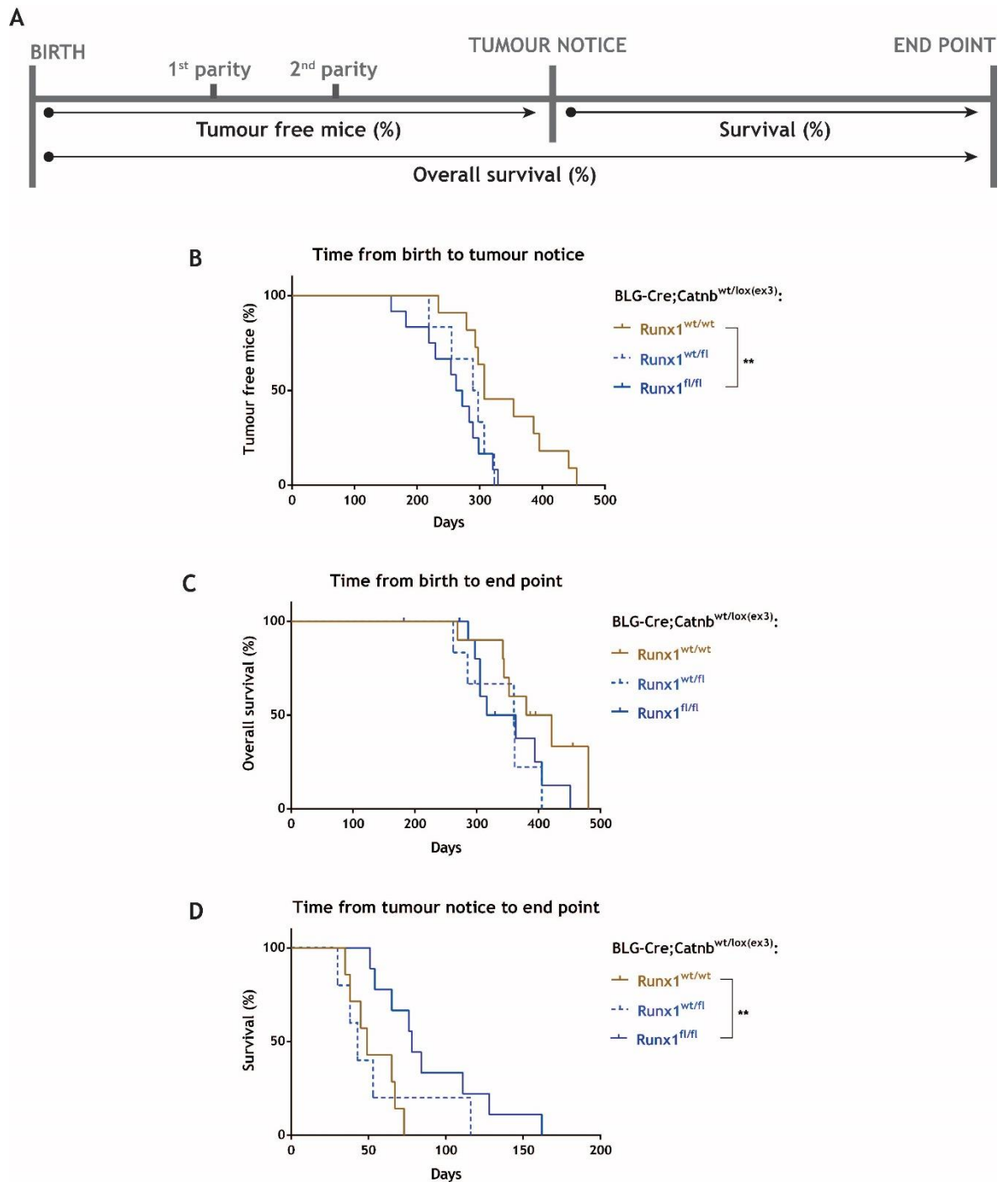


Figure 4. 1 *Runx1* deletion accelerates Wnt/ β -catenin-driven mammary tumourigenesis, yet it does not affect survival of the mice.

(A) Schematic of the three parameters used to assess the impact of *Runx1* deletion upon Wnt/ β -catenin-driven mammary tumourigenesis. 12 week old females were mated to undergo two rounds of parities in order to maximize the expression of the BLG-Cre driver. Mice were monitored twice a week for tumour formation and sacrificed once a mammary tumour lesion reached clinical end point. (B, C, D) Kaplan-Meier curves of MP *BLG-Cre;Catnb^{wt/lox(ex3)}* mice, in the absence of one copy (*Runx1^{wt/fl}*) or both copies (*Runx1^{fl/fl}*) of the *Runx1* allele. (B) Time from birth to tumour notice of *Runx1^{wt/wt}* (n=11), *Runx1^{wt/fl}* (n=6) and *Runx1^{fl/fl}* (n=12) mice. (C) Time from birth to clinical end point of *Runx1^{wt/wt}* (n=10), *Runx1^{wt/fl}* (n=6) and *Runx1^{fl/fl}* (n=12) mice. (D) Time from tumour notice to end point of *Runx1^{wt/wt}* (n=7), *Runx1^{wt/fl}* (n=5) and *Runx1^{fl/fl}* (n=9) mice. Statistical analysis was performed using the Log-rank (Mantel-Cox) test in GraphPad Prism. ***P*<0.01. MP, multiparous.

In view of the previously described role for RUNX2 in regulating mammary stemness (Ferrari et al., 2015), the same experimental pipeline was utilized to assess the impact of *Runx2* deletion upon Wnt/ β -catenin driven mammary tumorigenesis (Figure 4. 2A). In doing so, only mice carrying one deleted copy of the *Runx2* gene (*Runx2^{wt/fl}*) displayed a significant acceleration of palpable tumour formation (231 average days), whereas excision of both copies of the gene (*Runx2^{fl/fl}*) showed no difference compared to *Runx2^{wt/wt}* control mice (367 and 341 average days, respectively) (Figure 4. 2B). On the contrary, a significantly improved overall survival was found in *Runx2^{fl/fl}* mice (451 average days) when compared to both the *Runx2^{wt/fl}* and the *Runx2^{wt/wt}* cohorts (338 and 370 average days, respectively) (Figure 4. 2C). Lastly, whilst the time from tumour notice to clinical end point appeared prolonged in the absence of *Runx2*, this parameter was not statistically significant among cohorts, probably due to the low number of mice (Figure 4. 2D).

To fully understand the above results, it is important to mention that the *Runx2^{fl/fl}* transgenic line of mice was found to be affected by the presence of an hypomorphic allele. Thus, upon systemic reduction of RUNX2 levels, the majority of mice belonging to the *BLG-Cre;Catnb^{wt/lox(ex3)};Runx2^{fl/fl}* cohort generally appeared skinnier, lighter in weight and often characterized by breathing difficulties. For the same reason, many animals had to be censored out of the survival analysis due to tumour-unrelated reasons. Nonetheless, based on the results obtained from the *Runx2^{wt/fl}* cohort of mice, *Runx2* appeared to act as a tumour suppressor gene in the early stage of Wnt/ β -catenin mammary tumorigenesis. If so, this could have explained the prolonged time from tumour notice to end point displayed by *Runx1^{fl/fl}* mice (Figure 4. 1D). Equally, the trend towards delayed tumour progression shown by both cohorts of *Runx2*-deficient mice could then be ascribed to the suppressive role of RUNX1. Altogether, these observations supported the notion of a high degree of homology displayed by the *Runx* genes, able to compensate for each other at least in the context of aberrant Wnt/ β -catenin signalling pathway.

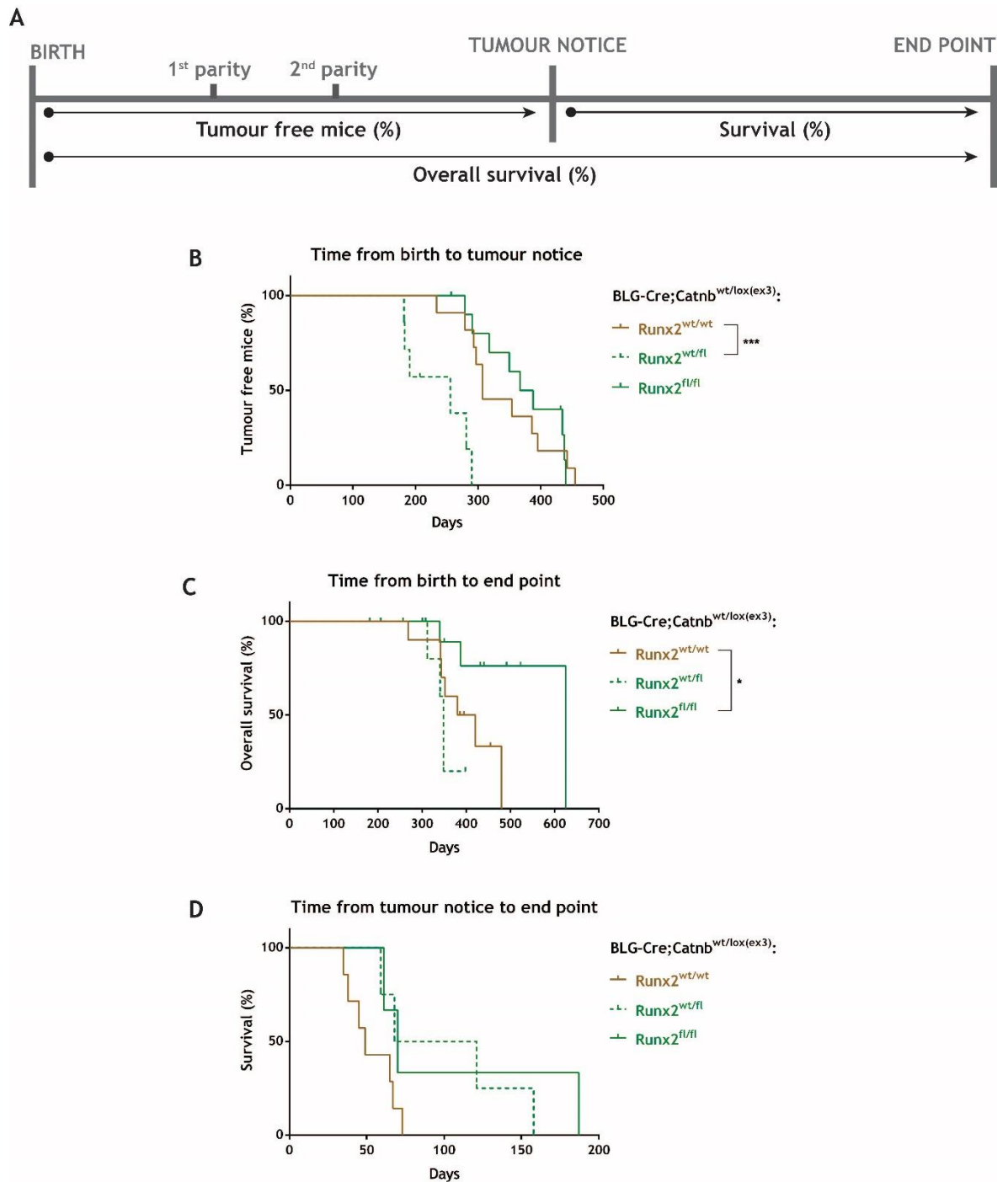


Figure 4. 2 Heterozygous deletion of *Runx2* accelerates Wnt/ β -catenin-driven mammary tumourigenesis, yet it does not affect survival of the mice.

(A) Schematic of the three parameters used to assess the impact of *Runx2* deletion upon Wnt/ β -catenin-driven mammary tumourigenesis. 12 week old females were mated to undergo two rounds of parities in order to maximize the expression of the BLG-Cre driver. Mice were monitored twice a week for tumour formation and sacrificed once a mammary tumour lesion reached clinical end point (i.e. 15 mm per width or length). (B, C, D) Kaplan-Meier curves of MP *BLG-Cre;Catnb^{wt/lox(ex3)}* mice, in the absence of one copy (*Runx2^{wt/fl}*) or both copies (*Runx2^{fl/fl}*) of the *Runx2* allele. (B) Time from birth to tumour notice of *Runx2^{wt/wt}* (n=11), *Runx2^{wt/fl}* (n=7) and *Runx2^{fl/fl}* (n=11) mice. (C) Time from birth to clinical end point of *Runx2^{wt/wt}* (n=10), *Runx2^{wt/fl}* (n=8) and *Runx2^{fl/fl}* (n=11) mice. (D) Time from tumour notice to end point of *Runx2^{wt/wt}* (n=7), *Runx2^{wt/fl}* (n=4) and *Runx2^{fl/fl}* (n=3) mice. Statistical analysis was performed using the Log-rank (Mantel-Cox) test in GraphPad Prism. * $P < 0.05$; *** $P < 0.001$. MP, multiparous.

It is important to mention that, regardless of the *Runx* status of the mice, all MP cohorts of *BLG-Cre;Catnb^{wt/lox(ex3)}* mice displayed a long tumour latency, comprised between 350 and 450 days. Of note, whilst maximizing the expression of the BLG-Cre driver, the use of parity is concomitantly characterized by the increased chance of incipient pre-neoplastic cells to be lost during involution. As such, to investigate the effect of parity upon Wnt/ β -catenin-mediated mammary tumourigenesis, corresponding nulliparous (NP) cohorts of *BLG-Cre;Catnb^{wt/lox(ex3)}* mice were generated. Interestingly, only three out of thirteen (23%) mice from the NP *Runx1^{wt/wt};Runx2^{wt/wt}* group developed mammary lesions around 493 days on average. Nonetheless, whilst two of them reached clinical end point (590 average days), the remaining tumour-bearing mouse and the rest of the animal cohort had to be sacrificed for unrelated reasons at an average time of 390 days. In regards to the latter, perhaps due to the leakiness of BLG-Cre expression in the liver (data not shown) and the crucial role exerted by Wnt/ β -catenin in the organ (Behari, 2010), the majority of animals appeared to suffer from gross hepatomegaly. Differently, when the *Runx1^{fl/fl}* MP and NP cohorts of *BLG-Cre;Catnb^{wt/lox(ex3)}* mice were compared with each other, no major differences were found among them, yet only in respect to MP *Runx1^{wt/wt}* control mice (Figure 4. 3). If on one hand this result ruled out the possibility of *Runx1*-deficient pre-neoplastic MMECs being lost during involution, on the other the absence for parity requirements highlighted the effect of deleting *Runx1* in the context of Wnt/ β -catenin-driven mammary tumourigenesis. Being the luminal layer predominantly remodelled during mammary gland reproductive development, these observations also hinted at the possibility of Wnt/ β -catenin-driven pre-neoplastic transformation occurring in the basal epithelial compartment of the organ. On the contrary, a significant delay in the time from birth to tumour notice was seen with NP *Runx2^{fl/fl}* mice (504 days on average), as compared to both MP *Runx2^{fl/fl}* and *Runx2^{wt/wt}* cohorts (367 and 341 average days, respectively) (Figure 4. 4B). No difference was instead found in regards to the other two parameters when comparing the NP and MP *Runx2^{fl/fl}* cohorts (Figure 4. 4C and D). In conclusion, albeit the inception of *Runx2*-deleted Wnt/ β -catenin driven mammary lesions resulted significantly accelerated in the MP cohort, the dependency of parity shown by *Runx2^{fl/fl}* mice could have just been a reflection of the hypomorphic allele affecting this transgenic line.

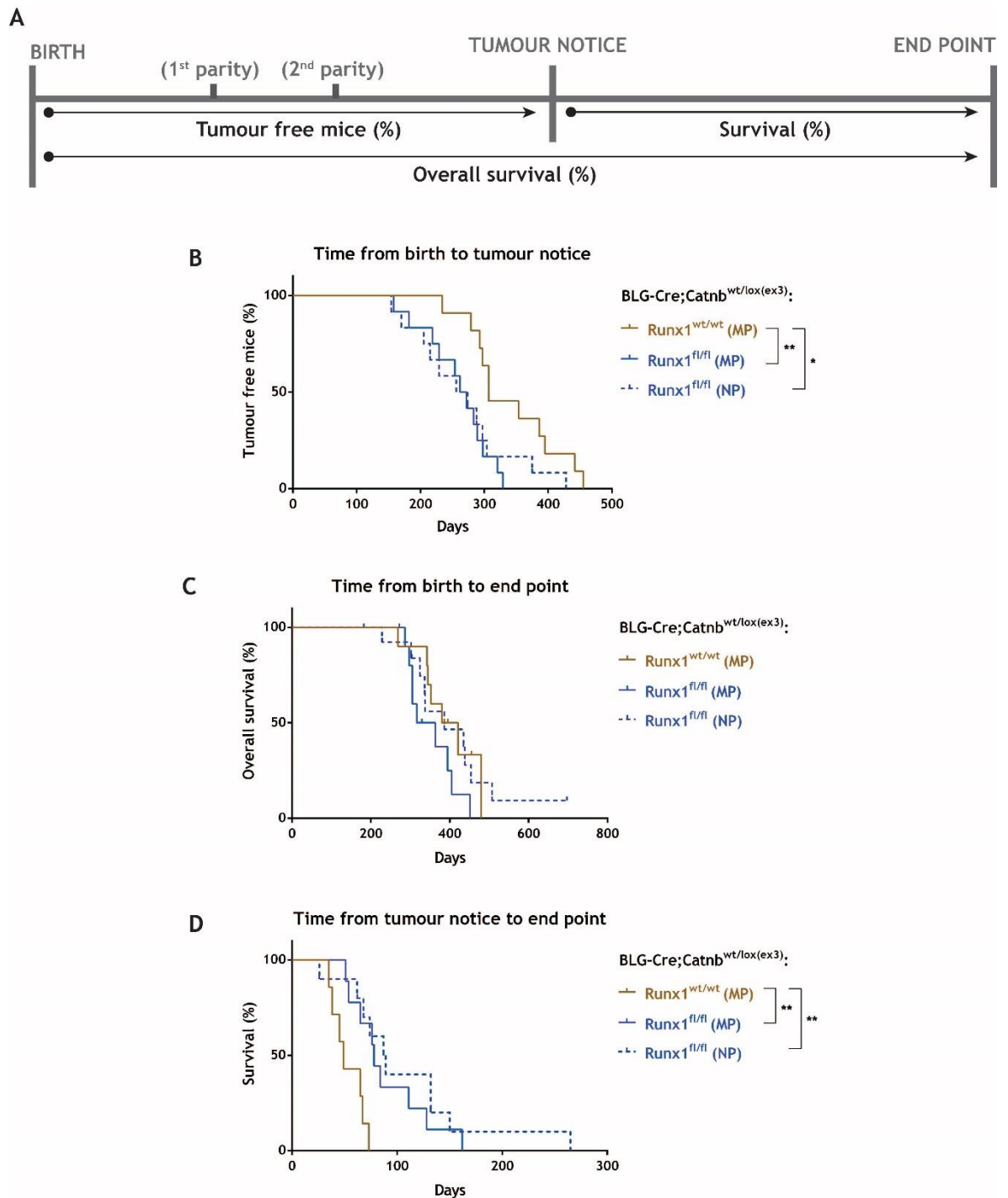


Figure 4. 3 Wnt/ β -catenin-driven mammary tumourigenesis, in the absence of *Runx1*, is not influenced by parity.

(A) Schematic of the three parameters used to assess the impact of *Runx1* deletion upon Wnt/ β -catenin-driven mammary tumourigenesis. Both MP and NP mice were monitored twice a week for tumour formation and sacrificed once a mammary tumour lesion reached end point. (B, C, D) Kaplan-Meier curves of *BLG-Cre;Catnb^{wt/lox(ex3)}* mice from the MP *Runx1^{wt/wt}*, MP *Runx1^{fl/fl}* and NP *Runx1^{fl/fl}* cohorts of mice. (B) Time from birth to tumour notice of MP *Runx1^{wt/wt}* (n=11), MP *Runx1^{fl/fl}* (n=12) and NP *Runx1^{fl/fl}* (n=12) mice. (C) Time from birth to clinical end point of MP *Runx1^{wt/wt}* (n=10), MP *Runx1^{fl/fl}* (n=12) and NP *Runx1^{fl/fl}* (n=13) mice. (D) Time from tumour notice to end point of MP *Runx1^{wt/wt}* (n=7), MP *Runx1^{fl/fl}* (n=9) and NP *Runx1^{fl/fl}* (n=10) mice. Statistical analysis was performed using the Log-rank (Mantel-Cox) test in GraphPad Prism. * $P < 0.05$; ** $P < 0.01$. MP, multiparous; NP, nulliparous.

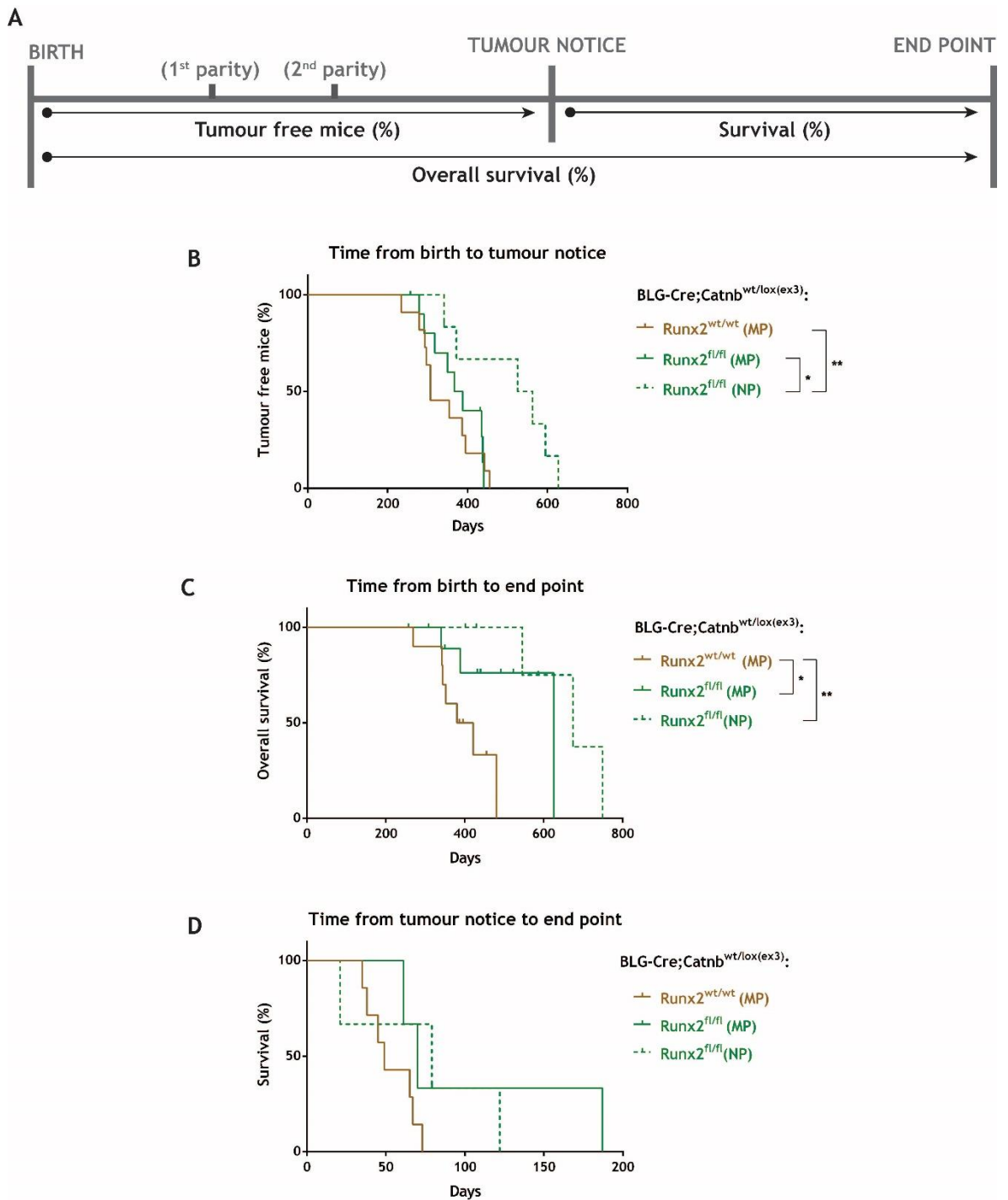


Figure 4. 4 Deletion of *Runx2*, in the absence of parity, delays the appearance of BLG-Cre driven Wnt/ β -catenin-activated mammary lesions.

(A) Schematic of the three parameters used to assess the impact of *Runx2* deletion upon Wnt/ β -catenin-driven mammary tumorigenesis. Both MP and NP mice were monitored twice a week for tumour formation and sacrificed once a mammary lesion reached end point. (B, C, D) Kaplan-Meier curves of *BLG-Cre;Catnb^{wt/lox(ex3)}* mice from the MP *Runx2^{wt/wt}*, MP *Runx2^{fl/fl}* and NP *Runx2^{fl/fl}* cohorts of mice. (B) Time from birth to tumour notice of MP *Runx2^{wt/wt}* (n=11), MP *Runx2^{fl/fl}* (n=11) and NP *Runx2^{fl/fl}* (n=6) mice. (C) Time from birth to clinical end point of MP *Runx2^{wt/wt}* (n=10), MP *Runx2^{fl/fl}* (n=11) and NP *Runx2^{fl/fl}* (n=6) mice. (D) Time from tumour notice to end point of MP *Runx2^{wt/wt}* (n=7), MP *Runx2^{fl/fl}* (n=3) and NP *Runx2^{fl/fl}* (n=3) mice. Statistical analysis was performed using the Log-rank (Mantel-Cox) test in GraphPad Prism. * $P < 0.05$; ** $P < 0.01$. MP, multiparous; NP, nulliparous.

4.3.2 Combined deletion of *Runx1* and *Runx2* results in a remarkable acceleration of Wnt/ β -catenin-driven mammary tumourigenesis

In view of the effects on tumour progression displayed by the *Runx1*^{fl/fl} and *Runx2*^{fl/fl} cohorts of mice, the high degree of homology existing between the two genes and the possibility of compensating for each other (Chuang et al., 2013), the combinatorial effect of *Runx1* and *Runx2* deletion upon Wnt/ β -catenin-driven mammary tumourigenesis was also evaluated. To this end, *BLG-Cre;Catnb*^{wt/lox(ex3)} mice were crossed onto *Runx1*^{fl/fl} and *Runx2*^{fl/fl} mice to generate a new cohort of *BLG-Cre;Catnb*^{wt/lox(ex3);Runx1}^{fl/fl};*Runx2*^{fl/fl} mice. Given the presence of the *Runx2*^{fl/fl} hypomorphic allele, the main aim of this analysis was to assess the contribution of deleting one or both copies of *Runx2* on a *Runx1*-null Wnt/ β -catenin activated background. Accordingly, deletion of one allele of the *Runx2* gene resulted in a remarkable acceleration of Wnt/ β -catenin driven mammary tumourigenesis (Figure 4. 5). On one hand, this was corroborated by the significant decreased timeframe from birth to tumour notice displayed by the *Runx1*^{fl/fl};*Runx2*^{wt/fl} cohort (131 average days), as compared to both *Runx1*^{fl/fl};*Runx2*^{wt/wt} (258 average days) and *Runx1*^{wt/wt};*Runx2*^{wt/wt} control mice (341 average days) (Figure 4. 5B). It was further supported by a significantly reduced overall survival shown by *Runx1*^{fl/fl};*Runx2*^{wt/fl} animals (235 average days), as opposed to the *Runx1*^{fl/fl};*Runx2*^{wt/wt} and *Runx1*^{wt/wt};*Runx2*^{wt/wt} cohorts (347 and 370 average days, respectively) (Figure 4. 5C). On the contrary, progression of established *Runx1*-deficient Wnt/ β -catenin-activated tumour lesions, intended as the timeframe from tumour notice to clinical end point, remained unchanged both in the presence or absence of *Runx2*. Nonetheless, whilst the delayed tumour progression shown by *Runx1*^{fl/fl};*Runx2*^{wt/wt} mice (90 average days) proved to be significantly different when compared to controls (53 average days), this was not the case for the *Runx1*^{fl/fl};*Runx2*^{wt/fl} cohort, wherein progression of established lesions occurred at an average time of 103 average days (Figure 4. 5D). Whilst emphasizing the tumour suppressive activity played by *Runx2* in the context of *Runx1* loss, these findings also highlighted the survival advantage displayed by recombined MMECs to survive upon activation of Wnt/ β -catenin, homozygous loss of *Runx1* and heterozygous deletion of *Runx2*.

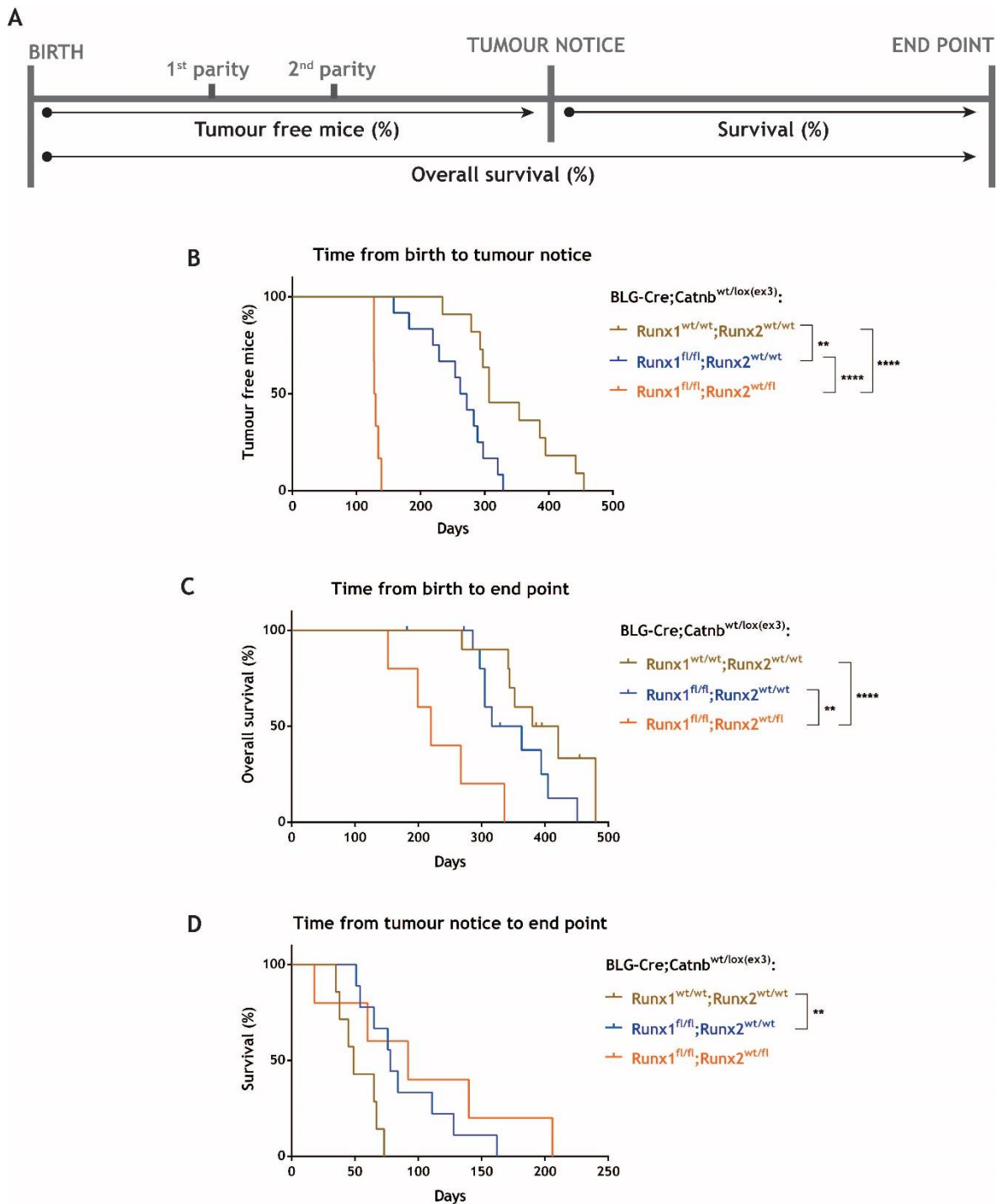


Figure 4. 5 Heterozygous deletion of *Runx2* significantly accelerates Wnt/ β -catenin-driven mammary tumourigenesis in a *Runx1*-null background.

(A) Schematic of the three parameters used to assess the impact of heterozygous *Runx2* deletion upon Wnt/ β -catenin-driven mammary tumourigenesis in a *Runx1*-null background. (B, C, D) Kaplan-Meier curves of *BLG-Cre;Catnb^{wt/lox(ex3)}* mice, in the presence (*Runx1^{fl/fl};Runx2^{wt/wt}*) or absence of one copy (*Runx1^{fl/fl};Runx2^{wt/fl}*) of the *Runx2* gene. (B) Time from birth to tumour notice of *Runx1^{wt/wt};Runx2^{wt/wt}* (n=11), *Runx1^{fl/fl};Runx2^{wt/wt}* (n=12) and *Runx1^{fl/fl};Runx2^{wt/fl}* (n=6) mice. (C) Time from birth to clinical end point of *Runx1^{wt/wt};Runx2^{wt/wt}* (n=10), *Runx1^{fl/fl};Runx2^{wt/wt}* (n=12) and *Runx1^{fl/fl};Runx2^{wt/fl}* (n=5) mice. (D) Time from tumour notice to end point of *Runx1^{wt/wt};Runx2^{wt/wt}* (n=7), *Runx1^{fl/fl};Runx2^{wt/wt}* (n=9) and *Runx1^{fl/fl};Runx2^{wt/fl}* (n=5) mice. All mice underwent two parities. Statistical analysis was performed using the Log-rank (Mantel-Cox) test in GraphPad Prism. ** $P < 0.01$; **** $P < 0.0001$.

To investigate how parity could affect the tumourigenesis displayed by *BLG-Cre;Catnb^{wt/lox(ex3)};Runx1^{fl/fl};Runx2^{wt/fl}* animals, a corresponding NP cohort of mice was generated and monitored over time for the formation of mammary lesions (Figure 4. 6). In doing so, NP *Runx1^{fl/fl};Runx2^{wt/fl}* mice were found to display a significant delay in the formation of palpable Wnt/ β -catenin-activated mammary tumours as compared to the corresponding MP cohort (181 and 131 average days, respectively). Nonetheless, this timeframe remained overall accelerated as compared to both MP cohorts of *Runx1^{fl/fl};Runx2^{wt/wt}* and *Runx1^{wt/wt};Runx2^{wt/wt}* mice (258 and 341 average days, respectively) (Figure 4. 6B). In view of its hormone responsiveness, this result reinforced the seminal role played by parity in potentiating the expression of BLG-Cre. When the overall survival of the mice was evaluated, no difference could be observed between the MP and NP cohorts of *Runx1^{fl/fl};Runx2^{wt/fl}* mice, which had to be sacrificed at an average time of 235 and 234 days, respectively. Nonetheless, the timeframe from birth to clinical end point displayed by NP *Runx1^{fl/fl};Runx2^{wt/fl}* mice resulted to be significantly different in relation to both MP *Runx1^{fl/fl};Runx2^{wt/wt}* and MP *Runx1^{wt/wt};Runx2^{wt/wt}* control mice (347 and 370 average days, respectively) (Figure 4. 6C). The delayed appearance of Wnt/ β -catenin driven palpable lesions displayed by NP *Runx1^{fl/fl};Runx2^{wt/fl}* mice, yet the absence of any difference in terms of overall survival as compared to the corresponding MP cohort could be explained by an accelerated tumour progression (Figure 4. 6D). Albeit not statistically significant to any of the other MP cohorts of *BLG-Cre;Catnb^{wt/lox(ex3)}* mice, probably due to small numbers, this result highlighted a controversial role for parity. If on one hand it accelerated the appearance of Wnt/ β -catenin-driven mammary lesions upon homozygous loss of *Runx1* and heterozygous loss of *Runx2*, on the other it also lessened their growth.

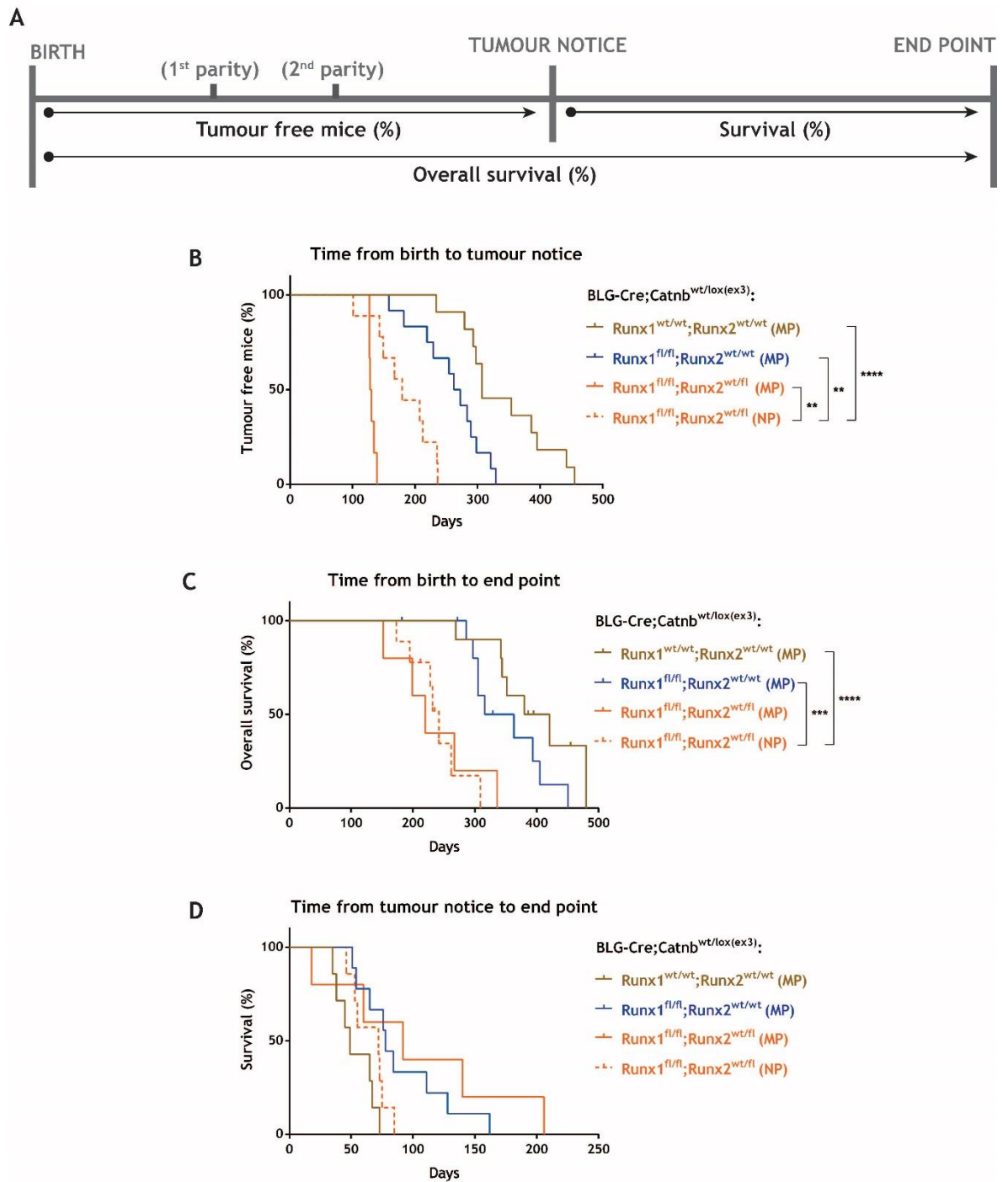


Figure 4. 6 The effect of parity on heterozygous loss of *Runx2* upon Wnt/ β -catenin-driven mammary tumourigenesis in a *Runx1*-null background.

(A) Schematic of the three parameters used to assess the impact of parity on heterozygous *Runx2* deletion upon Wnt/ β -catenin-driven mammary tumourigenesis in a *Runx1*-null background. (B, C, D) Kaplan-Meier curves of *BLG-Cre;Catnb^{wt/lox(ex3)}* mice from the MP *Runx1^{fl/fl};Runx2^{wt/wt}*, MP *Runx1^{fl/fl};Runx2^{wt/fl}* and NP *Runx1^{fl/fl};Runx2^{wt/fl}* cohorts. (B) Time from birth to tumour notice of *Runx1^{wt/wt};Runx2^{wt/wt}* (n=11), *Runx1^{fl/fl};Runx2^{wt/wt}* (n=12), MP *Runx1^{fl/fl};Runx2^{wt/wt}* (n=6) and NP *Runx1^{fl/fl};Runx2^{wt/fl}* (n=9) mice. (C) Time from birth to clinical end point of *Runx1^{wt/wt};Runx2^{wt/wt}* (n=10), *Runx1^{fl/fl};Runx2^{wt/wt}* (n=12), MP *Runx1^{fl/fl};Runx2^{wt/fl}* (n=5) and NP *Runx1^{fl/fl};Runx2^{wt/fl}* (n=9) mice. (D) Time from tumour notice to end point of *Runx1^{wt/wt};Runx2^{wt/wt}* (n=7), *Runx1^{fl/fl};Runx2^{wt/wt}* (n=9), MP *Runx1^{fl/fl};Runx2^{wt/fl}* (n=5) and NP *Runx1^{fl/fl};Runx2^{wt/fl}* (n=7) mice. Statistical analysis was performed using the Log-rank (Mantel-Cox) test in GraphPad Prism. ***P*<0.01; ****P*<0.001 *****P*<0.0001. MP, multiparous; NP, nulliparous.

Collectively, these results encouraged further investigation of the effect that deletion of both copies of *Runx2* might have had upon Wnt/ β -catenin-driven mammary tumourigenesis on a *Runx1*-null background. Thus, a cohort of *Runx1^{fl/fl};Runx2^{fl/fl}* mice was generated. As mentioned above, all females employed in this study were usually divided in two categories, a MP and NP ones, with the former comprising mice that have undergone two rounds of parities. The latter experimental approach, however, could not be achieved in this case, as co-deletion of both copies of *Runx2* on a *Runx1*-null background resulted in a highly significant acceleration of Wnt/ β -catenin-driven mammary tumourigenesis. This translated in the appearance of palpable mammary lesions at an average time of 56 days (Figure 4. 7B), as well as in a significantly decreased overall survival around 99 days (Figure 4. 7C). For the above reasons, these results remarkably distinguished the NP cohort of *Runx1^{fl/fl};Runx2^{fl/fl}* mice from all other MP cohorts of *BLG-Cre;Catnb^{wt/lox(ex3)}* animals. Nonetheless, when the time from palpable lesions to end point was assessed, the growth of established *Runx1^{fl/fl};Runx2^{fl/fl}*-deficient mammary lesions appeared to overlap to the one characterizing *Runx1^{wt/wt};Runx2^{wt/wt}* control tumours. On the contrary and as already discussed above, *Runx1*-null lesions, both in the presence (*Runx1^{fl/fl};Runx2^{wt/wt}*) or absence of only one copy of *Runx2* (*Runx1^{fl/fl};Runx2^{wt/fl}*), were significantly delayed in their tumour growth at this stage of disease progression (Figure 4. 7D). A definitive proof of the tumour suppressive role exerted by RUNX2 in halting the formation of *Runx1*-null Wnt/ β -catenin-driven mammary lesions was obtained. Altogether, these results confirmed the presence of a tantalizing interplay between the *Runx* genes and canonical Wnt signalling, whereby both RUNX1 and RUNX2 appear to act as “sentinels” of β -catenin. As such, only upon combined deletion of both genes the Wnt/ β -catenin pathway is fully unleashed resulting in a remarkable oncogenic transformation of the mammary epithelium. For an overview of MP *Runx1^{wt/wt};Runx2^{wt/wt}*, *Runx1^{fl/fl};Runx2^{wt/wt}*, *Runx1^{wt/wt};Runx2^{fl/fl}* and NP *Runx1^{fl/fl};Runx2^{fl/fl}* cohorts of *BLG-Cre;Catnb^{wt/lox(ex3)}* mice, refer to Figure 4. 8; for an overview of MP *Runx1^{wt/wt};Runx2^{wt/wt}* and NP *Runx1^{fl/fl};Runx2^{wt/wt}*, *Runx1^{wt/wt};Runx2^{fl/fl}* and *Runx1^{fl/fl};Runx2^{fl/fl}* cohorts of *BLG-Cre;Catnb^{wt/lox(ex3)}* mice, refer to Figure 4. 9.

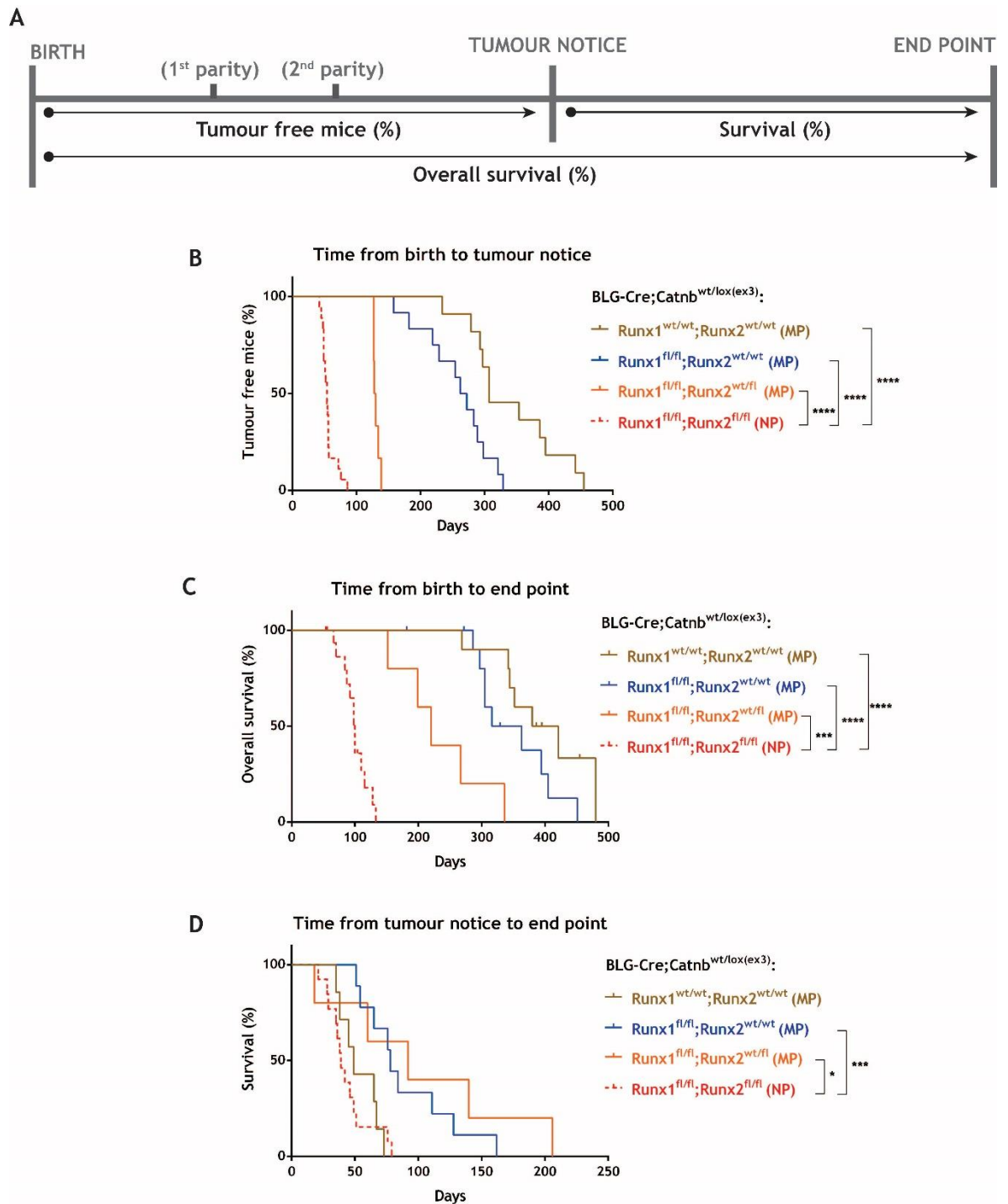


Figure 4. 7 Co-deletion of *Runx1* and *Runx2* significantly accelerates Wnt/ β -catenin-driven oncogenic transformation of the mammary epithelium.

(A) Schematic of the three parameters used to assess the impact of *Runx1* and *Runx2* co-deletion upon Wnt/ β -catenin-driven mammary tumourigenesis. (B, C, D) Kaplan-Meier curves of *BLG-Cre;Catnb^{wt/lox(ex3)}* mice from the MP *Runx1^{fl/fl};Runx2^{wt/wt}*, MP *Runx1^{fl/fl};Runx2^{wt/fl}* and NP *Runx1^{fl/fl};Runx2^{fl/fl}* cohorts. (B) Time from birth to tumour notice of *Runx1^{wt/wt};Runx2^{wt/wt}* (n=11), *Runx1^{fl/fl};Runx2^{wt/wt}* (n=12), *Runx1^{fl/fl};Runx2^{wt/fl}* (n=6) and *Runx1^{fl/fl};Runx2^{fl/fl}* (n=18) mice. (C) Time from birth to clinical end point of *Runx1^{wt/wt};Runx2^{wt/wt}* (n=10), *Runx1^{fl/fl};Runx2^{wt/wt}* (n=12), *Runx1^{fl/fl};Runx2^{wt/fl}* (n=5) and *Runx1^{fl/fl};Runx2^{fl/fl}* (n=18) mice. (D) Time from tumour notice to end point of *Runx1^{wt/wt};Runx2^{wt/wt}* (n=7), *Runx1^{fl/fl};Runx2^{wt/wt}* (n=9), *Runx1^{fl/fl};Runx2^{wt/fl}* (n=5) and *Runx1^{fl/fl};Runx2^{fl/fl}* (n=13) mice. Statistical analysis was performed using the Log-rank (Mantel-Cox) test in GraphPad Prism. * $P < 0.05$; *** $P < 0.001$ **** $P < 0.0001$. MP, multiparous; NP, nulliparous.

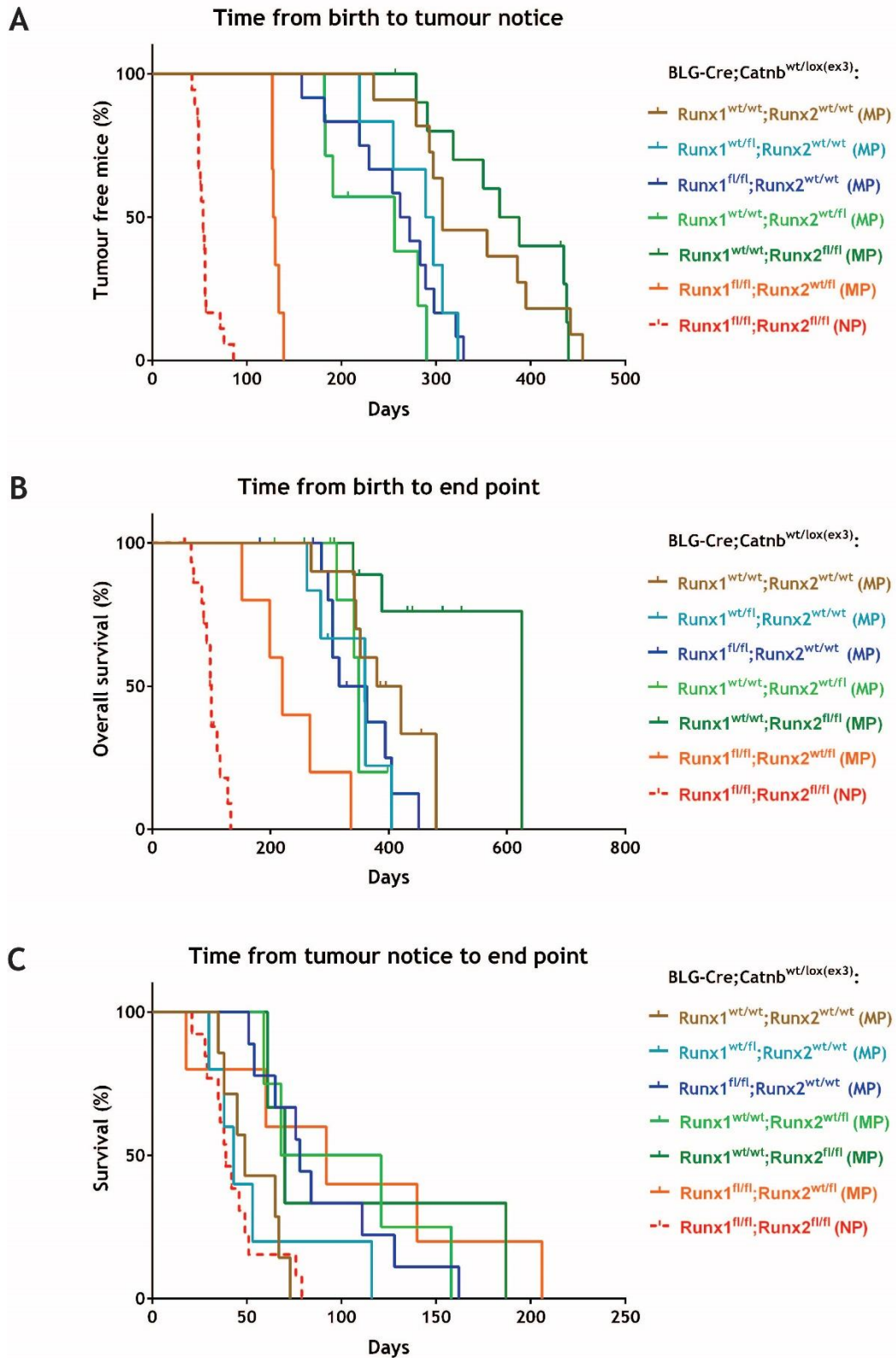


Figure 4. 8 Survival analysis of *Runx*-deficient cohorts of multiparous mice carrying an activated mutation of β -catenin.

Overview of the time from birth to tumour notice (A), from birth to end point (B) and from tumour notice to end point (C) of all MP *Runx*-deficient and NP *Runx1*^{fl/fl};*Runx2*^{fl/fl} cohorts of *BLG-Cre;Catnb*^{wt/lox(ex3)} cohorts. MP, multiparous; NP, nulliparous.

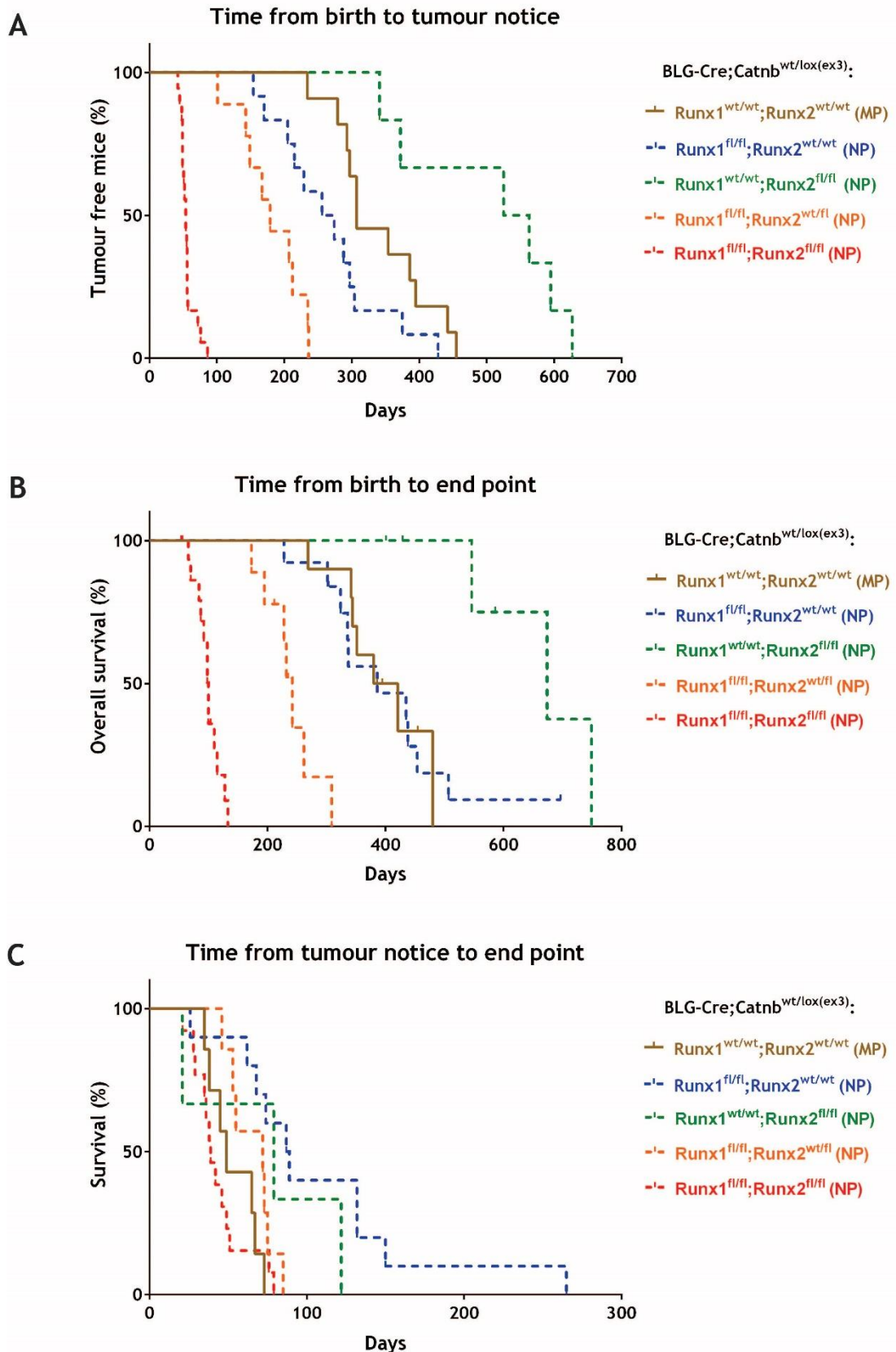


Figure 4. 9 Survival analysis of *Runx*-deficient cohorts of nulliparous mice carrying an activated mutation of β -catenin.

Overview of the time from birth to tumour notice (A), from birth to end point (B) and from tumour notice to end point (C) of all NP *Runx*-deficient and MP *Runx1*^{wt/wt};*Runx2*^{wt/wt} cohorts of *BLG-Cre;Catnb*^{wt/lox(ex3)} cohorts. MP, multiparous; NP, nulliparous.

4.3.3 Characterization of *Runx*-deficient breast cancer cohorts of mice carrying an activating mutation of β -catenin

When mice from all *BLG-Cre;Catnb^{wt/lox(ex3)}* cohorts reached clinical end point, these were sacrificed and both the body weight and the total weight of all ten tumour-bearing and non-tumour bearing mammary glands were recorded. Through the combination of these two parameters the tumour burden of the mouse was then calculated and expressed as the total weight of all mammary glands divided by the body weight of the mouse. In addition, the number of tumour burdened mammary glands was also noted. All cohorts of *Runx*-deficient *BLG-Cre;Catnb^{wt/lox(ex3)}* mice were characterized and compared with each other. Analysis of *Runx1*-deficient mice, comprising MP *Runx1^{wt/fl};Runx2^{wt/wt}* and both MP and NP *Runx1^{fl/fl};Runx2^{wt/wt}* cohorts, showed no difference in terms of body weight (Figure 4. 10A). Nonetheless, albeit not significant, all three *Runx1*-deleted cohorts displayed a trend towards higher tumour burden (Figure 4. 10B) and higher number of tumour burdened mammary glands (Figure 4. 10C), in respect to *Runx1^{wt/wt};Runx2^{wt/wt}* control mice. In line with pathological examination, these results suggested that deletion of *Runx1* favoured the appearance of multiple Wnt/ β -catenin-driven mammary lesions affecting more than one murine gland (n=3 on average). Loss of *Runx1* appeared to predispose a higher number of MMECs to Wnt/ β -catenin-driven oncogenic transformation. When the same analysis was performed on *Runx2*-deficient cohorts of *BLG-Cre;Catnb^{wt/lox(ex3)}* mice, both the MP and NP groups of *Runx1^{wt/wt};Runx2^{fl/fl}* mice displayed lighter body weights as compared to MP cohorts of *Runx1^{wt/wt};Runx2^{wt/fl}* and control *Runx1^{wt/wt};Runx2^{wt/wt}* animals (Figure 4. 11A). Albeit not significant, probably due to low number of animals, these findings reflected the previously discussed hypomorphic allele affecting the *Runx2^{fl/fl}* transgenic line. A significant increase of tumour burden was found to be displayed by *Runx1^{wt/wt};Runx2^{wt/fl}* mice, yet not from animals carrying homozygous deletion of *Runx2*, in respect to controls (Figure 4. 11B). No major differences were instead observed in relation to the number of mammary glands affected by Wnt/ β -catenin-driven mammary lesions (Figure 4. 11C).

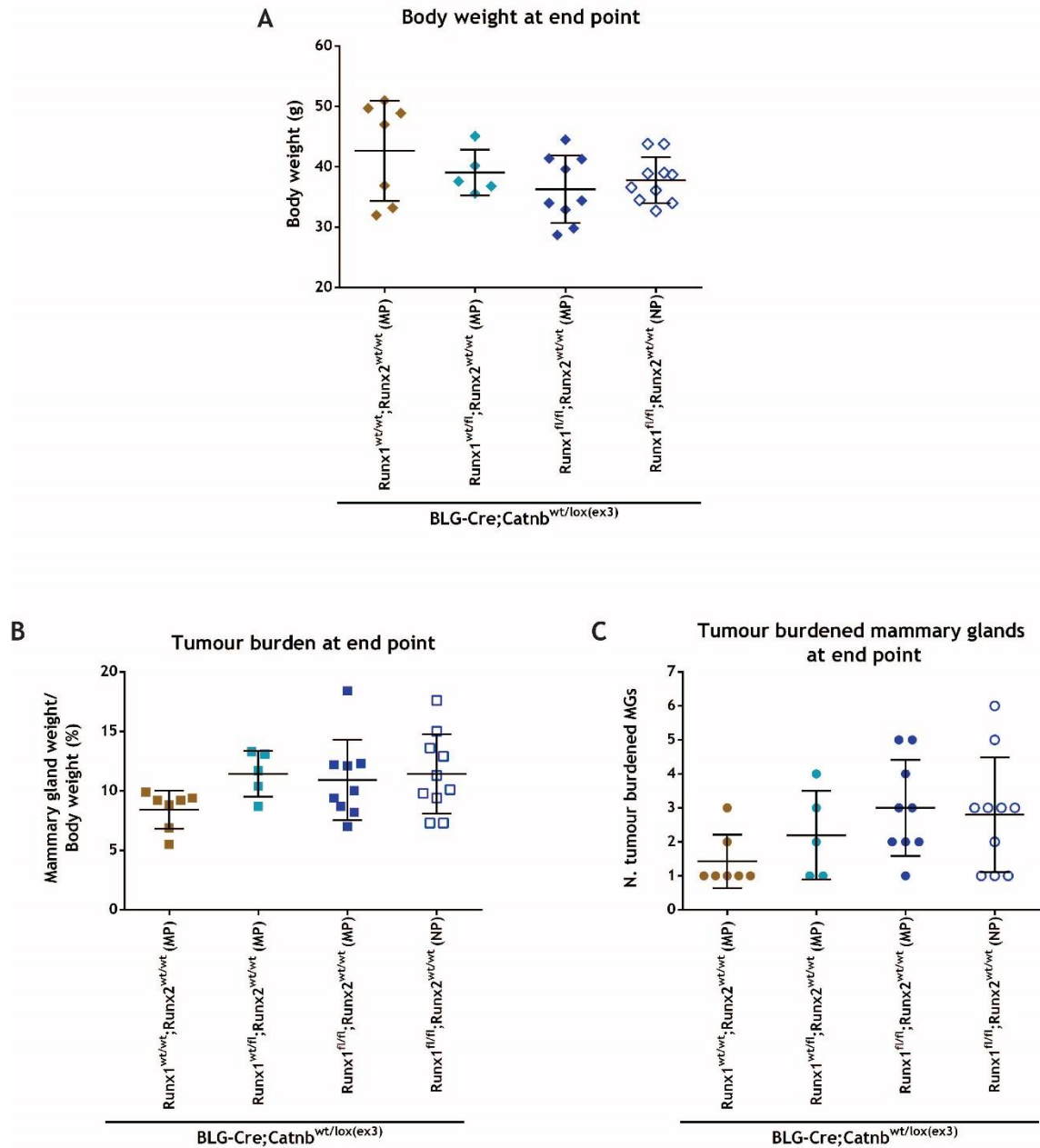


Figure 4. 10 Effect of *Runx1* loss on body weight, tumour burden and number of tumour burdened mammary glands in *Wnt/β-catenin* activated mutant mice at clinical end point.

Scatter dot plots of body weight (A), tumour burden (B) and number of tumour burdened mammary glands (C) from clinical end point *BLG-Cre;Catnb^{wt/lox(ex3)}* mice of the MP *Runx1^{wt/wt};Runx2^{wt/wt}*, MP *Runx1^{wt/fl};Runx2^{wt/wt}*, MP *Runx1^{fl/fl};Runx2^{wt/wt}* and NP *Runx1^{fl/fl};Runx2^{wt/wt}* cohorts of mice. Females from the MP cohorts were mated at the age of 12 week to undergo two rounds of parities. Both MP and NP cohorts (represented with full and empty symbols, respectively) were monitored twice a week for the presence of tumours. Once a lesion was noticed, its size was recorded and monitored over time. Mice were sacrificed when the first tumour lesion reached clinical end point. The number of tumour burden mammary glands represents the number of tumour bearing mammary glands over the total number of ten murine mammary glands. Statistical analysis was performed by the Kruskal-Wallis test with Dunn's multiple comparisons in GraphPad Prism. Error bars represent mean with SD (n≥5 per each cohort). No significant differences were found among cohorts. MP, multiparous; NP, nulliparous.

When characterization of clinical end point *BLG-Cre;Catnb^{wt/lox(ex3)}* mice carrying co-deletion of both *Runx1* and *Runx2* alleles was performed, the NP *Runx1^{fl/fl};Runx2^{fl/fl}* group displayed a significantly lower body weight in respect to both MP *Runx1^{fl/fl};Runx2^{wt/fl}* and control *Runx1^{wt/wt};Runx2^{wt/wt}* cohorts (Figure 4. 12A). This result was in line with the previously discussed reduced overall survival of NP *Runx1^{fl/fl};Runx2^{fl/fl}* occurring at a much younger age (average time of 99 days) (Figure 4. 7). Regardless, a significantly increased tumour burden as compared to controls was found in NP *Runx1*-null mice carrying either heterozygous or homozygous deletion of *Runx2* (Figure 4. 12B). The same could not be said for MP *Runx1^{fl/fl};Runx2^{wt/fl}* mice, even though the latter cohort showed an acceleration of tumourigenesis in respect to the NP counterpart (Figure 4. 6). This finding highlighted again the putative impact played by pregnancy, and subsequent involution stage, in the clearance of pre-neoplastic Wnt/ β -catenin driven tumour cells. Importantly, the increased tumour burden shown by NP *Runx1^{fl/fl};Runx2^{fl/fl}* mice was also reflected by a significantly increased number of tumour burdened mammary glands (n=8 on average), when compared with the *Runx1^{wt/wt};Runx2^{wt/wt}* group (n=1 on average). Although the same scenario did not apply to the MP and NP cohorts of *Runx1^{fl/fl};Runx2^{wt/fl}* mice, these also showed a higher trend towards increase tumour burdened glands in respect to controls (Figure 4. 12C). The distinctive features characterizing NP *Runx1^{fl/fl};Runx2^{fl/fl}* mice became even more striking when this group of mice was compared to all *Runx*-deficient MP (Figure 4. 13) and NP (Figure 4. 14) cohorts of *BLG-Cre;Catnb^{wt/lox(ex3)}* mice. Indeed, despite being the only group characterized by the lowest body weight, NP *Runx1^{fl/fl};Runx2^{fl/fl}* mice were always found to show the highest tumour burden, as well as the highest number of tumour burdened mammary glands among all cohorts. Thus, if *Runx1* deletion was already able to partly increase the percentage of MMECs susceptible to Wnt/ β -catenin oncogenic transformation (Figure 4. 10), deletion of *Runx2* on a *Runx1*-null background resulted in a complete exacerbation of this phenotype. Whilst reiterating the compensatory effect exerted by both genes, these findings highlighted once again the deleterious consequences of combined *Runx1* and *Runx2* deletion on a mammary-specific Wnt/ β -catenin activated background. Representative pictures of the gross pathology of clinical end point of *Runx*-deficient MP and NP cohorts of *BLG-Cre;Catnb^{wt/lox(ex3)}* mice are shown in Figure 4. 15.

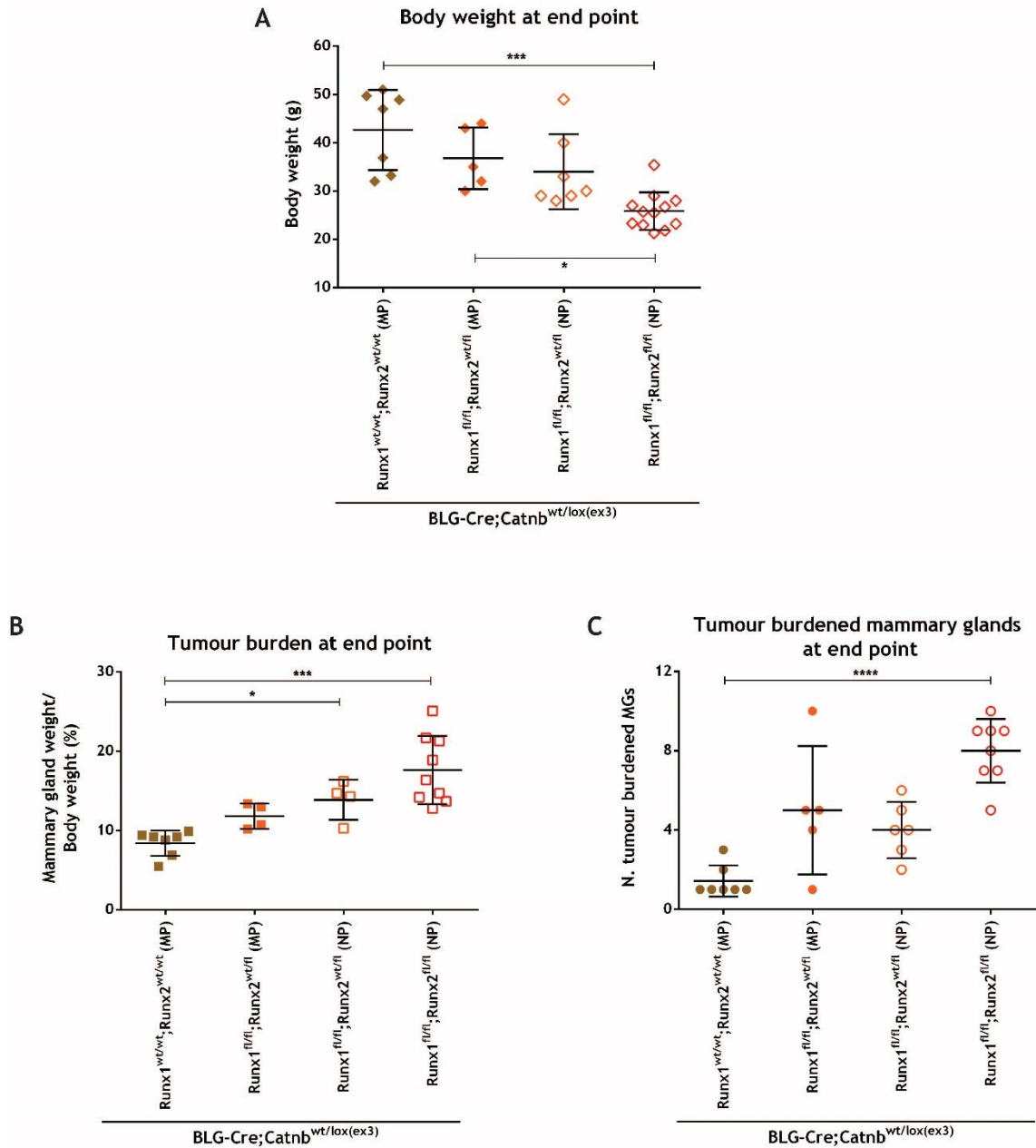


Figure 4. 12 Effect of combined *Runx1* and *Runx2* loss on body weight, tumour burden and number of tumour burdened mammary glands in *Wnt/β-catenin* activated mutant mice at clinical end point.

Scatter dot plots of body weight (A), tumour burden (B) and number of tumour burdened mammary glands (C) from clinical end point *BLG-Cre;Catnb^{wt/lox(ex3)}* mice of the MP *Runx1^{wt/wt};Runx2^{wt/wt}*, MP *Runx1^{fl/fl};Runx2^{wt/fl}*, NP *Runx1^{fl/fl};Runx2^{wt/fl}* and NP *Runx1^{fl/fl};Runx2^{fl/fl}* cohorts of mice. Females from the MP cohorts were mated at the age of 12 week to undergo two rounds of parities. Both MP and NP cohorts (represented with full and empty symbols, respectively) were monitored twice a week for the presence of tumours. Once a lesion was noticed, its size was recorded and monitored over time. Mice were sacrificed when the first tumour lesion reached clinical end point (i.e. 15 mm per width or length). The number of tumour burden mammary glands represents the number of tumour bearing mammary glands over the total number of ten murine mammary glands. Statistical analysis was performed by the Kruskal-Wallis test with Dunn's multiple comparisons in GraphPad Prism. Error bars represent mean with SD (n≥4 per each cohort). **P*<0.05, ****P*<0.001, *****P*<0.0001. MP, multiparous; NP, nulliparous.

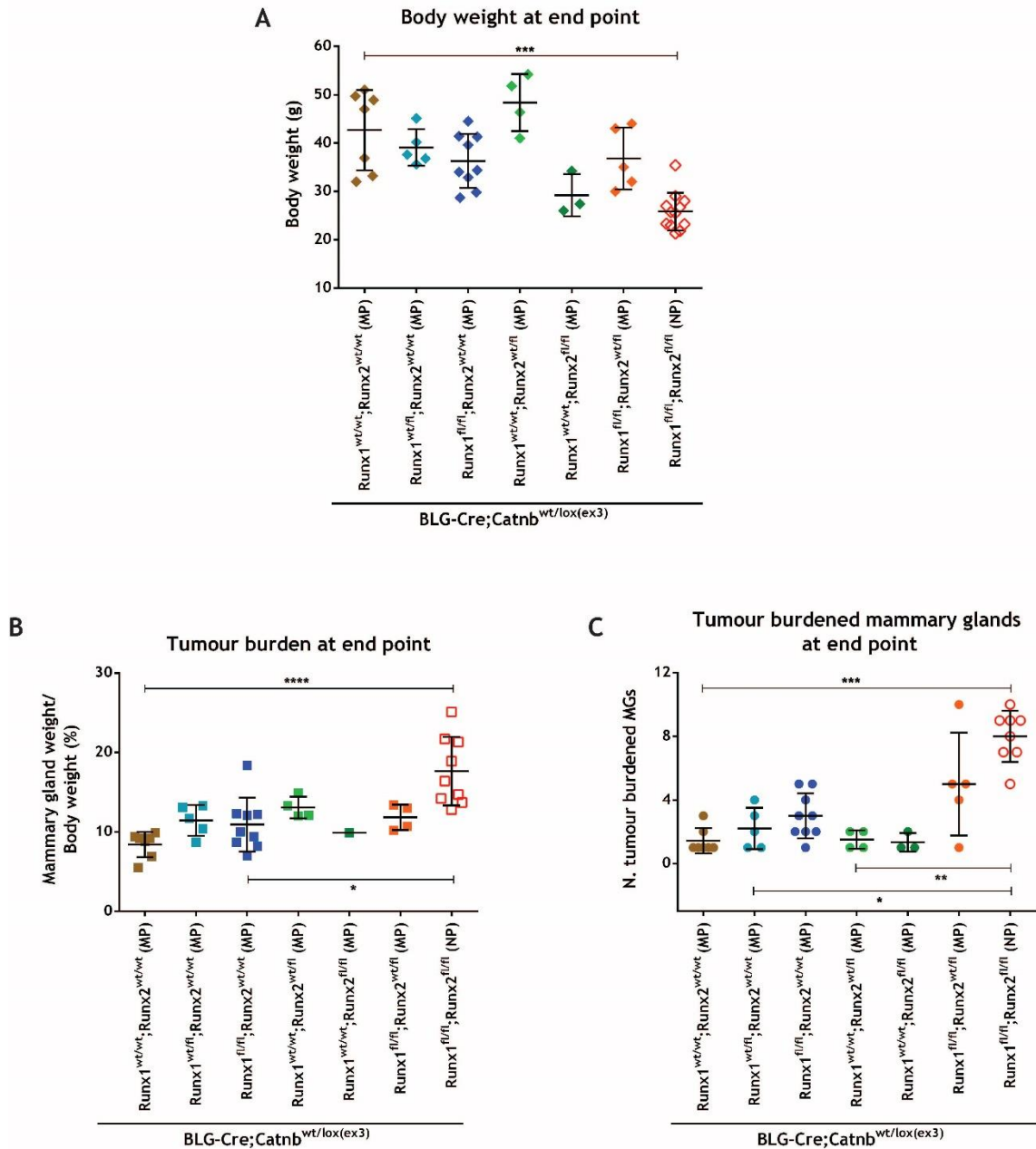


Figure 4. 13 Characterization of *Runx*-deficient multiparous cohorts of mice carrying a mammary-specific activating mutation of β -catenin.

Scatter dot plots of body weight (A), tumour burden (B) and number of tumour burdened mammary glands (C) from clinical end point *BLG-Cre;Catnb^{wt/lox(ex3)}* mice, upon loss of *Runx1* (MP *Runx1^{wt/fl};Runx2^{wt/wt}* and MP *Runx1^{fl/fl};Runx2^{wt/wt}*), *Runx2* (MP *Runx1^{wt/wt};Runx2^{wt/fl}* and MP *Runx1^{wt/wt};Runx2^{fl/fl}*), or combined deletion of both genes (MP *Runx1^{fl/fl};Runx2^{wt/fl}* and NP *Runx1^{fl/fl};Runx2^{fl/fl}*). All females, except those from the NP *Runx1^{fl/fl};Runx2^{fl/fl}* cohort, were mated at the age of 12 week to undergo two rounds of parities. Both MP and NP cohorts (represented with full and empty symbols, respectively) were monitored twice a week for the presence of tumours and sacrificed when the first lesion reached clinical end point. The number of tumour burdened mammary glands represents the number of tumour bearing mammary glands over the total number of ten murine mammary glands. Statistical analysis was performed by the Kruskal-Wallis test with Dunn's multiple comparisons in GraphPad Prism. Error bars represent mean with SD (n \geq 3 per each cohort, except for the tumour burden of MP *Runx1^{wt/wt};Runx2^{fl/fl}* with n=1). **P*<0.05, ***P*<0.01, ****P*<0.001, *****P*<0.0001. MP, multiparous; NP, nulliparous.

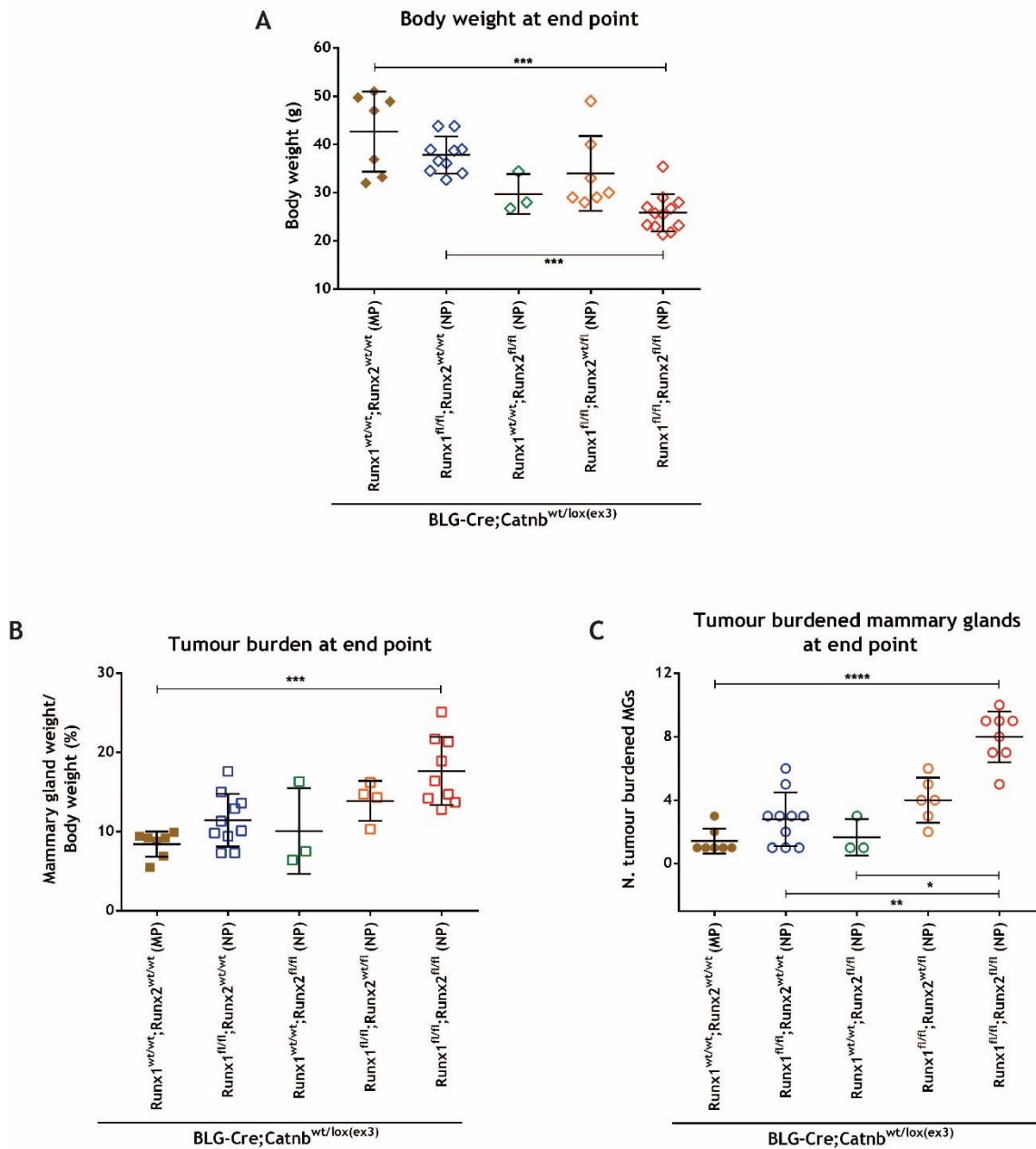


Figure 4. 14 Characterization of *Runx*-deficient nulliparous cohorts of mice carrying a mammary-specific activating mutation of β -catenin.

Scatter dot plots of body weight (A), tumour burden (B) and number of tumour burdened mammary glands (C) from clinical end point *BLG-Cre;Catnb^{wt/lox(ex3)}* mice, upon loss of *Runx1* (NP *Runx1^{fl/fl};Runx2^{wt/wt}*), *Runx2* (NP *Runx1^{wt/wt};Runx2^{fl/fl}*), or combined deletion of both genes (NP *Runx1^{fl/fl};Runx2^{wt/fl}* and NP *Runx1^{fl/fl};Runx2^{fl/fl}*). All MP females were mated at the age of 12 week to undergo two rounds of parities. Both MP and NP cohorts (represented with full and empty symbols, respectively) were monitored twice a week for the presence of tumours and sacrificed when a lesion reached clinical end point. The number of tumour burdened mammary glands represents the number of tumour bearing mammary glands over the total number of ten murine mammary glands. Statistical analysis was performed by the Kruskal-Wallis test with Dunn's multiple comparisons in GraphPad Prism. Error bars represent mean with SD (n \geq 3 per each cohort). * $P < 0.05$, ** $P < 0.01$, *** $P < 0.001$, **** $P < 0.0001$. MP, multiparous; NP, nulliparous.

BLG-Cre;Catnb^{wt/lox(ex3)}

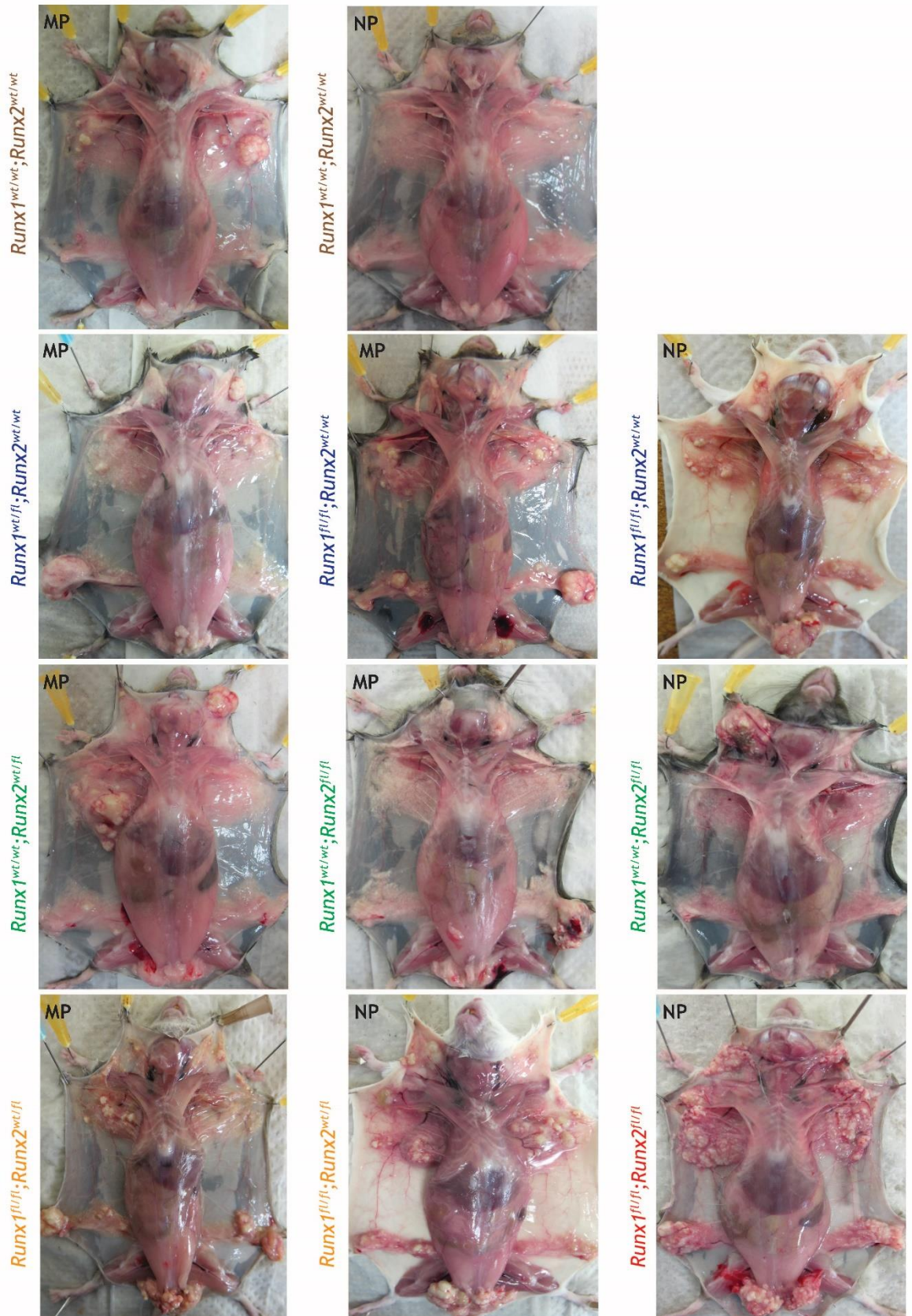


Figure 4. 15 Gross appearance of the phenotypical changes affecting the mammary glands of *Wnt/β-catenin*-activated mutant mice upon loss of the *Runx* genes.

Pictures of *BLG-Cre;Catnb^{wt/lox(ex3)}* *Runx*-deficient mice. MP, multiparous; NP, nulliparous.

4.3.4 Activation of the Wnt/ β -catenin signalling pathway leads to the formation of adenosquamous mammary lesions

When mice from all *Runx*-deficient *BLG-Cre;Catnb^{wt/lox(ex3)}* cohorts reached clinical end point, their mammary tumours were dissected out and formalin-fixed paraffin-embedded in order to preserve tissue architecture. Tissue blocks were then sectioned to generate corresponding blanks, which were used for H&E staining and IHC analysis. Examination of H&E stained tumour sections from *BLG-Cre;Catnb^{wt/lox(ex3)}* mice revealed the presence of a highly disorganized mammary structure, characterized by the formation of adenosquamous lesions reminiscent of metaplastic human breast cancer (Figure 4. 16). These highly differentiated and heterogenous elements were found to be composed of two main epithelial compartments, i.e. dense glandular regions and enlarged keratin pearls, surrounded by extensive areas of connective tissue. In an attempt to dissect the composition of the lesions, both basal (CK5, CK14 and p63) and luminal (CK8/18) epithelial markers were used. As such, if dense epithelial glandular elements displayed a higher amount of CK8/18 positivity, CK5 and CK14 positive cells appeared to be restricted to the external layer of keratin nodules. α SMA, a marker of myoepithelial cells, was found to surround both types of adenosquamous lesions. Importantly, whilst being predominantly localized at the plasma membrane in wild type mice, strong nuclear β -catenin staining was reported in both tumourigenic elements, which also displayed a modest amount of Ki67 positive cells (Figure 4. 16). This result aligned with the constitutive activation of canonical Wnt signalling characterizing *BLG-Cre;Catnb^{wt/lox(ex3)}* mice and highlighted a causative role for β -catenin in the conversion of a normal mammary epithelium into a tumourigenic one. In addition, macroscopic and microscopic examination of lungs, and other organs, revealed no evidence of metastasis shown by Wnt/ β -catenin activated GEMM of breast cancer. Of note, when the same analysis was applied to all cohorts of *BLG-Cre;Catnb^{wt/lox(ex3)}* mice, histopathological examination revealed no major differences depending on the *Runx* status of the mice (data not shown).

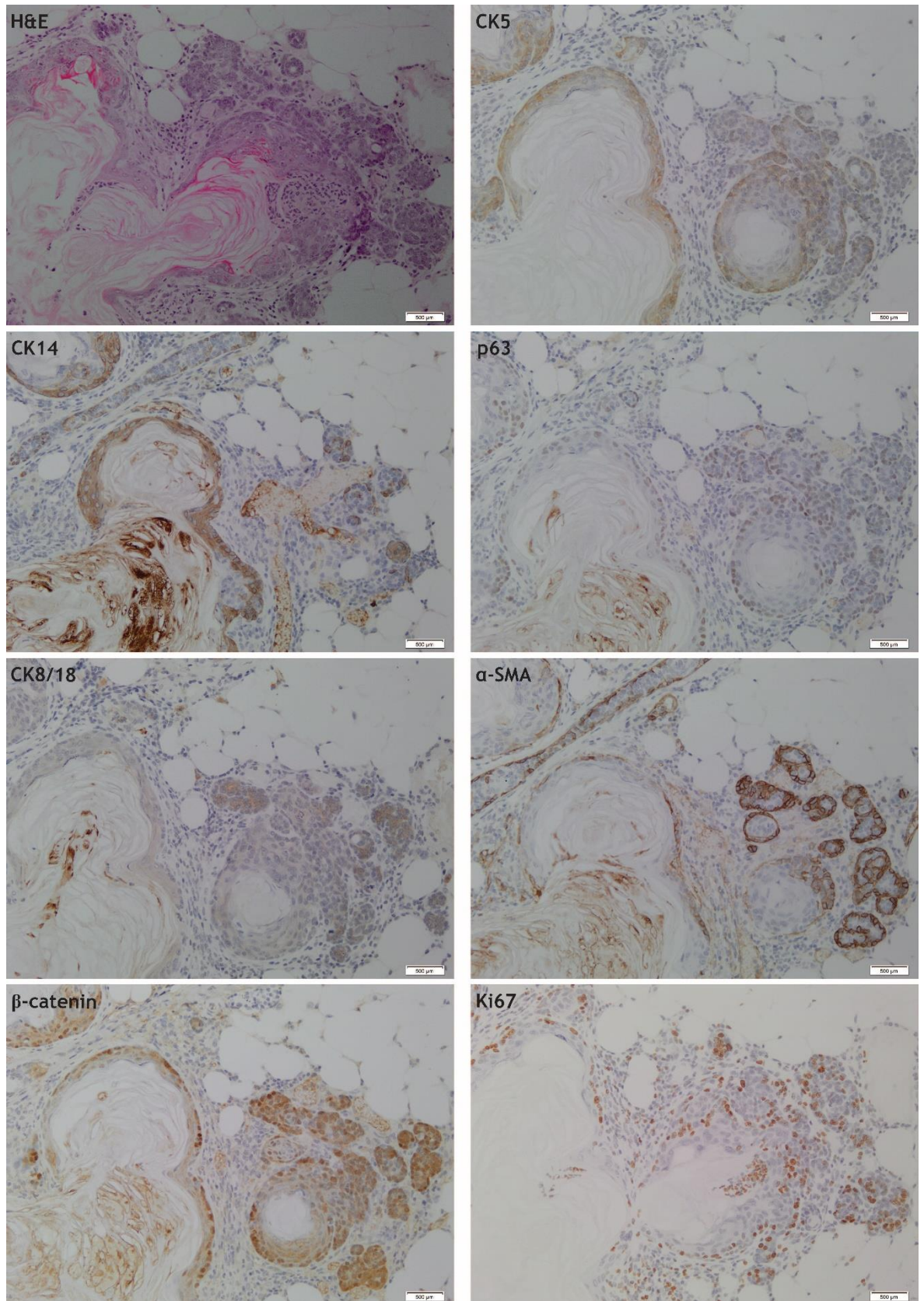


Figure 4. 16 Histopathological analysis of Wnt/ β -catenin driven adenosquamous lesions.

H&E and IHC staining of basal (CK5, CK14, p63), luminal (CK8/18), myoepithelial (α -SMA), proliferative (Ki67) and β -catenin makers on adenosquamous sections from clinical end point Wnt/ β -catenin-activated mutant mice. Scale bar, 500 μ m.

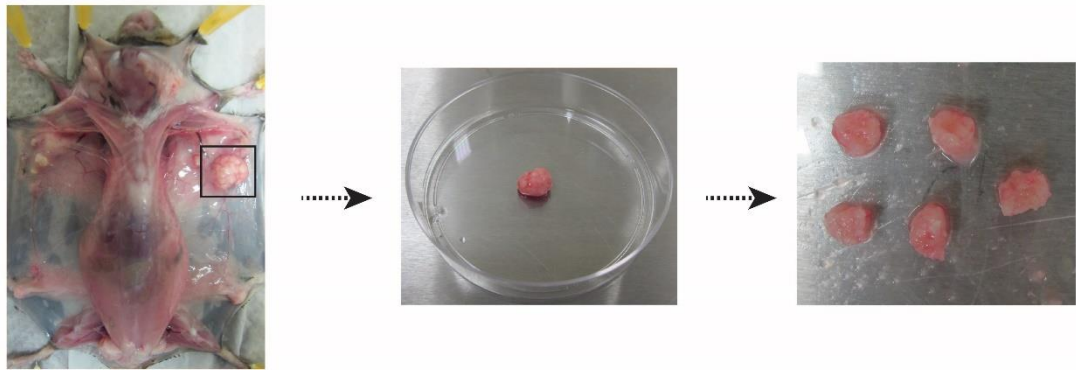
4.3.5 Investigating the tumourigenic potential of Wnt/ β -catenin-driven mammary lesions upon loss of the *Runx* genes

The significant acceleration of Wnt/ β -catenin-driven tumourigenesis, coupled with the increased tumour burden and number of tumour-burdened mammary glands displayed by NP *Runx1^{fl/fl};Runx2^{fl/fl}* mice may represent the expansion of a stem/progenitor mammary subpopulation. This hypothesis elicited an investigation of the stem-like properties characterizing Wnt/ β -catenin activated mammary tumours, in the context of *Runx1*, *Runx2* or *Runx1* and *Runx2* loss. Transplantation has for long been considered the gold standard assay to test the regenerative and tumourigenic potential of normal or transformed mammary tissues and/or MMECs. In view of this, two experimental approaches could have been employed: the first one refers to the injection of dissociated mammary tumour cells, either at fixed or limiting dilutions; the second one to the transplantation of mammary tumour-derived fragments. Due to the peculiar histopathology characterizing *BLG-Cre;Catnb^{wt/lox(ex3)}* mice, mechanical and enzymatic dissociation of Wnt/ β -catenin-driven adenosquamous lesions turned out to be extremely challenging. Therefore, to overcome these technical difficulties, the second approach was adopted. In addition, this choice allowed maintaining the intact structural architecture of Wnt/ β -catenin-driven tumours, so that interactions between cells of different compartments (epithelial and stromal) and of different potentials (stem, progenitor and differentiated) could be preserved.

As such, *BLG-Cre;Catnb^{wt/lox(ex3)}* mice of the MP *Runx1^{wt/wt};Runx2^{wt/wt}*, MP *Runx1^{fl/fl};Runx2^{wt/wt}*, MP *Runx1^{wt/wt};Runx2^{fl/fl}* and NP *Runx1^{fl/fl};Runx2^{fl/fl}* groups were sacrificed at clinical end point and their biggest tumour lesion dissected out. Each tumour was then sectioned into five tumour fragments, hereafter referred to as mouse-derived tumour fragments (MDTFs), which were independently transplanted into immunodeficient mice (Figure 4. 17). The growth of MDTFs generated from different *Runx*-deficient *BLG-Cre;Catnb^{wt/lox(ex3)}* cohorts was monitored over time and recipient mice were sacrificed when clinical end point was reached (Figure 4. 18). Based on the obtained results, 25% of MDTFs derived from the MP *Runx1^{wt/wt};Runx2^{wt/wt}* control cohort displayed the ability to transplant (Figure 4. 19A). Whilst an increased take rate was reported in the absence of *Runx1* (35%) (Figure 4. 19B) and combined deletion of *Runx1*

and *Runx2* (40%) (Figure 4. 19D), these differences did not appear to be statistically significant in respect to controls. Of note, examination of H&E stained tumour sections from all three cohorts of *BLG-Cre;Catnb^{wt/lox(ex3)}* mice revealed not only similarity among each other, yet also maintenance of the histopathology characterizing donor tumours (data not shown). A different scenario applied instead to the MP *Runx1^{wt/wt};Runx2^{fl/fl}* cohort, whose MDTFs failed to grow out in recipient mice (Figure 4. 19C), albeit this could be due to the low number of transplant experiments performed. Nonetheless, one ways to circumvent this issue could be to test the tumourigenic potential of MDTFs derived from the *MP Runx1^{wt/wt};Runx2^{wt/fl}* cohort of mice. The long tumour latency displayed by the majority of *BLG-Cre;Catnb^{wt/lox(ex3)}* cohorts, their mixed background and the expensive use of immunocompromised recipient, hindered the possibility to carry out serial transplantation analysis. In the near future, backcrossing of the *BLG-Cre*, *Catnb^{wt/lox(ex3)}*, *Runx1^{fl/fl}* and *Runx2^{fl/fl}* alleles onto a pure FVB background will enable the use of syngeneic recipient mice, wherein MDTFs could be transplanted either subcutaneously or orthotopically. Thus, implementation of the transplantation technique may allow clarification of how deletion of *Runx1*, *Runx2* or both genes impact upon the tumourigenic potential of Wnt/ β -catenin driven mammary tumours.

1. Clinical end point mammary tumour dissection



2. Mouse-derived tumour fragments transplantation



Figure 4. 17 Overview of the transplantation assay.

Workflow depicting the steps required to test the regenerative potential of Wnt/ β -catenin-driven mammary tumours upon loss of *Runx1*, *Runx2* or both genes through the use of the transplantation assay. *BLG-Cre;Catnb^{wt/lox(ex3)}* from all *Runx*-deficient cohorts mice were sacrificed at clinical end point and their biggest tumour lesion was dissected out. Each tumour was divided into five MDTFs (3 mm x 3 mm), which were independently transplanted into the right flank of five immunodeficient (athymic and CD1 nude) mice. The growth of MDTFs was monitored over time and recipient mice were sacrificed when clinical end point was reached. MDTF, mouse-derived tumour fragment.

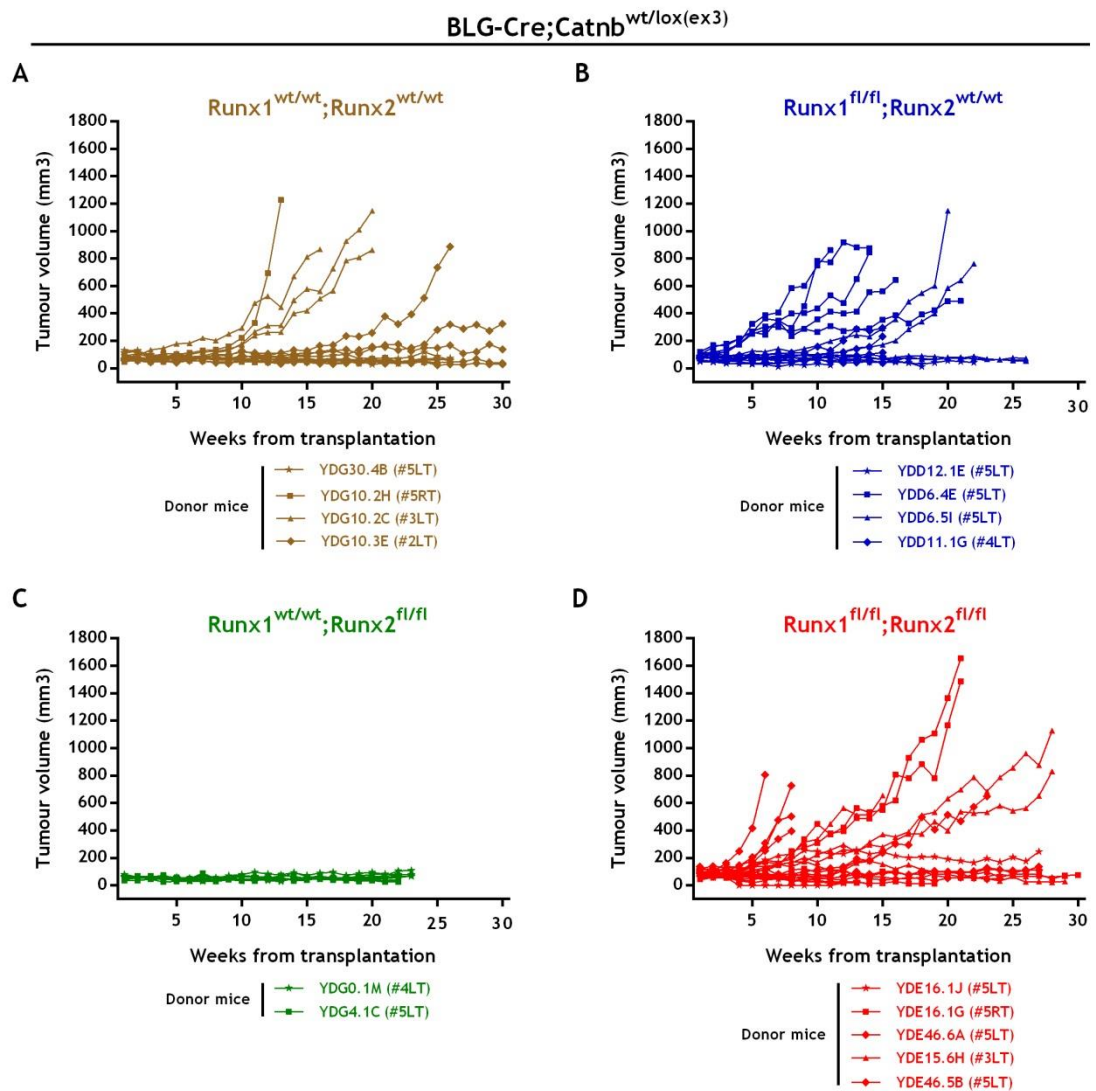


Figure 4. 18 Investigating the tumourigenic potential of Wnt/ β -catenin driven mammary tumours in the absence of the *Runx* genes.

Growth curves of MDTFs derived from *BLG-Cre;Catnb^{wt/lox(ex3)}* mice of the (A) MP *Runx1^{wt/wt};Runx2^{wt/wt}* (n=4 donor mice), (B) MP *Runx1^{fl/fl};Runx2^{wt/wt}* (n=4 donor mice), (C) MP *Runx1^{wt/wt};Runx2^{fl/fl}* (n=2 donor mice) and (D) NP *Runx1^{fl/fl};Runx2^{fl/fl}* (n=5 donor mice) cohorts. Donor mice from each *BLG-Cre;Catnb^{wt/lox(ex3)}* cohort are shown below each graph and are characterized by a different symbol. Donor mice were sacrificed at clinical end point, when their biggest tumour lesion was dissected out. Each tumour was sectioned into five independent MDTFs. Each MDTF was subcutaneously transplanted into an immunodeficient (recipient) mouse. The growth of each MDTF was monitored over time by measuring its volume (mm³) via the formula [(L x W x W)/2, with L>W] through the use of calipers. Recipient mice were euthanized when clinical end point was reached, that is when L or W of the tumour equalled 15 mm or if the lesion ulcerated. The growth of all five MDTFs derived from each donor mouse is displayed on the graph by five separate lines characterized by the same symbol. L, length; MDTF, mouse derived tumour fragment; MP, multiparous; NP, nulliparous; W, width.

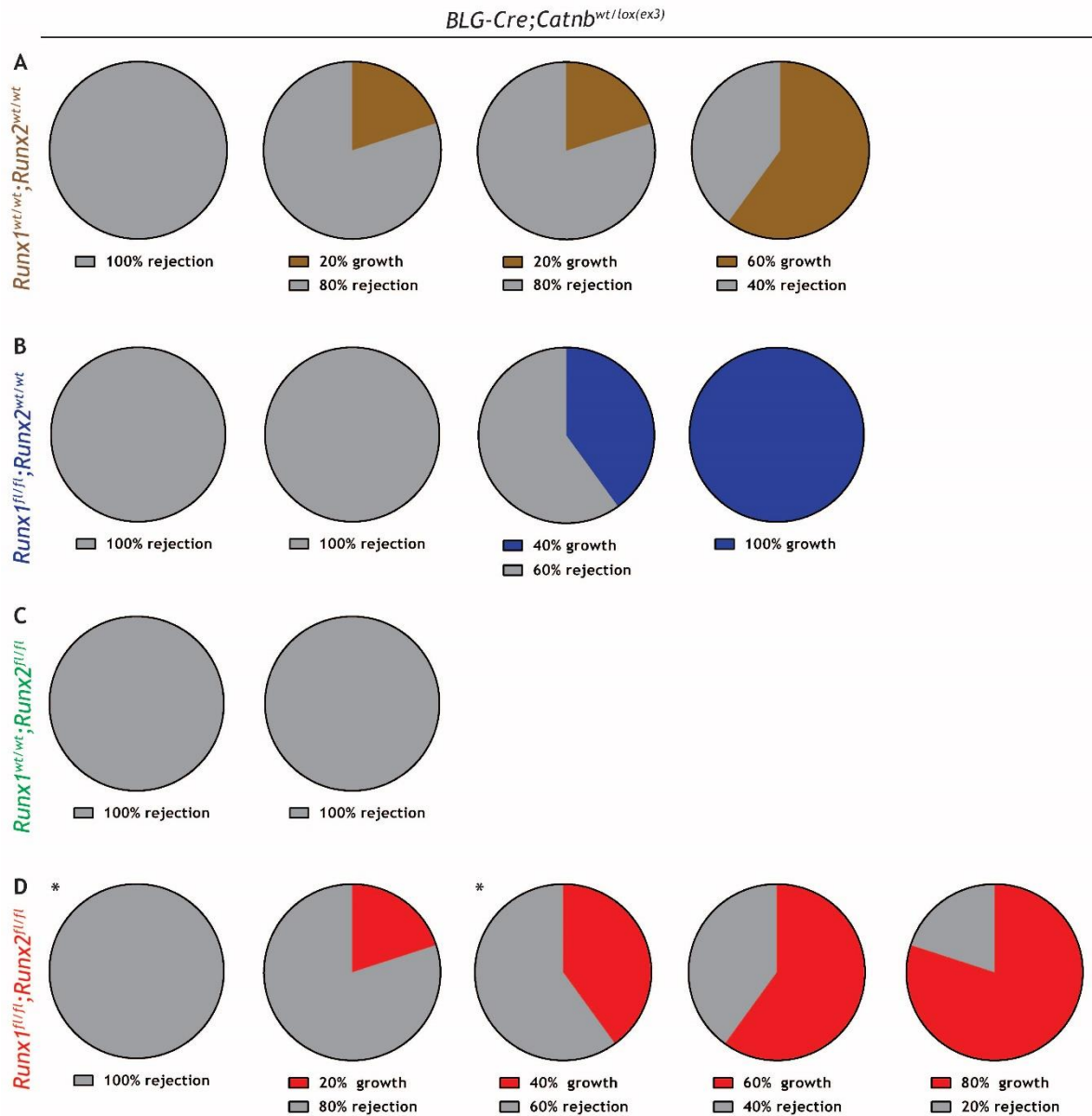


Figure 4. 19 Summary of the tumourigenic potential of Wnt/ β -catenin driven mammary tumours in the absence of the *Runx* genes.

Pie charts of the take rate displayed by the transplantation of MDTFs derived from *BLG-Cre;Catnb^{wt/lox(ex3)}* mice of the MP *Runx1^{wt/wt};Runx2^{wt/wt}* (n=4), MP *Runx1^{fl/fl};Runx2^{wt/wt}* (n=4), MP *Runx1^{wt/wt};Runx2^{fl/fl}* (n=2) and NP *Runx1^{fl/fl};Runx2^{fl/fl}* (n=5) cohorts. Donor mice were sacrificed at clinical end point and their biggest tumour lesion dissected out. Each tumour was divided into five MDTFs, which were independently transplanted into immunodeficient mice. Each pie chart represents the take rate of all five MDTFs derived from each donor GEMM. Underneath each pie chart, the percentage of MDTFs growth and/or rejection is displayed from that donor. Asterisk in the NP *Runx1^{fl/fl};Runx2^{fl/fl}* cohort of mice indicate the use of CD1 recipient mice. For all other transplants experiments, athymic nude mice were used. GEMM, genetically engineered mouse model; MDTF, mouse-derived tumour fragment; MP, multiparous; NP, nulliparous.

4.4 Discussion

It is now broadly accepted that Wnt signalling plays a major role in the mammary gland, wherein it exerts a tight control upon the self-renewal potential and proliferative capacity of mammary stem/progenitor cells. In addition, the pathway has been involved in the aetiology of many epithelial cancers, including breast cancer, raising the possibility that these two processes might be linked. Indeed, aberrant Wnt signalling was shown to override the aforementioned mechanisms, culminating in uncontrolled cycling and expansion of the MaSCs pool (Reya and Clevers, 2005). This appears to be particularly true for breast cancer, as corroborated by Wnt1-driven GEMMs whose mammary tumours displayed an accumulation of neoplastic cells with stem/progenitor-like features (Liu et al., 2004; Teissedre et al., 2009). In many cases, Wnt-driven tumourigenesis was shown to occur through dysregulation of the canonical pathway. This process could result from activation of Wnt receptors, inactivation of any member of the β -catenin destruction complex, such as deletion of APC, or from direct mutations of the *CTNNB1* gene (Polakis, 1999). In all cases, the net result is the stabilization of cytosolic β -catenin through prevention of its proteosomal degradation, whilst promotion of its translocation to the nucleus. This event can in turn lead to the persistent activation and/or repression of a multitude of downstream proto-oncogenes and tumour suppressors, resulting in aberrant cell growth and oncogenic transformation (Polakis, 2000). In line with the fact of taking part in the same signalling cascade, the majority of these genetic alterations were found to be mutually exclusive. In this regards, whilst APC inactivating mutations were predominantly linked to sporadic and inherited forms of colon cancers (Miyoshi et al., 1992), activating mutations of β -catenin were found in human hepatocellular (Miyoshi et al., 1998), uterine (Fukuki et al., 1998) and ovarian (Palacios and Gamallo, 1998) cancers. Albeit generally uncommon in human breast cancer (Lin et al., 2000) and often displayed only by benign fibromas (Abraham et al., 2002), genetic alterations of β -catenin were documented in a rare subtype of the disease referred to as metaplastic breast cancer (Hayes et al., 2008). Nonetheless, up to 40% of human breast cancer appears to be characterized by increased cytoplasmic and nuclear β -catenin and correlates with poor or worse patient prognosis (Lin et al., 2000). Altogether, these findings highlight that deregulation of upstream β -catenin elements are

likely to be the cause of aberrant Wnt signalling in breast cancer (Incassati et al., 2010).

Notwithstanding the paucity of β -catenin activating mutations, several breast cancer GEMMs have thus far relied on the use of β -catenin mutant alleles, including N-terminally truncated Δ N57, Δ N89, Δ N90 and *Catnb*^{wt/lox(ex3)} ones, to mimic constitutive activation of canonical Wnt signalling. Interestingly, despite all aiming at removal of the amino acid residuals critical for β -catenin degradation, the use of different Wnt/ β -catenin-driven GEMMs has led over time to very disparate results (Incassati et al., 2010). On one hand, the K5- Δ N57 β -catenin mouse model showed the development of invasive basal-type carcinomas (Teuliere et al., 2004). On the other, MMTV- or whey acidic protein-Cre-*Catnb*^{wt/lox(ex3)} GEMMs displayed squamous metaplasia (Miyoshi et al., 2002). In addition, when the MMTV promoter was used to drive recombination of the Δ N89 or Δ N90 β -catenin alleles, the formation of adenocarcinomas was observed (Imbert et al., 2001; Michaelson and Leder, 2001). This wide phenotypic variability was indicative of a highly context-dependent role played by β -catenin, depending on different epithelial compartments of the mammary gland, yet also on the specific targeted cell type within the latter (Incassati et al., 2010). In case the event that the same promoter driver was used to guide recombination, phenotypic differences were instead attributed to changes in β -catenin cellular levels, stemming perhaps from the use of different transgenic lines of mice (Miyoshi et al., 2002).

Despite not mimicking the genetic aberrations found in the majority of human breast cancer, the use of Wnt/ β -catenin-activated GEMMs has certainly reinforced the causative role played by canonical Wnt in the aetiology of the disease. Notwithstanding the potent oncogenic effect exerted by β -catenin, it is now widely accepted that cancer is characterized by a “multihit” nature, as it requires more than one genetic event to arise (Vogelstein, 1983). This notion was corroborated by the absence of gross adenosquamous lesions in the NP cohort of *BLG-Cre;Catnb*^{wt/lox(ex3)} control mice. In view of the hormone-responsiveness shown by the BLG-Cre driver, it was only after two rounds of parities that mammary tumours started to appear, albeit occurring at an average time of 341 days and affecting only a few mammary glands. Therefore, the long

tumour latency and the low penetrance of tumour formation supported the idea that BLG-Cre-mediated activation of β -catenin was not fully sufficient to drive breast tumourigenesis. In an effort to unveil new putative breast cancer players whose genetic aberrations were able to unleash aberrant activation of the Wnt/ β -catenin pathway in the mammary gland, attention was focused on the *Runx* family of genes. Highly expressed in the basal epithelial compartment (McDonald et al., 2014; van Bragt et al., 2014) and shown to play a role in the regulation of mammary stemness (Ferrari et al., 2015), an interplay between the Wnt signalling pathway and *Runx* genes was hypothesized. Accordingly, deletion of *Runx1* and heterozygous deletion of *Runx2* resulted in a significant acceleration of palpable tumour formation in respect to control mice, providing for the first time a compelling evidence for a tumour suppressive function exerted by these genes in a breast cancer GEMM. More importantly, whilst generally potentiated in the presence of multiple parities, the same BLG-Cre driven phenotype could also be observed in nulliparous mice, thus strengthening the effect of *Runx1* or *Runx2* deletion in the context of activated Wnt/ β -catenin signalling. What was particularly fascinating was the ability of *Runx1* and *Runx2* to seemingly compensate for the other deleted gene, as evidenced by the delayed tumour progression in *Runx1*- and *Runx2*-deficient cohorts. Further proof of this hypothesis was seen through combined deletion of both genes, which resulted in the appearance of Wnt/ β -catenin-driven lesions at around 56 days and in the overall survival of the mice at 99 days. If on one hand these results showed the potent tumour suppressive effects exerted by *Runx1* and *Runx2*, on the other these emphasized the remarkable survival advantage displayed by Wnt/ β -catenin-activated MMECs upon homozygous loss of *Runx1* and *Runx2*. In addition, what emerged from the analysis was also the long latency, yet fast tumour progression characterizing the *Runx1*^{wt/wt};*Runx2*^{wt/wt} control cohort of mice. Of note, this intriguing pattern of BLG-Cre-mediated Wnt/ β -catenin-driven mammary tumourigenesis appeared indicative of the presence of secondary hits. Considering the similar tumour progression displayed by *Runx1*^{wt/wt};*Runx2*^{wt/wt} and *Runx1*^{fl/fl};*Runx2*^{fl/fl} mice, it is tempting to speculate that these secondary hits might refer to *Runx1* and *Runx2*.

If acceleration of tumourigenesis denoted a tumour suppressive role played by the *Runx* genes, the increased tumour burden and number of tumour burdened

mammary glands upon combined *Runx1* and *Runx2* deletion hinted towards the expansion of a stem/progenitor subpopulation susceptible to Wnt/ β -catenin-driven transformation. Interestingly, a trend towards increased tumour burden and higher number of tumour-burdened mammary glands was also observed upon deletion of *Runx1*, yet not *Runx2*. Therefore, the extent to which these genes act and perhaps the context wherein they function may be different. Nonetheless, when the tumourigenic potential of *Runx*-deficient lesions was assessed using an *in vivo* transplantation assay, deletion of *Runx1* or combined deletion of *Runx1* and *Runx2* resulted in higher take rates as compared to controls (albeit numbers were too low to show significant differences). In addition, despite the lack of outgrowth displayed by the *Runx2*-deficient group of mice, no conclusion could be drawn in view of the low number of transplants performed. If first passage tumours displayed equal transplantability, perhaps the future use of serial transplants on syngeneic mice might help unravel how deletion of *Runx1*, *Runx2* or both genes impinges upon the long-term tumourigenic potential of Wnt/ β -catenin-driven mammary lesions.

Finally, upon histopathological examination, all cohorts of *BLG-Cre;Catnb^{wt/lox(ex3)}* mice, regardless of their *Runx* status, were found to be characterized by the presence of adenosquamous lesions. Nonetheless, this is not the first time this phenotype was reported among *Catnb^{wt/lox(ex3)}*-driven breast cancer GEMMs. In fact, due to its prominent role as a major determinant of epidermal epithelium, stabilization of β -catenin was already shown to induce trans-differentiation of the mammary epithelium into an epidermal one (Miyoshi et al., 2002). As such, one could then imagine that the identity and differentiation of mammary gland can only be achieved through tight regulation of the Wnt/ β -catenin signalling pathway. In view of the suppressive role shown by the *Runx* genes in the context of activated Wnt/ β -catenin signalling, it is then tempting to speculate that RUNX1 and RUNX2 might act as “sentinels” of mammary epithelial cell fate and identity.

5 Dissecting the role played by *Runx1* and *Runx2* in the early stages of Wnt/ β -catenin driven breast tumourigenesis

5.1 Introduction

In contrast to the majority of genetic diseases, cancer arises from the sequential accumulation of several somatic mutations hitting one or a few cells-of-origin. In line with the multi-hit nature of tumourigenesis is also the fact that cancer incidence dramatically increases with age (Vogelstein et al., 1983). Although the steps of this gradual evolution are well-documented for some types of cancer, yet not so much for others, common traits can be defined. It is proposed in fact that cancers grow through a process of clonal expansion, whereby, upon the acquisition of sequential mutations, targeted cells would proliferate, leading to the abnormal expansion of their progeny. In this way, oncogenic transformation of normal tissues would give rise to benign lesions. Acquisition of further hits will allow growth of benign tumours. Over time, cells within incipient pre-neoplastic lesions will keep acquiring different somatic mutations giving rise to distinct subclones. Lastly, through a process of Darwinian evolution or “selective sweep”, fittest sub-clones will dominate over others, thus converting benign tumours into malignant ones (Nowell, 1976). In view of above, the significant acceleration of tumourigenesis, the decrease in overall survival and increase in tumour burden displayed by *BLG-Cre;Catnb^{wt/lox(ex3)};Runx1^{fl/fl};Runx2^{fl/fl}* mice (see Chapter 3) were all indicative hints of a precocious Wnt/ β -catenin-driven transformation of the mammary epithelium. As ‘*in solving a problem of this sort, the grand thing is to be able to reason backwards*’ (Sherlock Holmes - Sir Arthur Conan Doyle), a thorough investigation of the early effects of MMECs transformation following activation of the Wnt/ β -catenin signalling pathway was next performed.

5.2 Results

5.2.1 Activation of Wnt/ β -catenin signalling alters mammary development in the absence of *Runx1* and *Runx2*

One of the main advantages of the murine mammary gland relates to the fact that its development takes place predominantly after birth (Medina et al., 1996). To investigate if BLG-Cre-driven activation of the Wnt/ β -catenin signalling pathway in the context of *Runx* gene deletion was impinging on an established mammary epithelium, or rather on an incipient one, a thorough characterization of all cohorts of *BLG-Cre;Catnb^{wt/lox(ex3)}* mice was carried out. In parallel, to discriminate between the role exerted by RUNX1 and RUNX2 in a Wnt/ β -catenin-activated context or in a physiological background, the corresponding cohorts of *BLG-Cre;Catnb^{wt/wt}* virgin mice were also analysed.

5.2.1.1 Analysis of mammary gland pubertal development in 9 week old virgin female mice

As the majority of *BLG-Cre;Catnb^{wt/lox(ex3)};Runx1^{fl/fl};Runx2^{fl/fl}* mice developed palpable mammary tumour lesions around 56 days on average, it was reckoned that the 9 week developmental time-point might capture the conversion of the normal mammary epithelium into a pre-neoplastic one. Of note, all 9 week old *Runx* deficient mice displayed lighter body weights compared to *BLG-Cre;Catnb^{wt/lox(ex3)}* control mice, but results were found to be statistically significant only in the absence of *Runx2* (Figure 5. 1A). However, no differences were observed among groups in relation to cumulative mammary gland weight (Figure 5. 1B). Differently, whilst 9 week old *BLG-Cre;Catnb^{wt/wt}* mice showed generally comparable body weights, regardless of their *Runx* status (Figure 5. 1C), a decrease in cumulative mammary gland weight was found in the *Runx1^{fl/fl}* cohort of mice (Figure 5. 1D). When #4 mammary glands from *BLG-Cre;Catnb^{wt/lox(ex3)}* mice were analysed by whole-mount examination, these showed thickened epithelial ducts across all genotypes, in line with the presence of mammary pre-neoplastic lesions observed by H&E stains (Figure 5. 2; compare to

Figure 5. 3). This phenotype, however, appeared exacerbated in the *Runx1^{fl/fl};Runx2^{fl/fl}* cohort of mice, whose mammary glands displayed lack of normal tissue architecture (Figure 5. 2D). On the other hand, BLG-Cre combined excision of *Runx1* and/or *Runx2* in the mammary epithelium of wild type mice did not appear to affect mammary gland morphology at this stage (

Figure 5. 3). Indeed, all cohorts of 9 week old *BLG-Cre;Catnb^{wt/wt}* mice were characterized by ramified mammary trees, with elongated epithelial ducts extending throughout the mammary fat pad. These results suggested a peculiar function exerted by RUNX1 and RUNX2 particularly in the context of activated Wnt/ β -catenin signalling pathway (Figure 5. 2;

Figure 5. 3).

To investigate the extent to which the presence of thickened epithelial ducts reported by control, *Runx1^{fl/fl}* and *Runx2^{fl/fl}* mice, and the disrupted tissue

architecture of *Runx1^{fl/fl};Runx2^{fl/fl}* animals have impinged on ductal morphogenesis, quantification of the ductal elongation of #4 mammary glands was carried out. This was achieved by measuring the distance of the three longest TEBs to/from the lymph node, taken as a reference point. In doing so, whilst no differences were found depending on the *Runx* status of the mice, a severe delay in ductal elongation was reported by all cohorts of *BLG-Cre;Catnb^{wt/lox(ex3)}* when compared to *BLG-Cre;Catnb^{wt/wt}* females (Figure 5. 4). It should be noted, however, that a high degree of variability was evident in all Wnt/ β -catenin activated mice, perhaps due to the mixed background or to differences in the level of BLG-Cre-mediated recombination (Figure 5. 4A).

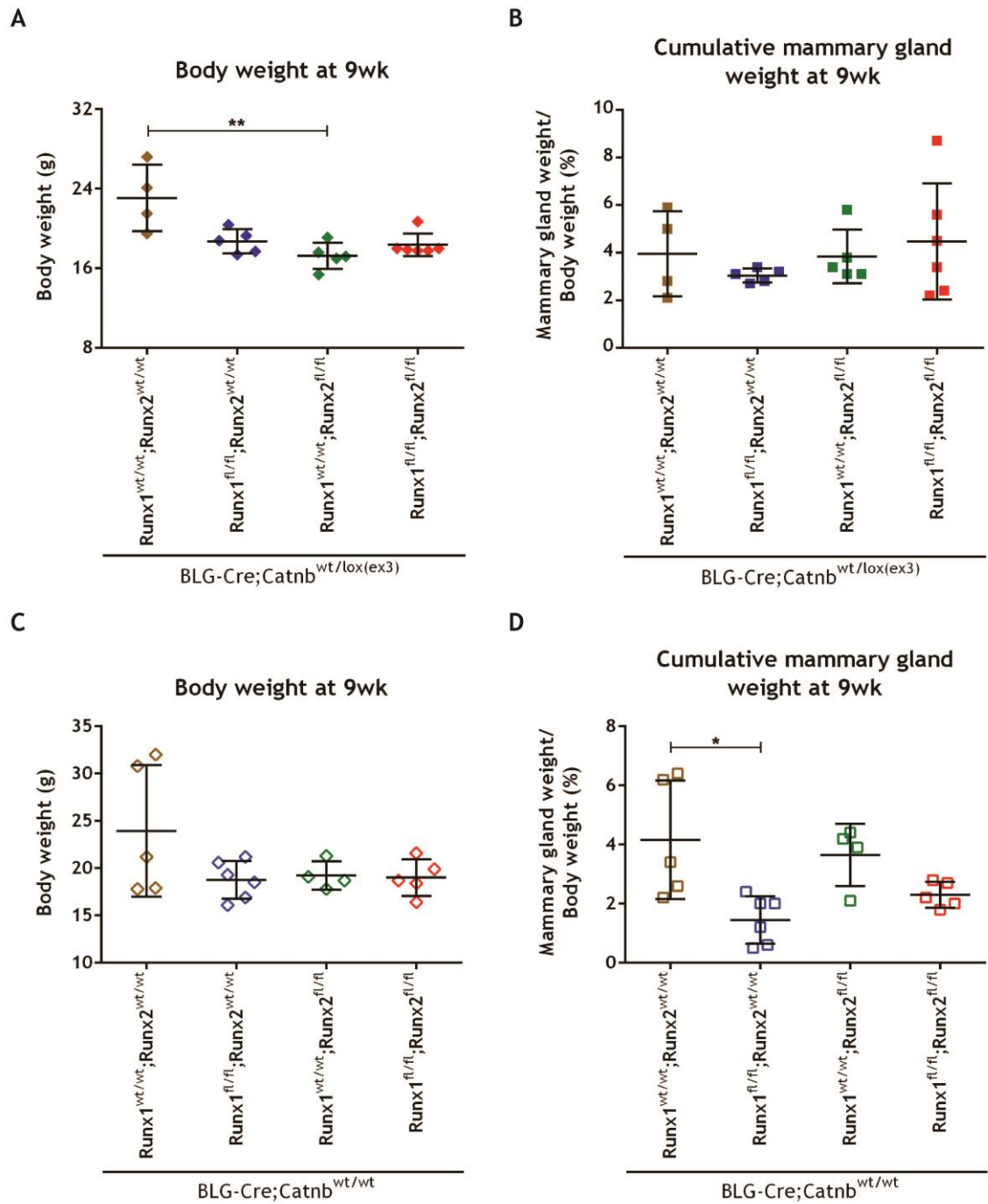


Figure 5. 1 Effect of mammary specific *Runx1* and *Runx2* loss on body weight and cumulative mammary gland weight in 9 week old *Wnt/β-catenin* mutant and wild type mice.

Scatter dot plots of body weight and cumulative mammary gland weight of 9 week old *BLG-Cre;Catnb^{wt/lox(ex3)}* (A, B) and *BLG-Cre;Catnb^{wt/wt}* (C, D) female mice upon loss of *Runx1*, *Runx2* or both genes. Cumulative mammary gland weight was expressed as a percentage of total mammary gland weight divided by the body weight of the animal. Statistical analysis was performed by the Kruskal-Wallis test with Dunn's multiple comparisons in GraphPad Prism. Error bars represent mean with SD (n≥4 per each cohort). **P*<0.05, ***P*<0.01.

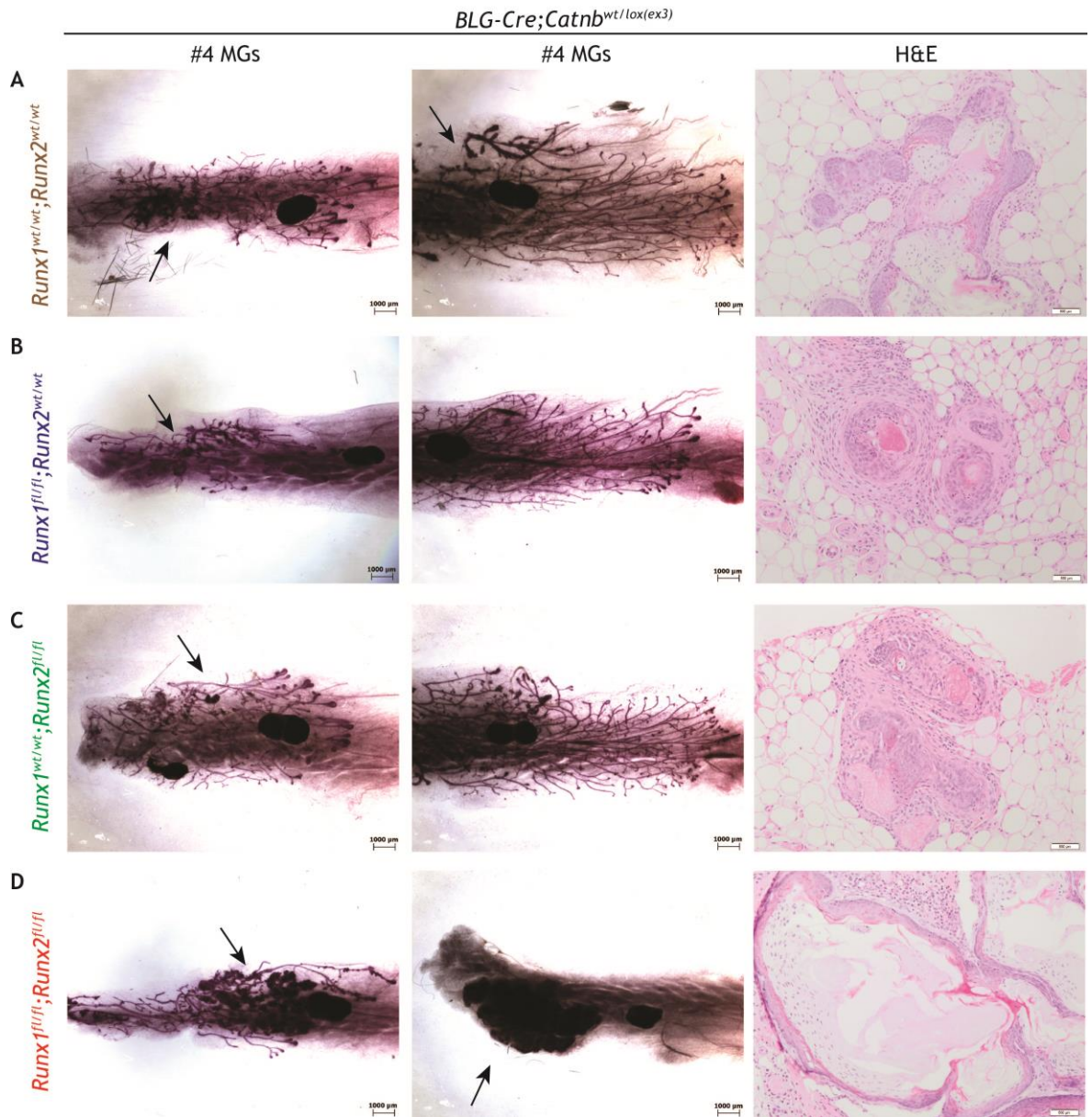


Figure 5. 2 Combined loss of *Runx1* and *Runx2* results in a dramatic impairment of ductal morphogenesis upon activation of the Wnt/ β -catenin signalling in late puberty.

Whole-mounts of #4 MGs (first two left columns) and corresponding H&Es (right column) from 9 week old *BLG-Cre;Catnb^{wt/lox(ex3)}* female mice of the *Runx1^{wt/wt};Runx2^{wt/wt}* (A), *Runx1^{fl/fl};Runx2^{wt/wt}* (B), *Runx1^{wt/wt};Runx2^{fl/fl}* (C) and *Runx1^{fl/fl};Runx2^{fl/fl}* (D) cohorts. Two representative whole-mount pictures of ≥ 4 are shown per genotype to highlight the variability within each cohort. One representative H&E image of ≥ 4 is shown per genotype. Arrows indicate the presence of thickened epithelial ducts. Scale bar of whole-mounts, 1000 μm . Scale of H&Es, 500 μm . H&E, haematoxylin eosin stain; MG, mammary gland.

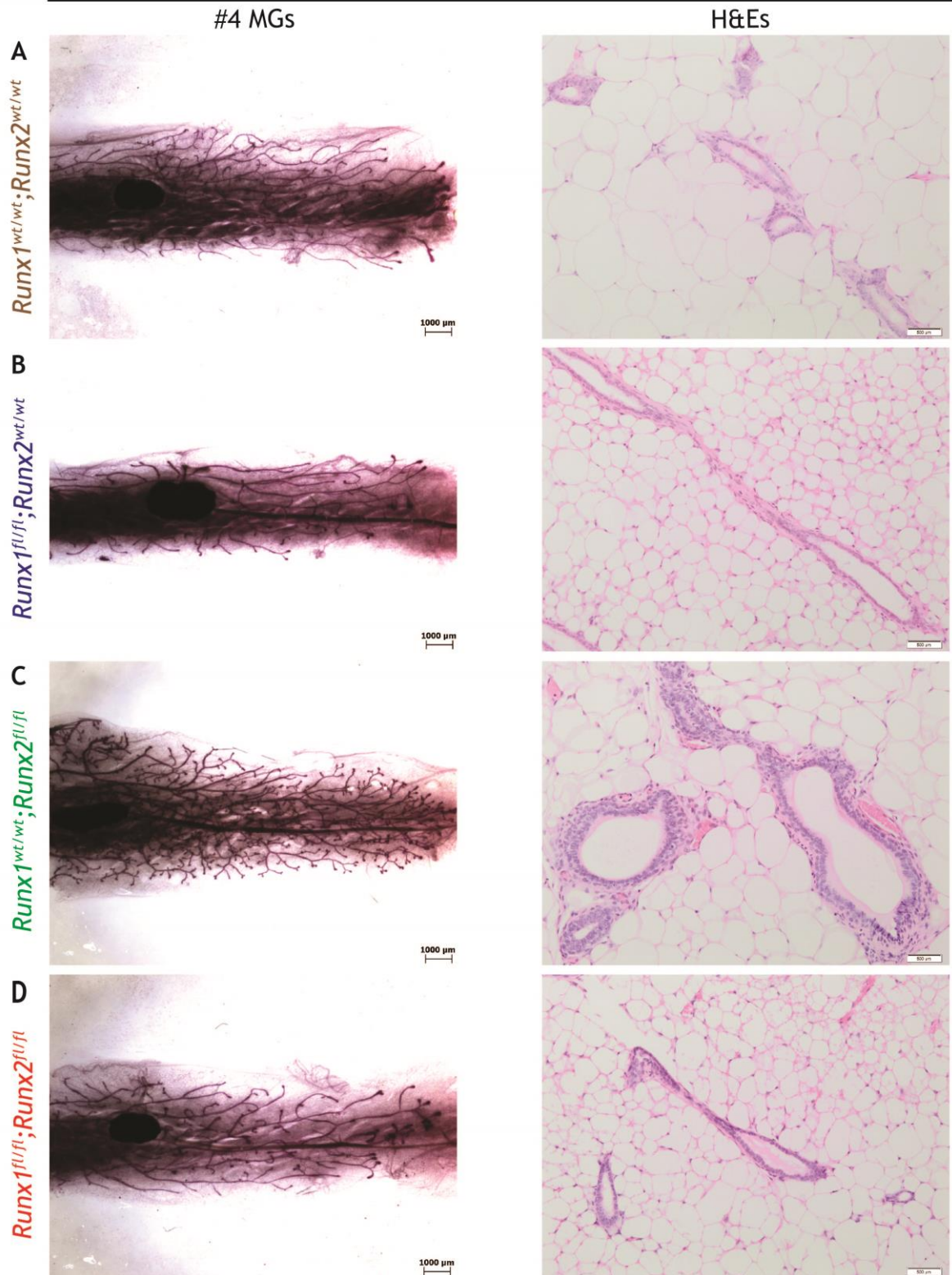
BLG-Cre;Catnb^{wt/wt}

Figure 5. 3 Mammary-specific deletion of *Runx1* and *Runx2* does not affect ductal morphogenesis of Wnt/ β -catenin wild type mice in late puberty.

Whole-mounts of #4 MGs (left column) and corresponding H&E (right column) from 9 week old *BLG-Cre;Catnb^{wt/wt}* female mice (A), upon loss of *Runx1* (*Runx1^{fl/fl};Runx2^{wt/wt}*) (B), *Runx2* (*Runx1^{wt/wt};Runx2^{fl/fl}*) (C), or both genes (*Runx1^{fl/fl};Runx2^{fl/fl}*) (D). One representative whole-mount and H&E image of $n \geq 4$ is shown per cohort. Scale bar of whole-mounts, 1000 μm . Scale of H&Es, 500 μm . H&E, haematoxylin eosin stain; MG, mammary gland.

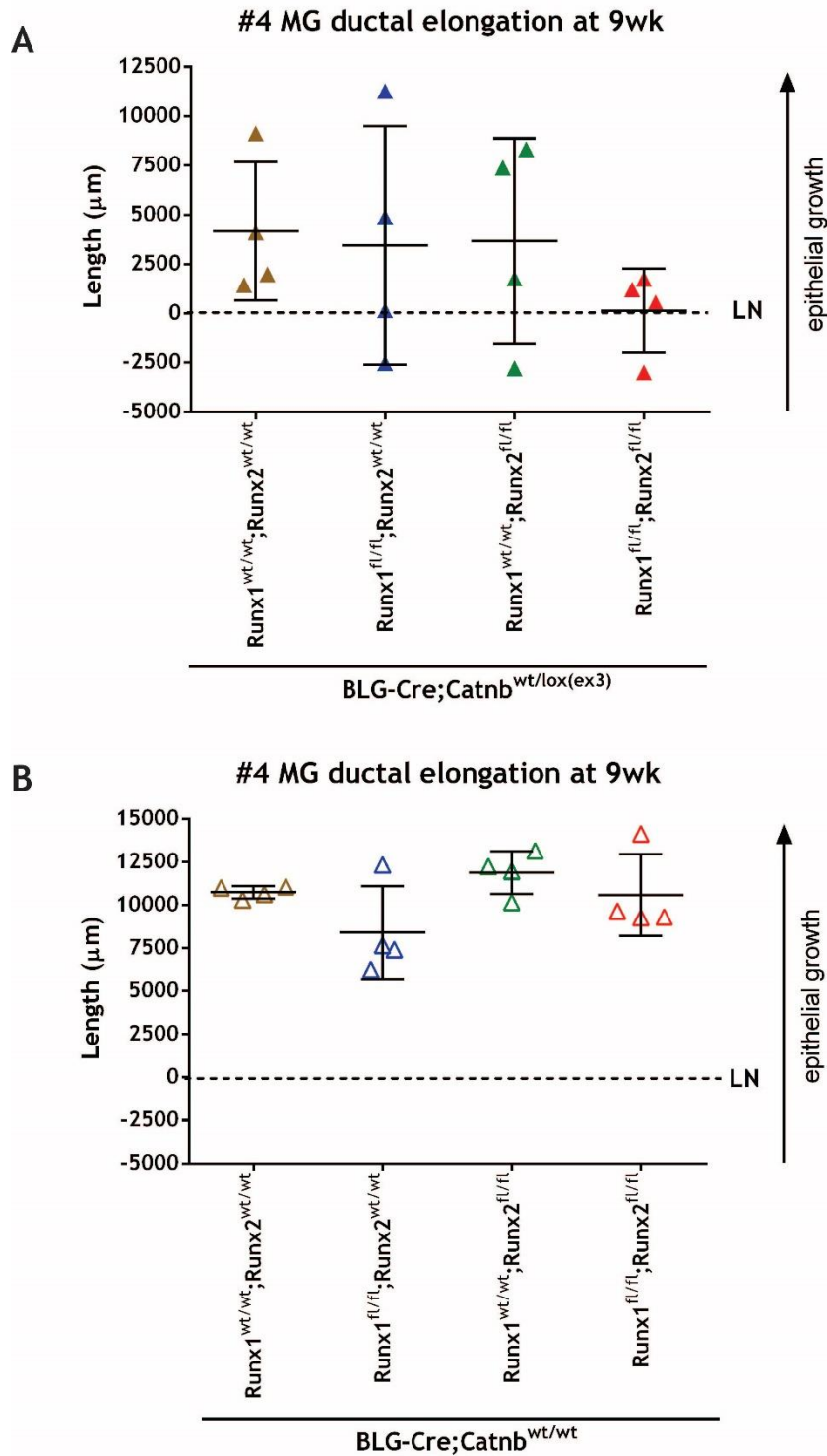


Figure 5. 4 Effect of *Runx1* and *Runx2* loss on mammary ductal elongation in 9 weeks old *Wnt*/ β -catenin activated mutant and wild type mice.

Scatter dot plot showing the ductal elongation of #4 MGs from 9 weeks old *BLG-Cre;Catnb*^{wt/lox(ex3)} (A) and *BLG-Cre;Catnb*^{wt/wt} (B) female mice upon loss of *Runx1*, *Runx2* or both genes. Ductal elongation was assessed by measuring the length of the epithelial tree to and from the LN. Arrows represent the direction of epithelial growth through the mammary fat pad. Statistical analysis was performed by the Kruskal-Wallis test with Dunn's multiple comparisons in GraphPad Prism. Error bars represent mean with SD (n=4 per each *BLG-Cre;Catnb*^{wt/lox(ex3)} and *BLG-Cre;Catnb*^{wt/wt} cohort). No significance was found. LN, lymph node; MG, mammary gland.

5.2.1.2 Analysis of mammary gland pubertal development in 6 week old virgin female mice

The presence of gross morphological differences observed in the whole-mounts and H&Es of 9 week old *BLG-Cre;Catnb^{wt/lox(ex3)}* mice suggested a more precocious transformation of the mammary epithelium upon activation of the Wnt/ β -catenin signalling pathway. This prompted an analysis at earlier stages of pubertal mammary gland development. When the 6 week developmental time-point was analysed, both single knock-out *Runx1^{fl/fl}* and *Runx2^{fl/fl}* cohorts of *BLG-Cre;Catnb^{wt/lox(ex3)}* mice displayed a significantly lighter body weights compared to wild type controls (Figure 5. 5A). The same phenotype could also be observed upon combined deletion of *Runx1* and *Runx2*, albeit the difference was not significant. Nonetheless, only *Runx1^{fl/fl}* animals presented with a significantly reduced cumulative mammary gland weight, whereas the other cohorts of *Runx2^{fl/fl}* and *Runx1^{fl/fl};Runx2^{fl/fl}* behaved like control mice (Figure 5. 5B). Lighter body weights were also observed among the *BLG-Cre;Catnb^{wt/wt}* groups of mice, yet only upon loss of *Runx2* or combined excision of *Runx1* and *Runx2* (Figure 5. 5C). No changes, however, were found in relation to cumulative mammary gland weight of the latter groups of mice (Figure 5. 5D). When #4 mammary glands were examined, both whole-mounts and H&E stains from all groups of *BLG-Cre;Catnb^{wt/lox(ex3)}* mice displayed altered mammary trees characterized by the presence of Wnt/ β -catenin-driven mammary pre-neoplastic lesions (Figure 5. 6; compare to Figure 5. 7). Nonetheless, whilst an epithelial ramified structure could still be visible in the control and single knock-out cohorts of mice, this appeared lost upon combined deletion of *Runx1* and *Runx2* (Figure 5. 6D). As in the case of the 9 week developmental stage, mammary-specific combined excision of *Runx1* and *Runx2* did not appear to influence ductal morphogenesis of wild type mice (Figure 5. 7), indicating the specificity of the aforementioned phenotype to the context of an activated Wnt/ β -catenin signalling pathway. Quantification of the ductal elongation characterizing #4 mammary glands revealed a significant delay of epithelial growth only for the double knock-out cohorts of *BLG-Cre;Catnb^{wt/lox(ex3)}* mice as compared to control (Figure 5. 8A). Albeit the same trend was noticed in the corresponding *BLG-Cre;Catnb^{wt/wt}* group of mice, no significant differences emerged in this case (Figure 5. 8B). Nonetheless, all *BLG-Cre;Catnb^{wt/wt}* displayed more elongated ductal trees as compared to *BLG-Cre;Catnb^{wt/lox(ex3)}* mice.

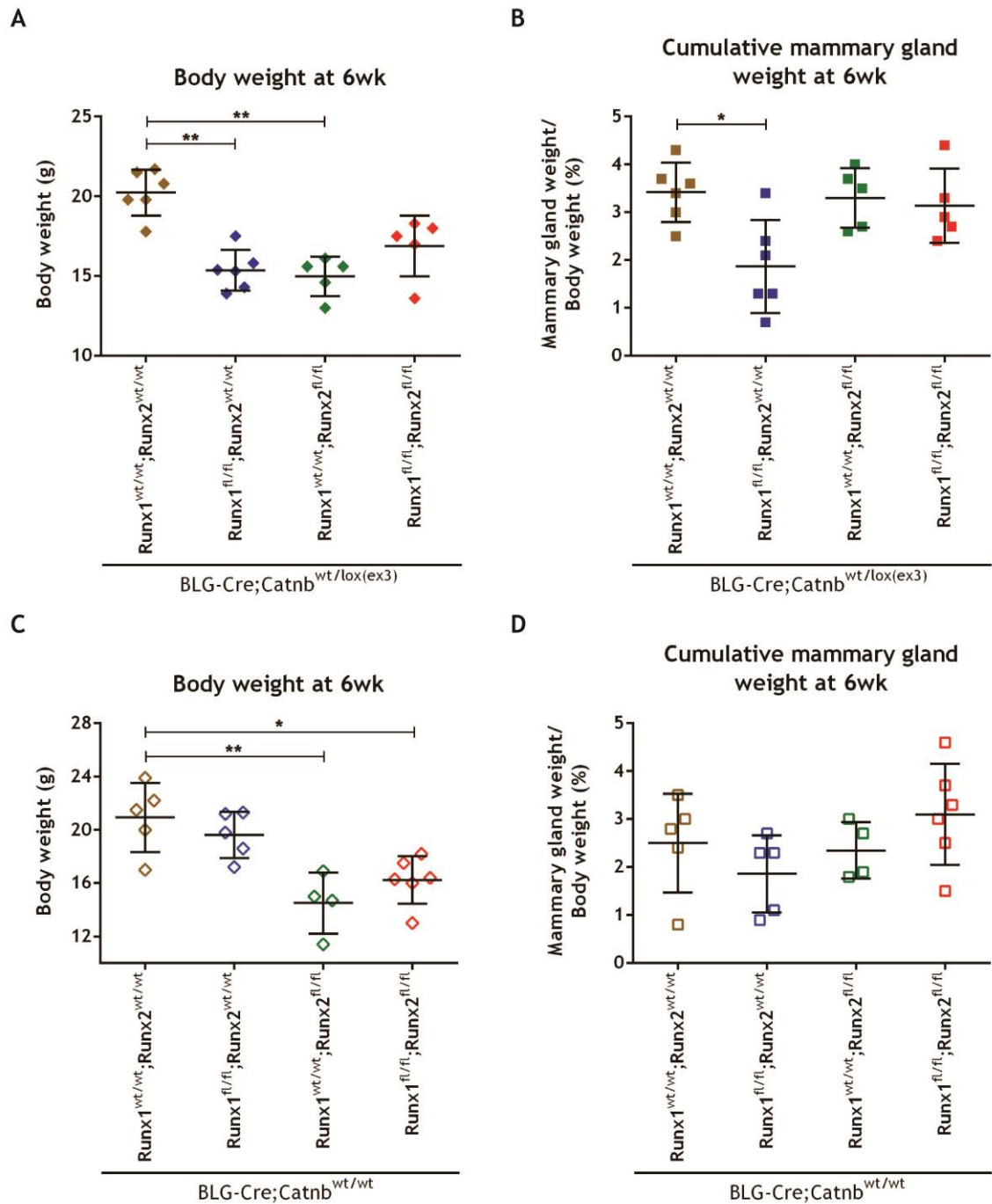


Figure 5. 5 Effect of mammary specific *Runx1* and *Runx2* loss on body weight and cumulative mammary gland weight in 6 week old Wnt/ β -catenin mutant and wild type mice.

Scatter dot plots of body weight and cumulative mammary gland weight of 6 week old *BLG-Cre;Catnb*^{wt/lox(ex3)} (A, B) and *BLG-Cre;Catnb*^{wt/wt} (C, D) female mice upon loss of *Runx1*, *Runx2* or both genes. Cumulative mammary gland weight was expressed as a percentage of total mammary gland weight divided by the body weight of the animal. Statistical analysis was performed by the Kruskal-Wallis test with Dunn's multiple comparisons in GraphPad Prism. Error bars represent mean with SD (n \geq 4 per each cohort). *P<0.05, **P<0.01.

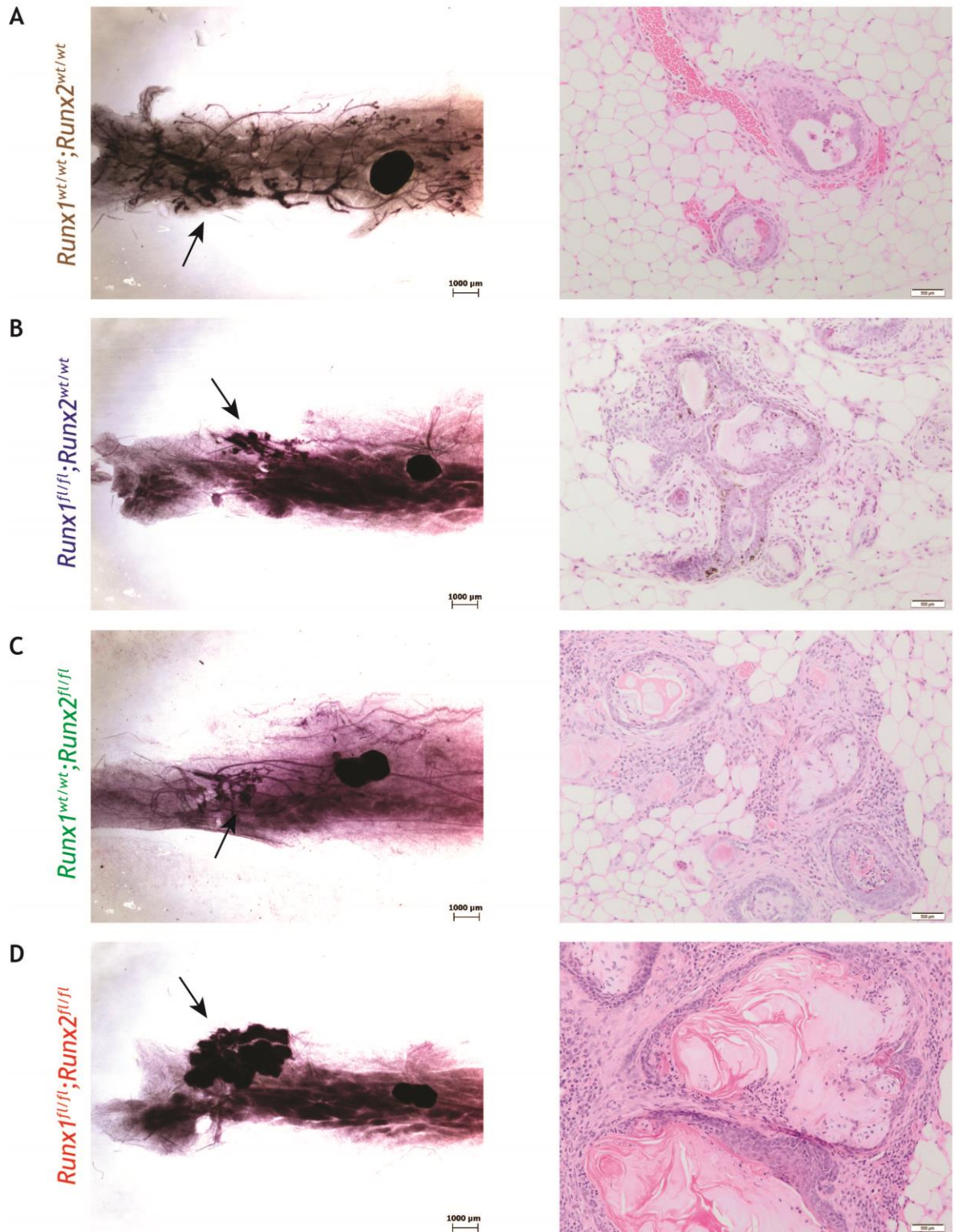
BLG-Cre;Catnb^{wt/lox(ex3)}

Figure 5. 6 Combined loss of *Runx1* and *Runx2* results in a dramatic impairment of ductal morphogenesis upon activation of the Wnt/ β -catenin signalling pathway in mid puberty.

Whole-mounts of #4 MGs (left column) and corresponding H&Es (right column) from 6 weeks old *BLG-Cre;Catnb^{wt/lox(ex3)}* female mice of the *Runx1^{wt/wt};Runx2^{wt/wt}* (A), *Runx1^{fl/fl};Runx2^{wt/wt}* (B), *Runx1^{wt/wt};Runx2^{fl/fl}* (C) and *Runx1^{fl/fl};Runx2^{fl/fl}* (D) cohorts. One representative whole-mount and H&E image of $n \geq 5$ is shown per genotype. Arrows indicate the presence of thickened epithelial ducts. Scale bar of whole-mounts, 1000 μ m. Scale of H&Es, 500 μ m. H&E, haematoxylin eosin stain; MG, mammary gland.

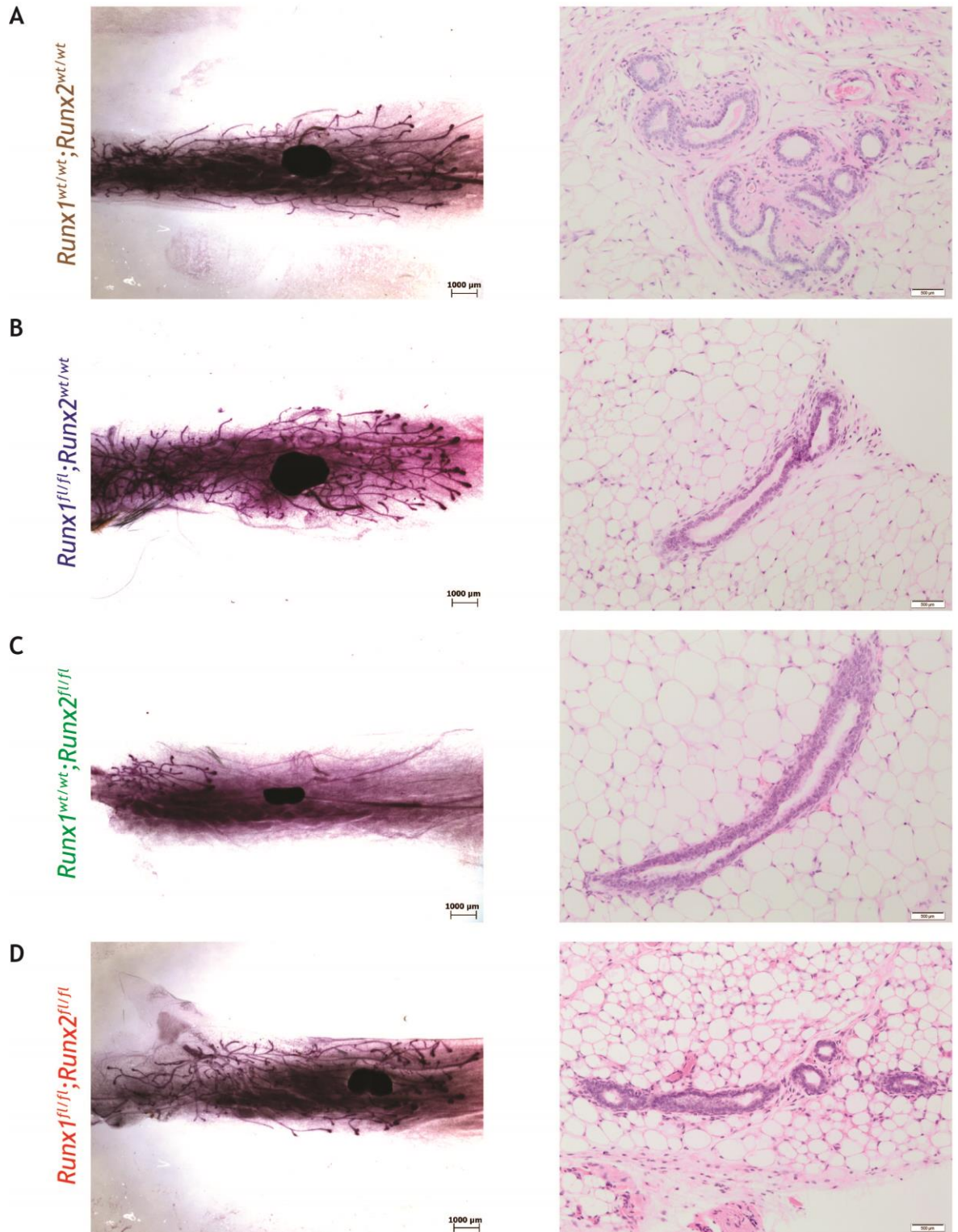
BLG-Cre;Catnb^{wt/wt}

Figure 5. 7 Mammary-specific deletion of *Runx1* and *Runx2* does not affect ductal morphogenesis of *Wnt/β-catenin* wild type mice in mid puberty.

Whole-mounts of #4 MGs (left column) and corresponding H&E (right column) from 6 week old *BLG-Cre;Catnb^{wt/wt}* female mice of the *Runx1^{wt/wt};Runx2^{wt/wt}* (A), *Runx1^{fl/fl};Runx2^{wt/wt}* (B), *Runx1^{wt/wt};Runx2^{fl/fl}* (C) and *Runx1^{fl/fl};Runx2^{fl/fl}* (D) cohorts. One representative whole-mount and H&E image of $n \geq 4$ is shown per cohort. Scale bar of whole-mounts, 1000 μm . Scale of H&Es, 500 μm . H&E, haematoxylin eosin stain; MG, mammary gland.

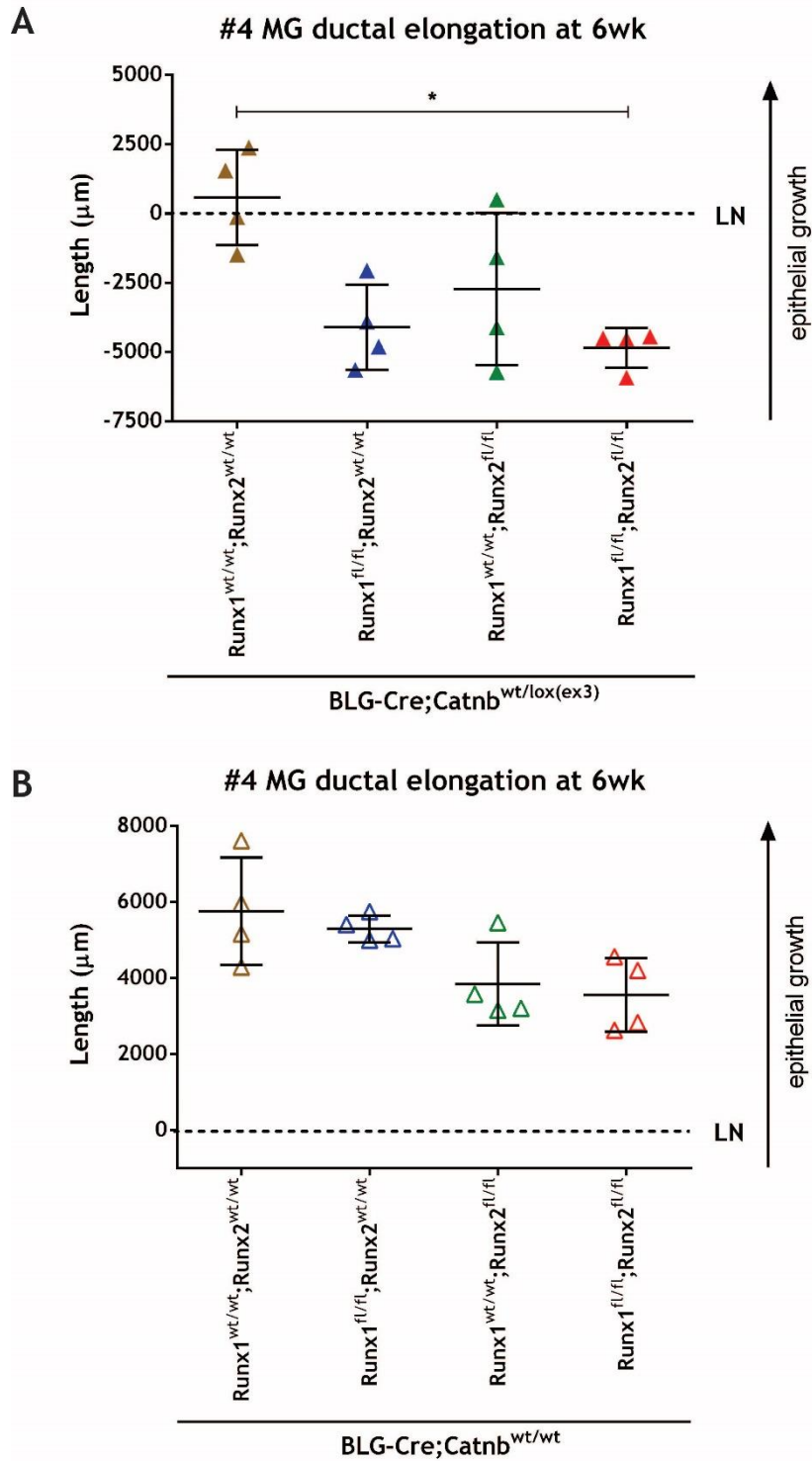


Figure 5. 8 Effect of *Runx1* and *Runx2* loss on mammary ductal elongation in 6 week old Wnt/ β -catenin activated mutant and wild type mice.

Scatter dot plots showing the ductal elongation of #4 MGs from 6 weeks old *BLG-Cre;Catnb*^{wt/lox(ex3)} (A) and *BLG-Cre;Catnb*^{wt/wt} (B) female mice upon loss of *Runx1*, *Runx2* or both genes. Ductal elongation was assessed by measuring the length of the epithelial tree to and from LN. Arrows represent the direction of epithelial growth through the mammary fat pad. Statistical analysis was performed by the Kruskal-Wallis test with Dunnet's multiple comparisons in GraphPad Prism. Error bars represent mean with SD (n=4 per each *BLG-Cre;Catnb*^{wt/lox(ex3)} and *BLG-Cre;Catnb*^{wt/wt} cohort). **P*<0.05. LN, lymph node; MG, mammary gland.

5.2.1.3 Analysis of mammary gland pre-pubertal development in 3 week old virgin female mice

The evidently altered mammary epithelium observed in all cohorts of 6 week old *BLG-Cre;Catnb^{wt/lox(ex3)}* female mice led to the hypothesis that perhaps activation of the Wnt/ β -catenin pathway was impinging on the pre-pubertal formation of mammary glands. Therefore, the status of the glands was assessed at the 3 week developmental time-point. Here, all single and double *Runx* knock-out cohorts of *BLG-Cre;Catnb^{wt/lox(ex3)}* and *BLG-Cre;Catnb^{wt/wt}* mice displayed lighter body weights and reduced cumulative mammary gland weight compared to wild type controls (Figure 5. 9). However, these differences did not appear to be statistically significant, possibly due to the small number of animals assessed or the high inter-mouse variation. When whole-mount analysis of #1 and #4 mammary glands were performed, no morphological differences could be discerned among the single and double knock-out cohorts of *BLG-Cre;Catnb^{wt/lox(ex3)}* mice. In fact, in contrast to the 6 and 9 week developmental time-points, all three *Runx* deficient groups of animals displayed a dramatically distorted mammary anlage compared to control mice (Figure 5. 10, left and mid panels). Importantly, this phenotype displayed 100% penetrance, as it was found to equally affect all five pairs of murine mammary glands. In addition, considering the high abundance of TEBs present at this developmental stage, it was not surprising to find the presence of Wnt/ β -catenin pre-neoplastic mammary lesions affecting the latter, as shown by H&E stains (Figure 5. 10, right panel). The same scenario did not hold true for *BLG-Cre;Catnb^{wt/wt}* mice, which displayed normal-looking mammary anlagen, regardless of their *Runx* status (Figure 5. 11). As directional growth of the mammary epithelial rudiment starts with ovary maturation and hormone release, quantification of ductal elongation was not carried out at this hormone-independent developmental stage.

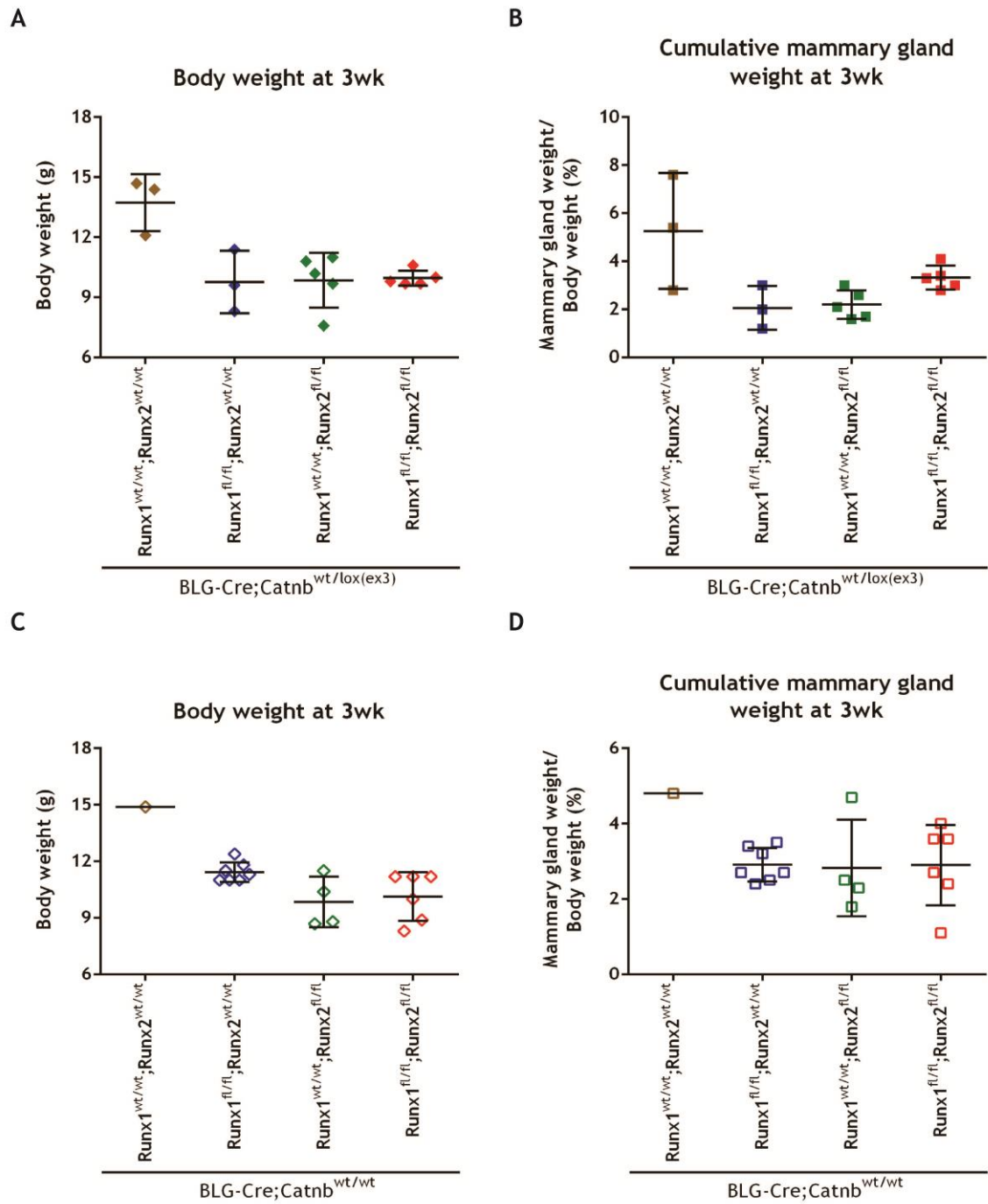


Figure 5. 9 Effect of mammary specific *Runx1* and *Runx2* loss on body weight and cumulative mammary gland weight in 3 week old *Wnt/β-catenin* mutant and wild type mice.

Scatter dot plots of body weight and cumulative mammary gland weight of 3 week old *BLG-Cre;Catnb^{wt/lox(ex3)}* (A, B) and *BLG-Cre;Catnb^{wt/wt}* (C, D) female mice upon loss of *Runx1*, *Runx2* or both genes. Cumulative mammary gland weight was expressed as a percentage of total mammary gland weight divided by the body weight of the animal. Statistical analysis was performed by the Kruskal-Wallis test with Dunn's multiple comparisons in GraphPad Prism. Error bars represent mean with SD ($n \geq 3$ per each cohort, except for *BLG-Cre;Catnb^{wt/wt};Runx1^{wt/wt};Runx2^{wt/wt}* with $n=1$). No significance was found among groups. No statistical test could be run for the *BLG-Cre;Catnb^{wt/wt}* cohort, as only was mouse was present in the *Runx1^{wt/wt};Runx2^{wt/wt}* group.

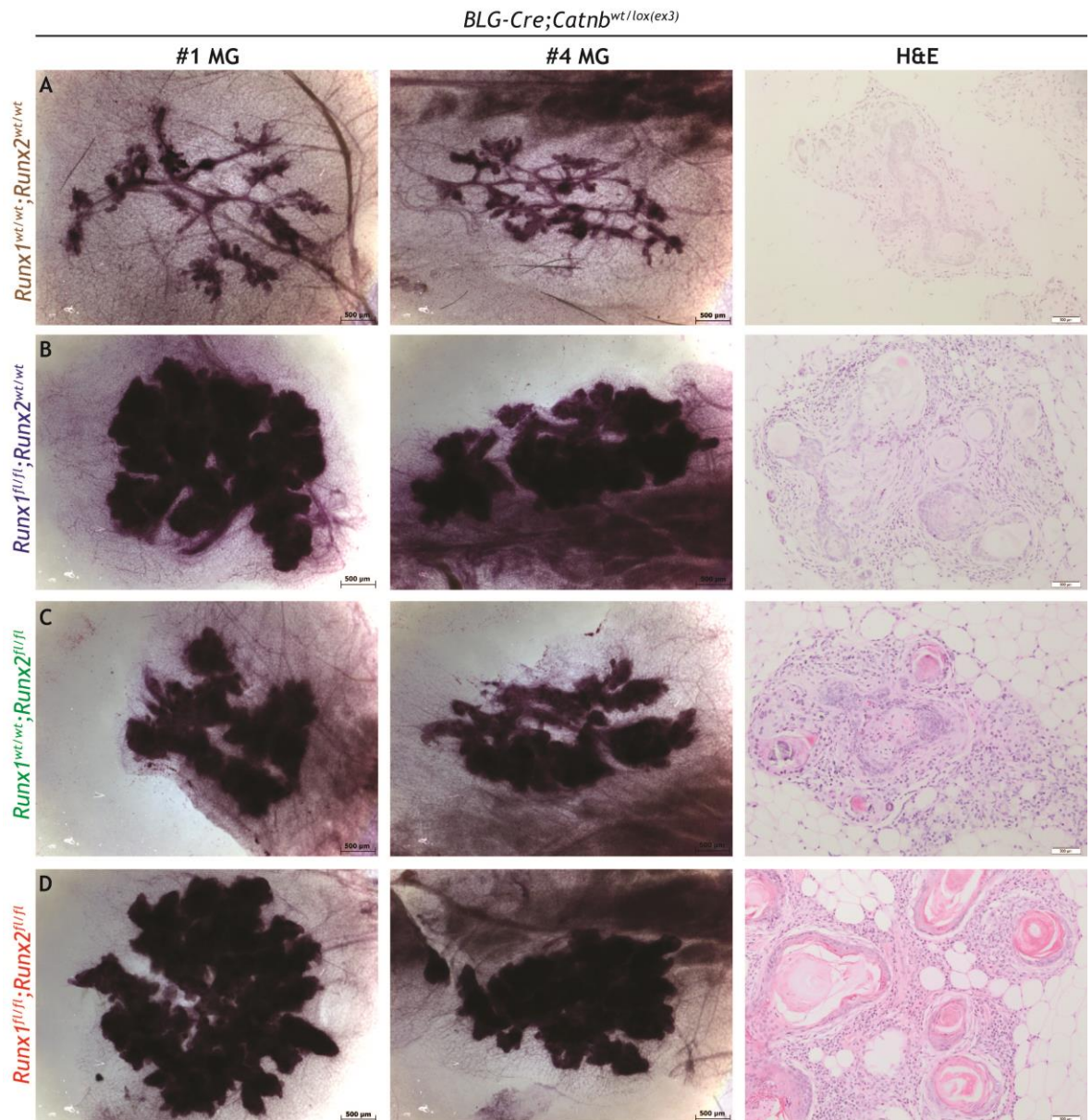


Figure 5. 10 Individual or combined loss of *Runx1* and *Runx2* severely compromise the morphology of the mammary anlage in the presence of activated Wnt/ β -catenin signalling.

Whole-mounts of cervical (#1) and abdominal (#4) MGs (left and mid columns) and representative H&Es (right column) from 3 week old *BLG-Cre;Catnb^{wt/lox(ex3)}* female mice of the *Runx1^{wt/wt};Runx2^{wt/wt}* (A), *Runx1^{fl/fl};Runx2^{wt/wt}* (B), *Runx1^{wt/wt};Runx2^{fl/fl}* (C) and *Runx1^{fl/fl};Runx2^{fl/fl}* (D) cohorts. One representative whole-mount and H&E image of $n \geq 3$ is shown per genotype. Scale bar of whole-mounts, 500 μ m. Scale of H&Es, 500 μ m. H&E, haematoxylin eosin; MG, mammary gland.

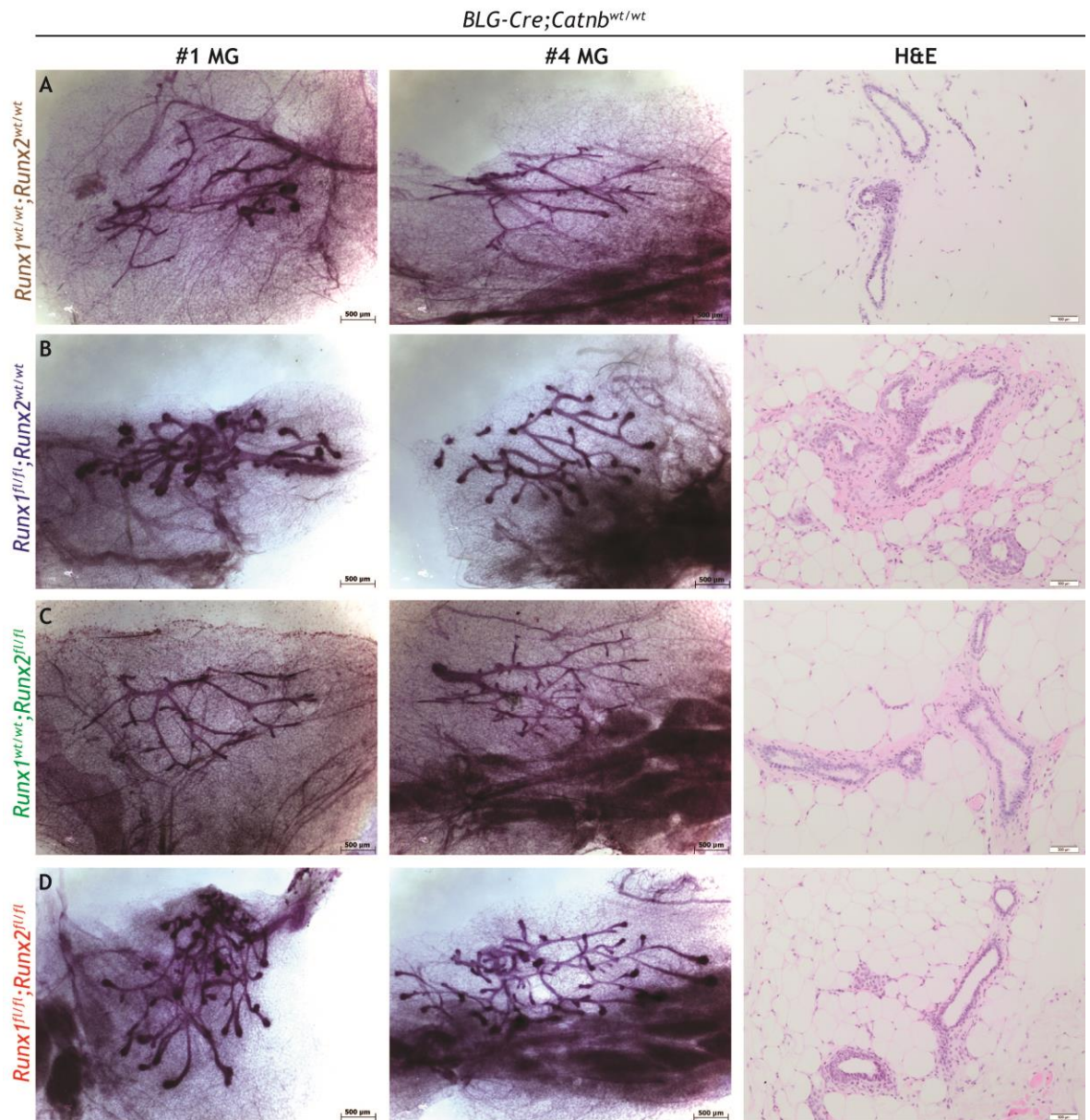


Figure 5. 11 Mammary-specific deletion of *Runx1* and *Runx2* does not affect the morphology of the anlage of Wnt/ β -catenin wild type mice.

Whole-mounts of cervical (#1) and abdominal (#4) MGs (left and mid columns) and representative H&Es (right column) from 3 week old *BLG-Cre;Catnb^{wt/wt}* female mice of the *Runx1^{wt/wt};Runx2^{wt/wt}* (A), *Runx1^{fl/fl};Runx2^{wt/wt}* (B), *Runx1^{wt/wt};Runx2^{fl/fl}* (C) and *Runx1^{fl/fl};Runx2^{fl/fl}* (D) cohorts. One representative whole-mount and H&E image of $n \geq 4$ is shown per genotype, but for *Runx1^{wt/wt};Runx2^{wt/wt}* with $n=1$. Scale bar of whole-mounts, 500 μ m. Scale of H&Es, 500 μ m. H&E, haematoxylin eosin; MG, mammary gland.

5.2.2 Investigating the tumour suppressive mechanisms exerted by RUNX1 and RUNX2

To investigate how deletion of *Runx1* and/or *Runx2* affected the proliferative signals conveyed by mammary-specific activation of the Wnt/ β -catenin signalling pathway, an analysis of the growth of pre-neoplastic mammary lesions was performed. To this end, 6 week old *BLG-Cre;Catnb^{wt/lox(ex3)}* pubertal mice were injected with BrdU and their mammary glands harvested two hours after injection. Tissues from all animal cohorts were formalin-fixed paraffin-embedded and stained with an anti-BrdU antibody to assess the presence of cycling (BrdU+) cells within incipient mammary lesions. Being the mammary gland a heterogeneous organ composed of both epithelial and stromal compartments, it was first necessary to determine the amount of total epithelium (TE) present per each slide analysed, across all different genotypes.

Quantification of TE revealed a moderate increase of epithelial tissue only upon combined loss of *Runx1* and *Runx2*, yet not in the absence of each individual gene (Figure 5. 12A). A significant difference, however, was found between *Runx1^{fl/fl};Runx2^{fl/fl}* and *Runx1^{fl/fl}* mice, in line with the enlarged mammary structure displayed by the whole-mounts of double floxed mice, versus the thinner and smaller mammary trees observed upon loss of *Runx1* (Figure 5. 6). In view of the use of a conditional GEMM wherein BLG-Cre-driven activation would have occurred only in a subset of MMECs, it was important to further distinguish between the amount of normal and abnormal epithelium (NE and AE, respectively) present per slide. By doing so, results of the analysis revealed a trend towards increased NE displayed by both single knock-out cohorts of mice (Figure 5. 12B), counterbalanced by a higher amount of AE observed in both control and *Runx1^{fl/fl};Runx2^{fl/fl}* animals (Figure 5. 12C). In both cases, significant differences emerged specifically between the *Runx2^{fl/fl}* and *Runx1^{fl/fl};Runx2^{fl/fl}* groups of mice (Figure 5. 12).

Interestingly, when the proliferative index displayed by each epithelial layer (i.e. TE, NE and AE) was quantified, no significant differences emerged between *Runx1^{fl/fl};Runx2^{fl/fl}* mice and the other cohorts of *BLG-Cre;Catnb^{wt/lox(ex3)}* animals (Figure 5. 13). What emerged, instead, was a trend to increased TE proliferation displayed by *Runx1^{fl/fl}* animals (Figure 5. 13A). Of note, this increase appeared

to be due to moderate levels of proliferation occurring in both NE (Figure 5. 13B) and AE (Figure 5. 13C). Albeit not significant, these results were perhaps indicative of a compensatory mechanism occurring in the absence of *Runx1*.

Nonetheless, when TE, NE and AE proliferative indices were multiplied by the percentage occupied by each layer within the analysed mammary gland tissue, *Runx1^{fl/fl};Runx2^{fl/fl}* mice displayed significantly higher levels of TE proliferation compared to *Runx1^{fl/fl}* mice, yet not to wild type *BLG-Cre;Catnb^{wt/lox(ex3)}* animals (Figure 5. 14A). Of note, this increase appeared to relate to the high cell turnover characterizing AE (Figure 5. 14C), but not NE (Figure 5. 14B). Representative histological sections of anti-BrdU staining of pre-neoplastic mammary lesions from all cohorts *BLG-Cre;Catnb^{wt/lox(ex3)}* mice are shown in Figure 5. 15.

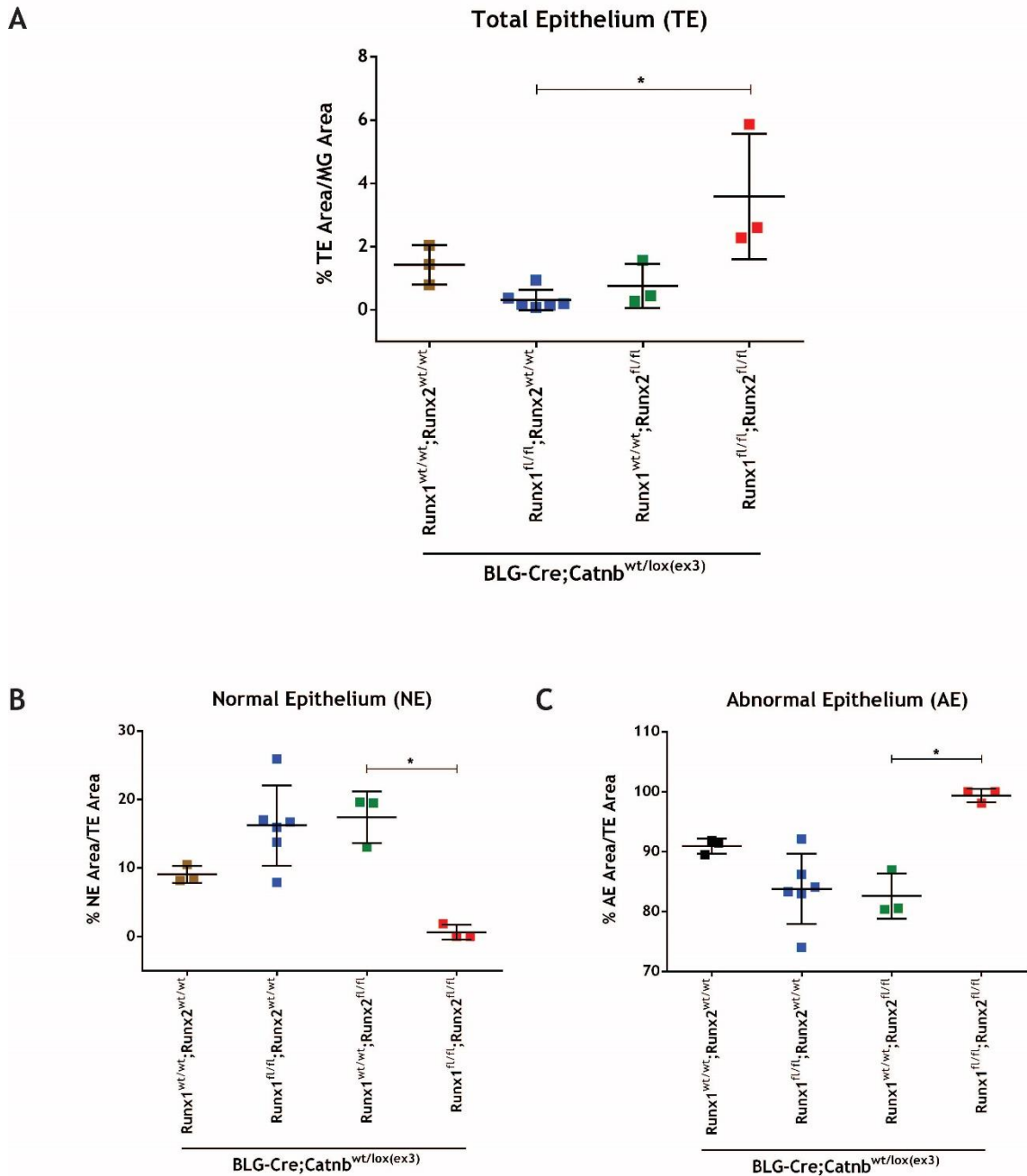
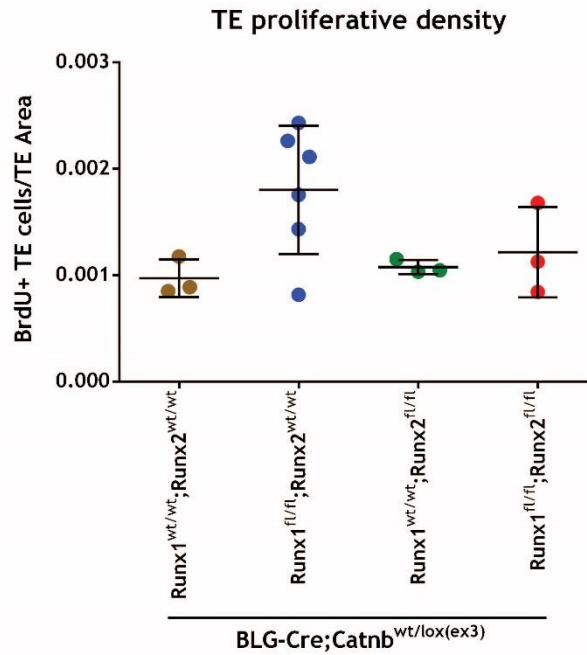


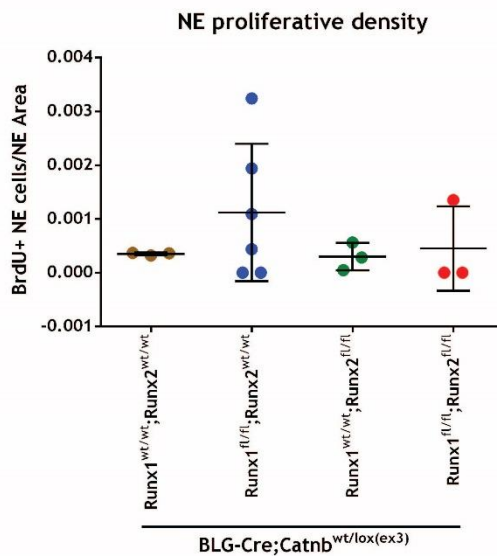
Figure 5. 12 Perturbation of pubertal mammary epithelium upon activation of the Wnt/ β -catenin pathway in the absence of *Runx1* and *Runx2*.

Scatter dot plots showing the distribution of TE (A), NE (B) and AE (C) displayed by 6 week old *BLG-Cre;Catnb^{wt/lox(ex3)}* female mice in the absence of *Runx1*, *Runx2* or both genes. (A) TE was calculated as a percentage of total mammary gland area. (B) NE and (C) AE were calculated as percentages of TE area. Statistical analysis was performed by the Kruskal-Wallis test with Dunn's multiple comparisons in GraphPad Prism. Error bars represent mean with SD ($n \geq 3$ per each cohort). * $P < 0.05$. AE, abnormal epithelium; NE, normal epithelium; TE, total epithelium.

A



B



C

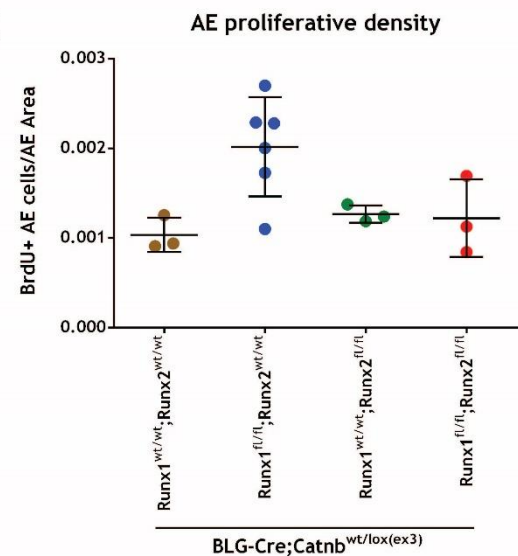


Figure 5. 13 Quantification of the proliferative density of pubertal mammary epithelium upon activation of the Wnt/B-catenin pathway in the absence of *Runx1* and *Runx2*.

Scatter dot plots of TE (A), NE (B) and AE (C) proliferative density displayed by 6 week old *BLG-Cre;Catnb*^{wt/lox(ex3)} female mice in the absence of *Runx1*, *Runx2* or both genes. Mice were injected with BrdU, their mammary glands harvested after 2 hours, and the tissues stained with anti-BrdU. (A) TE proliferative density was calculated dividing the number of BrdU+ cells within TE by TE area. (B) NE proliferative density was calculated dividing the number of BrdU+ cells within NE by NE area. (C) AE proliferative density was calculated dividing the total number of BrdU+ cells with AE by AE area. Statistical analysis was performed by the Kruskal-Wallis test with Dunn's multiple comparisons in GraphPad Prism. Error bars represent mean with SD ($n \geq 3$ per each cohort). No significant differences were found among groups. AE, abnormal epithelium; BrdU, bromodeoxyuridine; NE, normal epithelium; TE, total epithelium.

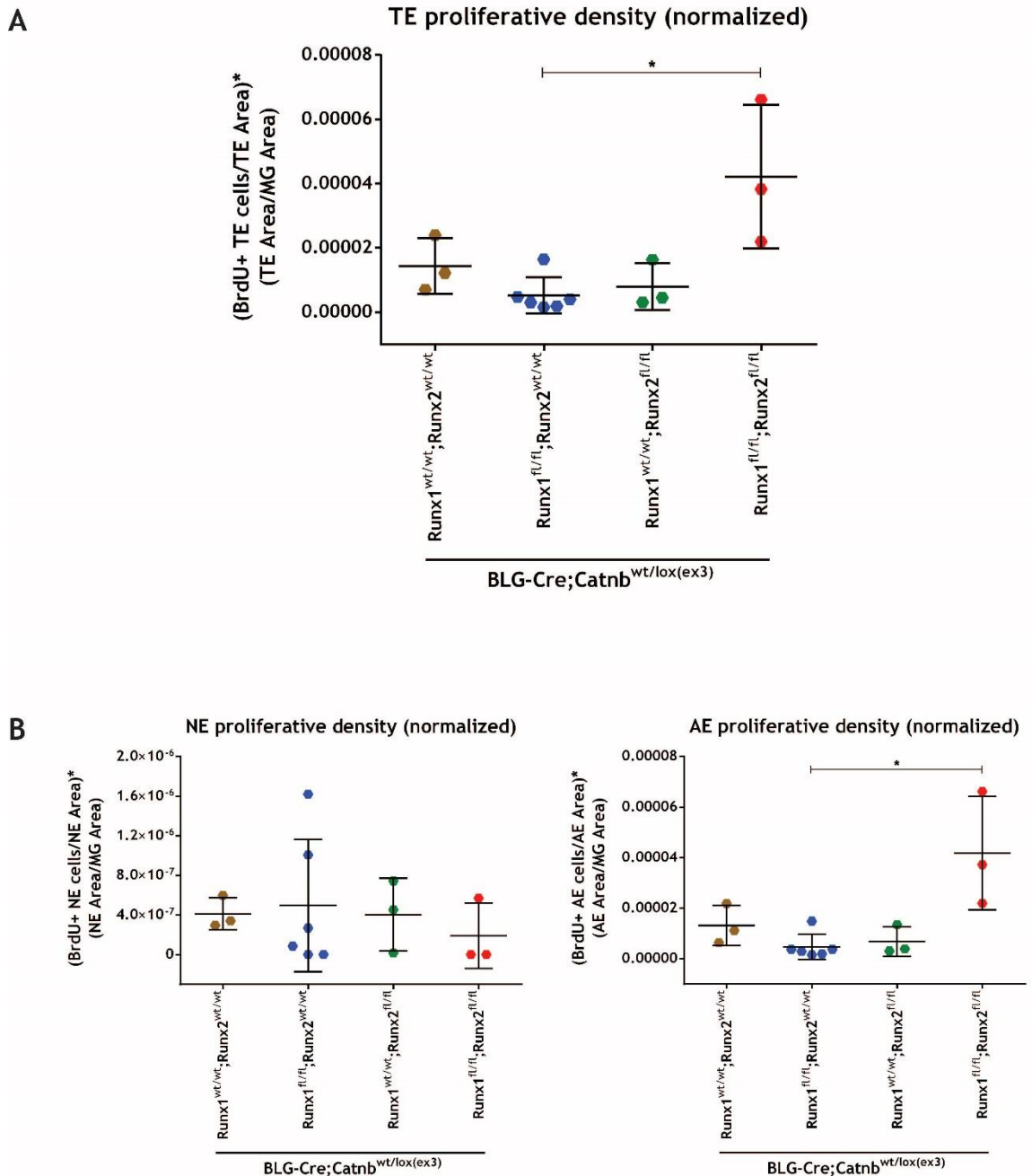


Figure 5. 14 Normalized proliferative density of pubertal mammary epithelium upon activation of the Wnt/ β -catenin pathway in the absence of *Runx1* and *Runx2*.

Scatter dot plots of normalized TE (A), NE (B) and AE (C) proliferative density displayed by MGs of 6 week old *BLG-Cre;Catnb*^{wt/lox(ex3)} female mice in the absence of *Runx1*, *Runx2* or both genes. Mice were injected with BrdU, their mammary glands harvested after 2 hours, and the tissues stained with anti-BrdU. (A) TE proliferative density was normalized by dividing it by the % TE area. (B) NE proliferative density was normalized by dividing it by the % NE area. (C) AE proliferative density was normalized by dividing it by the % AE area. Statistical analysis was performed by the Kruskal-Wallis test with Dunn's multiple comparisons in GraphPad Prism. Error bars represent mean with SD (n \geq 3 per each cohort). *P<0.05. AE, abnormal epithelium; BrdU, bromodeoxyuridine; NE, normal epithelium; TE, total epithelium.

BLG-Cre;Catnb^{wt/lox(ex3)}

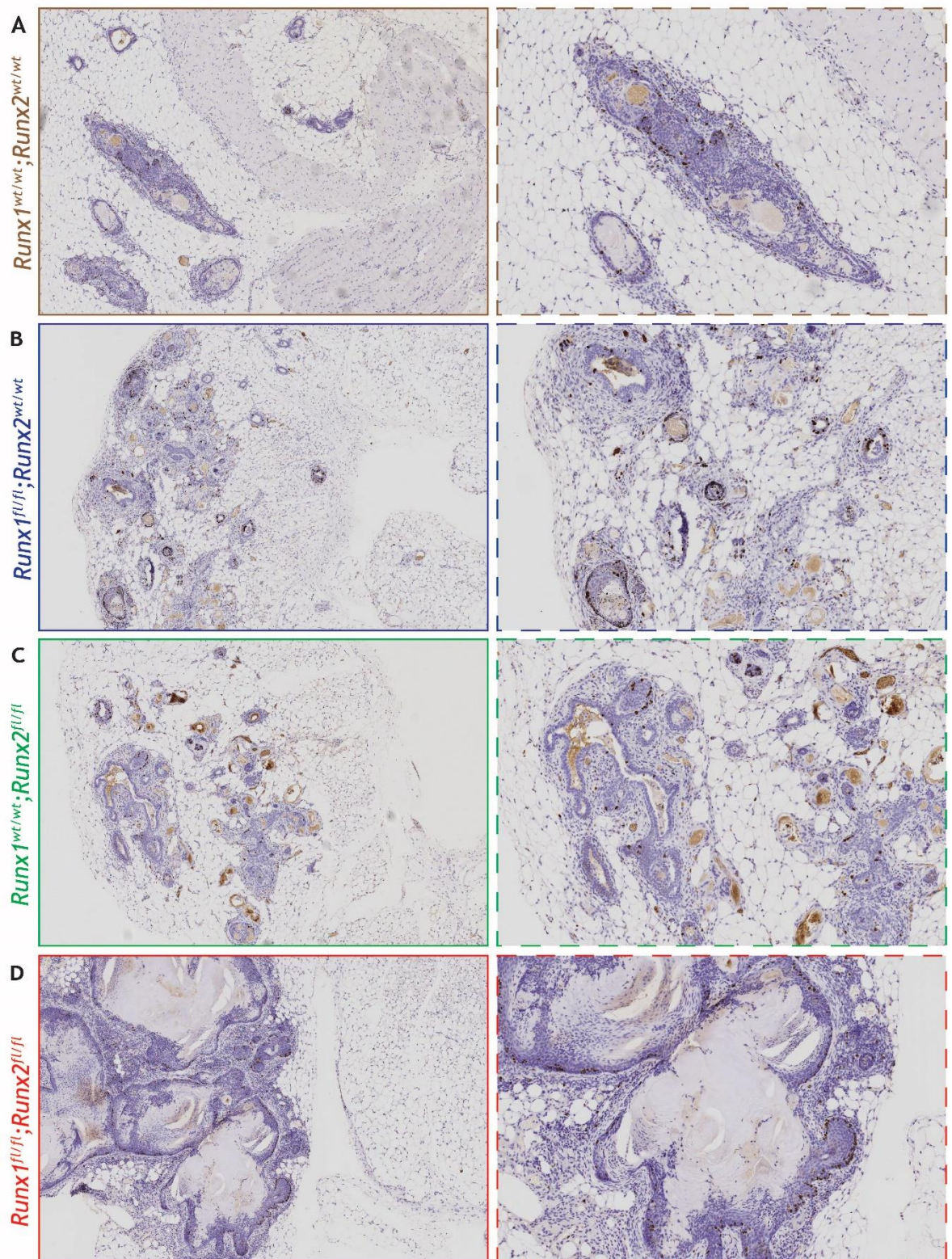


Figure 5. 15 Immunohistochemistry for BrdU on pre-neoplastic Wnt/ β -catenin mammary lesions upon loss of *Runx1* and *Runx2*.

Histological sections of anti-BrdU stained mammary glands from 6 week old *BLG-Cre;Catnb^{wt/lox(ex3)}* mice of the *Runx1^{wt/wt};Runx2^{wt/wt}* (A), *Runx1^{fl/fl};Runx2^{wt/wt}* (B), *Runx1^{wt/wt};Runx2^{fl/fl}* (C) and *Runx1^{fl/fl};Runx2^{fl/fl}* (D) cohorts. One representative image of n=3, but for the *Runx1^{fl/fl};Runx2^{wt/wt}* group with n=6, is shown per genotype. Images were captured via the HALO software, using the 2X (left column) and 10X (right column) lenses.

5.2.3 Histopathological characterization of Wnt/ β -catenin preneoplastic lesions in the absence of the *Runx* genes

In an attempt to perform a thorough characterization of the histopathological features displayed by pre-neoplastic Wnt/ β -catenin-driven mammary lesions, 6 week old *BLG-Cre;Catnb^{wt/lox(ex3)}* mice were euthanized and their mammary glands formalin-fixed paraffin-embedded for H&E and IHC analysis. Upon H&E examination, *Runx1^{wt/wt};Runx2^{wt/wt}* animals displayed a distorted mammary tissue architecture with presence of adenosquamous lesions (Figure 5. 16). In line with the causative tumourigenic role played by canonical Wnt signalling, strong nuclear β -catenin could be observed in specific foci of the mammary gland. In the rest of the organ, the protein was instead found to be mainly located at the cell membrane, exerting its function as a cell-adhesion molecule. IHC analysis of CK5 and CK8/18 staining indicated the simultaneous presence of abnormally expanded basal and luminal MMECs, respectively. In addition, CK10 positive cells could also be detected within the centre of most lesions, confirming trans-differentiation of MMECs into epidermal cells upon Wnt/ β -catenin-driven oncogenic transformation. Lastly, strong α -SMA staining was found to delineate the majority of pre-neoplastic lesions, which also showed levels of ER α and PR positivity. Interestingly, whilst the pattern of hormone receptors expression is reported to be evenly scattered across normal mammary ducts, the presence of contiguous HR+ cells was often observed in Wnt/ β -catenin-driven mammary lesions (Figure 5. 16). The same histopathological features were visible in *Runx1^{fl/fl};Runx2^{wt/wt}* animals, albeit to a smaller extent of control mice due to the low amount of epithelial mammary tissue displayed upon loss of *Runx1* (Figure 5. 17). In addition, correct interpretation of IHC staining in this cohort of mice was often confounded by the unknown presence of infiltrating melanocytes, which appeared brown in colour as with all IHC positive MMECs. Regardless, strong nuclear β -catenin staining was also evident in the mammary glands of *Runx1^{fl/fl};Runx2^{wt/wt}* mice, yet this time in a fewer percentage of MMECs. As in the case of control mice, *Runx1*-deleted pre-neoplastic lesions appeared to be composed of both basal (CK5+) and luminal (CK8/18+) cells, surrounded by a layer of myoepithelial (α -SMA) MMECs. On the contrary, only non-specific CK10 staining could be observed, suggesting a lower degree of epithelial trans-differentiation upon loss of *Runx1*. As in the case of

control mice, ER α and PR positive cells were found to be highly abundant within Wnt/ β -catenin-driven mammary lesions, suggesting perhaps a dependency on hormonal cues, at least at the developmental stage analysed (Figure 5. 17). When the same analysis was applied to *Runx1*^{wt/wt};*Runx2*^{fl/fl} mice, a high degree of mammary epithelial transformation was visible by H&Es (Figure 5. 18). Like in the case of controls, several foci of strong nuclear β -catenin staining were interspersed with disorganized mammary ducts, wherein the protein remained located at the plasma membrane. In line with both *Runx1*^{wt/wt};*Runx2*^{wt/wt} and *Runx1*^{fl/fl};*Runx2*^{wt/wt} mice, *Runx2*-deleted pre-neoplastic lesions appeared characterized by the presence of basal (CK5 and α -SMA) and luminal (CK8/18) markers, again indicative of an abnormal expansion of both epithelial lineages. No staining could instead be observed for the epidermal marker CK10. Interestingly, however, when the hormonal status of incipient lesions was assessed, these displayed very strong ER α staining, with positive cells often found adjacent to each other (Figure 5. 19). In line with whole-mount examinations, Wnt/ β -catenin pre-neoplastic lesions appeared to dominate the mammary gland landscape of *Runx1*^{fl/fl};*Runx2*^{fl/fl} mice, displaying a more widespread β -catenin expression as compared to all other cohorts of *BLG-Cre;Catnb*^{wt/lox(ex3)} mice (Figure 5. 19). Akin to the other groups, *Runx1*- and *Runx2*-deleted mammary lesions were characterized by the presence of both CK5 and CK8/18 positive cells. Nonetheless, a reduction of α -SMA, as well as ER α and PR staining, was seen in this cohort. On the contrary, the highest levels of CK10 positivity appeared to distinguish *Runx1*^{fl/fl};*Runx2*^{fl/fl} animals, suggesting a prominent Wnt/ β -catenin mediated trans-differentiation of the mammary epithelium upon loss of *Runx* genes (Figure 5. 19). IHC analysis for RUNX1 and RUNX2, as displayed by all cohorts of *BLG-Cre;Catnb*^{wt/lox(ex3)} mice, is shown in Figure 5. 20. In line with previous analysis done in our lab (McDonald et al., 2014), RUNX1 epithelial expression appeared stronger than RUNX2, which instead was occasionally found in the stroma surrounding pre-neoplastic lesions of *Runx1*^{wt/wt};*Runx2*^{wt/wt} animals. Albeit *Runx1*^{fl/fl};*Runx2*^{fl/fl} mice showed the lowest levels of expression for both genes, correlating RUNX1 and RUNX2 expression with the genotype of *Runx*-deficient *BLG-Cre;Catnb*^{wt/lox(ex3)} mice revealed to be a challenging task, probably due to the high prevalence of BLG-Cre negative, *Runx*-proficient MMECs.

BLG-Cre;Catnb^{wt/lox(ex3);Runx1^{wt/wt};Runx2^{wt/wt}}

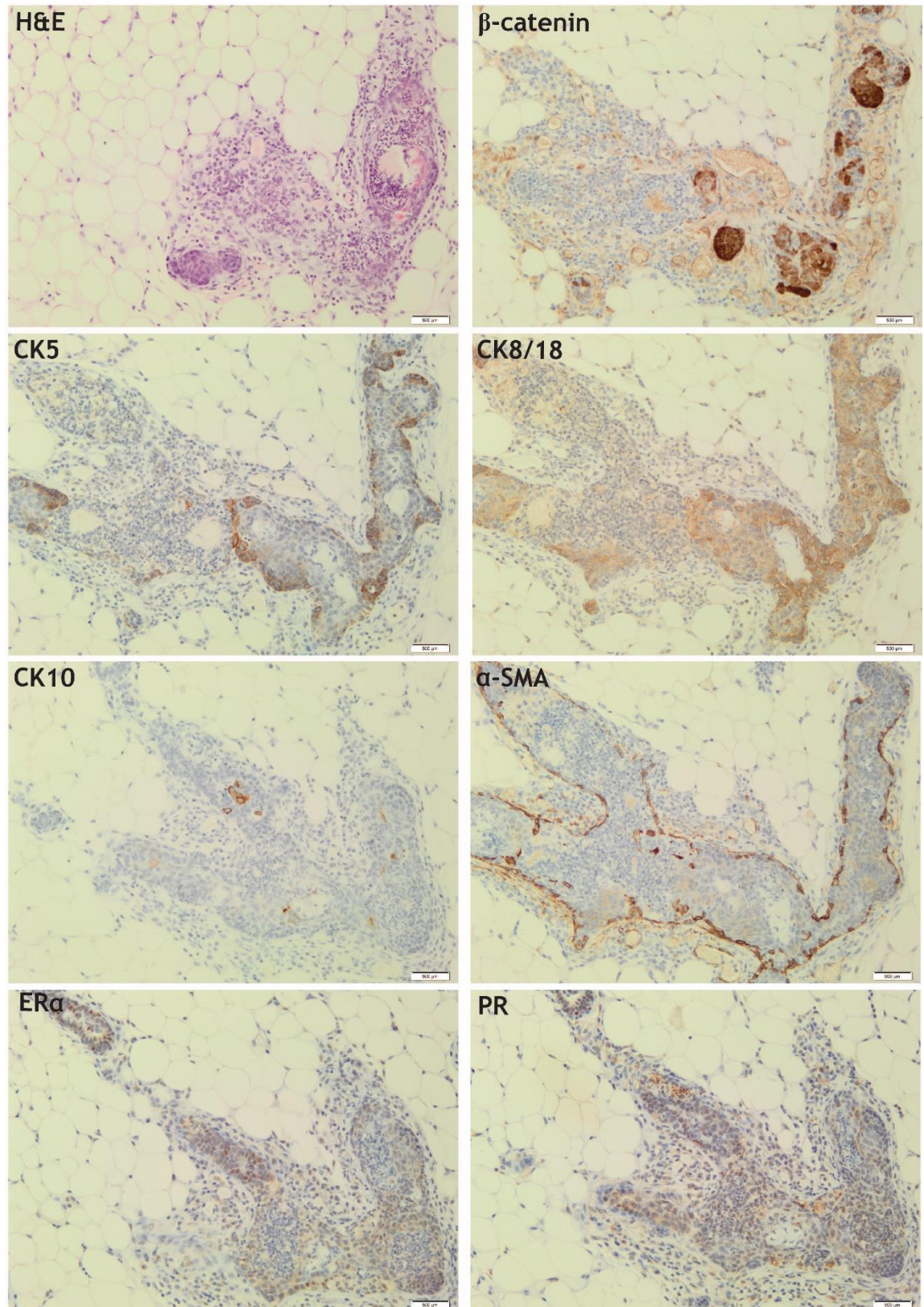


Figure 5. 16 Histopathological analysis of Wnt/ β -catenin driven pre-neoplastic lesions.

H&E and IHC staining of β -catenin, basal (CK5), luminal (CK8/18), epidermal (CK10), myoepithelial (α -SMA) and hormonal (ER α , PR) makers on pre-neoplastic mammary tumour lesions from 6 week old *BLG-Cre;Catnb^{wt/lox(ex3);Runx1^{wt/wt};Runx2^{wt/wt}}* mice. Representative pictures of n=3 mice. Scale bar, 500 μ m. H&E, haematoxylin eosin; IHC, immunohistochemistry.

BLG-Cre;Catnb^{wt/lox(ex3)};Runx1^{fl/fl};Runx2^{wt/wt}

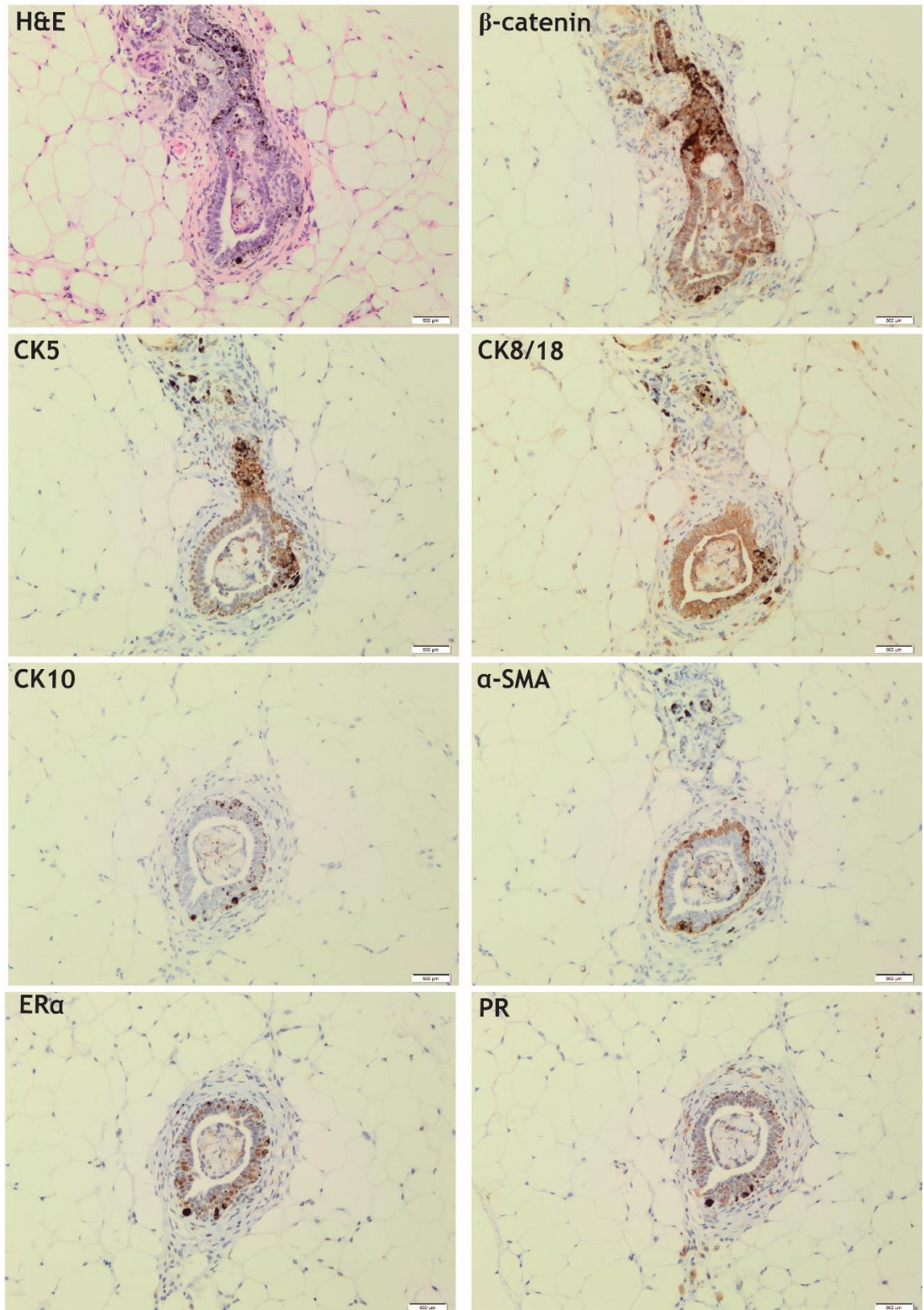


Figure 5. 17 Histopathological analysis of Wnt/ β -catenin driven lesions upon *Runx1* loss.

H&E and IHC staining of β -catenin, basal (CK5), luminal (CK8/18), epidermal (CK10), myoepithelial (α -SMA) and hormonal (ER α , PR) makers on pre-neoplastic mammary tumour lesions from 6 week old *BLG-Cre;Catnb^{wt/lox(ex3)};Runx1^{fl/fl};Runx2^{wt/wt}* mice. Representative pictures of n=3 mice. Scale bar, 500 μ m. H&E, haematoxylin eosin; IHC, immunohistochemistry.

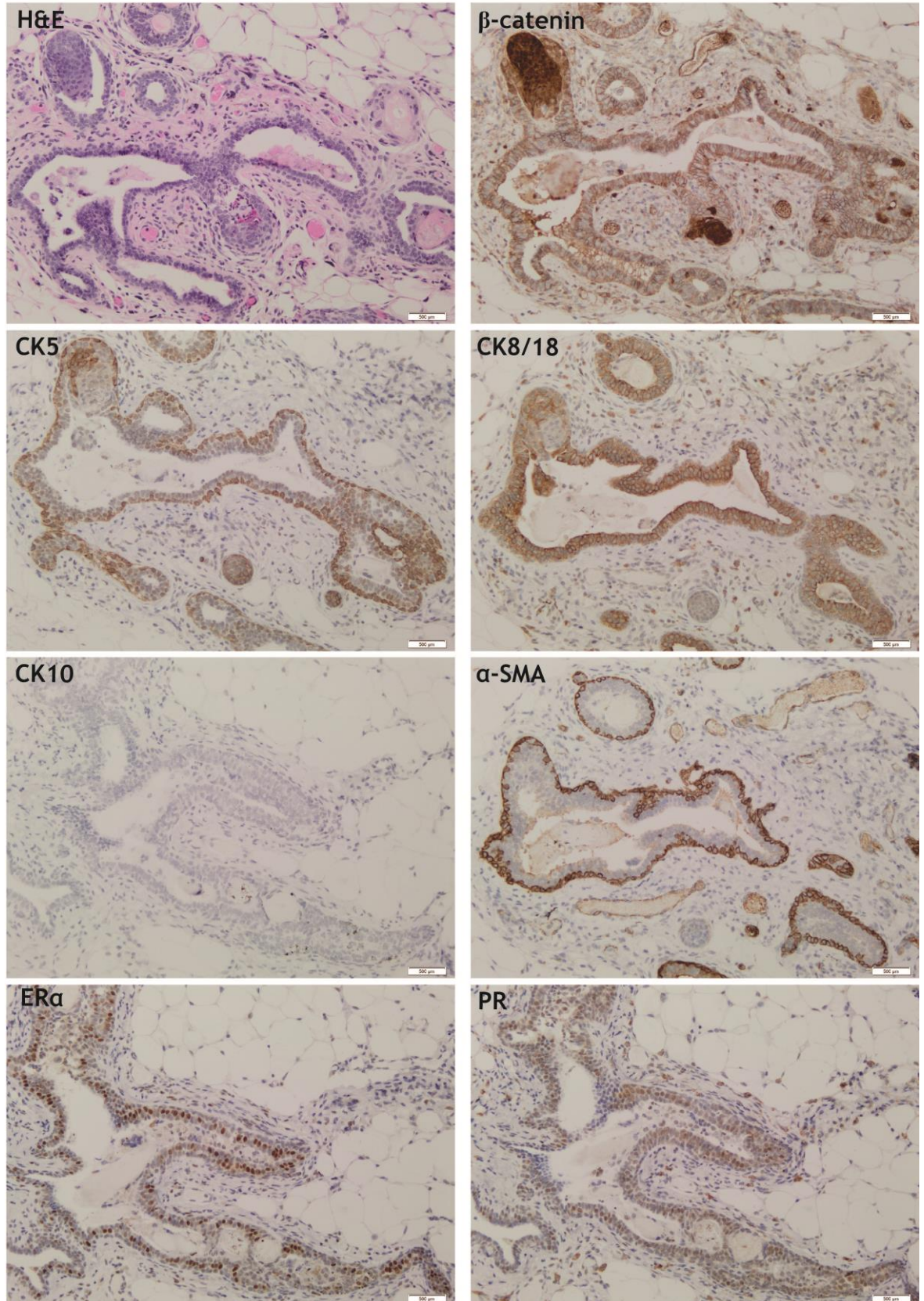
BLG-Cre;Catnb^{wt/lox(ex3)};Runx1^{wt/wt};Runx2^{fl/fl}

Figure 5. 18 Histopathological analysis of Wnt/ β -catenin driven lesions upon *Runx2* loss.

H&E and IHC staining of β -catenin, basal (CK5), luminal (CK8/18), epidermal (CK10), myoepithelial (α -SMA) and hormonal (ER α , PR) makers on pre-neoplastic mammary tumour lesions from 6 week old *BLG-Cre;Catnb^{wt/lox(ex3)};Runx1^{wt/wt};Runx2^{fl/fl}* mice. Representative pictures of n=3 mice Scale bar, 500 μ m. H&E, haematoxylin eosin; IHC, immunohistochemistry.

BLG-Cre;Catnb^{wt/lox(ex3);Runx1^{fl/fl};Runx2^{fl/fl}}

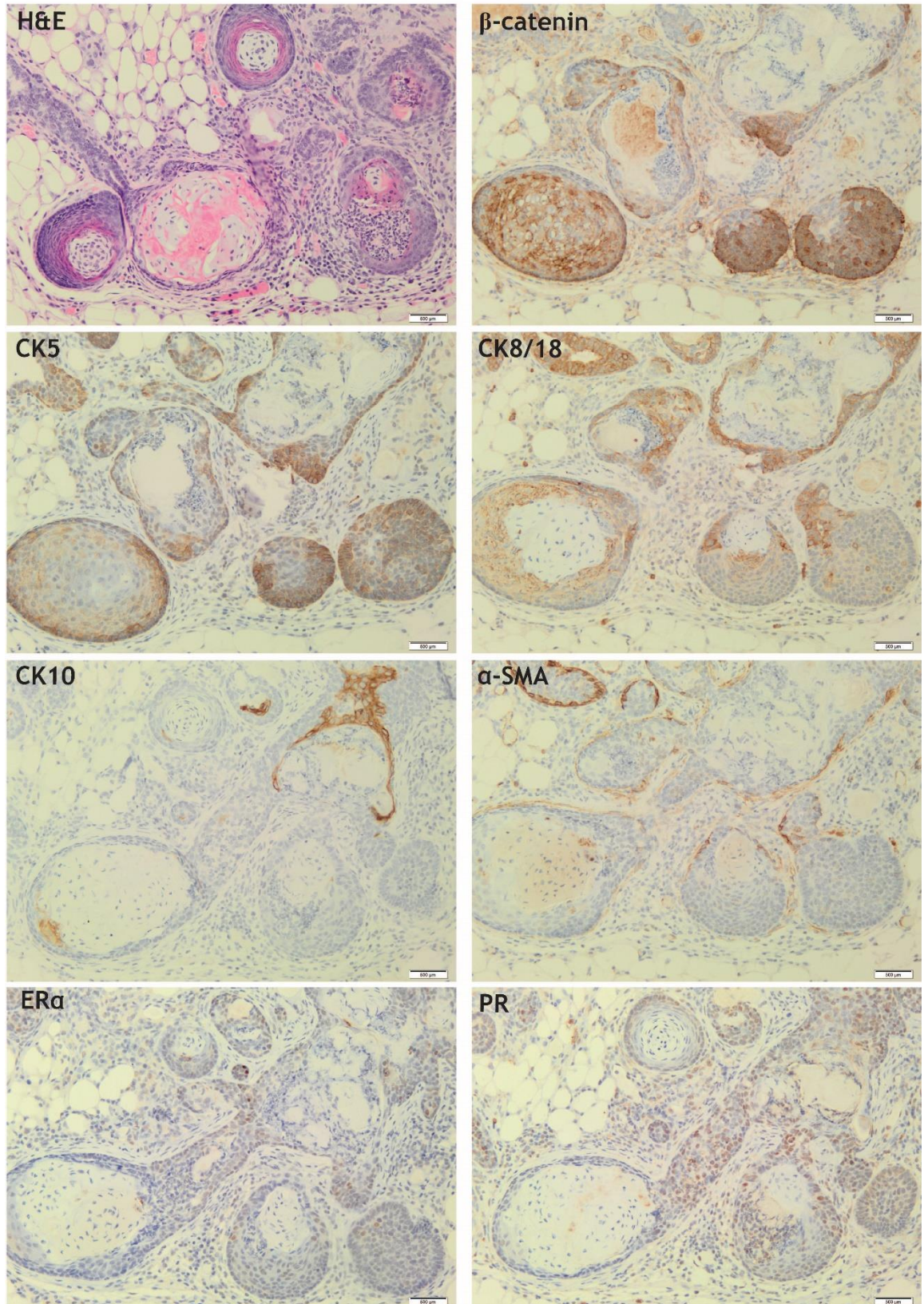


Figure 5. 19 Histopathological analysis of Wnt/ β -catenin lesions upon loss of *Runx* genes.

H&E and IHC staining of β -catenin, basal (CK5), luminal (CK8/18), epidermal (CK10), myoepithelial (α -SMA) and hormonal (ER α , PR) makers on pre-neoplastic mammary tumour lesions from 6 week old *BLG-Cre;Catnb^{wt/lox(ex3);Runx1^{fl/fl};Runx2^{fl/fl}}* mice. Representative pictures of n=3 mice Scale bar, 500 μ m. H&E, haematoxylin eosin; IHC, immunohistochemistry.

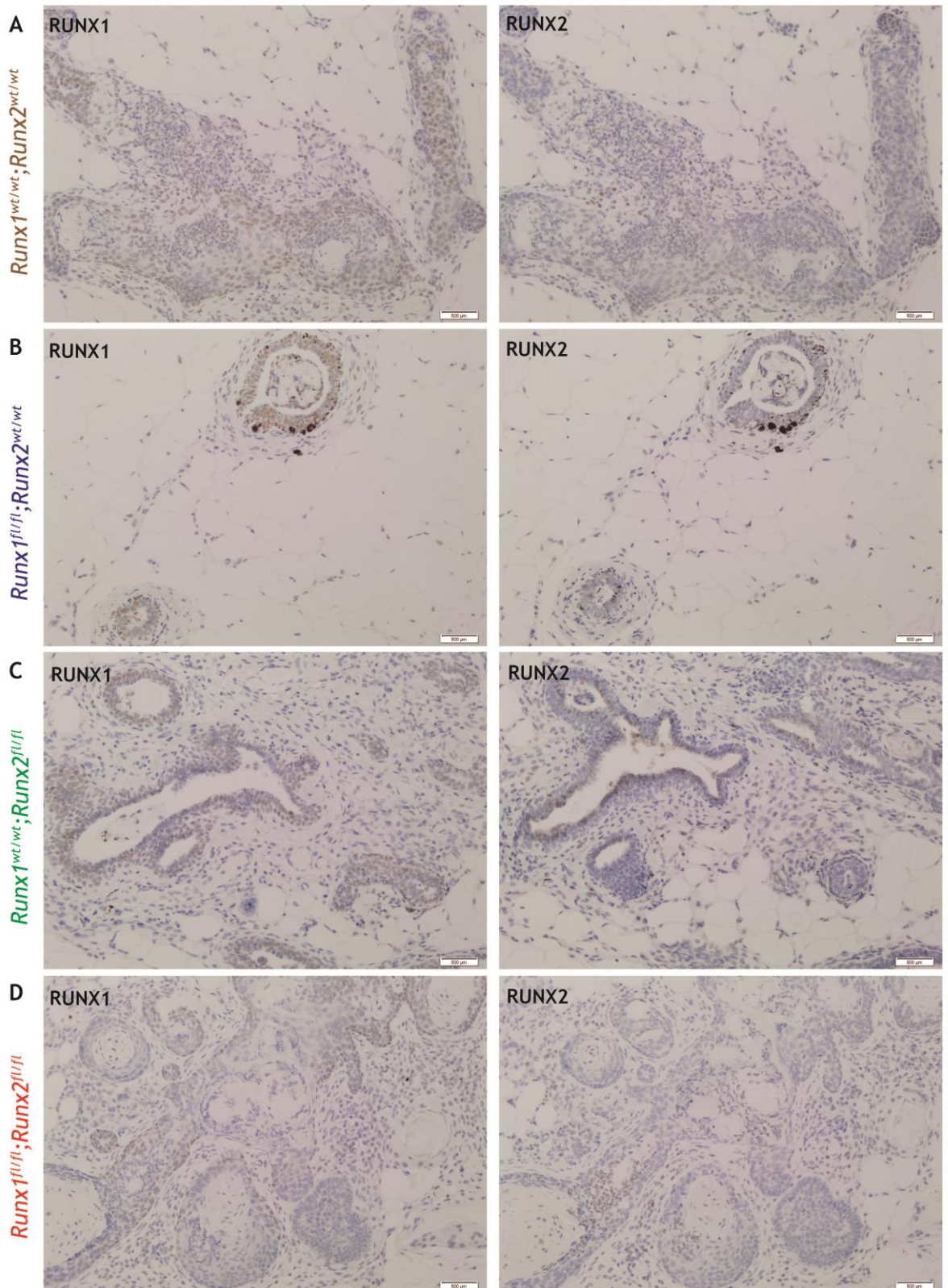
BLG-Cre;Catnb^{wt/lox(ex3)}

Figure 5. 20 RUNX1 and RUNX2 analysis of Wnt/ β -catenin driven adenosquamous lesions.

Representative IHC images of RUNX1 and RUNX2 staining from 6 week old *BLG-Cre;Catnb^{wt/lox(ex3)}* mice of the *Runx1^{wt/wt};Runx2^{wt/wt}* (A), *Runx1^{fl/fl};Runx2^{wt/wt}* (B), *Runx1^{wt/wt};Runx2^{fl/fl}* (C) and *Runx1^{fl/fl};Runx2^{fl/fl}* (D) cohorts. One representative image of n=3 is shown per cohort. IHC. Immunohistochemistry.

5.2.4 Expression analysis of Wnt/ β -catenin target genes upon loss of *Runx* genes

In view of the presence of strong nuclear β -catenin foci found within the vast majority of pre-neoplastic lesions displayed by *BLG-Cre;Catnb^{wt/lox(ex3)}* animals, a preliminary analysis of Wnt/ β -catenin target genes was performed. In this regards, *Runx1^{wt/wt};Runx2^{wt/wt}*, *Runx1^{fl/fl};Runx2^{wt/wt}*, *Runx1^{wt/wt};Runx2^{fl/fl}* and *Runx1^{fl/fl};Runx2^{fl/fl}* mice were euthanized at the age of 6 weeks and all ten mammary glands dissected out for collection. Organs were then processed as previously described (Chapter 3), in order to obtain a single cell suspension enriched in MMECs. Following RNA extraction and cDNA synthesis, qPCR analysis for a restricted panel of Wnt/ β -catenin target genes was carried out. As already discussed in Chapter 4, nuclear translocation of unphosphorylated β -catenin leads to the formation of a bipartite transcription factor complex composed by members of the TCF/LEF family (Eastman et al., 1999). This result in a transient, yet potent, activation of gene transcription affecting a wide range of β -catenin targeted genes (Daniels et al., 2005). Albeit the identity of the majority of them is still elusive, some others have well-been documented. Among the latter category, *Ccnd1* and *Myc* represent major drivers of β -catenin-induced cell proliferation (Lin et al., 2000), whereas *Lgr5*, *Cd44* and *Ascl2* genes are crucial mediators of the role played by canonical Wnt signalling in the regulation of mammary stemness (Zeng et al., 2010). Accordingly, whilst high *Ccnd1* levels were consistently shown for *Runx1^{wt/wt};Runx2^{fl/fl}* mice, all three *Runx*-deficient cohorts showed a reduction of *Myc* expression as compared to controls (Figure 5. 21). Nonetheless, a significant difference in *Myc* levels was only found upon combined deletion of *Runx1* and *Runx2* ($P=0.00384$). Thus, it could be speculated that *Myc* might represent a downstream target of the *Runx* genes. When analysis of Wnt/ β -catenin stem-like genes was performed, a modest increase in *Lgr5* levels was displayed by all *Runx*-deficient cohorts of mice, as compared to *Runx1^{wt/wt};Runx2^{wt/wt}* animals, albeit a significant difference was only reported upon deletion of *Runx2* ($P=0.00638$). Whilst some variability was found in relation to *Cd44*, both within and across cohorts, an intriguing pattern of expression was observed in the case of the *Ascl2* gene, which showed a trend towards increased levels in both *Runx1^{fl/fl};Runx2^{wt/wt}* and *Runx1^{fl/fl};Runx2^{fl/fl}* cohorts of *BLG-Cre;Catnb^{wt/lox(ex3)}* mice (Figure 5. 21).

Wnt/ β -catenin target genes

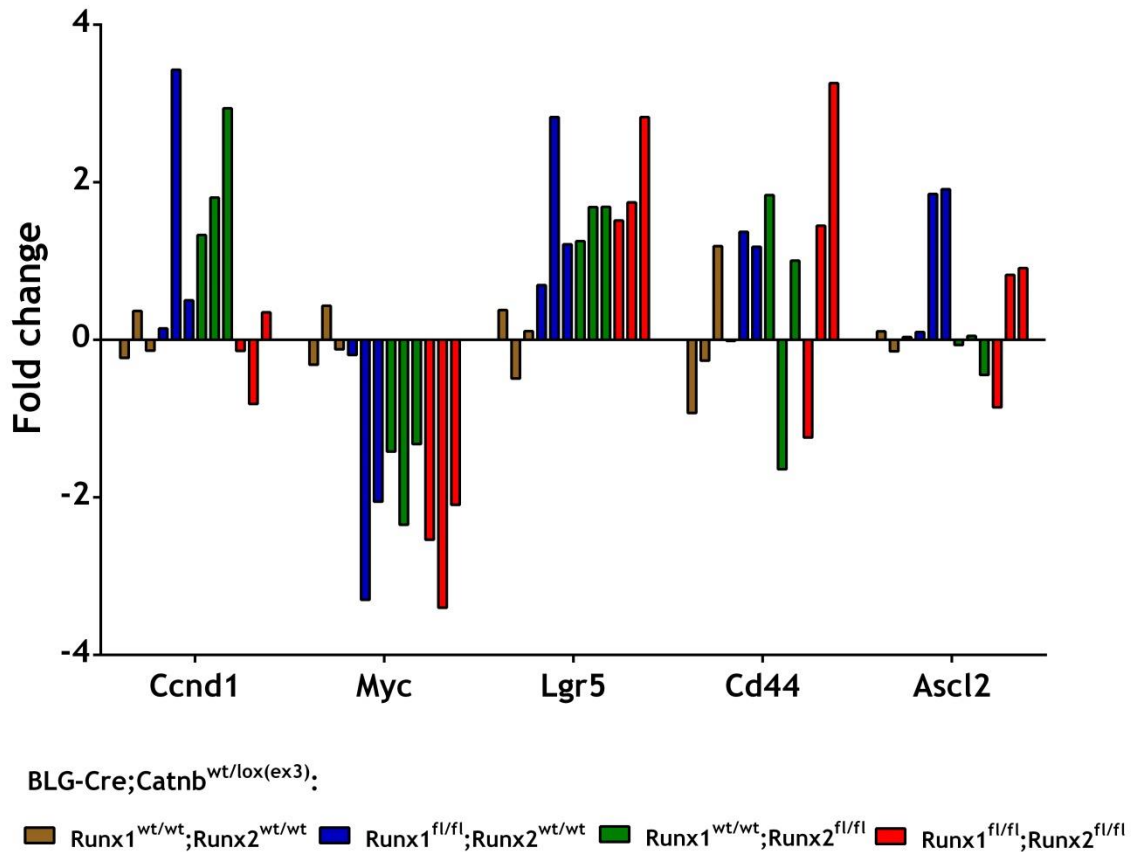


Figure 5. 21 Expression analysis of Wnt/ β -catenin target genes upon loss of *Runx1* and *Runx2*.

Bar chart showing mRNA expression levels of five Wnt/ β -catenin target genes in *Runx1*^{wt/wt};*Runx2*^{wt/wt}, *Runx1*^{fl/fl};*Runx2*^{wt/wt}, *Runx1*^{wt/wt};*Runx2*^{fl/fl} and *Runx1*^{fl/fl};*Runx2*^{fl/fl} cohort of BLG-Cre;Catnb^{wt/lox(ex3)} mice. Animals were euthanized at 6 weeks of age and their mammary glands dissected out for collection. Organs were mechanically and enzymatically digested in order to obtain a single cell suspension enriched in MMECs. Samples were then processed for RNA extraction, cDNA synthesis and qPCR analysis. Three replicates per cohort are shown individually to highlight the variability within each group. Each replicate contains mammary glands from more than one animal. Data analysis was performed using the CFX Manager software, version 3.1 (BioRad) and the GenEx Standard software, version 6.1 (MultiD Analyses). Data were first normalized to *Actin* and *Fbxo38* reference genes and then expressed as fold change of *Runx1*^{wt/wt};*Runx2*^{wt/wt} control mice. The x axis indicates five different Wnt/ β -catenin target genes (*Ccnd1*, *Myc*, *Lgr5*, *Cd44* and *Ascl2*); the y axis shows expression values after log₂ transformation, where 0 represents the base value. Anything above 0 is up-regulated, whilst anything below 0 is downregulated in respect to *Runx1*^{wt/wt};*Runx2*^{wt/wt} mice. Statistical analysis (shown in the text) was performed by the multiple comparisons t-test with the Dunn-Bonferroni correction method, comparing each cohort to the *Runx1*^{wt/wt};*Runx2*^{wt/wt} group. Cut off value of this analysis is 0.006379. RNA extraction, cDNA synthesis and qPCR analysis was done by Dimitris Athineos.

5.3 Discussion

Overall, this analysis revealed a precocious transformation of the mammary epithelium in response to BLG-Cre-driven activation of the Wnt/ β -catenin signalling pathway. Proof of oncogenic changes relate to the presence of thickened epithelial ducts in mammary whole-mounts and H&E pre-neoplastic lesions at both pre-pubertal (3 weeks) and pubertal (6 and 9 weeks) time-points. Nonetheless, the mammary anlage and the subsequent elongation of the incipient ductal tree characterizing *Runx* wild type *BLG-Cre;Catnb^{wt/lox(ex3)}* control mice did not appear to be severely compromised. In net contrast, individual or combined deletion of *Runx1* and *Runx2* resulted in the formation of enlarged mammary rudiments at 3 weeks of age. By 6 weeks, this phenotype dramatically impinged on the subsequent elongation of pubertal mammary glands, whereby growth of ductal trees appeared halted in the absence of *Runx1* and *Runx2*, yet augmented upon combined loss of both genes. At the end of puberty (9 weeks), whilst ductal elongation and mammary gland morphogenesis were partly restored in the vast majority of both *Runx1^{fl/fl}* and *Runx2^{fl/fl}* mice, a similar rescue of the phenotype was not observed in the absence of both genes. Thus, it could be speculated that activation of the Wnt/ β -catenin signalling pathway might target a population of stem/progenitor cells present in the TEBs of pre-pubertal mice. Whilst expansion of this pre-neoplastic subset of cells would occur upon individual and combined loss of *Runx1* and *Runx2*, its survival would appear to be enhanced in the absence of both genes. Altogether, this hints towards a potent tumour suppressive role played by *Runx1* and *Runx2* in the early stages of Wnt/ β -catenin-mediated mammary tumourigenesis.

Of note, one of the most common mechanisms by which activated Wnt/ β -catenin signalling drives tumourigenesis is via an increase in cell proliferation (Zeng et al., 2010). However, on the basis of the results explained above, the enlarged mammary tree arising from combined loss of *Runx1* and *Runx2* cannot be solely justified by the moderate rate of TE proliferative density. Moreover, in line with the high predominance of pre-neoplastic lesions evident by IHC, proliferation appears to be tightly linked to the subsequent differentiation of the incipient mammary epithelium. Due to the experimental procedure used, which involves the incorporation of BrdU by proliferating cells and its gradual decrease over cell

division, it might be possible that fast cycling cells could not be captured by this technique. Alternatively, the enlarged epithelial structure seen upon loss of *Runx1* and *Runx2* might stem from either a decrease in cell death or from changes in MaSC behaviour. MaSCs would use the balance between ACD and SCD in order to self-renew and differentiate (ACD) or to expand the SC pool (SCD) (Ballard et al., 2015). It is also known that, while committed progenitors arising via ACD display a high proliferative rate, MaSCs are generally believed to be slow cycling cells (Welm et al., 2002; Visvader et al., 2016). As such, it could be speculated that BLG-Cre-driven activation of the Wnt/ β -catenin signalling pathway switches the balance from ACD to SCD in the absence of *Runx1* and *Runx2*. Due to their intrinsic differences in cell proliferation, the use of a label-retaining approach might help discriminate between the presence of an expanded MaSC pool (the result of SCD) versus the presence of transient amplifying cells (the result of ACD). Albeit the same phenotype was not observed in *Runx1^{fl/fl}* mice, the latter displayed the highest levels of TE proliferative density. However, if TE proliferation of *Runx1^{fl/fl}* mice did not lead to a corresponding increase in the amount of total TE, compensatory processes have to exist. This could point towards an increased cell death, a reduced cell survival, or to the presence of a tumour suppressive mechanism able to halt Wnt/ β -catenin driven pre-neoplastic transformation in the absence of *Runx1*. Due to the phenotype displayed with the concomitant absence of *Runx2*, there is a high chance these two genes might compensate for each other's absence.

Following histopathological characterization of pre-neoplastic Wnt/ β -catenin-driven mammary lesions, foci of strong nuclear β -catenin staining could be observed across all cohorts of pubertal (6 week old) mice. These data reiterated the causative tumourigenic role played by canonical Wnt signalling, able to cause a precocious transformation of the mammary epithelium. As suggested by IHC analysis, signs of this transformation were displayed by distorted mammary ducts composed by abnormally expanded basal and luminal epithelial cells, surrounded by an almost intact MYO layer. Culmination of this phenotype was represented by the presence of epidermal cells found within the centre of pre-neoplastic lesions, particularly upon combined deletion of both *Runx1* and *Runx2*. Interestingly, high levels of HRs were also found across all mouse cohorts, with ER α positive cells often located in close proximity to each other.

These observations suggested a link between canonical Wnt and hormone signalling and hinted towards the possibility of a targeted HR positive cell-of-origin. Preliminary analysis of Wnt/ β -catenin target genes showed an increase of *Lgr5* expression displayed by all three cohorts of *Runx*-deficient mice. In addition, a modest increase of the *Ascl2* transcription factor was specifically found upon deletion of *Runx1*, both in the presence or absence of *Runx2*. In view of its well-known function as a stem cell identity gene in the colon (Schuijers et al., 2015), these findings might point towards the expansion of a stem-like population of MMECs in the absence of *Runx1* or combined loss of both *Runx* genes. Nonetheless, a considerable amount of variability was found within each group of mice. These discrepancies could be ascribed to the peculiar developmental time point chosen, characterized by the presence of both normal and pre-neoplastic mammary tissue. In addition, being all cohorts on a mixed background, strain-related differences cannot be ruled out. Future directives might be focused on increasing not only the panel of Wnt/ β -catenin target genes, but also the number of experimental animals per each cohort. Lastly, given the multitude of signalling pathways the Wnt/ β -catenin signalling interact with, an unbiased analysis of RNA-sequencing might help unveil the contribution played by *Runx* genes loss upon Wnt/ β -catenin-driven mammary tumourigenesis.

6 Characterization of Wnt/ β -catenin activated mammary epithelial cells upon *Runx* deletion

6.1 Introduction

Mammary-specific activation of the Wnt/ β -catenin signalling pathway showed a remarkable disruption of postnatal mammary gland development in the absence of *Runx1* and *Runx2* (see Chapter 5). In order to capture the early stages of oncogenic transformation, responsible for converting a normal mammary epithelium into an incipient pre-neoplastic one, an experimental *ex vivo*-based approach was exploited. This consisted in the extraction and characterization of the functional and phenotypic features displayed by Wnt/ β -catenin-activated MMECs, in the attempt to better understand the mechanism(s) underpinning the tumour suppressive function exerted by RUNX1 and RUNX2 in the context of Wnt signalling.

6.2 Experimental procedures

In view of the phenotypic variability visible by whole-mounts affecting all cohorts of *BLG-Cre;Catnb^{wt/lox(ex3)}* mice and the low amount of epithelial tissue correlated with some genotypes, MMEC extraction was performed by harvesting mammary glands from 7 to 8 week old females. Considering the subtle molecular differences reported between different pairs of mammary glands (Veltmaat et al., 2013), all ten murine glands were harvested at any time, with removal of the inguinal lymph nodes. In addition, although some experiments were performed with one mouse per group, some others were carried out pulling together mammary glands from more than one animal per genotype. As for any fractionation studies, one of the main hurdles of this technique consisted in obtaining a single cell suspension from solid mammary gland tissues. Indeed, the ramified ductal structure of the mammary gland lays its foundation on the properties of MMECs, which appear to be tightly connected to each other, as well as to the extracellular matrix. In brief, mammary glands were firstly mechanically dissociated with the use of a tissue chopper and secondly enzymatically digested via a mixture of collagenase and hyaluronidase. Following

a series of washes to remove all cell debris and the majority of non-epithelial cells, the digested tissue was subjected to red blood cell lysis. Lastly, after two sequential steps of trypsinization and filtration, a single-cell suspension could be obtained and used for different *ex vivo* experimental assays (Figure 6. 1).

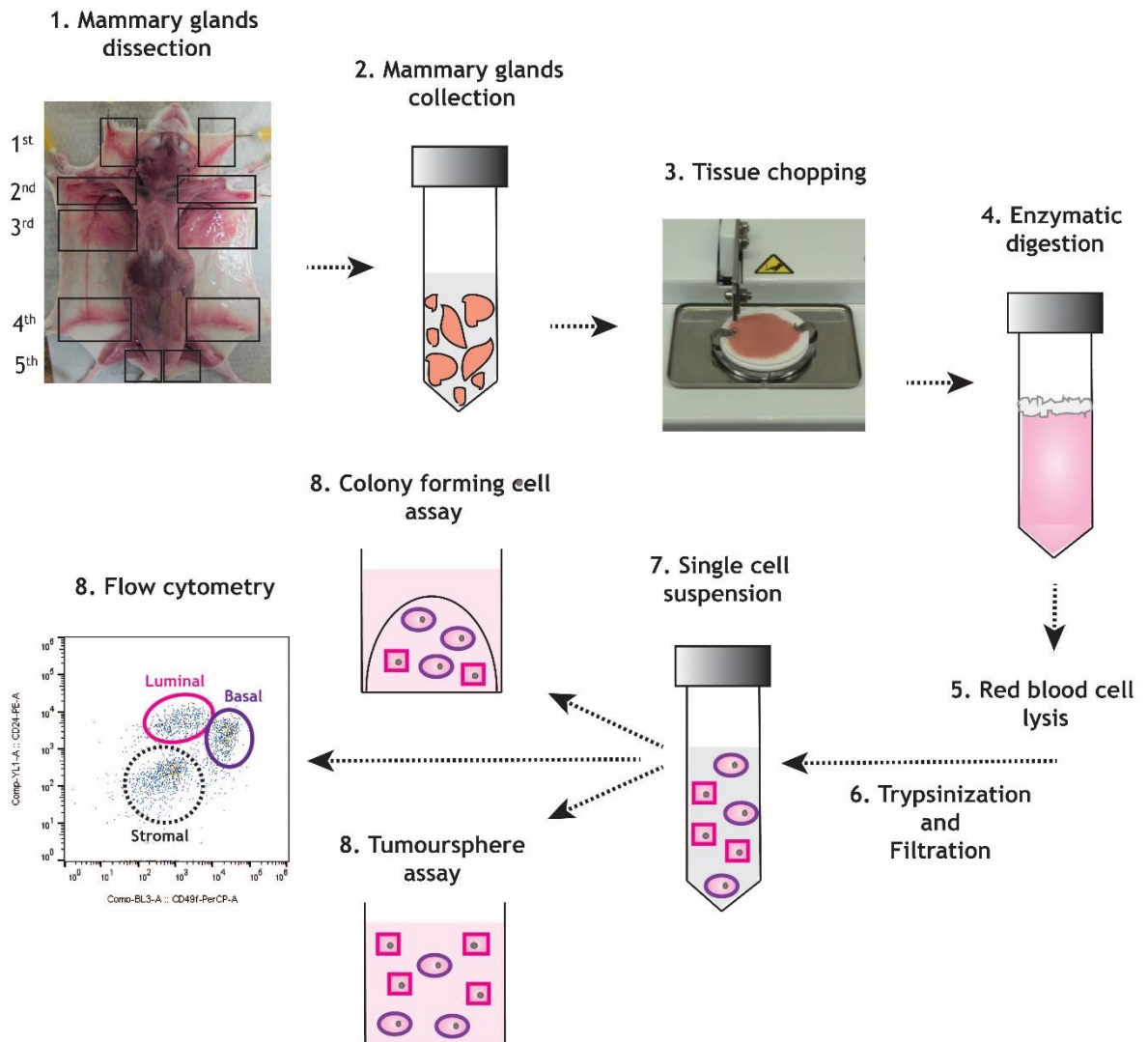


Figure 6. 1 Pipeline for the extraction and characterization of mammary epithelial cells.

Workflow of the eight steps required to extract and characterize the properties of MMECs. (1) All five pairs of mammary glands are dissected out and (2) placed in a 50 ml tube with PBS. (3) Mammary glands are mechanically disrupted with a tissue chopper until a fine tissue paste is obtained. (4) Chopped tissue is enzymatically digested at 37°C for 1.5 hours in medium containing collagenase and hyaluronidase. (5) Digested tissue is treated with NH_4Cl for 5 minutes at room temperature to lyse red blood cells. (6) The lysate is trypsinized for 10 minutes at 37°C and filtered through 70 μm pores. (7) A single cell suspension enriched in MMECs is obtained. (8) The properties of MMECs can be tested via different *ex vivo* functional assays: tumoursphere assay, MMEC, mouse mammary epithelial cell; PBS, phosphate buffered saline.

6.3 Results

6.3.1 Investigating how loss of *Runx1* and *Runx2* impinges on Wnt/ β -catenin-driven mammary stemness

The Wnt/ β -catenin signalling pathway plays a major role in regulating self-renewal potential and proliferative ability of stem/progenitor cells. Not surprisingly, aberrant Wnt/ β -catenin signalling has also been shown to exploit the latter mechanisms to drive malignant transformation of several tissues, including the breast (Reya and Clevers, 2005). In an attempt to investigate if individual or combined deletion of *Runx1* and *Runx2* impinged on the stemness properties exhibited by Wnt/ β -catenin-activated MMECs, the tumoursphere assay was employed. Following optimization of the appropriate culture conditions, freshly extracted MMECs from all cohorts of *BLG-Cre;Catnb^{wt/lox(ex3)}* mice were plated in non-adherent conditions at a density of 10,000 live cells per well. After 6 days, spheres were manually counted and photographed to assess their morphology. Nonetheless, as the accurate number of spheres was confounded by the presence of aggregates and cell debris, sphere size was used as a surrogate measure of stem/progenitor activity. Accordingly, whilst all *BLG-Cre;Catnb^{wt/lox(ex3)}* derived MMECs demonstrated the ability to grow in suspension (Figure 6. 2A), a significant reduction in the frequency of small size spheres was found in the absence of *Runx2* as compared to *Runx*-wild type controls (Figure 6. 2B). However, when all groups were compared with each other, *Runx1^{fl/fl};Runx2^{fl/fl}* cultures displayed a significantly higher frequency of small tumourspheres in respect to both *Runx1^{fl/fl}* and *Runx2^{fl/fl}*-derived MMECs.

When primary tumoursphere-derived cells were re-plated at a density of 5,000 live cells per well under the same non-adherent conditions, genotypes showed the ability to form secondary tumourspheres (Figure 6. 3A). These appeared to be significantly bigger upon loss of *Runx2* (Figure 6. 3B). Albeit combined deletion of *Runx1* and *Runx2* did not seem to affect the size of secondary tumourspheres in relation to *Runx*-wild type cohorts (Figure 6. 3), these were found to be significantly smaller in relation to *Runx2^{fl/fl}*-derived MMECs. In addition, *Runx1^{fl/fl};Runx2^{fl/fl}*-derived secondary tumourspheres generally appeared to be lower in number compared to all other groups of *BLG-Cre;Catnb^{wt/lox(ex3)}* mice (data not shown).

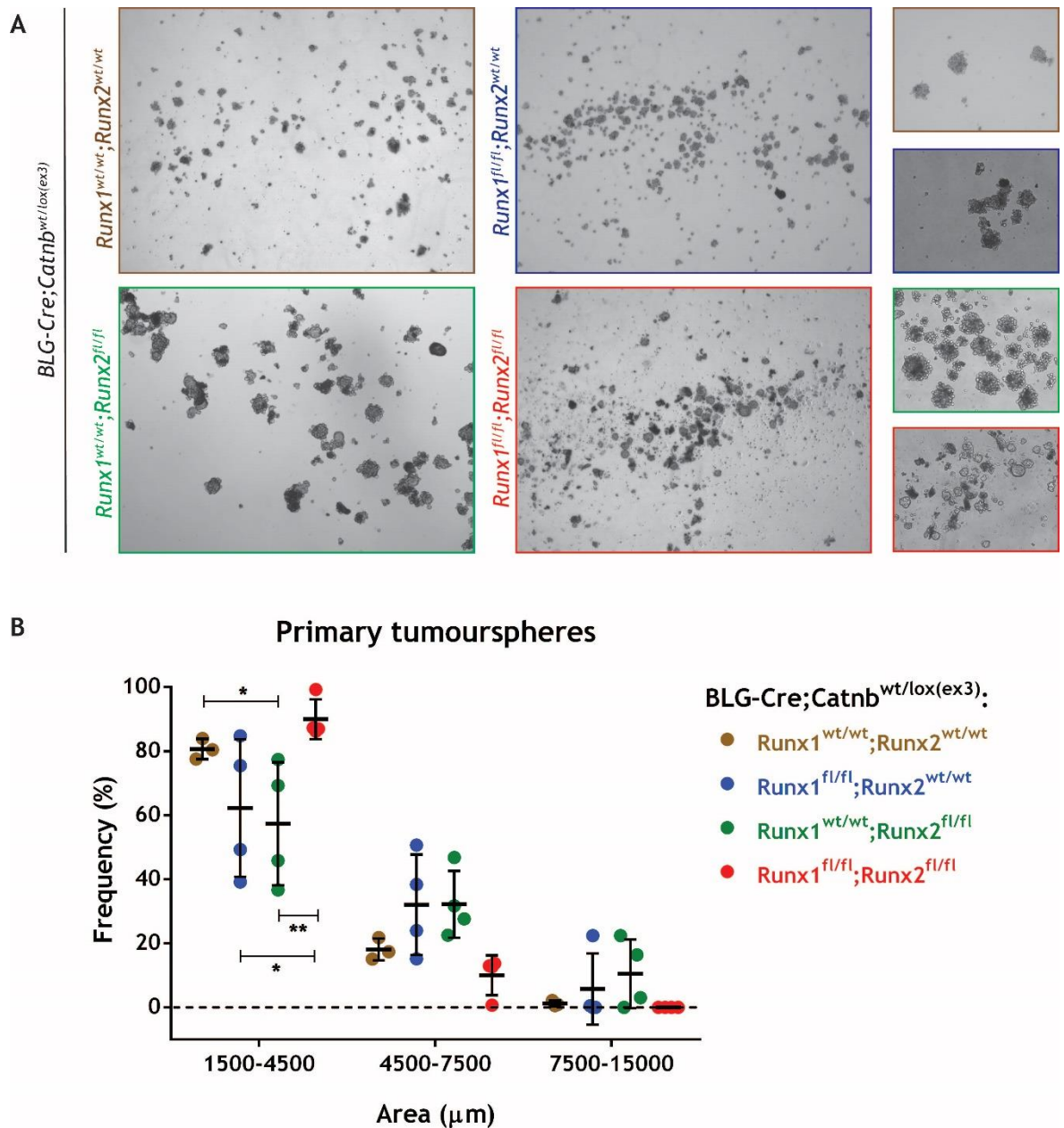


Figure 6. 2 Primary tumoursphere growth of Wnt/ β -catenin activated mammary epithelial cells in the absence of *Runx1* and/or *Runx2*.

Representative pictures (A) and scatter dot plot of the area (B) of primary tumourspheres derived from the extraction of MMECs from 7 to 8 week old *BLG-Cre; Catnb^{wt/lox(ex3)}* female mice, in the absence of *Runx1* (*Runx1^{fl/fl}; Runx2^{wt/wt}*), *Runx2* (*Runx1^{wt/wt}; Runx2^{fl/fl}*), or both genes (*Runx1^{fl/fl}; Runx2^{fl/fl}*). Images were captured with the 4X (left and mid columns) and 10X (right column) objective lens of the Olympus CKX41 microscope. One representative picture of $n \geq 3$ is shown per genotype. Spheres area (μm) was calculated via ImageJ and grouped into three ranges: 1500-4500, 4500-7500, 7500-15000. The graph shows the frequency (%) of measured spheres according to each range across all genotypes. Statistical analysis was performed by the two-way ANOVA test in GraphPad Prism. The Dunnett's multiple comparisons test was used to compare all genotypes to the *Runx1^{wt/wt}; Runx2^{wt/wt}* control cohort; the Tukey's multiple comparisons test was used to compare all genotypes with each other. Error bars represent mean with SD ($n \geq 3$ for *Runx1^{wt/wt}; Runx2^{wt/wt}*, $n \geq 4$ for the other cohorts). * $P < 0.05$; ** $P < 0.01$. MMEC, mouse mammary epithelial cells.

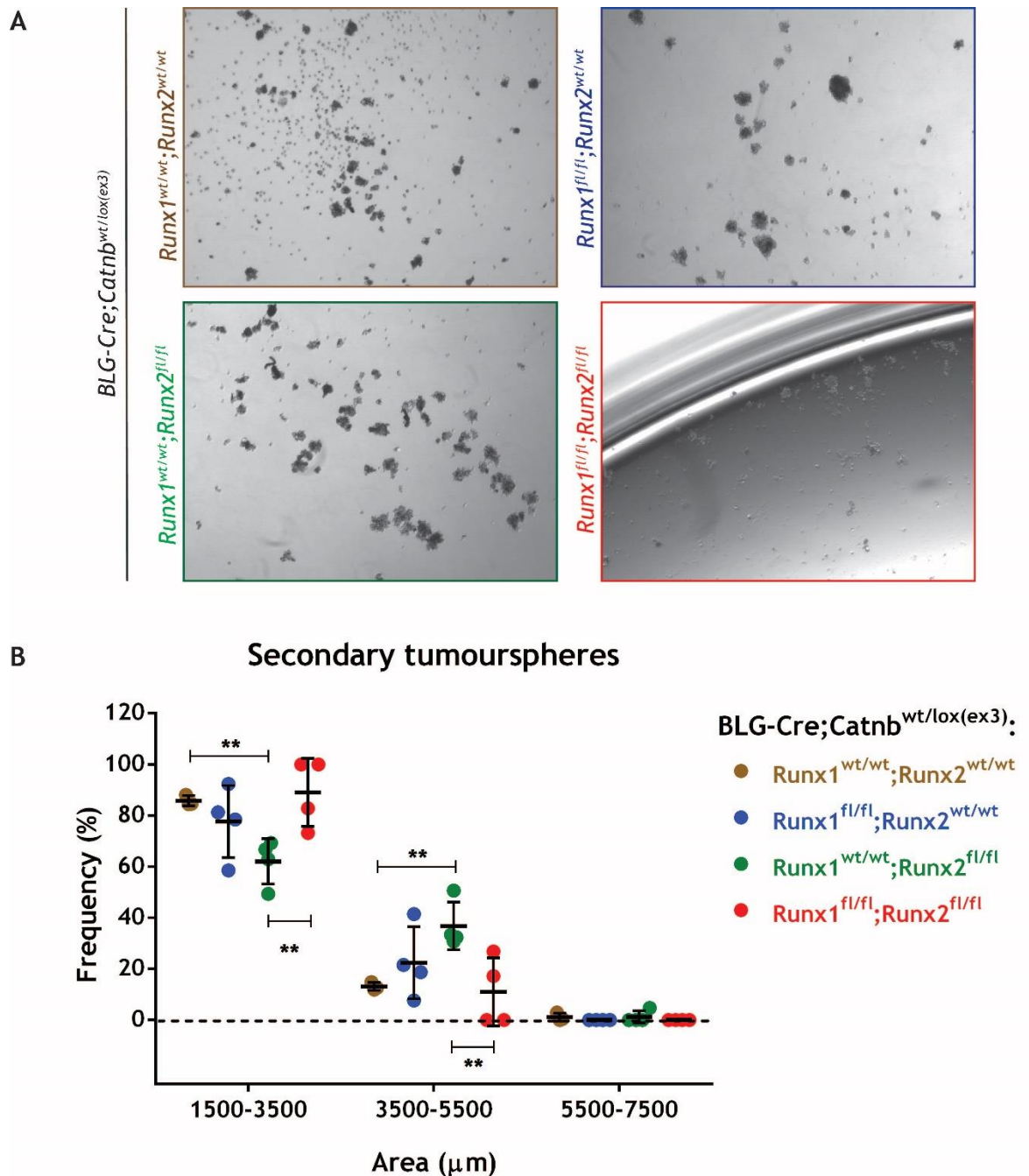


Figure 6. 3 Secondary tumoursphere growth of Wnt/ β -catenin activated mammary epithelial cells in the absence of *Runx1* and/or *Runx2*.

Representative pictures (A) and scatter dot plot of the area (B) of secondary tumourspheres derived from the extraction of MMECs from 7 to 8 week old *BLG-Cre;Catnb^{wt/lox(ex3)}* female mice, in the absence of *Runx1* (*Runx1^{fl/fl};Runx2^{wt/wt}*), *Runx2* (*Runx1^{wt/wt};Runx2^{fl/fl}*), or both genes (*Runx1^{fl/fl};Runx2^{fl/fl}*). Images were captured with the 4X objective lens of the Olympus CKX41 microscope. One representative image of $n \geq 3$ is shown per genotype. Spheres area (μm) was calculated via ImageJ and grouped into three ranges: 1500-3500, 3500-5500, 5500-7500. The graph shows the frequency (%) of measured spheres according to each range across all genotypes. Statistical analysis was performed by the two-way ANOVA test in GraphPad Prism. The Dunnet's multiple comparisons test was used to compare all genotypes to the *Runx1^{wt/wt};Runx2^{wt/wt}* control cohort; the Tukey's multiple comparisons test was used to compare all genotypes with each other. Error bars represent mean with SD ($n \geq 3$ for *Runx1^{wt/wt};Runx2^{wt/wt}*, $n \geq 4$ for the other cohorts). ** $P < 0.001$. MMEC, mouse mammary epithelial cells.

6.3.2 Loss of *Runx1* favours the expansion of a basal subpopulation of mammary cells upon activated Wnt/ β -catenin signalling

To investigate if Wnt/ β -catenin pre-neoplastic transformation of the mammary epithelium was due to the expansion of a progenitor subpopulation of MMECs in the absence of the *Runx* genes, the CFC assay was employed. By embedding freshly extracted MMECs from 7 to 8 week old *BLG-Cre;Catnb^{wt/lox(ex3)}* mice in matrigel in the presence of GFs-enriched medium, the activity of different progenitor populations could be inferred via the formation of discrete colonies. However, due to the high degree of cellular heterogeneity present in the MG and the low reliability of epithelial versus non-epithelial cell count, the number of generated colonies per cohort could not be taken into account. Nonetheless, whilst the latter is a general reflection of progenitor cell' activity, colony morphology is indicative of the different types of active progenitors present in the original cell mixture. It is in fact believed that cells enriched in the Lin⁻CD24⁺CD49f^{low} subgroup, containing LPs, would mainly give rise to acinar-like colonies, whereas cells enriched in the Lin⁻CD24⁺CD49f^{high} subpopulation, comprising BPs/MRUs, would form solid-like colonies (Stingl et al., 2006; Joshi et al., 2010).

When the ratio of solid versus acinar colonies was calculated, it was found that *BLG-Cre;Catnb^{wt/lox(ex3)}*-derived MMECs predominantly formed solid colonies in the absence of *Runx1* (Figure 6. 4). Interestingly, this phenotype appeared to be independent of the *Runx2* status, as *Runx1^{fl/fl};Runx2^{fl/fl}*-derived MMECs also showed a similar behaviour. On the contrary, MMECs extracted from *Runx1^{wt/wt};Runx2^{wt/wt}* and *Runx2^{fl/fl}* mice displayed a ratio equal to one, indicating comparable levels of solid versus acinar colonies. Whilst the size of acinar colonies was found to be unchanged between groups, MMECs extracted from *Runx1^{fl/fl}* and *Runx1^{fl/fl};Runx2^{fl/fl}* mice generated a significantly lower frequency of 0-100 μ m and higher frequency of 100-200 μ m solid spheres as compared to controls (Figure 6. 5). This result perhaps suggested an increased proliferative activity displayed by BPs in the absence of *Runx1*. It is important to point out, however, that none of MMECs extracted from each cohort of *BLG-Cre;Catnb^{wt/lox(ex3)}* mice managed to form any discrete colonies in the absence of GFs (EGF, FGF2 and Insulin), indicating an equal dependency of Wnt/ β -catenin driven MMECs towards external cues (data not shown).

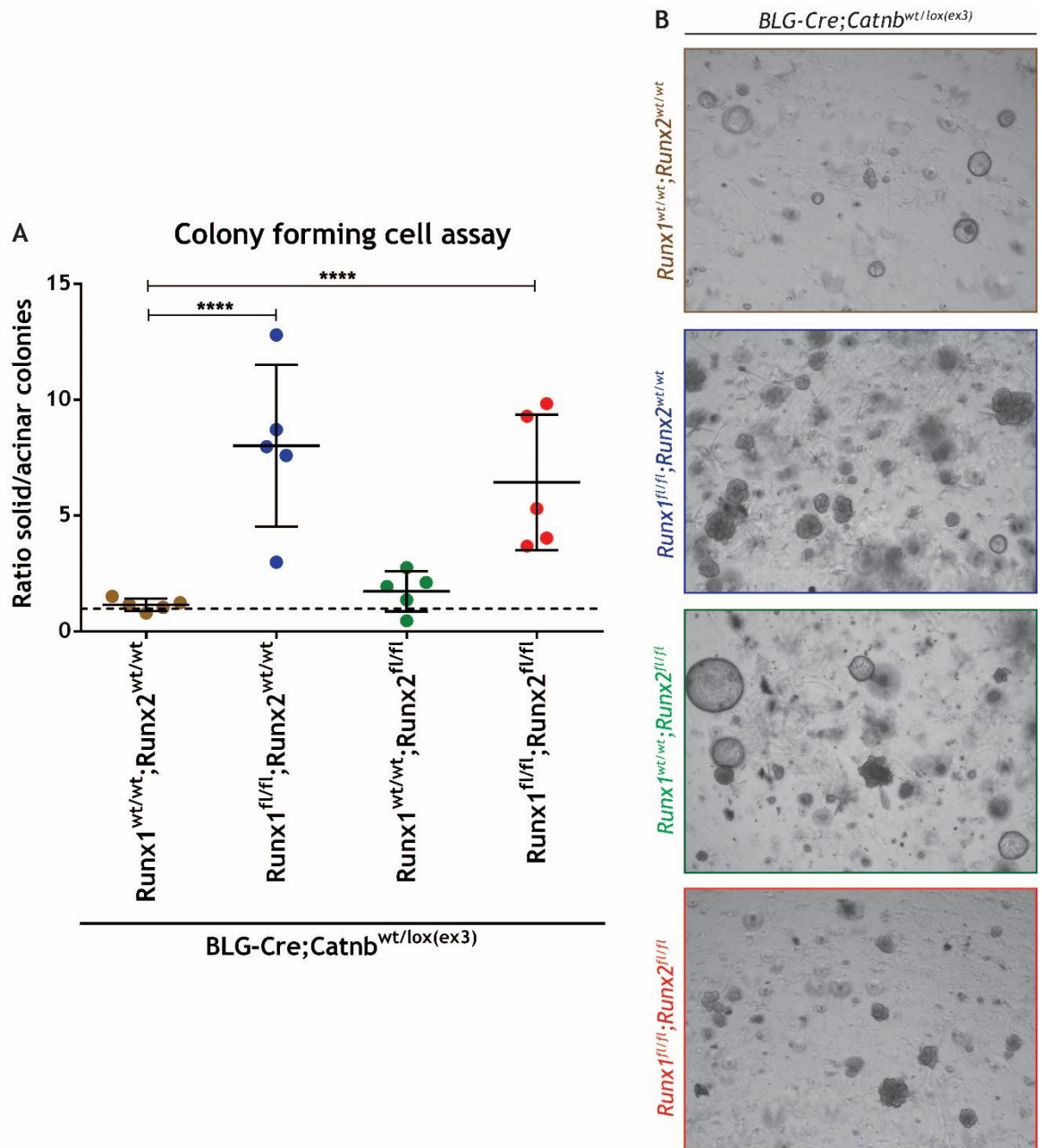


Figure 6. 4 Deletion of *Runx1* favours the formation of basal colonies on a Wnt/ β -catenin activated background.

(A) Scatter dot plot of the ratio of solid versus acinar colonies generated by MMECs extracted from 7 to 8 week old $BLG-Cre; Catnb^{wt/lox(ex3)}$ female mice, in the absence of *Runx1* ($Runx1^{fl/fl}; Runx2^{wt/wt}$), *Runx2* ($Runx1^{wt/wt}; Runx2^{fl/fl}$), or both genes ($Runx1^{fl/fl}; Runx2^{fl/fl}$). 5,000 live MMECs were plated per well in a 20 μ l drop of matrigel, covered with medium supplemented with GFs. Cells were fed after 3 days with the addition of fresh medium and cultured for up to 6 days. For each genotype, the ratio between solid and acinar colonies was calculated per well and averaged among all 12 technical replicates. Each dot represents an independent biological replicate. (B) One representative picture of n=5 displaying solid and acinar colonies is shown per each cohort. Images were taken with the 4X objective lens of the Olympus CKX41 microscope. Statistical analysis was performed by the two-way ANOVA test with Dunnet's multiple comparisons in GraphPad Prism. Error bars represent mean with SD (n=5 per each cohort). **** $P < 0.0001$. MMEC, mouse mammary epithelial cell.

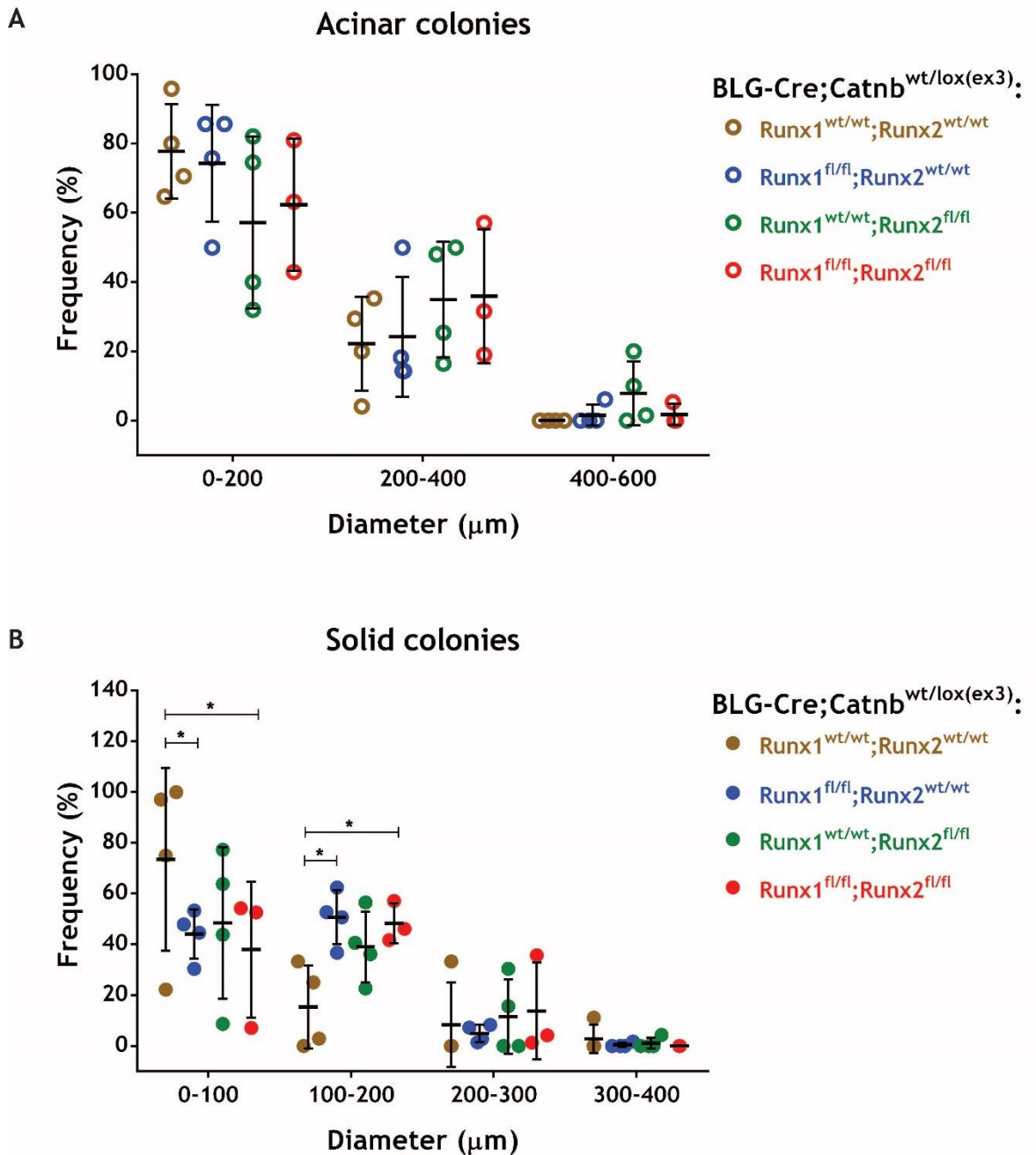


Figure 6. 5 Size of acinar and solid colonies formed by Wnt/ β -catenin activated mammary epithelial cells upon loss of *Runx1* and *Runx2*.

Analysis of the diameter displayed by acinar (A) and solid (B) colonies formed by MMECs extracted from 7 to 8 week old *BLG-Cre;Catnb^{wt/lox(ex3)}* female mice, in the absence of *Runx1* ($Runx1^{fl/fl};Runx2^{wt/wt}$), *Runx2* ($Runx1^{wt/wt};Runx2^{fl/fl}$), or both genes ($Runx1^{fl/fl};Runx2^{fl/fl}$). 5,000 live MMECs were plated per well in a 20 μ l drop of matrigel, covered with medium supplemented with GFs. Cells were fed after 3 days with the addition of fresh medium and cultured for up to 6 days. Pictures of each of the 12 technical replicates were taken at day 6 with the 4X objective lens of the Olympus CKX41 microscope. The diameter of both acinar and solid colonies was analysed via the use of ImageJ. Statistical analysis was performed by the two-way ANOVA test with Dunnett's multiple comparisons in GraphPad Prism. Error bars represent mean with SD ($n \geq 3$ per each cohort). * $P < 0.05$. MMEC, mouse mammary epithelial cell.

Perhaps as a reflection of the cellular heterogeneity displayed by the basal compartment of the mammary gland, three different morphological types of solid colonies could be distinguished among all *BLG-Cre;Catnb^{wt/lox(ex3)}* cohorts of mice: regularly-shaped, branched-shaped and irregularly-shaped. On the basis of evidence reported by the literature (Petersen et al., 1992; Stingl et al., 2006), regularly-shaped colonies could be due to the presence of BPs, whereas the other two types of colonies to the activity of MRUs. However, while branched-shaped colonies might arise from the activity of normal MRUs (N-MRUs), irregularly-shaped colonies could arise from abnormal MRUs (A-MRUs) (Figure 6. 6A). Interestingly, the morphological appearance of basal colonies appeared to correlate with the *Runx* status of *BLG-Cre;Catnb^{wt/lox(ex3)}* mice, as the majority of *Runx1*-deficient MMECs, both in the presence or absence of *Runx2*, generated a significantly lower frequency of regularly-shaped colonies versus a higher frequency of irregularly-shaped ones. On the contrary, both control and *Runx2*-floxed MMECs predominantly formed regularly-shaped colonies, albeit a trend towards increased irregular-colonies was also found upon deletion of *Runx2* (Figure 6. 6B). Of note, albeit diestrus-staged animals have been shown to give rise to more solid- versus acinar-like colonies due to the high levels of progesterone (Joshi et al., 2010), no correlation was found between colony morphology and the oestrous cycle of the mice in this study (data not shown). Collectively, these data suggested that, in the absence of *Runx1*, activation of the Wnt/ β -catenin signalling pathway might lead to the expansion of a transformed subpopulation of stem/progenitor cells contained within the basal compartment of the mammary gland and display a moderate rate of proliferative ability in 3D culture. Nonetheless, as in the case of the tumoursphere assay, it remains to be seen whether the heterogeneity displayed by solid colonies can be truly ascribed to activation of the Wnt/ β -catenin pathway or is rather a reflection of the different proportions of normal and abnormal MMECs present in mammary glands. Lastly, despite the cellular heterogeneity of the luminal epithelial compartment of the mammary gland discussed in the introduction, no morphological differences were observed among acinar colonies across all different cohorts of *BLG-Cre;Catnb^{wt/lox(ex3)}* mice. This finding supported the idea that perhaps BLG-Cre mediated activation of the Wnt/ β -catenin signalling pathway might target a subpopulation of MMECs lying within the basal epithelial lineage.

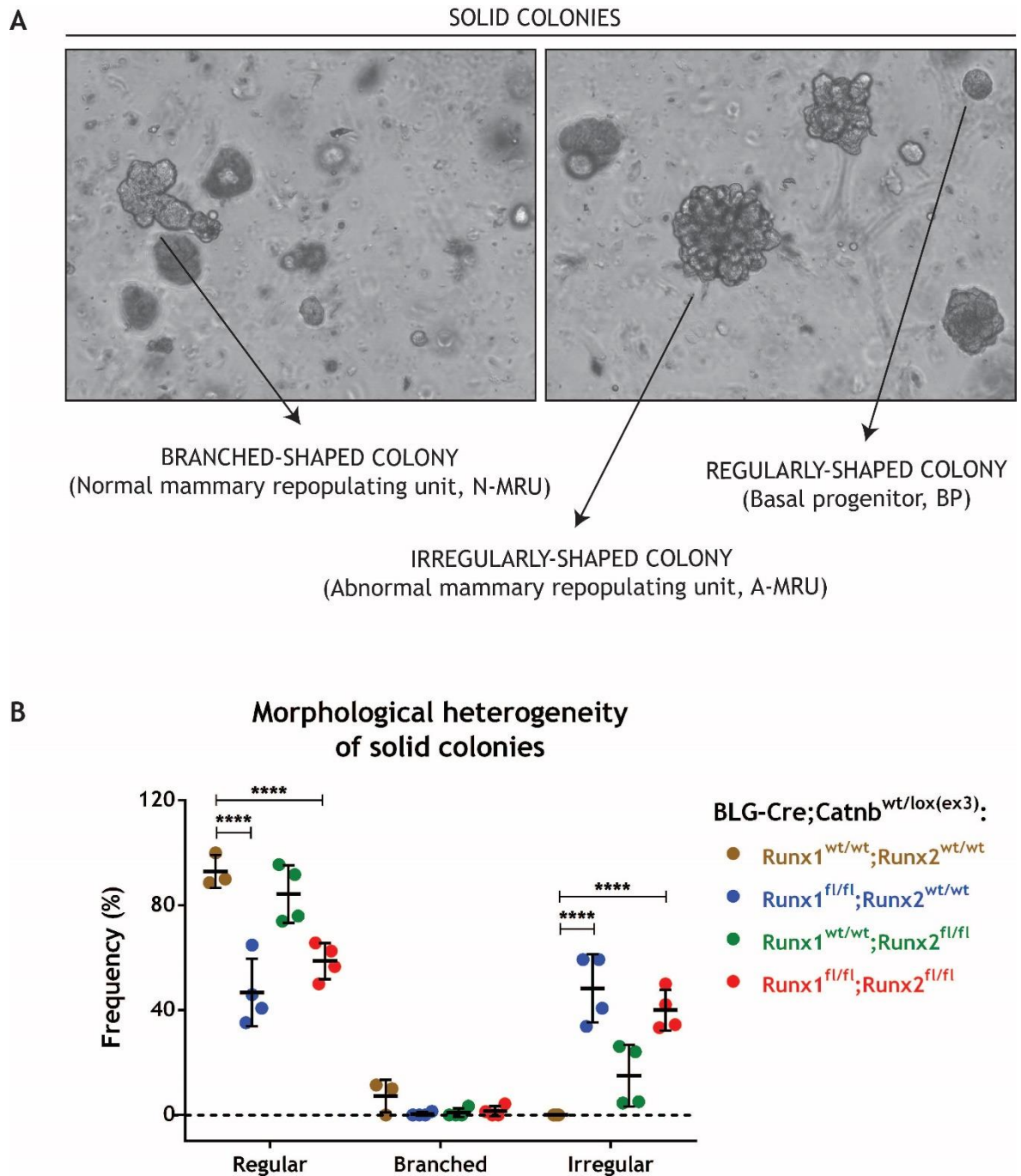


Figure 6. 6 Morphological heterogeneity displayed by Wnt/ β -catenin activated solid colonies upon loss of *Runx1* and *Runx2*.

(A) Two representative pictures showing three different morphological types of solid colonies, such as branched-shaped, irregularly-shaped and regularly-shaped, arising from N-MRUs, A-MRUs and BPs, respectively. (B) Scatter dot plot of three types of solid colonies generated by extracted MMECs from 7 to 8 week old *BLG-Cre; Catnb*^{wt/lox(ex3)} female mice, in the absence of *Runx1* (*Runx1*^{fl/fl}; *Runx2*^{wt/wt}), *Runx2* (*Runx1*^{wt/wt}; *Runx2*^{fl/fl}), or both genes (*Runx1*^{fl/fl}; *Runx2*^{fl/fl}). 5,000 live MMECs were plated per well in a 20 μ l drop of matrigel, covered with medium supplemented with GFs. Cells were fed with fresh medium after 3 days and cultured for up to 6 days. Pictures of each of the 12 replicates were taken at day 6 with the 10X objective lens of the Olympus CKX41 microscope. Statistical analysis was performed by the two-way ANOVA test with Dunnett's multiple comparisons in GraphPad Prism. Error bars represent mean with SD ($n \geq 3$ per each cohort). **** $P < 0.0001$. A-MRU, abnormal mammary repopulating unit; BP, basal progenitor; N-MRU, normal mammary repopulating unit; MMEC, mouse mammary epithelial cells.

6.3.3 Phenotypic characterization of Wnt/ β -catenin-driven mammary epithelial cells

Based on the *ex vivo* functional analysis reported above, *Runx* genes deletion was shown to significantly alter the properties of Wnt/ β -catenin-activated pre-neoplastic MMECs, perhaps by interfering with the basal stem/progenitor subset of the latter. Thus, in the attempt to capture the molecular changes displayed by the mammary epithelium of all cohorts of *BLG-Cre;Catnb^{wt/lox(ex3)}* mice, an experimental flow cytometry-based approach was exploited. As for previous analysis, the same experimental procedure was also applied to all corresponding groups of *BLG-Cre;Catnb^{wt/wt}* mice, so that the different contribution of *Runx* genes deletion occurring in a tumourigenic (Wnt/ β -catenin activated) and non-tumourigenic (Wnt/ β -catenin wild type) setting could be discerned. While doing so, it was felt important to avoid any *in vitro* culture step in order to minimize the presence of putative molecular mechanisms of cell adaptation to non-physiological conditions. As such, freshly extracted MMECs from all cohorts of 7 to 8 week old *BLG-Cre* mice were analysed by flow cytometry within the same day to preserve cell viability. In view of the high degree of cellular heterogeneity displayed by the mammary gland, a panel of different fluorochrome-conjugated antibodies had to be used in the first place to eliminate the majority of contaminating haematopoietic and endothelial cells from the original mixture (see Materials and Methods). Afterwards, MMEC enrichment was achieved via the combinatorial use of two main cell surface markers, i.e. CD24 and CD49f. CD24 (heat stable antigen) is a protein detected in the apical membrane and cytoplasm of human luminal cells (Jones et al., 2004), whereas in mice its expression appears to be more widespread, being present in epithelial, as well as endothelial and adipocyte cells (Stingl et al., 2006). CD49f ($\alpha 6$ -integrin), instead, seems to be located in the basal layer of the human skin (Carter et al., 1990) and in the basal compartment of the murine mammary epithelium (Stingl et al., 2006). By following this pipeline, three different subpopulations of Lin⁻ mammary cells could be resolved: stromal (CD24⁻CD49f⁻), luminal (CD24⁺CD49f^{low}) and basal (CD24⁺CD49f^{high}) (Stingl et al., 2006; Asselin-Labat et al., 2010) (Figure 6. 1).

6.3.3.1 Epithelial versus stromal cells

As discussed in Chapter 1, murine mammary gland postnatal development undergoes two distinct phases: a hormone-independent one, when the mammary anlage grows isometrically with the rest of the body; and a hormone-dependent one, during which the mammary epithelial tree proliferates and elongates throughout the stromal fat pad in response to external hormonal cues. As such, one could then imagine that the morphological appearance displayed by the mammary gland in late puberty stems from the subsequent contribution of these two interconnected processes, as well as from the interaction between the epithelial and stromal compartment. In view of the remarkable phenotypes observed in the whole-mounts of all virgin *BLG-Cre;Catnb^{wt/lox(ex3)}* mice (see Chapter 5), it was first investigated whether mammary specific deletion of *Runx1*, *Runx2* or both genes, caused an unbalance between the percentage of epithelial and stromal cells expressed over total Lin⁻ MMECs.

As perhaps expected from the developmental time-point analysed (i.e. 7 to 8 weeks), the percentage of stromal cells generally appeared to be greater than the epithelial counterpart, in both tumourigenic and non-tumourigenic settings across all different genotypes (Figure 6. 7). The only exception occurred within the *Runx1^{fl/fl};Runx2^{fl/fl}* cohort of *BLG-Cre;Catnb^{wt/lox(ex3)}* mice, wherein epithelial and stromal cells equalled each other (Figure 6. 7A). Albeit no significant differences were found when comparing each *Runx*-deficient cohort to its corresponding *BLG-Cre;Catnb^{wt/lox(ex3)}* and *BLG-Cre;Catnb^{wt/wt}* control group, deletion of *Runx1* resulted in a significant decrease of epithelial and increase of stromal cells when compared to *Runx1^{fl/fl};Runx2^{fl/fl}* mice of the *BLG-Cre;Catnb^{wt/lox(ex3)}* cohort (Figure 6. 7A). Of note, this result tided up not only with findings from the 6 and 9 weeks whole-mount analysis, whereby a small *Runx1*-deficient tree contrasted the presence of an enlarged mammary structure in the absence of both genes, but also to the previously shown quantification of TE, which appeared decreased upon deletion of *Runx1* yet increased with combined excision of both genes (see Chapter 5). Altogether, these data might suggest that the restricted proliferative ability of Wnt/ β -catenin-driven *Runx1*-deficient MMECs might only be unleashed in the absence of *Runx2*.

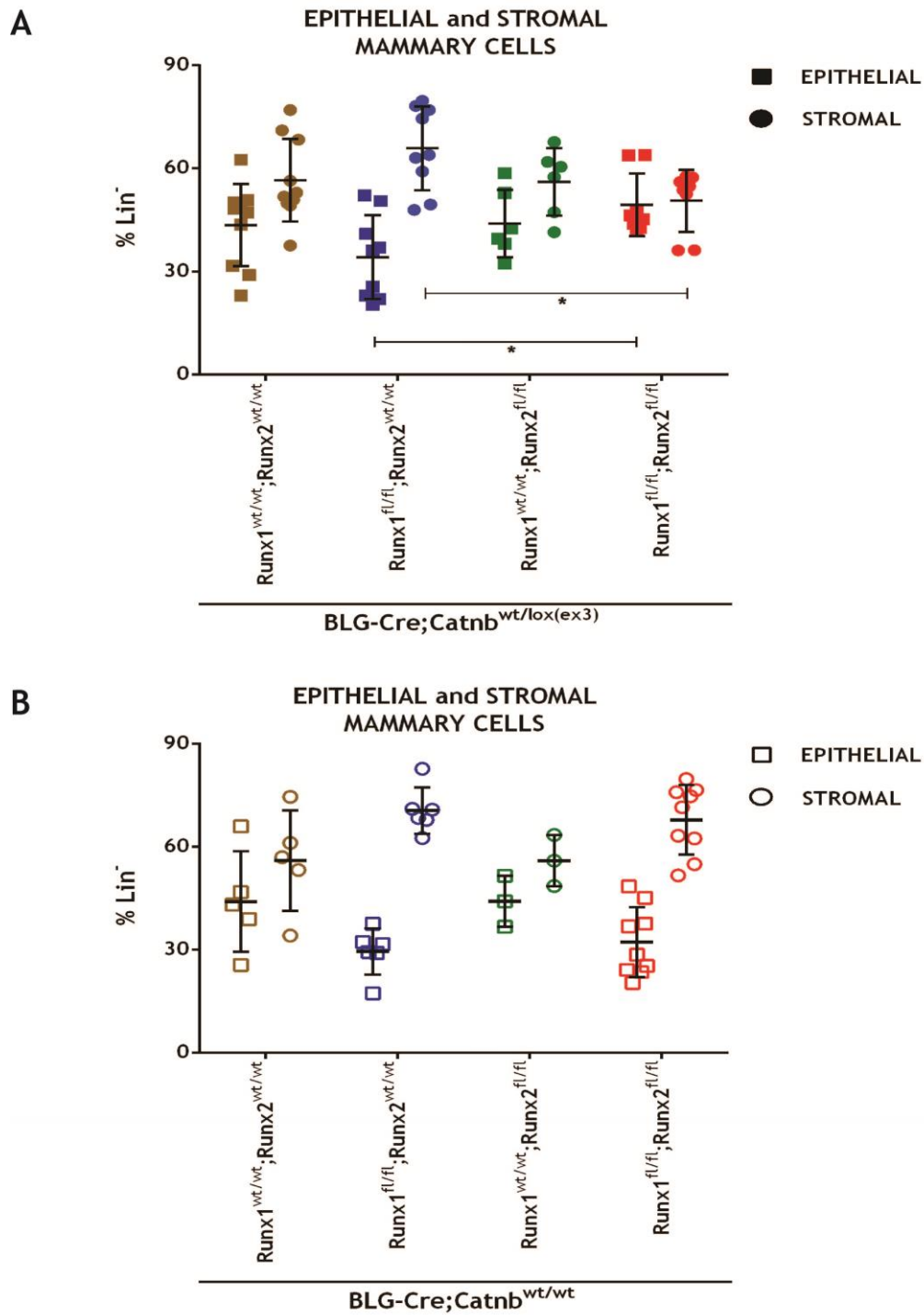


Figure 6. 7 Effects of *Runx1* and *Runx2* deletion on mammary epithelial and stromal cells in a *Wnt/β-catenin* activated and wild type setting.

Scatter dot plots showing the proportion of epithelial and stromal cells from (A) *BLG-Cre;Catnb^{wt/lox(ex3)}* and (B) *BLG-Cre;Catnb^{wt/wt}* mice, upon deletion of *Runx1* (*Runx1^{fl/fl};Runx2^{wt/wt}*), *Runx2* (*Runx1^{wt/wt};Runx2^{fl/fl}*) or both genes (*Runx1^{fl/fl};Runx2^{fl/fl}*). Cells were extracted from all five pairs of mammary glands of 7 to 8 weeks old female mice and are expressed as a percentage of total Lin⁻ cells. Statistical analysis was performed by the two-way ANOVA with the Tukey's multiple comparisons test in GraphPad Prism. Error bars represent mean with SD (n≥3 for each cohort). *P<0.05. Lin⁻, lineage negative.

6.3.3.2 Luminal versus basal cells

To accomplish its milk-producing function, the epithelial compartment of the mammary gland is composed of two main cell lineages: luminal cells, devoted to the production and secretion of milk into the ductal lumen of the gland, and basal/MYO cells, allowing the former in the process of milk ejection during lactation. As such, a balance between the two populations is fundamental to both mammary gland pubertal development, as well as homeostasis during adulthood. To investigate if activation of the Wnt/ β -catenin signalling pathway altered the equilibrium between the luminal and basal layers of the mammary gland in the context of *Runx* genes deletion, the proportion of each subset of MMECs was analysed and expressed as a percentage of total Lin⁺ cells. In doing so, deletion of *Runx1* resulted in a significant decrease of the percentage of luminal cells compared to *Runx1* wild type *BLG-Cre;Catnb^{wt/lox(ex3)}* control mice. Whilst deletion of *Runx2* displayed a similar, yet not significant, trend, combined loss of both genes was found to significantly restore both *Runx1*- and *Runx2*-deficient luminal population to slightly higher level than controls (Figure 6. 8A). Thus, the decreased epithelial subset showed by *Runx1*-deficient *BLG-Cre;Catnb^{wt/lox(ex3)}* glands (Figure 6. 7A) might be attributed to changes affecting the luminal compartment of the mammary gland. A similar pattern was also observed in a Wnt/ β -catenin wild type setting, whereby mammary specific deletion of *Runx1* or *Runx2* resulted in a moderate (yet not significant) reduction of luminal cells, which was rescued to the levels of *BLG-Cre;Catnb^{wt/wt}* control glands upon combined excision of both genes (Figure 6. 8B). However, in contrast to the tumourigenic context, even the basal subset of MMECs appeared perturbed upon *Runx* genes loss. In particular, the latter showed a reduction in both *Runx1^{fl/fl}* and *Runx1^{fl/fl};Runx2^{fl/fl}* mice, whilst a significant increase in the absence of *Runx2* (Figure 6. 8). Altogether, these results are indicative of a context-dependent interplay existing between RUNX1 and RUNX2, which seems to depend not only on the epithelial compartment of the mammary gland, but also on the presence of a tumourigenic or non-tumourigenic setting affecting the latter. Representative density plots of the luminal and basal expression profiles displayed by each cohort of *BLG-Cre;Catnb^{wt/lox(ex3)}* and *BLG-Cre;Catnb^{wt/wt}* mice are shown in Figure 6. 9 and Figure 6. 10, respectively.

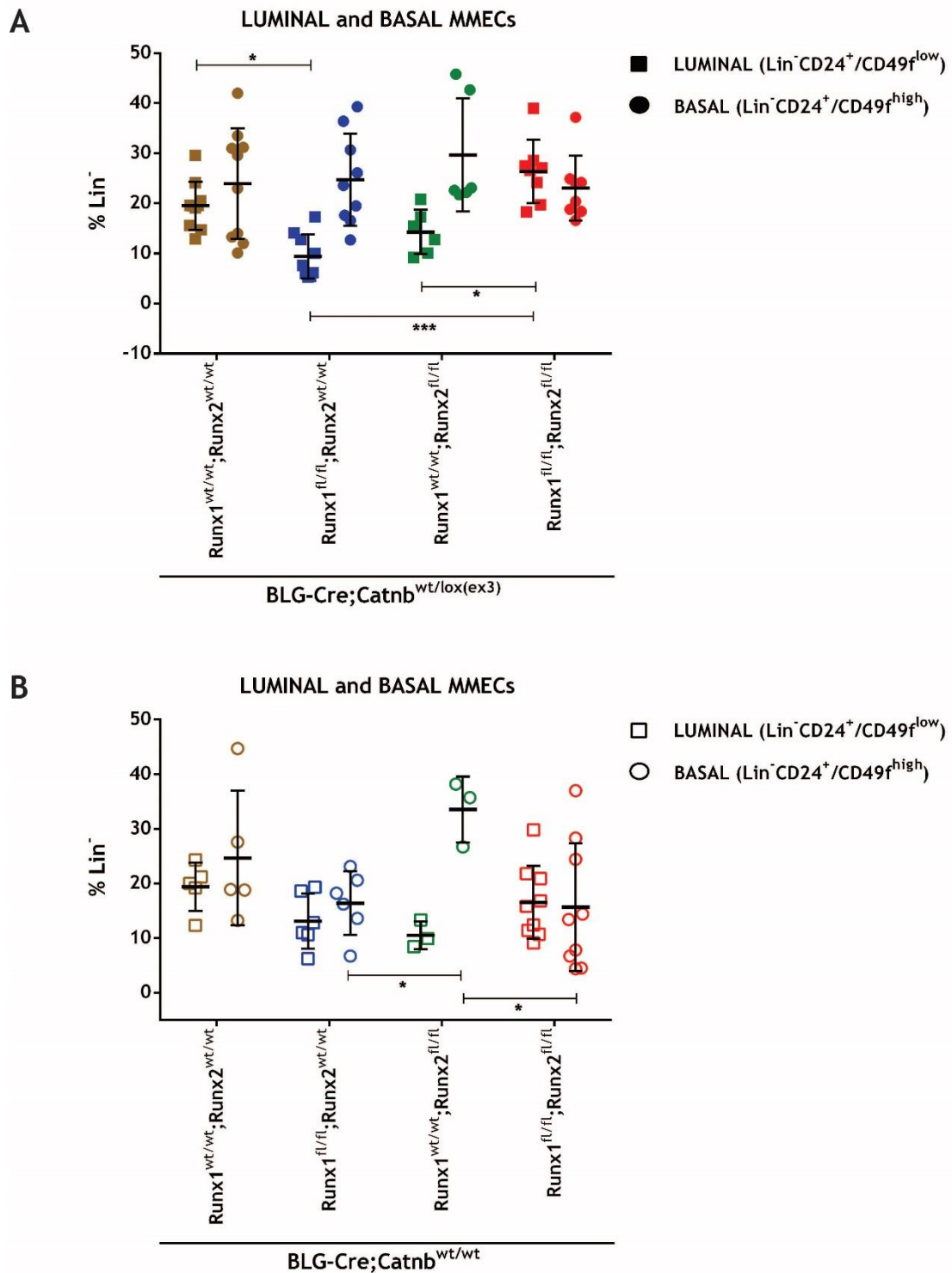


Figure 6. 8 Effects of *Runx1* and *Runx2* deletion on luminal and basal mammary epithelial cells in a Wnt/ β -catenin activated and wild type setting.

Scatter dot plots of luminal and basal MMECs from (A) *BLG-Cre;Catnb^{wt/lox(ex3)}* and (B) *BLG-Cre;Catnb^{wt/wt}* mice, upon deletion of *Runx1* (*Runx1^{fl/fl};Runx2^{wt/wt}*), *Runx2* (*Runx1^{wt/wt};Runx2^{fl/fl}*) or both genes (*Runx1^{fl/fl};Runx2^{fl/fl}*). Cells were extracted from all five pairs of mammary glands of 7 to 8 weeks old female mice and are expressed as a percentage of total Lin⁻ cells. Error bars represent mean with SD (n \geq 3 for each cohort). Statistical analysis was performed by the two-way ANOVA with the Tukey's multiple comparisons test in GraphPad Prism. **P*<0.05, *** *P*<0.001. Lin⁻, lineage negative; MMEC, mouse mammary epithelial cell.

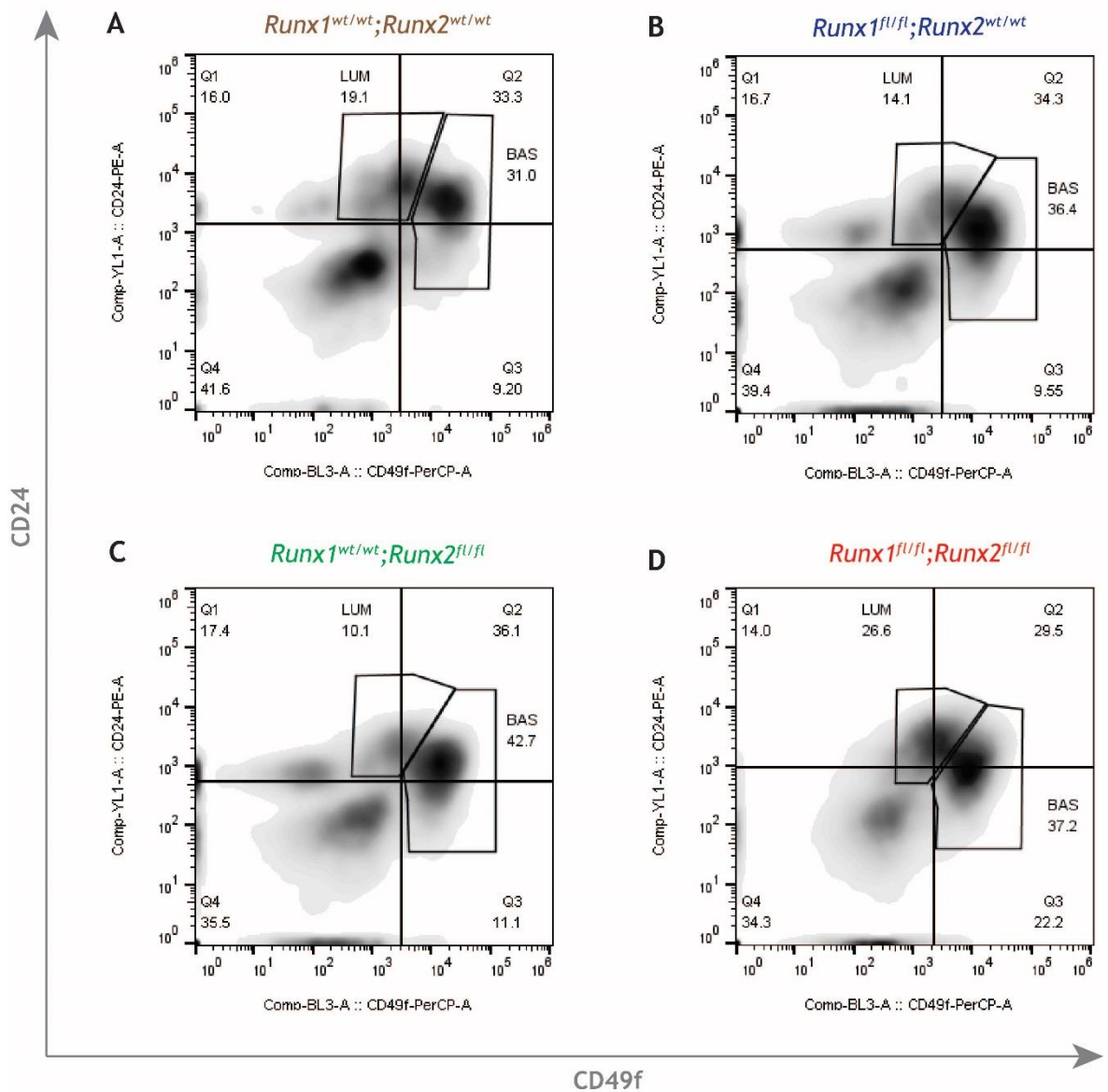


Figure 6. 9 Expression profiles of luminal and basal mammary epithelial cells upon deletion of *Runx1* and *Runx2* in a *Wnt*/ β -catenin activated mutant background.

Representative density plots showing the distribution of the luminal (LUM) and basal (BAS) subpopulations of MMECs extracted from *BLG-Cre;Catnb^{wt/lox(ex3)}* mice (A), upon deletion of *Runx1* (*Runx1^{fl/fl};Runx2^{wt/wt}*) (B), *Runx2* (*Runx1^{wt/wt};Runx2^{fl/fl}*) (C), or both genes (*Runx1^{fl/fl};Runx2^{fl/fl}*) (D). Five pairs of mammary glands, extracted from 7 to 8 week old females, were mechanically chopped and enzymatically digested to obtain a single cell suspension. This was labelled with a panel of fluorochrome-conjugated antibodies in order to enrich for MMECs. Luminal and basal cells were resolved with the combinatorial use of the CD24 and CD49f cell surface markers and expressed as a percentage of total Lin⁻ cells. Luminal cells are enriched in the Lin⁻CD24⁺CD49f^{low} subset, whilst basal cells are enriched in the Lin⁻CD24⁺CD49f^{high} one. One representative graph of n \geq 6 is shown per genotype. BAS, basal; Lin⁻, lineage negative; LUM, luminal; MMEC, mouse mammary epithelial cell.

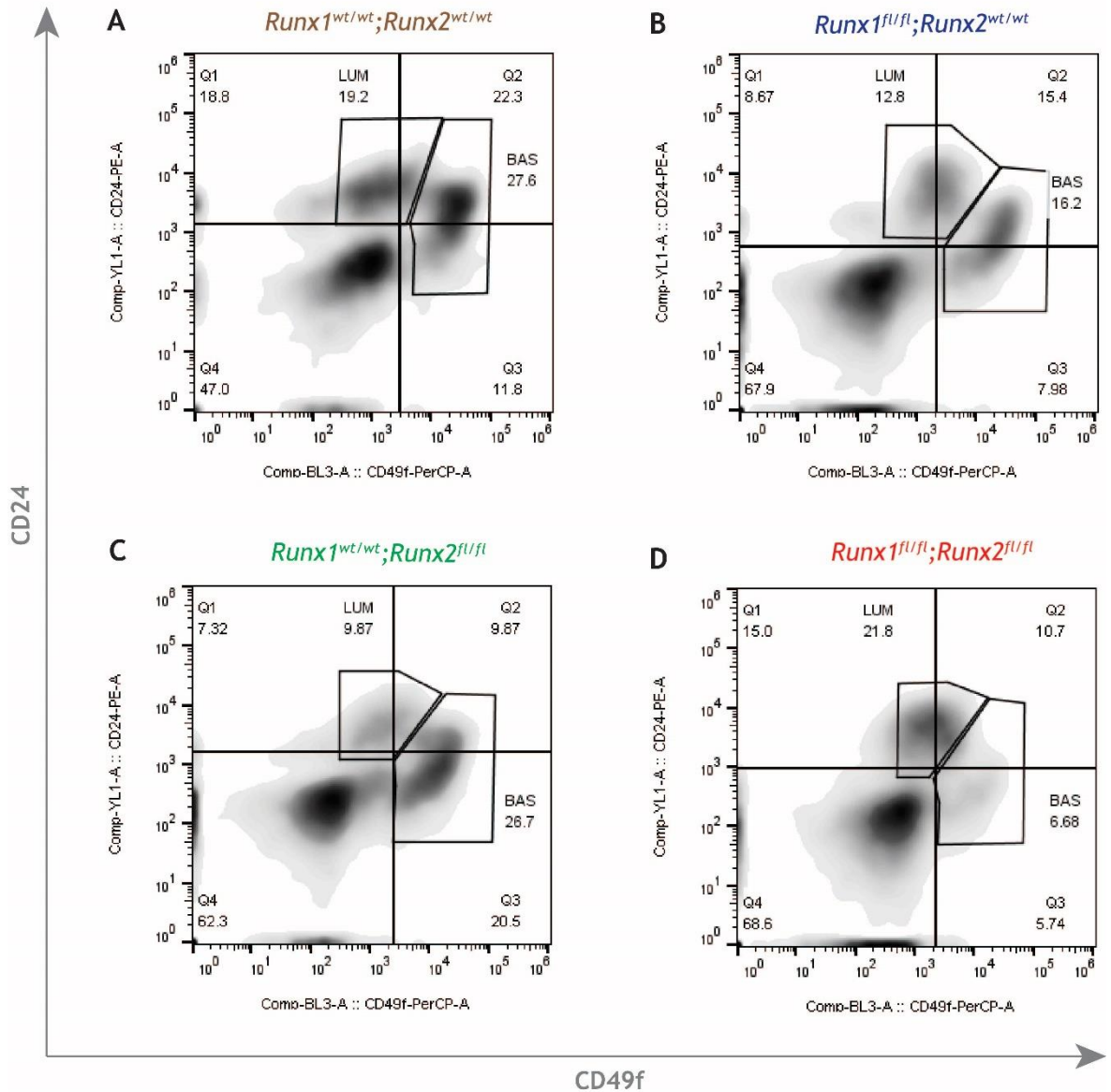


Figure 6. 10 Expression profiles of luminal and basal mammary epithelial cells upon deletion of *Runx1* and *Runx2* in a *Wnt*/ β -catenin wild type background.

Representative density plots showing the distribution of the luminal (LUM) and basal (BAS) subpopulations of MMECs extracted from *BLG-Cre;Catnb*^{wt/wt} mice (A), upon deletion of *Runx1* (*Runx1*^{fl/fl};*Runx2*^{wt/wt}) (B), *Runx2* (*Runx1*^{wt/wt};*Runx2*^{fl/fl}) (C), or both genes (*Runx1*^{fl/fl};*Runx2*^{fl/fl}) (D). Five pair of mammary glands, extracted from 7 to 8 week old females, were mechanically chopped and enzymatically digested to obtain a single cell suspension. This was labelled with a panel of fluorochrome-conjugated antibodies in order to enrich for MMECs. Luminal and basal cells were resolved with the combinatorial use of the CD24 and CD49f cell surface markers and expressed as a percentage of total Lin⁻ cells. Luminal cells are enriched in the Lin⁻CD24⁺CD49f^{low} subset, whilst basal cells are enriched in the Lin⁻CD24⁺CD49f^{high} one. One representative graph of n \geq 3 is shown per genotype. BAS, basal; Lin⁻, lineage negative; LUM, luminal; MMEC, mouse mammary epithelial cell.

6.3.3.3 Sca-1 expression in the luminal compartment

The decrease of luminal MMECs displayed by *Runx1^{fl/fl}* or *Runx2^{fl/fl}* mice, whilst its rescue seen in the *Runx1^{fl/fl};Runx2^{fl/fl}* cohort, unleashed the question as to whether deletion of one or both genes had a preferential effect on specific subsets of luminal cells. As mentioned in Chapter 1, the luminal compartment of the mammary gland is characterized by a high degree of heterogeneity, being composed of different types of LPs and differentiated MMECs, including ER⁺/PR⁺ (sensor) and ER⁻/PR⁻ (effector) cells of the ductal and alveolar subtypes, respectively (Clarke et al., 1997). In an attempt to capture such variability, different cell surface markers have been employed over time, one of them being Sca-1. Early studies looking at Sca-1 expression in the mammary gland found positive cells mainly scattered in the luminal epithelium, being more expressed in TEBs as opposed to terminal ducts (Welm et al., 2002). Long-term labelling experiments also showed that Sca-1⁺ MMECs contained a slow cycling population and displayed a higher outgrowth potential compared to the negative counterpart upon transplants. Thus, Sca-1 was proposed as a marker to enrich for a quiescent population of stem/progenitors thought to reside in the luminal epithelium (Welm et al., 2002). However, as transplant experiments were performed on total Sca-1⁺ and Sca-1⁻ MMECs without prior sorting for the luminal or basal subpopulations, proper identification of Sca-1⁺ cells was hampered. Furthermore, although Sca-1-enriched MMECs showed an increased ability to generate an outgrowth in cleared fat pads, their self-renewal potential was not tested in subsequent transplants. Lastly, Sca-1 expression in the mammary gland was assessed without the use of any markers for the basal or luminal lineage, thus hindering the exact location of Sca-1⁺ cells. According to later studies, Sca-1 expression was found to be restricted to a specific subset of luminal cells displaying high levels of hormone-related genes (e.g. *Esr-1*, *Pr*, *Prlr*), thus being recognized as a marker for ER α + LPs and mature cells (Sleeman et al., 2007; Shehata et al., 2012). When the proportion of Sca-1⁺ and Sca-1⁻ luminal cells was examined, no significant differences were found among all *BLG-Cre;Catnb^{wt/lox(ex3)}* cohorts of mice (Figure 6. 11A). What emerged, instead, was a significant increase of Sca-1⁺ luminal cells showed by *Runx1^{fl/fl}* mice in respect to *BLG-Cre;Catnb^{wt/wt}* controls (Figure 6. 11B). Interestingly, very preliminary data revealed an opposite trend for *Runx2*, whereby deletion of the gene would result in a decrease of Sca-1⁺ cells. However, extremely caution is noted as this

result is only based on one mouse. On the other hand, combined loss of both genes appeared to rescue the phenotype of both *Runx1^{fl/fl}* and *Runx2^{fl/fl}* mice to the levels of controls (Figure 6. 11B).

6.3.3.4 Sca-1 expression in the basal compartment

When the basal subset of MMECs was analysed for Sca-1 expression, results showed a significant increase in the percentage of Sca-1⁺ cells in the *Runx1^{fl/fl};Runx2^{fl/fl}* cohort of *BLG-Cre;Catnb^{wt/lox(ex3)}* mice as compared to controls (Figure 6. 12 and Figure 6. 13). In addition, when all groups of animals were compared with each other, such increase resulted to be significant even in relation to both *Runx1^{fl/fl}* and *Runx2^{fl/fl}* mice (data not shown). Instead, no differences were found among the corresponding cohorts of *BLG-Cre;Catnb^{wt/wt}* mice, wherein the proportion of Sca-1⁻ cells always exceeded the positive counterpart (Figure 6. 12B). If the role played by Sca-1 in the luminal epithelium has been better elucidated, the picture does not seem to be so clear for the basal compartment of the mammary gland. As discussed in the introduction, cumulative evidences have argued against the regenerative potential displayed by Sca-1⁺ basal cells, claiming that the marker cannot be used to enrich for MaSCs (Shackleton et al., 2006; Stingl et al., 2006). Albeit in agreement with the latter, Dall et al. (2017) have recently found the Lin⁻CD24⁺CD49f^{high}Sca-1⁺ subset of cells particularly abundant in young mice as compared to old mice. In the former, Sca-1⁺ basal cells were shown to be an actively cycling population, mainly located in TEBs versus terminal ducts, and displaying both basal as well as luminal markers (e.g. ERα and PR). Thus, it was hypothesized that Sca-1⁺ basal cells may represent a subset of hormone-responsive pubertal MaSCs, particularly committed to ductal morphogenesis. Their decrease occurring with age could be indicative of a negative regulation exerted by E2, whereby the hormone might prompt CD24⁺CD49f^{high}Sca-1⁺ cells proliferation, as well as differentiation into the negative subset. In view of their hormone responsiveness and the carcinogen sensitivity shown by TEBs (Russo et al., 1983), Sca-1⁺ basal cells might represent a transient, yet vulnerable target for oncogenic transformation (Dall et al., 2017).

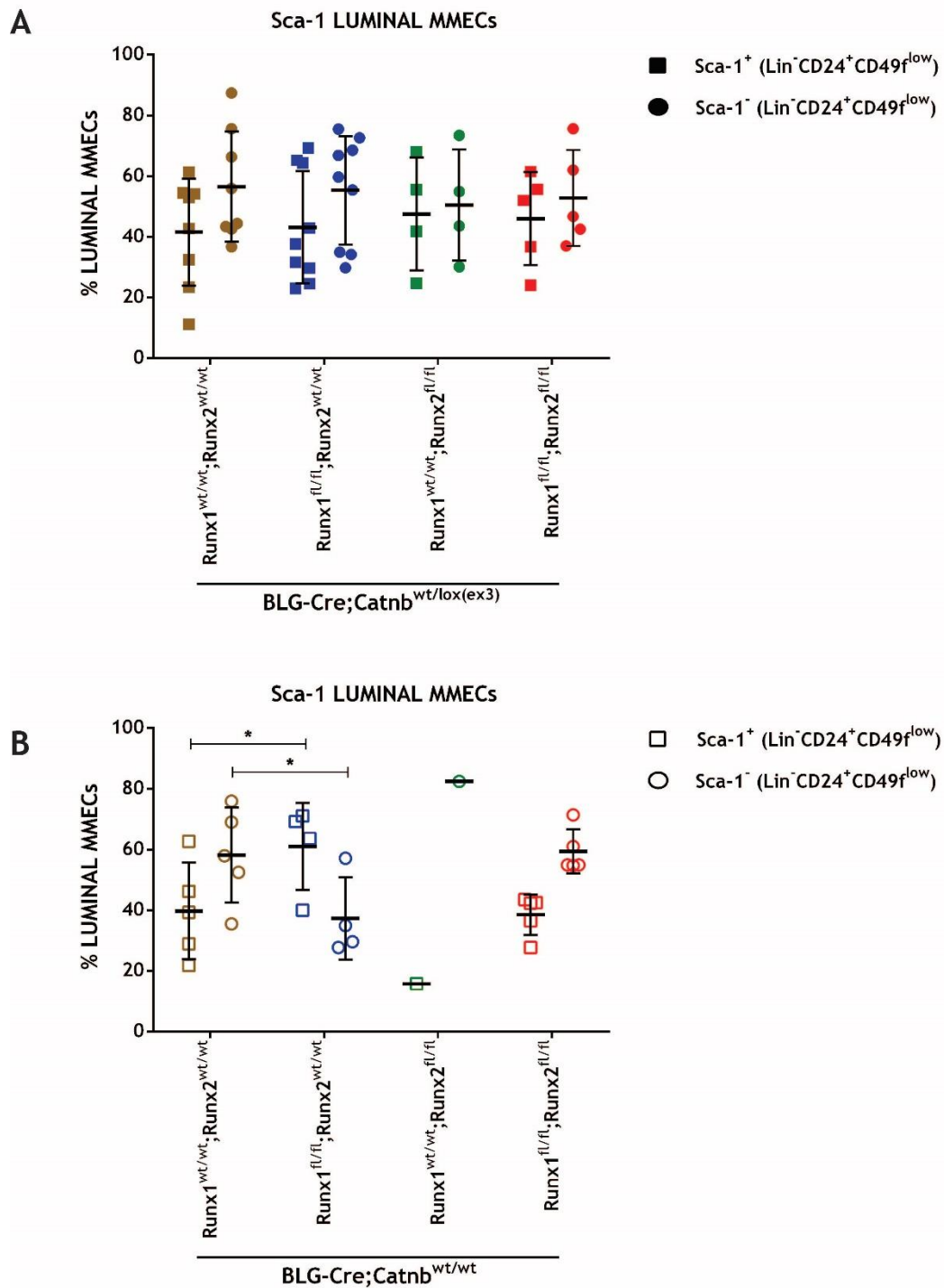


Figure 6. 11 Effects of *Runx1* and *Runx2* deletion on the expression profile of Sca-1 luminal mammary cells in a Wnt/ β -catenin activated mutant and wild type setting.

Scatter dot plots of Sca-1⁺ and Sca-1⁻ luminal MMECs from *BLG-Cre;Catnb*^{wt/lox(ex3)} (A) and *BLG-Cre;Catnb*^{wt/wt} (B) mice, upon deletion of *Runx1* (*Runx1*^{fl/fl};*Runx2*^{wt/wt}), *Runx2* (*Runx1*^{wt/wt};*Runx2*^{fl/fl}) or both genes (*Runx1*^{fl/fl};*Runx2*^{fl/fl}). Cells were extracted from mammary glands of 7 to 8 week old female mice, resolved with the combinatorial use of CD24 and CD49f and expressed as a percentage of total luminal (Lin⁻CD24⁺CD49f^{low}) MMECs. Error bars represent mean with SD (n \geq 4 for each cohort, but for the *Runx2*^{fl/fl} group of *BLG-Cre;Catnb*^{wt/wt} mice with n=1). Statistical analysis was performed by the two-way ANOVA with the Dunnett's multiple comparisons test in GraphPad Prism. *P<0.05. MMEC, mouse mammary epithelial cells.

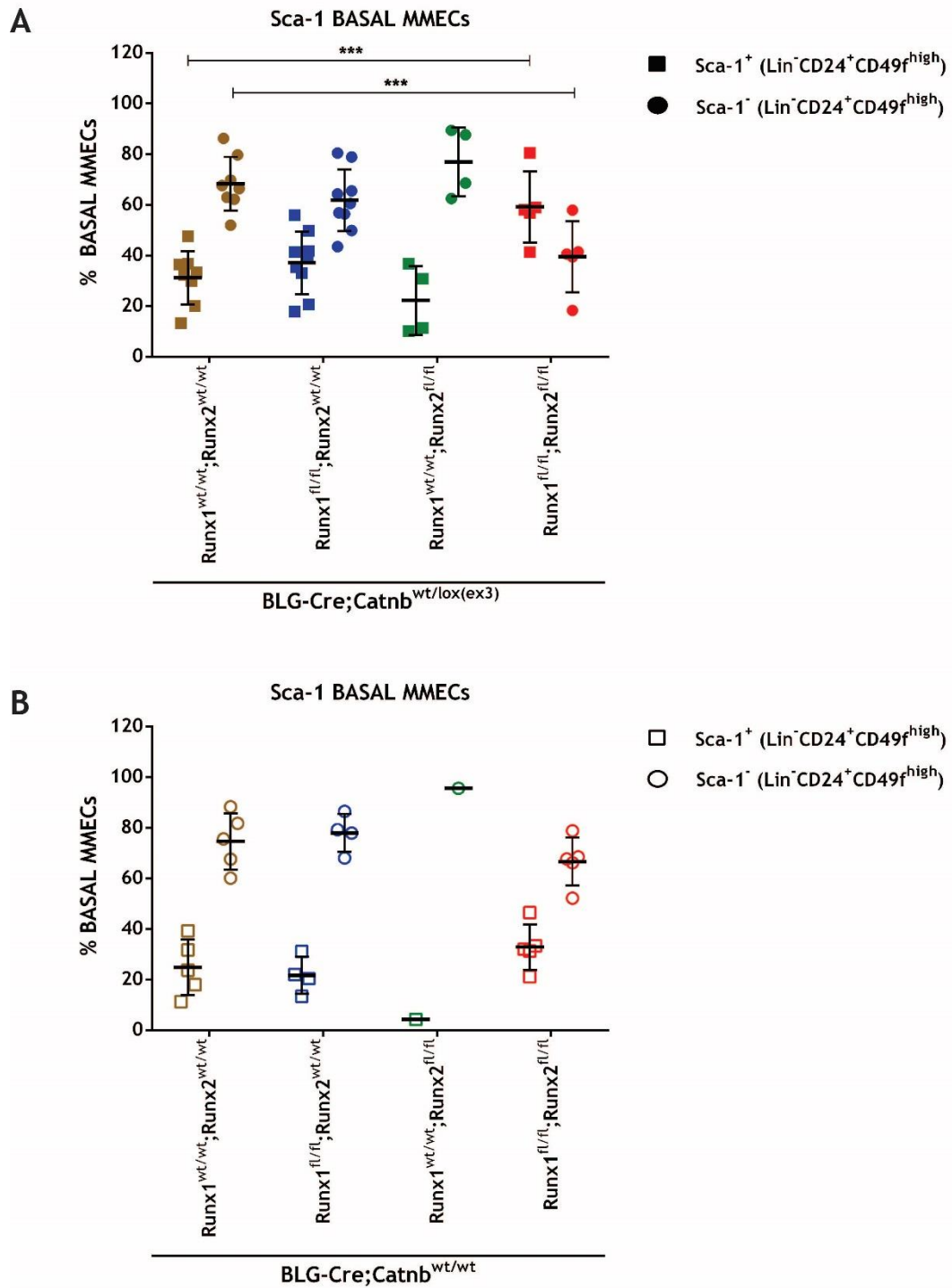


Figure 6. 12 Effects of *Runx1* and *Runx2* deletion on the expression profile of Sca-1 basal mammary cells in a Wnt/ β -catenin activated mutant and wild type setting.

Scatter dot plots of Sca-1⁺ and Sca-1⁻ basal MMECs from *BLG-Cre;Catnb*^{wt/lox(ex3)} (A) and *BLG-Cre;Catnb*^{w/wt} (B) mice, upon deletion of *Runx1* (*Runx1*^{fl/fl};*Runx2*^{wt/wt}), *Runx2* (*Runx1*^{wt/wt};*Runx2*^{fl/fl}) or both genes (*Runx1*^{fl/fl};*Runx2*^{fl/fl}). Cells were extracted from mammary glands of 7 to 8 week old female mice, resolved with the combinatorial use of CD24 and CD49f and expressed as a percentage of total luminal (Lin⁻CD24⁺CD49f^{high}) MMECs. Error bars represent mean with SD (n≥4 for each cohort, but for *BLG-Cre;Catnb*^{w/wt};*Runx2*^{fl/fl} mice with n=1). Statistical analysis was performed by the two-way ANOVA with the Dunnett's multiple comparisons test in GraphPad Prism. *P<0.05. MMEC, mouse mammary epithelial cells.

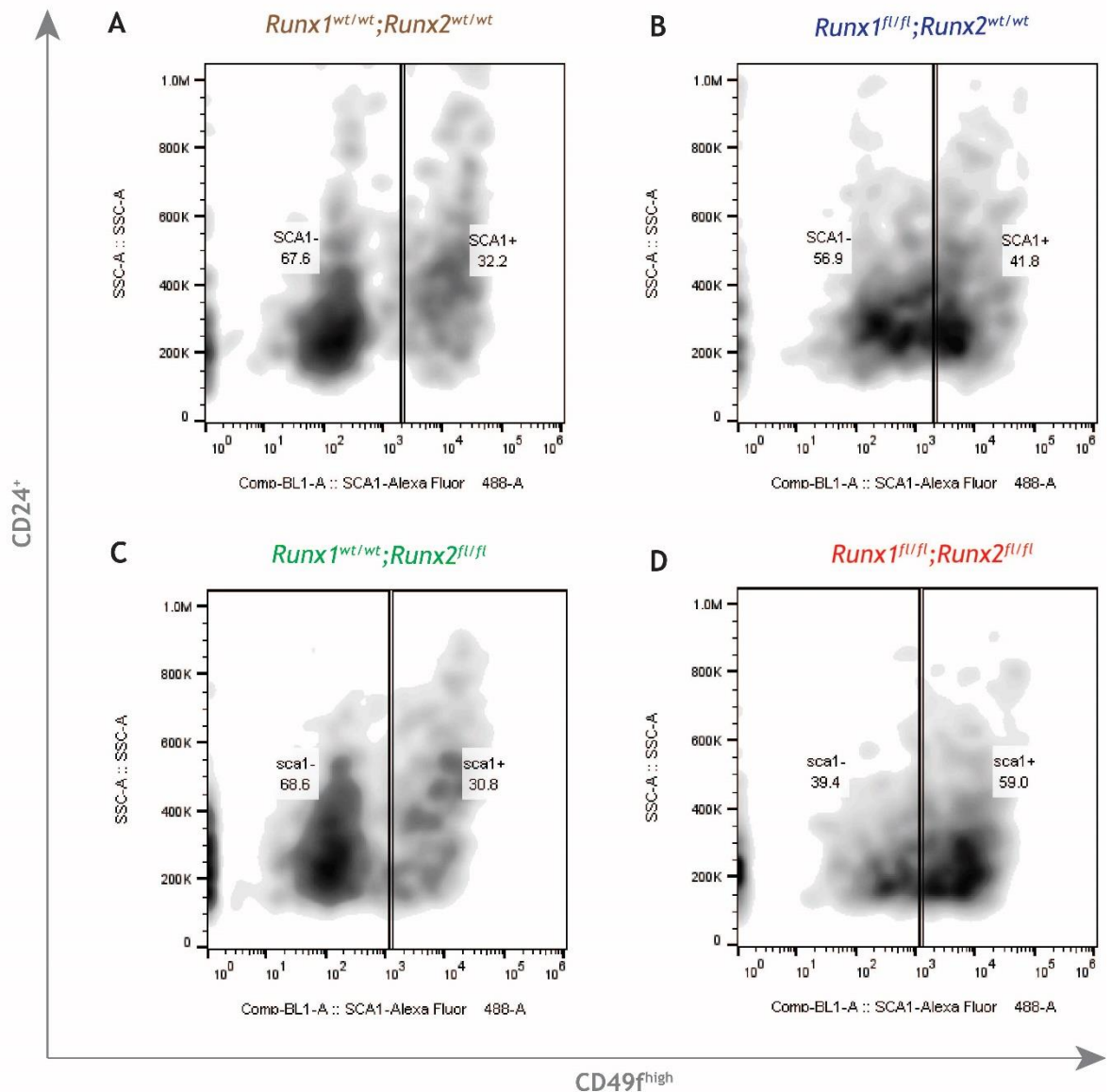


Figure 6. 13 Sca-1 expression profile of basal mouse mammary epithelial cells upon loss of *Runx1* and *Runx2* deletion in a *Wnt/β-catenin* activated background.

Representative density plots showing the distribution of Sca-1⁺ and Sca-1⁻ basal MMEC from *BLG-Cre;Catnb*^{wt/lox(ex3)} mice (A), upon deletion of *Runx1* (*Runx1*^{fl/fl}; *Runx2*^{wt/wt}) (B), *Runx2* (*Runx1*^{wt/wt}; *Runx2*^{fl/fl}) (C), or both genes (*Runx1*^{fl/fl}; *Runx2*^{fl/fl}) (D). Mammary glands, extracted from 7 to 8 week old females, were mechanically chopped and enzymatically digested to obtain a single cell suspension. This was labelled with a panel of fluorochrome-based antibodies in order to enrich for MMECs. Basal cells were resolved with the combinatorial use of the CD24 and CD49f cell surface markers and found to be enriched in the Lin⁻CD24⁺CD49f^{high} subset. Sca-1⁺ and Sca-1⁻ basal cells are expressed as a percentage of total basal (Lin⁻CD24⁺CD49f^{high}) MMECs. One representative graph of n≥4 is shown per genotype. MMEC, mouse mammary epithelial cell; Lin⁻, lineage negative.

6.4 Discussion

As mentioned in Chapter 1, the results obtained with transplantation studies have revealed the existence of a “*growth-regulating system*” within the mammary gland (Faulkin et al., 1960). This has been ascribed to the presence and peculiar properties owned by MaSCs, able to govern both mammary pubertal development and homeostasis during adulthood through the formation of a highly organized hierarchical structure of cells. Of note, “*the ability to override this growth-regulating system appears to be the principal characteristic of neoplastic tissue*” (Faulkin et al., 1960). In this regard, the presence of overtly disrupted mammary tissues upon activation of the Wnt/ β -catenin pathway in the absence of *Runx1* and *Runx2* leads to the hypothesis that this dysregulation might originate from changes affecting the mammary epithelial cell hierarchy. However, in view of the high degree of cellular heterogeneity characterizing the latter (see Chapter 1), this is not an inconsequential premise to dissect. As such, it was reckoned that only through the combinatorial use of multiple techniques it would have been possible to characterize the functional and phenotypic characteristics displayed by Wnt/ β -catenin-activated MMECs in the context of *Runx* genes deletion. To begin, as the significant acceleration of tumourigenesis and high penetrance of tumour burden displayed by *BLG-Cre;Catnb^{wt/lox(ex3)};Runx1^{fl/fl};Runx2^{fl/fl}* mice (observed in Chapter 4) hinted at the presence of an altered stem/progenitor subpopulation, the tumoursphere and CFC assays were employed.

Correct interpretation of the sphere assay has so far been hindered by the presence of confounding results reported by the literature. One of the main arguments concerns the rapidity of sphere formation, which could not be inferred solely to the clonal expansion of MaSCs. As such, spheres would rather appear to be formed by a mixture of stem and progenitor (or transient amplifying) cells (Clarke et al., 2006). If that holds true, sphere formation could be considered the result of a combination of both SCD and ACD. In addition, whilst the size of spheres would be an indirect measure of the proliferative ability of stem/progenitor cells (via ACD and SCD), the number of secondary spheres would mainly reflect MaSCs’ self-renewal potential. In this regards, the bigger size of primary and secondary spheres shown by *Runx2^{fl/fl}*-derived MMECs

of the *BLG-Cre;Catnb^{wt/lox(ex3)}* cohort might be indicative of an increased proliferative ability owned by stem/progenitor cells in the absence of the gene. Nonetheless, with concomitant loss of *Runx1*, *Runx2*-deficient MMECs appeared to give rise to fewer and smaller spheres, with reduced self-renewal potential. It should be noted, however, that at the 7 to 8 week developmental time-point, both control and single knock-out *Runx1^{fl/fl}* and *Runx2^{fl/fl}* cohorts of *BLG-Cre;Catnb^{wt/lox(ex3)}* mice displayed a higher percentage of normal epithelium, in contrast to *Runx1^{fl/fl};Runx2^{fl/fl}* animals, characterized by a higher amount of abnormal epithelium (see Chapter 5). Therefore, only results obtained from the latter cohort of mice could be more confidently ascribed to the predominant presence of Wnt/ β -catenin transformed MMECs, and not to remaining normal MMECs. If that is the case, then BLG-Cre driven constitutive activation of the Wnt/ β -catenin signalling pathway is able to reduce the proliferative and self-renewal potential of stem/progenitor cells in the absence of both *Runx1* and *Runx2*. But if this hypothesis holds true, how can the enlarged mammary structure displayed by *Runx1^{fl/fl};Runx2^{fl/fl}* whole-mounts be explained? Perhaps by envisioning a Wnt/ β -catenin-driven switch from ACD to SCD which might foster the expansion of slow-cycling cells. The reduced self-renewal potential shown by secondary tumourspheres might in turn arise from the sudden terminal differentiation route taken by the latter population. Whilst the previously discussed use of the transplantation technique was employed in the attempt to test this hypothesis (see Chapter 4), this has only been carried out with primary transplants to date and requires serial passaging of MDTFs *in vivo*. Through backcrossing of the *BLG-Cre;Catnb^{wt/lox(ex3)}* line in a pure FVB background, it will be possible to explore the *in vivo* regenerative potential of Wnt/ β -catenin-activated *Runx1^{fl/fl};Runx2^{fl/fl}*-deficient mammary lesions upon serial transplantations. In addition, considering the precocious transformation of the mammary epithelium, it would be worthwhile applying the same experimental pipeline to pre-neoplastic MMECs extracted from all virgin cohorts of *BLG-Cre;Catnb^{wt/lox(ex3)}* mice.

If the different types of discrete colonies formed by MMECs when challenged in CFC assays can be truly ascribed to the presence of specific subpopulations of stem/progenitor cells, then activation of the Wnt/ β -catenin signalling pathway upon loss of *Runx1* might favour the expansion of a transformed subset of cells

lying within the basal lineage. Importantly, this phenotype appears to be independent of the *Runx2* status carried by *Runx1*-deficient MMECs, as a predominance of solid colonies was also observed in the *Runx1^{fl/fl};Runx2^{fl/fl}* cohort of *BLG-Cre;Catnb^{wt/lox(ex3)}* mice. In agreement with the notion that ‘*all pathological changes are merely physiological modified ones*’ (Beatson, 1896), preliminary results showed that extraction of MMECs from *BLG-Cre;Catnb^{wt/wt}* cohorts of mice also led to a higher predominance of solid colonies upon loss of *Runx1* or combined deletion of *Runx1* and *Runx2*. On the contrary, *Runx2*-deficient and control-derived MMECs displayed a ratio equal to one, indicating the absence of any preferential addiction towards basal or acinar colony formation (data not shown). These pieces of evidence suggest a different role played by RUNX1 and RUNX2 in regulating mammary epithelial cell fates. In view of the role shown by progesterone in driving the expansion of MaSCs (Joshi et al., 2010), it was surprising not to find a correlation between the oestrous cycle of the animals and the type of morphological colonies generated by matrigel-embedded MMECs. Three main hypotheses have been put forward to explain this discrepancy. Firstly, in view of the changes in oestrous cycle dynamics displayed by different strains of mice (Barkley and Bradford, 1981), the lack of correlation might stem from the fact that both cohorts of *BLG-Cre;Catnb^{wt/lox(ex3)}* and *BLG-Cre;Catnb^{wt/wt}* mice are on a mixed background. Secondly, it might be that mammary-specific activation of the Wnt/ β -catenin signalling pathway can override the effects that ovarian hormones have on the mammary epithelial cell hierarchy. However, the fact that no correlation was found among all groups of *BLG-Cre;Catnb^{wt/wt}* mice would argue against this hypothesis. Thirdly, the peak of progesterone at each diestrus cycle might indeed favour the expansion of a Wnt/ β -catenin-activated subset of basal stem/progenitor cells, which could then expand upon loss of *Runx1* and persist across all stages of the oestrous cycle.

Whilst hinting towards the basal compartment as the putative primary source of the aberrant mammary structures displayed by Wnt/ β -catenin-activated *Runx1*-deficient mice, these *ex vivo* assays could not explain the different timeframes of palpable tumour formation and overall survival displayed by *Runx1^{fl/fl}* and *Runx1^{fl/fl};Runx2^{fl/fl}* mice. Thus, to gain a better insight into how deletion of *Runx1* or combined excision of both *Runx1* and *Runx2* could differently affect Wnt/ β -catenin-driven tumourigenesis, the phenotypic profile of extracted

MMECs was assessed. What emerged from the analysis was a significant decrease of epithelial cells displayed by *Runx1^{fl/fl}* mice, which might stem from a reduction of the luminal rather than the basal compartment. Importantly, whilst no similar observations could be found upon combined loss of *Runx1* and *Runx2*, a significant increase of Sca-1⁺ basal cells seemed to exclusively characterize the *Runx1^{fl/fl};Runx2^{fl/fl}* cohort of mice as compared to all other *BLG-Cre;Catnb^{wt/lox(ex3)}* groups. In view of its high abundance in young mice and its preferential location in TEBs (Dall et al., 2017), it is tempting to speculate that the Lin⁻CD24⁺CD49f^{high}Sca-1⁺ subset might represent the “cell-of-origin” of BLG-Cre mediated Wnt/ β -catenin driven breast tumourigenesis (Figure 6. 14). Proposed as a hormone-responsive MaSC subpopulation particularly devoted to ductal morphogenesis (Dall et al., 2017), it could be assumed that the physiological role of the Lin⁻CD24⁺CD49f^{high}Sca-1⁺ subset would be to feed into both the basal and luminal layers of incipient pubertal ducts. Thus, one could envision the possibility of a Wnt/ β -catenin driven *Runx1*- and *Runx2*-deficient subpopulation of Sca-1⁺ basal cells, entering the cell cycle in response to E2, expanding abnormally within TEBs and disseminating its pre-neoplastic progeny along subtending ducts (Figure 6. 14). In this regards, the absence of a similar increase in *Runx1^{fl/fl}* mice might be indicative of either a decreased survival capability of Sca-1⁺ basal cells in the absence of the gene or the presence of a compensatory tumour suppressive mechanism, perhaps exerted by RUNX2. This could explain why there is a delay in ductal elongation and the presence of fewer epithelia in 6 week whole-mounts, but also a partial disappearance of pre-neoplastic lesions in 9 week old *Runx1^{fl/fl}* mice. What needs to be addressed next is how deletion of *Runx1*, *Runx2* or both genes, impinges on the tumourigenic potential of Wnt/ β -catenin-activated Sca-1⁺ basal cells. One way to test this hypothesis would be to isolate the cells via FACS and carry out a thorough molecular and functional characterization of the population. If an active Wnt/ β -catenin signalling pathway and deletion of *Runx* can be validates in these Sca-1⁺ cells, these could then be challenged in serial transplantation assays.

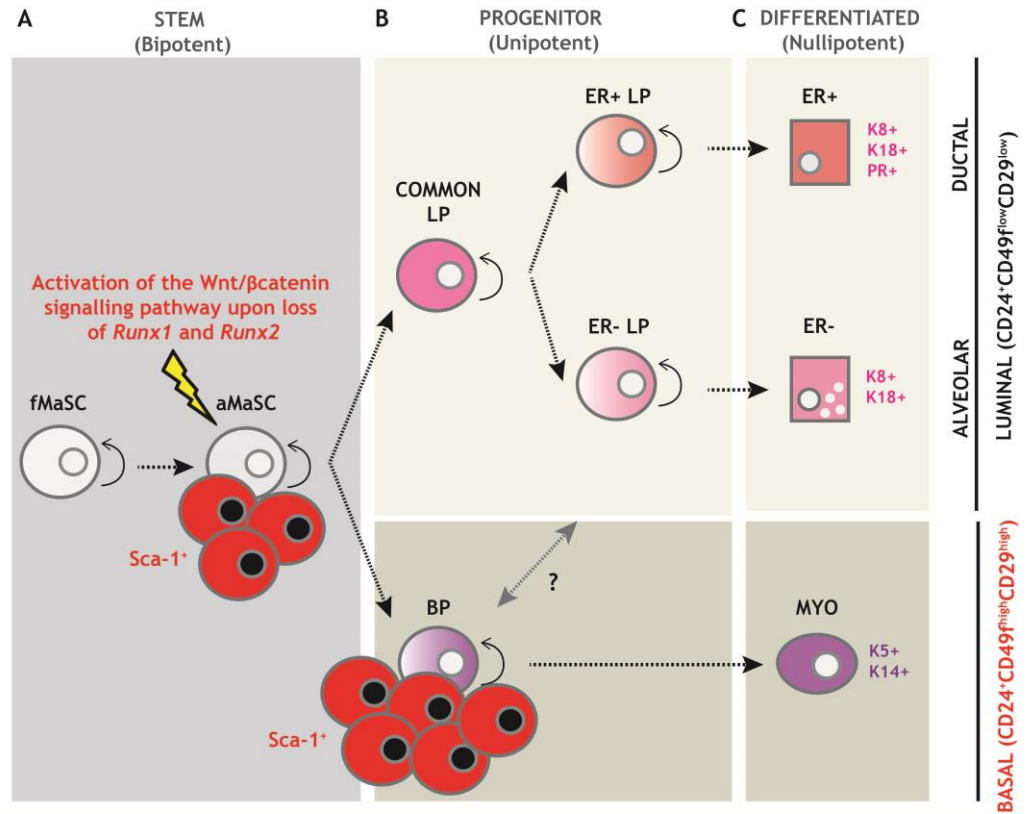


Figure 6. 14 Working model.

Schematic diagram illustrating the putative “cell-of-origin” of BLG-Cre driven Wnt/ β catenin mammary tumours upon combinatorial loss of *Runx1* and *Runx2*. Deletion of both genes may favour the abnormal expansion of a stem/progenitor subpopulation of Sca-1⁺ cells residing in the basal layer of the mammary gland. Particularly abundant in terminal end buds, Sca-1⁺ basal cells are believed to drive the ductal elongation of the epithelial tree upon release of hormonal cues occurring at the onset of puberty. An abnormal expansion and increased survival of this peculiar subpopulation may negatively impact on the highly organized structure of the mammary epithelial cell hierarchy, eventually resulting in the formation of Wnt/ β catenin mammary lesions.

Interestingly, a trend towards decreased epithelium characterizing *Runx1^{fl/fl}* mice was also observed on a Wnt/ β -catenin wild type background in relation to *Runx1^{wt/wt}* animals (29% and 45%, respectively) (Table 6. 1). This time, however, the reduction appeared to stem from a lower percentage displayed by both luminal (13%) and basal cells (16%) in respect to controls (19% and 26%, respectively). Differently, BLG-Cre mediated deletion of *Runx2* appeared to cause a reduction of the luminal subpopulation (10%), yet an increase of the basal one (33%) compared to controls. Combined deletion of both genes was instead able to partly restore both the luminal (16%) and basal (16%) subpopulations (Table 6. 1). These results are indicative of a context-dependent interplay between RUNX1 and RUNX2, which might exert similar effects within the luminal compartment, while opposite functions in the basal one. In regards to the luminal compartment, three different scenarios might be proposed. According to the first one, RUNX1 and RUNX2 might have tumour suppressive effects. As such, deletion of *Runx1* or *Runx2* would result in a decreased luminal population in view of the suppressive function of the remaining gene, whereas deletion of both genes would rescue the phenotype. What remains puzzling, however, is how the presence or absence of both *Runx1* and *Runx2* leads to a similar percentage of luminal cells. Perhaps, one could presume that in a physiological context RUNX1 and RUNX2 would be responsible for keeping the luminal population under control (making sure the percentage does not go over 19%), whereas in their absence compensatory mechanism would take their place to avoid any increase of luminal cells. According to the second scenario, both RUNX1 and RUNX2 might have promoting effects. This would explain why deletion of *Runx1* or *Runx2* causes a decrease of the luminal population, although it does not justify how the absence of both genes restores the luminal subset to the level of control mice. Furthermore, this hypothesis would not take into account the possibility of the remaining gene to compensate for the missing one. According to the third one, the genes might have dualist effect exerted on different subsets of luminal cells. In support of the latter, several lines of evidence have suggested a role for RUNX1 as a master regulator of luminal cell fate decisions, by promoting the ER program whilst inhibiting the alveolar one (van Bragt et al., 2014). In addition, as corroborated by the reduction of ER+ cells upon MMTV-Cre mediated excision of *Runx1*, the gene appears to be required for the survival of the latter population. Nonetheless, results obtained

from the BLG-Cre driven mouse model led to opposite findings, as deletion of the gene resulted in a significant increase of Sca-1⁺ (ER⁺) luminal cells. Interestingly, deletion of *Runx2* had the opposite effect, whereas the absence of both genes restored the Sca-1⁺ subset to the levels of control mice. This result is of particular interest in view of the previously discussed tumour suppressive role played by RUNX1 in ER⁺ cells (see Chapter 1). As such, it could be envisioned that, whilst loss of *Runx1* leads to a moderate decrease of the luminal compartment, the latter experiences an increase of ER+Sca-1⁺ and decrease of ER-Sca-1⁻ cells. In view of the fundamental role exerted by hormonal paracrine circuits between ER+Sca-1⁺ (sensor) and ER-Sca-1⁻ (effector) cells, it would be interesting to see if upon loss of *Runx1*, ER+Sca-1⁺ sensor cells might expand, whilst losing their ability to “feed” the effector cellular counterpart through release of paracrine molecules. Although expression of both genes does not appear to be very high in extracted luminal cells as compared to basal MMECs (McDonald et al., 2014; van Bragt et al., 2014), this data is indicative of an important role played by RUNX1 and RUNX2 in the luminal layer of the mammary gland. Nonetheless, owing to the heterogeneity of the luminal lineage, it would be necessary to dissect the specific function played by each gene by characterizing their expression in different luminal subpopulations, including ER⁺ and ER⁻ cells. This, for instance, could be achieved by performing co-immunofluorescence for ER and RUNX1 or RUNX2 or by isolating different subsets of luminal cells by FACS. A different, yet more straightforward, scenario might hold true for the basal compartment, wherein both *Runx1* and *Runx2* appear to be more expressed (McDonald et al., 2014; van Bragt et al., 2014). Within the latter, RUNX1 seems to exert a positive effect (as its deletion leads to a decrease of basal cells), whereas RUNX2 appears to have a negative function (since its excision yields to an expansion of the population). By counterbalancing each other, deletion of both genes results in the rescue of basal cells to the level of control mice. In line with this hypothesis, cumulative evidence has labelled RUNX1 as a master regulator of MaSCs differentiation, as its deletion was shown to block stem/progenitor cells in a bipotent/undifferentiated state susceptible to oncogenic transformation (Sokol et al., 2015). Accordingly, an increase in the basal population has been observed in the *Runx1^{fl/fl}* cohort of *BLG-Cre;Catnb^{wt/lox(ex3)}* mice, further corroborating the role of the latter compartment as the primary source of Wnt/ β -catenin transformation.

At the bottom of all the aforementioned questions lies the uncertainty of the “cell-of-origin” of Wnt/ β -catenin mammary lesions. Indeed, while trying to understand the phenotype of any conditional mouse model, it is imperative to consider not only the genetic aberrations carried by the latter, but also the driver of those recombination events (Holen et al., 2017). As mentioned in chapter 3, the novelty of the *BLG-Cre;Catnb^{wt/lox(ex3)}* breast cancer mouse model allowed the possibility to study for the first time the effects of *Runx* genes deletion in the context of activated Wnt/ β -catenin, yet also the fact that both genetic events are driven by the BLG-Cre. As for any other conditional model, if the *in vivo* phenotype is assumed to stem from a cell-autonomous effect, then one way to unveil its cell-of-origin is by guiding the expression of a reporter gene under the control of the same driver. In this regards, the absence of a reporter gene within the *BLG-Cre;Catnb^{wt/lox(ex3)}* cohorts of mice hampered the possibility to specifically ascribe the changes observed within each MMEC subpopulation to activation of Wnt/ β -catenin and deletion of *Runx1*, *Runx2* or both genes. Nonetheless, characterization of BLG-Cre expression in a Wnt/ β -catenin wild type setting was previously performed by N. Ferrari (unpublished; PhD thesis) through the use of the Z/EG (*lacZ/EGFP*) reporter line of mice (Novak et al., 2000). Due to the presence of a lox-stop-lox cassette preceding the enhanced green fluorescent protein (*EGFP*) transgene, visualization of GFP could only be observed upon Cre excision (Novak et al., 2000). When *BLG-Cre;Z/EG* mice were crossed with *Runx1^{fl/fl}*, *Runx2^{fl/fl}* and *Runx1^{fl/fl};Runx2^{fl/fl}* animals, monitoring of the GFP signal allowed to evaluate the effect of *Runx1* and/or *Runx2* deletion upon specific subpopulation of MMECs (Table 6. 1). If analysis of 12 weeks old *BLG-Cre;Z/EG* mice showed an 18% of GFP positivity in regards to total Lin⁻ cells, the signal appeared to be significantly reduced in the absence of *Runx1* (12%) or *Runx2* (11%), yet rescued upon loss of both genes (17%). In line with the literature (Selbert et al., 1998), when the percentage of GFP⁺ cells was calculated in respect to the two epithelial compartments of the mammary gland, BLG-Cre was found to be more expressed by luminal (38%) versus basal (4%) cells. Interestingly, a significant reduction in the percentage of GFP⁺ luminal MMECs was observed in both *Runx1^{fl/fl}* (26%) and *Runx2^{fl/fl}* (19%) mice, as well as in the *Runx1^{fl/fl};Runx2^{fl/fl}* cohort (21%). In regards to the basal compartment, results showed decreased positivity displayed by *Runx2^{fl/fl}* (2%) mice, versus a significant increase of GFP⁺ cells upon combined excision of

Runx1 and *Runx2* (23%), as compared to control (4%) (Table 6. 1). This analysis offered important insights in interpreting the changes of the luminal and basal MMECs subpopulations displayed by all cohorts of *BLG-Cre;Catnb^{wt/wt}* mice upon loss of the *Runx* genes. On one hand, in view of the high level of BLG-Cre expression reported in the luminal layer (38%), the results obtained from the GFP expression analysis mirrored the reduction of luminal cells seen upon deletion of *Runx1* and *Runx2*. On the other hand, considering the low levels of BLG-Cre expression present in the basal layer (4%), these data helped clarify the changes affecting the basal compartment of *Runx*-deficient *BLG-Cre;Catnb^{wt/wt}* mice. Thus, albeit *BLG-Cre;Catnb^{wt/wt}* mice showed a higher percentage of total basal cells as compared to *Runx1^{fl/fl};Runx2^{fl/fl}* mice (26% and 16%, respectively), analysis of GFP expression revealed a higher proportion of positivity within the latter group (Table 6. 1).

Table 6. 1 BLG-Cre mediated effects of *Runx1* and *Runx2* loss in the mammary epithelium.

Virgin (7-8 week)		<i>BLG-Cre;Catnb^{wt/wt}</i>			
Cohorts		<i>Runx1^{wt/wt};Runx2^{wt/wt}</i>	<i>Runx1^{fl/fl};Runx2^{wt/wt}</i>	<i>Runx1^{wt/wt};Runx2^{fl/fl}</i>	<i>Runx1^{fl/fl};Runx2^{fl/fl}</i>
%Lin ⁻	Epithelial	45	29	43	32
	Luminal	19	13	10	16
	Basal	26	16	33	16
Virgin (12 week)		<i>BLG-Cre;Z/EG</i>			
Cohorts		<i>Runx1^{wt/wt};Runx2^{wt/wt}</i>	<i>Runx1^{fl/fl};Runx2^{wt/wt}</i>	<i>Runx1^{wt/wt};Runx2^{fl/fl}</i>	<i>Runx1^{fl/fl};Runx2^{fl/fl}</i>
GFP ⁺ cells	% Lin ⁻	18	12	11	17
	% Luminal	38	26	19	21
	% Basal	4	7	2	23

Altogether these data indicate that BLG-Cre mediated deletion of both *Runx1* and *Runx2* confers basal cells a selective advantage over the wild type counterpart. As part of future directives, it will be necessary to validate these findings by crossing all *Runx*-deficient *BLG-Cre;Catnb^{wt/lox(ex3)}* cohorts with a reporter strain of mice. This will allow a thorough investigation of how deletion of the *Runx* genes impinges on the survival capability of Wnt/ β -catenin activated MMECs. Presently, it is obvious that there exists an important role played by *Runx1* and *Runx2* in the mammary epithelial cell hierarchy, wherein these genes appear to govern the intersection between fundamental cell fate decisions between the luminal and basal lineages. Thus, a deeper understanding on the function exerted by these genes is worth of further investigation.

7 Conclusions

[The following discussion has been in part adapted from Riggio and Blyth (2017)].

Cancer is a very heterogeneous disease which exploits a multitude of strategies, referred to as “hallmarks”, in order to convert a normal tissue into a malignant one (Hanahan and Weinberg, 2011). Even though these hallmarks have significantly contributed to our comprehension of the disease, cancer still remains a black box. Within the latter, breast cancer represents the leading cause of tumour-related death in women worldwide (Torre et al., 2016). The reason behind this could be ascribed to several factors, including: a family history at risk; the lifetime exposure to hormones; the reproductive path of a woman (including the decision of not having children, the trend to have late pregnancies and the low rate of breast feeding); and the adoption of bad life-style behaviours (e.g. alcohol and high-calorie food intake, tobacco, stress and long-working hours) (Eccles et al., 2013). Notwithstanding the causative role played by each factor, cancer (and therefore breast cancer) is primarily a genetic disease. However, differently from most genetic diseases, cancer is caused by somatic mutations, and not solely by germ-line mutations. In addition, whilst genetic diseases often require a single mutation to arise, cancer is the result of a “multi-hit” process, whereby different genetic alterations accumulate over time in one or a few cell(s)-of-origin (Vogelstein, 1983). Importantly, this sequence of genetic events uniquely defines the genomic landscape of each type of cancer. In regards to breast cancer, only a few ‘mountains’, that is frequently altered genes, and many more ‘hills’, that is infrequently mutated genes, were shown to characterize the genomic landscape of the disease (Wood et al., 2007). However, whilst the function of frequently mutated genes is well-documented, the identity and role played by infrequently altered genes is still elusive. Following the discovery in the last five years of *RUNX1* somatic mutations in biopsies of breast cancer patients (Banerji et al., 2012; Cancer Genome Atlas, 2012; Ellis et al., 2012), a new ‘hill’ has been finally unveiled. As the sole presence of genetic alterations is not necessarily indicative of a causative role played by a gene in the aetiology of the corresponding disease, it remained to be seen whether *RUNX1* genetic alterations were passenger or driver events in the context of breast tumourigenesis. When NGS data was coupled with structural

analysis to look at the pattern and pathogenicity of the identified mutations, the majority of *RUNX1* genetic alterations were predicted to cause *loss-of-function* of the protein (van Bragt et al., 2014) and confer a selective growth advantage to the insulted cells. In view of this, *RUNX1* was ascribed among the list of breast cancer driver genes together with its heterodimerization partner CBF β (Nik-Zainal et al., 2016; Pereira et al., 2016). Notwithstanding the utility of these predictive analyses, the ultimate proof of the causative role played by *RUNX1* in the initiation, maintenance and/or progression of breast cancer could only be achieved by studying its function *in vivo*. As such, using two genetic models of breast cancer, characterized by two distinct oncogenes (i.e. PyMT and β -catenin) driven by different mammary-specific Cre-recombinases (i.e. MMTV-Cre and BLG-Cre, respectively), deletion of *Runx1* resulted in a significantly accelerated onset of mammary tumourigenesis. These results are the first to provide compelling functional evidence for a tumour suppressive function played by *RUNX1* in the context of breast tumourigenesis.

In an effort to delve into the root of *RUNX1*'s behaviour, and in view of the fact that '*pathological changes are merely physiological modified ones*' (Beatson, 1896), attention has focused on the role played by the gene in the physiology of the murine mammary gland. Expression of *Runx1* was found to fluctuate during mammary gland post-natal development, increasing in virgin and involuting mice, whilst decreasing during pregnancy and lactation (Blyth et al., 2010). These results were indicative of a function played by *RUNX1* specifically during mammary gland pubertal growth, as well as remodelling of the organ occurring at weaning. When expression of the gene was analysed in extracted murine mammary cells, *Runx1* was found to be present in both epithelial compartments, albeit showing a preferential enrichment for the basal versus the luminal one (McDonald et al., 2014). As no expression was reported in the fat pad, these findings hinted towards a specific requirement for the gene in the epithelium of the mammary gland. Studying the effects of *Runx1* deletion in the basal epithelium via the use of the K14-Cre driver was hampered by the ubiquitous expression of the K14 promoter and the peculiar function played by the gene in the development of dental epithelium (Yamashiro et al., 2002). This resulted in the generation of small sized mice characterized by the presence of crooked teeth (data not shown). Nonetheless, when whole-mount analysis of inguinal

mammary glands from 20 week old mice was analysed, this revealed the presence of delayed mammary epithelial ductal trees as compared to *Runx1*-proficient mice. Based on these preliminary observations and as ductal morphogenesis is under the tight control of ovarian hormones and paracrine molecules, it would be interesting to investigate whether *Runx1* deletion could impinge on the hormonal paracrine circuits taking place in the mammary gland. In view of the caveats displayed by the K14-Cre model, most of the studies herein focused on the effects of BLG-Cre mediated excision of *Runx1*. Expression of BLG-Cre recombinase was shown to be temporally regulated in the mammary gland, with minimal levels recorded in pubertal/adult mice (7%), while maximal expression observed during lactation (70-80%). The reason behind this fluctuation was ascribed to hormones, as *BLG* encodes for a milk-secreted protein released by luminal cells during lactation (Selbert et al., 1998). Nonetheless, results from a former PhD student in our lab (N. Ferrari, unpublished) are indicative of a different pattern of BLG-Cre expression, evaluated through the use of the *EGFP* reported gene. This revealed in fact a higher percentage of BLG-Cre levels (18%) detected in 12 week virgin females. Although animals presented with normal-looking mammary trees able to undergo pregnancy, lactation and involution, a significant decreased of the luminal population was found to affect the mammary epithelial cell hierarchy upon BLG-Cre mediated deletion of *Runx1* (N. Ferrari, unpublished). RUNX1 has in fact been shown to be a crucial orchestrator of the luminal compartment, wherein it might favour the ductal ER⁺ program over the alveolar one through repression of *Elf5* (van Bragt et al., 2014). As an enrichment of the p53 signature was displayed by luminal cells in the absence of the gene, RUNX1 expression appeared fundamental for the survival and maintenance of a subset of luminal cells (van Bragt et al., 2014). To investigate this further, BLG-Cre mediated excision of *Runx1* is currently being studied in our lab in the context of a *p53*-null background. If loss of *Runx1* causes death of luminal cells, then loss of p53 should rescue the phenotype, allowing survival and oncogenic transformation of *Runx1*-deleted cells.

In support of a peculiar function played by the gene in the luminal epithelium of the mammary gland is also the fact that fluctuation of *Runx1* levels during the reproductive stages of the organ is reminiscent of ER α and PR expression. Both

HRs were in fact found to be elevated during puberty and involution, yet absent at pregnancy and lactation (Shyamala et al., 2002; van Keymeulen et al., 2017). In addition, as the presence of both HR+ sensor and HR- effector cells could be observed in the luminal compartment, seemingly RUNX1 IHC staining showed a mosaic pattern of expression, with positive cells found adjacent to negative ones. Altogether, these observations could lead to the hypothesis that RUNX1 expression in the luminal layer of the murine gland might be restricted to HR+ sensor cells. In support of the latter, a tantalizing interplay between RUNX1 and the ER signalling pathway has recently emerged, whereby the gene appears to modulate oestrogen-ER gene transcription via both a tethering and non-tethering mechanism of action (Riggio and Blyth, 2017). This was shown to be particularly true for the *AXIN1* locus, with RUNX1 acting as a positive regulator of *AXIN1* expression, whilst oestrogen-ER complexes suppressing it (Chimge et al., 2016). This antagonist relationship provided mechanistic evidence for a tumour suppressive function exerted by RUNX1 in HR+ sensor cells, wherein the gene's role might be to fine-tune oestrogens-ER α -mediated proliferation. As a dependency for hormonal cues is required for incipient PyMT-driven lesions, yet not by established tumours (Berebbi et al., 1990), this could offer important insights into how the formation of mammary lesions shown by the *MMTV-PyMT* model was accelerated in the absence of *Runx1*. Seemingly, this could also explain the precocious appearance of *Runx1*-deleted Wnt/ β -catenin-driven pre-neoplastic lesions, which also displayed high levels of ER and PR expression. To investigate this further, the first thing to do will be to confirm if expression of RUNX1 is indeed restricted to ER+ mammary epithelial cells. This could be achieved via the use of a *Runx1*-CreER inducible line, wherein expression of *Runx1* could be monitored over time through visualization of a Cre-dependent reporter gene (Samokhvalov et al., 2007). In conjunction with the latter, the employment of co-immunofluorescence or FACS techniques might allow to visualize the presence of double positive RUNX1/ER mammary epithelial cells and detect a concomitant enrichment for *Runx1* and *Esr-1* expression in sorted luminal cells, respectively. Secondly, it will be important to assess if deletion of *Runx1* in the context of an activated oncogene caused an aberrant proliferation of ER+ cells and/or of neighbouring ER- cells. Lastly, in support of the intriguing link between RUNX1 and hormone signalling is the recent reclassification of the five intrinsic subtypes of breast cancer (luminal A, luminal B, basal-like, HER2+

and normal-like) (Perou et al., 2000; Sorlie et al., 2001) into 10 Integrative Clusters of the disease (Curtis et al., 2012; Dawson et al., 2013). Accordingly, *RUNX1* mutations were reported to occur within Integrative Cluster 3, comprised of Luminal A tumours and characterized by a high prevalence of *PIK3CA* and *CDH1* mutations. Albeit displaying the best prognosis above all clusters, Luminal A breast tumours were shown to have the highest likelihood of local and/or distant relapse in the long term (Haque et al., 2012). Therefore, these findings may offer not only valuable clues on the most relevant genetic context wherein to study the consequences of *RUNX1* loss, but could also hold the key for the generation of more refined GEMMs of luminal breast cancer.

Prior to breast cancer, the first hints for a tumour suppressive role played by *RUNX1* came from the haematopoietic field. Here, the gene was found to be absolutely required for the conversion of endothelial cells to HSCs, yet dispensable for the maintenance and survival of the latter population in the adult organ. Accordingly, while *Runx1* knock-out mice displayed an embryonic lethal phenotype (Wang et al., 1996), deletion of *Runx1* in the adult haematopoietic compartment allowed mice to survive for more than 5 months. These, however, reported mild to severe haematopoietic abnormalities due to an expanded HSC pool, stemming from the presence of a myeloproliferative phenotype, as opposed to a block in lymphoid development (Growney et al., 2005). In line with the latter, homozygous loss of *RUNX1* was observed in patients with M0 (undifferentiated) acute myeloid leukaemia cells (AML) (Roumier et al., 2003), yet not with acute lymphoid leukaemia (Osato et al., 1999). This suggested that persistence of AML cells, characterized by a high self-renewing ability and a limited differentiation capability, could only occur in the absence of *RUNX1*. For the above reasons, *RUNX1* was proposed to act as a major cell fate and differentiation determinant, whose absence appears to increase self-renewal potential by maintaining the cells in a more undifferentiated state (Growney et al., 2005). Interestingly, very similar observations were recently made in the breast field, wherein inhibition of *RUNX1* in the human MCF-10A line was shown to trap cells in a bipotent state, thus preventing their differentiation into the ductal and lobular phenotypes (Sokol et al., 2015). Evidence for an expanded stem/progenitor pool of cells was also proposed in the Wnt/ β -catenin-driven breast cancer GEMM, as corroborated by the increase of a basal

subpopulation upon deletion of *Runx1* (Chapter 6). This phenotype, however, displayed a remarkable exacerbation when combined deletion of both *Runx1* and *Runx2* was achieved, resulting in the formation of enlarged mammary anlagen (Chapter 5), increased tumour burden and significantly decreased overall survival displayed by the mice (Chapter 4). Based on preliminary analyses, an expanded pool of Sca-1+ basal cells appeared to lay the foundation of this peculiar phenotypic behaviour (Chapter 6). Particularly abundant in TEBs and deemed to be responsive to hormonal cues, these results pointed again towards an exquisite tumour suppressive function exerted by the *Runx* genes in HR+ mammary cells. Similar to TEBs, cumulative evidence also suggest that corresponding human TDLUs are the most preferential site for neoplastic transformation (Russo et al., 2005; Visvader, 2009). Importantly, susceptibility of TDLUs to breast cancer appears to be intimately linked to the differentiation status of the epithelial tissue, which is in turn profoundly influenced by the presence or absence of pregnancy. As such, nulliparous women, characterized by a less differentiated epithelium, are believed to be at higher risk of breast cancer than parous ones, which on the contrary are less susceptible to neoplastic transformation in view of the higher prevalence of differentiated cells (Russo et al., 2005). Due to the remarkable parallels between the murine and the human cellular hierarchies (Visvader, 2009), it is tempting to envision *RUNX1* and *RUNX2* as guardians of mammary epithelial cell fate decisions and differentiation potential. As impairment of the mammary epithelial cell hierarchy is key for the aetiology of breast cancer, a deeper understanding on the function exerted by the *RUNX* family of genes is worth of further investigation.

In this regard, if the absence of *Runx1* caused an acceleration of breast tumourigenesis, it should also be noted that deletion of the gene resulted in delayed growth of established PyMT- and β -catenin-driven mammary lesions. This is not the first time a chameleon-like role has been proposed for *RUNX1*, acting as a tumour suppressor and an oncogene not only in different tissues, but also in different tissue-contexts (Chuang et al., 2013). Over the past recent years multiple breast cancer associated genetic events were reported to affect the gene, including deep deletion, mutations (truncating, inframe and missense), but also amplification events (Rooney, Riggio et al., 2017). In support of a pro-oncogenic role played by the gene, different transcriptomic studies

reported *RUNX1* mRNA upregulation in the TN subtype of breast cancer (Karn et al., 2011; Rody et al., 2011). In addition, expression of the protein was found by our lab to significantly correlate with poor overall survival of ER- and TN breast cancer patients (Ferrari et al., 2014). Preliminary analysis of MDAMB231 TN cells also showed an *in vitro* and *in vivo* impairment of cell proliferation upon *Runx1* knock-down (Riggio and Ferrari, unpublished). Importantly, whilst trying to dissect the dualistic behaviour shown by RUNX1, several factors should be taken into account. Firstly, the RUNX1-CBF β complex functions as an organizing platform which recruits additional co-factors (co-activators or co-repressors) to regulate gene transcription, contributing to its physiological capability as both a transcriptional activator and repressor (Blyth et al., 2005). Furthermore, not only is the *RUNX1* gene transcribed from two distinct promoters, but also the originating mRNAs can be subjected to alternative splicing, giving rise to multiple isoforms which appear to possess unique functions and differing patterns of tissue-specificity (Levanon et al., 1996; Miyoshi et al., 1995). It is therefore conceivable that RUNX1's complex role might be due to the presence of differentially expressed isoforms. Additionally, the function of RUNX1 can be markedly affected by post-translational modifications, including phosphorylation, acetylation and ubiquitination (Bae and Lee, 2006). As such, RUNX1's transcriptional activity was shown to be enhanced by extracellular signal-regulated kinase-mediated phosphorylation (Tanaka et al., 1996), whereas ubiquitin-dependent degradation is responsible for the tight control of RUNX1 protein levels (Huang et al., 2001), an event shown to be inhibited through CBF β heterodimerization. Accordingly, *Cbfb*-null mice display poorly detectable RUNX1 levels, leading to the hypothesis that perhaps the effective amount of RUNX1 within the cells might be dependent upon existing CBF β levels. Finally, RUNX1 can drive both proliferation and differentiation, two biological processes always thought of as antagonists (Coffman, 2003). Thus, a deeper investigation into the regulatory network impinging on its expression, stability and activity will pave the way towards a better understanding of the context-dependent role displayed by RUNX1 in breast cancers.

In conclusion, far from being a “modern” disease, cancer is probably the oldest malady that humans have ever encountered, with proof of its existence tracing back to Egyptian mummies. Despite the remarkable advances made in the

research field, cancer remains “*the defining plague of our generation*” (Siddharta, 2010). With a total of 55,200 new cases diagnosed in the UK in 2014, and 11,433 reported deaths in the same year, almost 78% of breast cancer patients are believed to survive the disease for 10 or more years (<https://www.cancerresearchuk.org/>; accessed October 2017). Nonetheless, to avoid the remaining 22% of women succumbing to this malignancy and improve the quality of life of surviving patients, a deeper understanding of the molecular mechanisms underpinning the biology of the mammary gland and of breast cancer is imperative. To achieve this aim, as the disease appears to be the result of the concerted interaction between multiple low-frequently altered genes (e.g. *RUNX1*), the identity of all these players needs to be investigated. Elucidation of the signalling pathways controlled by breast cancer-associated genes through the use of different *in vitro* and *in vivo* experimental models might help add an extra dowel to the incomplete puzzle of breast cancer.

Bibliography

- Abraham, S.C., Reynolds, C., Lee, J.H., Montgomery, E.A., Baisden, B.L., Krasinskas, A.M., and T.T. Wu. 2002. Fibromatosis of the breast and mutations involving the APC/beta-catenin pathway. *Human Pathology*. 33(1):39-46.
- Ahlbory-Dieker, D.L., B.D. Stride, G. Leder, J. Schkoldow, S. Trolenberg, H. Seidel, C. Otto, A. Sommer, M.G. Parker, G. Schutz, and T.M. Wintermantel. 2009. DNA binding by estrogen receptor-alpha is essential for the transcriptional response to estrogen in the liver and the uterus. *Molecular endocrinology*. 23:1544-1555.
- Alexander, C.M., Goel, S., Fakhralden, S.A., and S. Kim. 2012. Wnt signaling in mammary glands: plastic cell fates and combinatorial signaling. *Cold Spring Harbour Perspectives in Biology*. 4(10):a008037.
- Al-Hajj, M., M.S. Wicha, A. Benito-Hernandez, S.J. Morrison, and M.F. Clarke. 2003. Prospective identification of tumorigenic breast cancer cells. *Proceedings of the National Academy of Sciences of the United States of America*. 100:3983-3988.
- Andersen, C.L., Jensen, J.L., and T.F. Orntoft. 2004. Normalization of real-time quantitative reverse transcription-PCR data: a model-based variance estimation approach to identify genes suited for normalization, applied to bladder and colon cancer data sets. *Cancer Research*. 64(15):5245-5250.
- Andrechek, E.R., W.R. Hardy, P.M. Siegel, M.A. Rudnicki, R.D. Cardiff, and W.J. Muller. 2000. Amplification of the neu/erbB-2 oncogene in a mouse model of mammary tumorigenesis. *Proceedings of the National Academy of Sciences of the United States of America*. 97(7):3444-3449.
- Asghar, U.S., A.R. Barr, R. Cutts, M. Beaney, I. Babina, D. Sampath, J. Giltane, J.A. Lacap, L. Crocker, A. Young, A. Pearson, M.T. Herrera-Abreu, C. Bakal, and N.C. Turner. 2017. Single-Cell Dynamics Determines Response to CDK4/6 Inhibition in Triple-Negative Breast Cancer. *Clinical cancer research : an official journal of the American Association for Cancer Research*. 23:5561-5572.
- Asselin-Labat, M.L., M. Shackleton, J. Stingl, F. Vaillant, N.C. Forrest, C.J. Eaves, J.E. Visvader, and G.J. Lindeman. 2006. Steroid hormone receptor status of mouse mammary stem cells. *J Natl Cancer Inst*. 98:1011-1014.
- Asselin-Labat, M.L., K.D. Sutherland, H. Barker, R. Thomas, M. Shackleton, N.C. Forrest, L. Hartley, L. Robb, F.G. Grosveld, J. van der Wees, G.J. Lindeman, and J.E. Visvader. 2007. Gata-3 is an essential regulator of mammary-gland morphogenesis and luminal-cell differentiation. *Nature cell biology*. 9:201-209.
- Asselin-Labat, M.L., K.D. Sutherland, F. Vaillant, D.E. Gyorki, D. Wu, S. Holroyd, K. Breslin, T. Ward, W. Shi, M.L. Bath, S. Deb, S.B. Fox, G.K. Smyth, G.J. Lindeman, and J.E. Visvader. 2011. Gata-3 negatively regulates the tumor-initiating capacity of mammary luminal progenitor cells and targets the putative tumor suppressor caspase-14. *Molecular and cellular biology*. 31:4609-4622.
- Asselin-Labat, M.L., F. Vaillant, J.M. Sheridan, B. Pal, D. Wu, E.R. Simpson, H. Yasuda, G.K. Smyth, T.J. Martin, G.J. Lindeman, and J.E. Visvader. 2010. Control of mammary stem cell function by steroid hormone signalling. *Nature*. 465:798-802.
- Aure, M.R., V. Vitelli, S. Jernstrom, S. Kumar, M. Krohn, E.U. Due, T.H. Haukaas, S.K. Leivonen, H.K. Vollan, T. Luders, E. Rodland, C.J. Vaske,

- W. Zhao, E.K. Moller, S. Nord, G.F. Giskeodegard, T.F. Bathen, C. Caldas, T. Tramm, J. Alsner, J. Overgaard, J. Geisler, I.R. Bukholm, B. Naume, E. Schlichting, T. Sauer, G.B. Mills, R. Karesen, G.M. Maelandsmo, O.C. Lingjaerde, A. Frigessi, V.N. Kristensen, A.L. Borresen-Dale, K.K. Sahlberg, and Osbreac. 2017. Integrative clustering reveals a novel split in the luminal A subtype of breast cancer with impact on outcome. *Breast cancer research : BCR*. 19:44.
- Bae, S.C., and Y.H. Lee. 2006. Phosphorylation, acetylation and ubiquitination: the molecular basis of RUNX regulation. *Gene*. 366:58-66.
- Bai, J., H.M. Yong, F.F. Chen, W.B. Song, C. Li, H. Liu, and J.N. Zheng. 2013. RUNX3 is a prognostic marker and potential therapeutic target in human breast cancer. *Journal of cancer research and clinical oncology*. 139:1813-1823.
- Bai, L., and L.R. Rohrschneider. 2010. s-SHIP promoter expression marks activated stem cells in developing mouse mammary tissue. *Genes Dev*. 24:1882-1892.
- Ballard, M.S., A. Zhu, N. Iwai, M. Stensrud, A. Mapps, M.P. Postiglione, J.A. Knoblich, and L. Hinck. 2015. Mammary Stem Cell Self-Renewal Is Regulated by Slit2/Robo1 Signaling through SNAI1 and mNSC. *Cell reports*. 13:290-301.
- Banerji, S., K. Cibulskis, C. Rangel-Escareno, K.K. Brown, S.L. Carter, A.M. Frederick, M.S. Lawrence, A.Y. Sivachenko, C. Sougnez, L. Zou, M.L. Cortes, J.C. Fernandez-Lopez, S. Peng, K.G. Ardlie, D. Auclair, V. Bautista-Pina, F. Duke, J. Francis, J. Jung, A. Maffuz-Aziz, R.C. Onofrio, M. Parkin, N.H. Pho, V. Quintanar-Jurado, A.H. Ramos, R. Rebollar-Vega, S. Rodriguez-Cuevas, S.L. Romero-Cordoba, S.E. Schumacher, N. Stransky, K.M. Thompson, L. Uribe-Figueroa, J. Baselga, R. Beroukhim, K. Polyak, D.C. Sgroi, A.L. Richardson, G. Jimenez-Sanchez, E.S. Lander, S.B. Gabriel, L.A. Garraway, T.R. Golub, J. Melendez-Zajgla, A. Toker, G. Getz, A. Hidalgo-Miranda, and M. Meyerson. 2012. Sequence analysis of mutations and translocations across breast cancer subtypes. *Nature*. 486:405-409.
- Barker, N., S. Tan, and H. Clevers. 2013. Lgr proteins in epithelial stem cell biology. *Development*. 140:2484-2494.
- Barkley, M.S., and G..E. Bradford. 1981. Estrous cycle dynamics in different strains of mice. *Proceedings of the society for experimental biology and medicine*. 167:70-77.
- Barutcu, A.R., D. Hong, B.R. Lajoie, R.P. McCord, A.J. van Wijnen, J.B. Lian, J.L. Stein, J. Dekker, A.N. Imbalzano, and G.S. Stein. 2016. RUNX1 contributes to higher-order chromatin organization and gene regulation in breast cancer cells. *Biochimica et biophysica acta*. 1859:1389-1397.
- Beatson, G.T. 1896. On the treatment of inoperable cases of carcinoma of the mamma: suggestions for a new method of treatment, with illustrative cases. *The Lancet*. 148: 162-165.
- Behari, J. 2010. The Wnt/ β -catenin signaling pathway in liver biology and disease. *Expert Review of Gastroenterology and Hepatology*. 4(6):745-756.
- Beleut, M., R.D. Rajaram, M. Caikovski, A. Ayyanan, D. Germano, Y. Choi, P. Schneider, and C. Brisken. 2010. Two distinct mechanisms underlie progesterone-induced proliferation in the mammary gland. *Proceedings of the National Academy of Sciences of the United States of America*. 107:2989-2994.

- Ben-Porath, I., M.W. Thomson, V.J. Carey, R. Ge, G.W. Bell, A. Regev, and R.A. Weinberg. 2008. An embryonic stem cell-like gene expression signature in poorly differentiated aggressive human tumors. *Nature genetics*. 40:499-507.
- Berebby, M., Martin, P.M., Berthois, Y., Bernard, A.M., and D. Blangy. 1990. Estradiol dependence of the specific mammary tissue targeting of polyoma virus oncogenicity in nude mice. *Oncogene*. 5(4):505-509.
- Blanpain, C., and E. Fuchs. 2014. Stem cell plasticity. Plasticity of epithelial stem cells in tissue regeneration. *Science*. 344:1242281.
- Blyth, K., E.R. Cameron, and J.C. Neil. 2005. The RUNX genes: gain or loss of function in cancer. *Nature reviews. Cancer*. 5:376-387.
- Blyth, K., F. Vaillant, A. Jenkins, L. McDonald, M.A. Pringle, C. Huser, T. Stein, J. Neil, and E.R. Cameron. 2010. Runx2 in normal tissues and cancer cells: A developing story. *Blood cells, molecules & diseases*. 45:117-123.
- Booth, B.W., and G.H. Smith. 2006. Estrogen receptor-alpha and progesterone receptor are expressed in label-retaining mammary epithelial cells that divide asymmetrically and retain their template DNA strands. *Breast cancer research : BCR*. 8:R49.
- Brennan, K., M. Garcia-Closas, N. Orr, O. Fletcher, M. Jones, A. Ashworth, A. Swerdlow, H. Thorne, K.C. Investigators, E. Riboli, P. Vineis, M. Dorransoro, F. Clavel-Chapelon, S. Panico, N.C. Onland-Moret, D. Trichopoulos, R. Kaaks, K.T. Khaw, R. Brown, and J.M. Flanagan. 2012. Intragenic ATM methylation in peripheral blood DNA as a biomarker of breast cancer risk. *Cancer research*. 72:2304-2313.
- Brisken, C., Park, S., Vass, T., Lydon, J.P., and B.W. O'Malley. 1998. A paracrine role for the epithelial progesterone receptor in mammary gland development. *Proceedings of the National Academy of Sciences of the United States of America*. 95(9):5076-5081.
- Brisken, C., and B. O'Malley. 2010. Hormone action in the mammary gland. *Cold Spring Harb Perspect Biol*. 2:25.
- Browne, G., H. Taipaleenmaki, N.M. Bishop, S.C. Madasu, L.M. Shaw, A.J. van Wijnen, J.L. Stein, G.S. Stein, and J.B. Lian. 2015. Runx1 is associated with breast cancer progression in MMTV-PyMT transgenic mice and its depletion in vitro inhibits migration and invasion. *Journal of cellular physiology*. 230:2522-2532.
- Bruna, A., O.M. Rueda, W. Greenwood, A.S. Batra, M. Callari, R.N. Batra, K. Pogrebniak, J. Sandoval, J.W. Cassidy, A. Tufegdizic-Vidakovic, S.J. Sammut, L. Jones, E. Provenzano, R. Baird, P. Eirew, J. Hadfield, M. Eldridge, A. McLaren-Douglas, A. Barthorpe, H. Lightfoot, M.J. O'Connor, J. Gray, J. Cortes, J. Baselga, E. Marangoni, A.L. Welm, S. Aparicio, V. Serra, M.J. Garnett, and C. Caldas. 2016. A Biobank of Breast Cancer Explants with Preserved Intra-tumor Heterogeneity to Screen Anticancer Compounds. *Cell*. 167:260-274 e222.
- Byrne, C., Tainsky, M., and E. Fuchs. 1994. Programming gene expression in developing epidermis. *Development*. 120(9):2369-2383.
- Cailleau, R., Olive', M., and Q.V. Cruciger. 1978. Long-term human breast carcinoma cell lines of metastatic origin: preliminary characterization. *In vitro*. 14:911-915.
- Caley, A., and R. Jones. 2012. The principles of cancer treatment by chemotherapy. *Surgery (Oxford)*. 30:186-190.
- Caligioni, C.S. 2009. Assessing reproductive status/stages in mice. *Current protocols in neuroscience*. Appendix 4:Appendix 4I.

- Cancer Genome Atlas, N. 2012. Comprehensive molecular portraits of human breast tumours. *Nature*. 490:61-70.
- Cardiff, R.D., and S.R. Wellings. 1999. The comparative pathology of human and mouse mammary glands. *Journal of Mammary Gland Biology and Neoplasia*. 4(1):105-122.
- Carter, W. G., Kaur, P., Gil, S. G., Gahr, P. J., and E. A. Wayner. 1990. Distinct functions for integrins alpha 3 beta 1 in focal adhesions and alpha 6 beta 4/bullous pemphigoid antigen in a new stable anchoring contact (SAC) of keratinocytes: relation to hemidesmosomes. *Journal of cellular biology*. 111:3141-3154.
- Cerami, E., J. Gao, U. Dogrusoz, B.E. Gross, S.O. Sumer, B.A. Aksoy, A. Jacobsen, C.J. Byrne, M.L. Heuer, E. Larsson, Y. Antipin, B. Reva, A.P. Goldberg, C. Sander, and N. Schultz. 2012. The cBio cancer genomics portal: an open platform for exploring multidimensional cancer genomics data. *Cancer Discovery*. 2:401-404.
- Chaffer, C.L., and R.A. Weinberg. 2015. How does multistep tumorigenesis really proceed? *Cancer Discov*. 5:22-24.
- Chang, T.H.T, Kunasegaran, K., Tarulli, G.A., De Silva, D., Voorhoeve, P.M., and Pieterse, A.M. 2014. New insights into lineage restriction of mammary gland epithelium using parity-identified mammary epithelial cells. *Breast Cancer Research*. 16:R1.
- Chatterjee, A., and J.K. Erban. 2017. Neoadjuvant therapy for treatment of breast cancer: the way forward, or simply a convenient option for patients?. *Gland surgery*. 6:119-124.
- Chen, G., and A.J. Courey. 2000. Groucho/TLE family proteins and transcriptional repression. *Gene*. 249(1-2):1-16.
- Chen, W., M. Salto-Tellez, N. Palanisamy, K. Ganesan, Q. Hou, L.K. Tan, L.H. Sii, K. Ito, B. Tan, J. Wu, A. Tay, K.C. Tan, E. Ang, B.K. Tan, P.H. Tan, Y. Ito, and P. Tan. 2007. Targets of genome copy number reduction in primary breast cancers identified by integrative genomics. *Genes, chromosomes & cancer*. 46:288-301.
- Chen, X., Q. Liu, and E. Song. 2017. Mammary stem cells: angels or demons in mammary gland? *Signal Transduction and Targeted Therapy*. 2:16038.
- Chimge, N.O., S.K. Baniwal, J. Luo, S. Coetzee, O. Khalid, B.P. Berman, D. Tripathy, M.J. Ellis, and B. Frenkel. 2012. Opposing effects of Runx2 and estradiol on breast cancer cell proliferation: in vitro identification of reciprocally regulated gene signature related to clinical letrozole responsiveness. *Clinical cancer research : an official journal of the American Association for Cancer Research*. 18:901-911.
- Chimge, N.O., and B. Frenkel. 2013. The RUNX family in breast cancer: relationships with estrogen signaling. *Oncogene*. 32:2121-2130.
- Chimge, N.O., G.H. Little, S.K. Baniwal, H. Adisetiyo, Y. Xie, T. Zhang, A. O'Laughlin, Z.Y. Liu, P. Ulrich, A. Martin, P. Mhawech-Fauceglia, M.J. Ellis, D. Tripathy, S. Groshen, C. Liang, Z. Li, D.E. Schones, and B. Frenkel. 2016. RUNX1 prevents oestrogen-mediated AXIN1 suppression and beta-catenin activation in ER-positive breast cancer. *Nature communications*. 7:10751.
- Chu, E.Y., Hens, J., Andl, T., Kairo, A., Yamaguchi, T.P., Brisken, C., Glick, A., Wysolmerski, J.J., and S.E. Millar. 2004. Canonical WNT signaling promotes mammary placode development and is essential for initiation of mammary gland morphogenesis. *Development*. 131(19):4819-4829.

- Chuang, L.S., K. Ito, and Y. Ito. 2013. RUNX family: Regulation and diversification of roles through interacting proteins. *International journal of cancer*. 132:1260-1271.
- Ciarloni, L., S. Mallepell, and C. Brisken. 2007. Amphiregulin is an essential mediator of estrogen receptor alpha function in mammary gland development. *Proceedings of the National Academy of Sciences of the United States of America*. 104:5455-5460.
- Clarke, R.B., A. Howell, C.S. Potten, and E. Anderson. 1997. Dissociation between steroid receptor expression and cell proliferation in the human breast. *Cancer research*. 57:4987-4991.
- Clarke, M.F., Dick, J.E., Dirks, P.B., Eaves, C.J., Jamieson, C.H.M., Jones, D.L., Visvader, J., Weissman, I.L., and G.M. Wahl. 2006. Cancer Stem Cells - perspectives on current status and future directions: AACR workshop on cancer stem cells. *Cancer Research*. 66(19):9339-9344.
- Coffman, J. 2003. Runx transcription factors and the developmental balance between cell proliferation and differentiation. *Cell Biology International*. 27:315-324.
- Cornen, S., A. Guille, J. Adelaide, L. Addou-Klouche, P. Finetti, M.R. Saade, M. Manai, N. Carbuccia, I. Bekhouche, A. Letessier, S. Raynaud, E. Charafe-Jauffret, J. Jacquemier, S. Spicuglia, H. de The, P. Viens, F. Bertucci, D. Birnbaum, and M. Chaffanet. 2014. Candidate luminal B breast cancer genes identified by genome, gene expression and DNA methylation profiling. *PLoS One*. 9(1):e81843.
- Courtneidge, S.A., and A. Heber. 1987. An 81 kd protein complexed with middle T antigen and pp60^{c-src}: a possible phosphatidylinositol kinase. *Cell*. 50(7):1031-1037.
- Cowin, P., and B. Burke. 1996. Cytoskeleton-membrane interactions. *Current Opinion in Cell Biology*. 8(1):56-65.
- Cowin, P., and J. Wysolmerski. 2010. Molecular mechanisms guiding embryonic mammary gland development. *Cold Spring Harbour Perspectives in Biology*. 2(6):a003251.
- Curtis, C., S.P. Shah, S.F. Chin, G. Turashvili, O.M. Rueda, M.J. Dunning, D. Speed, A.G. Lynch, S. Samarajiwa, Y. Yuan, S. Graf, G. Ha, G. Haffari, A. Bashashati, R. Russell, S. McKinney, A. Langerod, A. Green, E. Provenzano, G. Wishart, S. Pinder, P. Watson, F. Markowitz, L. Murphy, I. Ellis, A. Purushotham, A.L. Borresen-Dale, J.D. Brenton, S. Tavare, C. Caldas, and S. Aparicio. 2012. The genomic and transcriptomic architecture of 2,000 breast tumours reveals novel subgroups. *Nature*. 486:346-352.
- Cuzick, J., I. Sestak, B. Bonanni, J.P. Costantino, S. Cummings, A. DeCensi, M. Dowsett, J.F. Forbes, L. Ford, A.Z. LaCroix, J. Mershon, B.H. Mittlak, T. Powles, U. Veronesi, V. Vogel, and D.L. Wickerham. 2013. Selective oestrogen receptor modulators in prevention of breast cancer: an updated meta-analysis of individual participant data. *The Lancet*. 381:1827-1834.
- Dall, G.V., Vieusseux, J.L., Korach, K.S., Arao, Y., Hewitt, S.C., Hamilton, K.J., Dzierzak, E., Boon, W.C., Simpson, E.R., Ramsay, R.G., Stein, T., Morris, J.S., Anderson, R.L., Risbridger, G.P., and K.L. Britt. 2017. SCA-1 labels a subset of estrogen-responsive bipotential repopulating cells within the CD24⁺CD49^{hi} mammary stem cell-enriched compartment. *Stem Cell Reports*. 8(2):417-431.
- Daniel, C.W., DeOme, K.B., Young, J.T., Blair, P.B., and L.J. Faulkin. 1968. The in vivo life span of normal and preneoplastic mouse mammary glands: a

- serial transplantation study. *Proceedings of the National Academy of Sciences of the United States of America*. 61(1):53-60.
- Daniels, D.L., and W.I. Weis. 2005. β -catenin directly displaces Groucho/TLE repressors from TCF/lef in Wnt-mediated transcription activation. *Nature Structural and Molecular Biology*. 12(4):364-371.
- Dassule, H.R., Lewis, P., Bei, M., Maas, R., and A.P. McMahon. 2000. Sonic hedgehog regulates growth and morphogenesis of the tooth. *Development*. 127(22):4775-4785.
- Davie, S.A., Maglione, J.E., Manner, C.K., Young, D., Cardiff, R.D., MacLeod, C.L., and L.G. Ellies. 2007. Effects of FVB/NJ and C57Bl/6J strain backgrounds on mammary tumor phenotype in inducible nitric oxide synthase deficient mice. *Transgenic Research*. 16(2):193-201.
- Dawe, C.J., Freund, R., Mandel, G., Ballmer-Hofer, K., Talmage, D.A., and T.L. Benjamin. 1987. Variations in polyoma virus genotype in relation to tumor induction in mice. Characterization of wild type strains with widely differing tumor profiles. *American Journal of Pathology*. 127(2):243-261.
- Dawson, S.J., O.M. Rueda, S. Aparicio, and C. Caldas. 2013. A new genome-driven integrated classification of breast cancer and its implications. *Embo J*. 32:617-628.
- de Visser, K.E., M. Ciampricotti, E.M. Michalak, D.W. Tan, E.N. Speksnijder, C.S. Hau, H. Clevers, N. Barker, and J. Jonkers. 2012. Developmental stage-specific contribution of LGR5(+) cells to basal and luminal epithelial lineages in the postnatal mammary gland. *The Journal of pathology*. 228:300-309.
- Defrank, J.T., and N. Brewer. 2010. A model of the influence of false-positive mammography screening results on subsequent screening. *Health psychology review*. 4:112-127.
- DeOme, F., Bern, Blair. 1959. Development of mammary tumors from hyperplastic alveolar nodules transplanted into gland-free mammary fat pads of female C3H mice. *Cancer research*. 19:515-520.
- DeRose, Y.S., K.M. Gligorich, G. Wang, A. Georgelas, P. Bowman, S.J. Courdy, A.L. Welm, and B.E. Welm. 2013. Patient-derived models of human breast cancer: protocols for in vitro and in vivo applications in tumor biology and translational medicine. *Current protocols in pharmacology*. Chapter 14:Unit14 23.
- Dieckmann, M., Dietrich, M.F., and J. Herz. 2010. Lipoprotein receptors - an evolutionarily ancient multifunctional receptor family. *The Journal of Biological Chemistry*. 391(11):1341-1363.
- Dontu, G., W.M. Abdallah, J.M. Foley, K.W. Jackson, M.F. Clarke, M.J. Kawamura, and M.S. Wicha. 2003. In vitro propagation and transcriptional profiling of human mammary stem/progenitor cells. *Genes Dev*. 17:1253-1270.
- Dulak, A.M., S.E. Schumacher, J. van Lieshout, Y. Imamura, C. Fox, B. Shim, A.H. Ramos, G. Saksena, S.C. Baca, J. Baselga, J. Taberner, J. Barretina, P.C. Enzinger, G. Corso, F. Roviello, L. Lin, S. Bandla, J.D. Luketich, A. Pennathur, M. Meyerson, S. Ogino, R.A. Shivdasani, D.G. Beer, T.E. Godfrey, R. Beroukhim, and A.J. Bass. 2012. Gastrointestinal adenocarcinomas of the esophagus, stomach, and colon exhibit distinct patterns of genome instability and oncogenesis. *Cancer research*. 72:4383-4393.

- Eastman, Q., and R. Grosschedl. 1999. Regulation of LEF-1/TCF transcription factors by Wnt and other signals. *Current Opinion in Cell Biology*. 11(2):233-240.
- Eccles, S.A., E.O. Aboagye, S. Ali, A.S. Anderson, J. Armes, F. Berditchevski, J.P. Blaydes, K. Brennan, N.J. Brown, H.E. Bryant, N.J. Bundred, J.M. Burchell, A.M. Campbell, J.S. Carroll, R.B. Clarke, C.E. Coles, G.J. Cook, A. Cox, N.J. Curtin, L.V. Dekker, S. Silva Idos, S.W. Duffy, D.F. Easton, D.M. Eccles, D.R. Edwards, J. Edwards, D. Evans, D.F. Fenlon, J.M. Flanagan, C. Foster, W.M. Gallagher, M. Garcia-Closas, J.M. Gee, A.J. Gescher, V. Goh, A.M. Groves, A.J. Harvey, M. Harvie, B.T. Hennessy, S. Hiscox, I. Holen, S.J. Howell, A. Howell, G. Hubbard, N. Hulbert-Williams, M.S. Hunter, B. Jasani, L.J. Jones, T.J. Key, C.C. Kirwan, A. Kong, I.H. Kunkler, S.P. Langdon, M.O. Leach, D.J. Mann, J.F. Marshall, L. Martin, S.G. Martin, J.E. Macdougall, D.W. Miles, W.R. Miller, J.R. Morris, S.M. Moss, P. Mullan, R. Natrajan, J.P. O'Connor, R. O'Connor, C. Palmieri, P.D. Pharoah, E.A. Rakha, E. Reed, S.P. Robinson, E. Sahai, J.M. Saxton, P. Schmid, M.J. Smalley, V. Speirs, R. Stein, J. Stingl, C.H. Streuli, A.N. Tutt, G. Velikova, R.A. Walker, C.J. Watson, K.J. Williams, L.S. Young, and A.M. Thompson. 2013. Critical research gaps and translational priorities for the successful prevention and treatment of breast cancer. *Breast cancer research : BCR*. 15:R92.
- Ellis, M.J., L. Ding, D. Shen, J. Luo, V.J. Suman, J.W. Wallis, B.A. Van Tine, J. Hoog, R.J. Goiffon, T.C. Goldstein, S. Ng, L. Lin, R. Crowder, J. Snider, K. Ballman, J. Weber, K. Chen, D.C. Koboldt, C. Kandoth, W.S. Schierding, J.F. McMichael, C.A. Miller, C. Lu, C.C. Harris, M.D. McLellan, M.C. Wendl, K. DeSchryver, D.C. Allred, L. Esserman, G. Unzeitig, J. Margenthaler, G.V. Babiera, P.K. Marcom, J.M. Guenther, M. Leitch, K. Hunt, J. Olson, Y. Tao, C.A. Maher, L.L. Fulton, R.S. Fulton, M. Harrison, B. Oberkfell, F. Du, R. Demeter, T.L. Vickery, A. Elhammali, H. Piwnica-Worms, S. McDonald, M. Watson, D.J. Dooling, D. Ota, L.W. Chang, R. Bose, T.J. Ley, D. Piwnica-Worms, J.M. Stuart, R.K. Wilson, and E.R. Mardis. 2012. Whole-genome analysis informs breast cancer response to aromatase inhibition. *Nature*. 486:353-360.
- Eriksson, L., P. Hall, K. Czene, I. Dos Santos Silva, V. McCormack, J. Bergh, J. Bjohle, and A. Ploner. 2012. Mammographic density and molecular subtypes of breast cancer. *Br J Cancer*. 107:18-23.
- Ethier, S.P., Mahacek, M.L., Gullick, W.J., Frank, T.S., and B.L. Weber. 1993. Differential isolation of normal luminal mammary epithelial cells and breast cancer cells from primary and metastatic sites using selective media. *Cancer Research*. 53(3):627-635.
- Faulkin, L.J., and K.B. DeOme. 1960. Regulation of growth and spacing of gland elements in the mammary fat pad of the C3H mouse. *Journal of the National Cancer Institute*. 24(4):953-969.
- Fernandez-Valdivia, R., and J.P. Lydon. 2012. From the ranks of mammary progesterone mediators, RANKL takes the spotlight. *Molecular and cellular endocrinology*. 357:91-100.
- Fernandez-Valdivia, R., A. Mukherjee, C.J. Creighton, A.C. Buser, F.J. DeMayo, D.P. Edwards, and J.P. Lydon. 2008. Transcriptional response of the murine mammary gland to acute progesterone exposure. *Endocrinology*. 149:6236-6250.

- Ferrari, N., L. McDonald, J.S. Morris, E.R. Cameron, and K. Blyth. 2013. RUNX2 in mammary gland development and breast cancer. *Journal of cellular physiology*. 228:1137-1142.
- Ferrari, N., Z.M. Mohammed, C. Nixon, S.M. Mason, E. Mallon, D.C. McMillan, J.S. Morris, E.R. Cameron, J. Edwards, and K. Blyth. 2014. Expression of RUNX1 correlates with poor patient prognosis in triple negative breast cancer. *PLoS One*. 9.
- Ferrari, N., A.I. Riggio, S. Mason, L. McDonald, A. King, T. Higgins, I. Rosewell, J.C. Neil, M.J. Smalley, O.J. Sansom, J. Morris, E.R. Cameron, and K. Blyth. 2015. Runx2 contributes to the regenerative potential of the mammary epithelium. *Scientific reports*. 5:15658.
- Frisch, S.M., and H. Francis. 1994. Disruption of epithelial cell-matrix interactions induces apoptosis. *The Journal of Cell Biology*. 124(4):619-626.
- Fukuchi, T., Sakamoto, M., Tsuda, H., Maruyama, K., Nozawa, S., and S. Hirohashi. 1998. β -catenin mutation in carcinoma of the uterine endometrium. *Cancer Research*. 58(16):3526-3528.
- Gao, J., B.A. Aksoy, U. Dogrusoz, G. Dresdner, B. Gross, S.O. Sumer, Y. Sun, A. Jacobsen, R. Sinha, E. Larsson, E. Cerami, C. Sander, and N. Schultz. 2013. Integrative analysis of complex cancer genomics and clinical profiles using the cBioPortal. *Sci Signal*. 6:2004088.
- Gerdes, J., Schwab, U., Lemke, H., and H. Stein. 1983. Production of a mouse monoclonal antibody reactive with a human nuclear antigen associated with cell proliferation. *International Journal of Cancer*. 31(1):13-20.
- Gey, G.O., Coffman, W.D., and M.T. Kubicek. 1952. Tissue culture studies of the proliferative capacity of cervical carcinoma and normal epithelium. *Cancer Research*. 12:264-265.
- Giangrande, P.H., and D.P. McDonnell. 1999. The A and B isoforms of the human progesterone receptor: two functionally different transcription factors encoded by a single gene. *Recent Prog Horm Res*. 54:291-313.
- Goodell, M.A., Brose, K., Paradis, G., Conner, A.S., and R.C. Mulligan. 1996. Isolation and functional properties of murine hematopoietic stem cells that are replicating in vivo. *The Journal of experimental medicine*. 183(4):1797.
- Gradishar, W.J., and V.C. Jordan. 1998. Endocrine therapy of breast cancer in: K.L. Bland, E.M. Copeland (Eds.), *The Breast*, 2nd Edition, Saunders, Philadelphia. 1350-1372.
- Graham, J.D., Mote, P.A., Salagame, U., van Dijk, J.H., Balleine, R.L., Huschtscha, L.I., Reddel, R.R., and C.L. Clarke. 2009. DNA replication licensing and progenitor numbers are increased by progesterone in normal human breast. *Endocrinology*. 150(7):3318-3326.
- Greenman, C., P. Stephens, R. Smith, G.L. Dalgliesh, C. Hunter, G. Bignell, H. Davies, J. Teague, A. Butler, C. Stevens, S. Edkins, S. O'Meara, I. Vastrik, E.E. Schmidt, T. Avis, S. Barthorpe, G. Bhamra, G. Buck, B. Choudhury, J. Clements, J. Cole, E. Dicks, S. Forbes, K. Gray, K. Halliday, R. Harrison, K. Hills, J. Hinton, A. Jenkinson, D. Jones, A. Menzies, T. Mironenko, J. Perry, K. Raine, D. Richardson, R. Shepherd, A. Small, C. Tofts, J. Varian, T. Webb, S. West, S. Widaa, A. Yates, D.P. Cahill, D.N. Louis, P. Goldstraw, A.G. Nicholson, F. Brasseur, L. Looijenga, B.L. Weber, Y.E. Chiew, A. DeFazio, M.F. Greaves, A.R. Green, P. Campbell, E. Birney, D.F. Easton, G. Chenevix-Trench, M.H. Tan, S.K. Khoo, B.T. Teh, S.T. Yuen,

- S.Y. Leung, R. Wooster, P.A. Futreal, and M.R. Stratton. 2007. Patterns of somatic mutation in human cancer genomes. *Nature*. 446:153-158.
- Growney, J.D., H. Shigematsu, Z. Li, B.H. Lee, J. Adelsperger, R. Rowan, D.P. Curley, J.L. Kutok, K. Akashi, I.R. Williams, N.A. Speck, and D.G. Gilliland. 2005. Loss of Runx1 perturbs adult hematopoiesis and is associated with a myeloproliferative phenotype. *Blood*. 106:494-504.
- Gu, G., D. Dustin, and S.A. Fuqua. 2016. Targeted therapy for breast cancer and molecular mechanisms of resistance to treatment. *Current opinion in pharmacology*. 31:97-103.
- Gumbiner, B.M. 1995. Signal transduction by beta-catenin. *Current Opinion in Cell Biology*. 7:634-640.
- Guo, W., Z. Keckesova, J.L. Donaher, T. Shibue, V. Tischler, F. Reinhardt, S. Itzkovitz, A. Noske, U. Zurrer-Hardi, G. Bell, W.L. Tam, S.A. Mani, A. van Oudenaarden, and R.A. Weinberg. 2012. Slug and Sox9 cooperatively determine the mammary stem cell state. *Cell*. 148:1015-1028.
- Guy, C.T., Cardiff, R.D., and W.J. Muller. 1992. Induction of mammary tumors by expression of polyomavirus middle T oncogene: a transgenic mouse model for metastatic disease. *Molecular and Cellular Biology*. 12(3):954-961.
- Hamilton, D.L., and K. Abremski. 1984. Site-specific recombination by the bacteriophage P1 lox-Cre system. Cre-mediated synapsis of two lox sites. *Journal of Molecular Biology*. 178(2):481-486.
- Han, X., J. Wang, and Y. Sun. 2017. Circulating Tumor DNA as Biomarkers for Cancer Detection. *Genomics, proteomics & bioinformatics*. 15:59-72.
- Hanahan, D., E.F. Wagner, and R.D. Palmiter. 2007. The origins of oncomice: a history of the first transgenic mice genetically engineered to develop cancer. *Genes Dev*. 21:2258-2270.
- Hanahan, D., and R.A. Weinberg. 2011. Hallmarks of cancer: the next generation. *Cell*. 144:646-674.
- Haque, R., S.A. Ahmed, G. Inzhakova, J. Shi, C. Avila, J. Polikoff, L. Bernstein, S.M. Enger, and M.F. Press. 2012. Impact of breast cancer subtypes and treatment on survival: an analysis spanning two decades. *Cancer epidemiology, biomarkers & prevention : a publication of the American Association for Cancer Research, cosponsored by the American Society of Preventive Oncology*. 21:1848-1855.
- Harada, N., Tamai, Y., Ishikawa, T., Sauer, B., Takaku, K., Oshima, M., and M.M. Taketo. 1999. Intestinal polyposis in mice with a dominant stable mutations of the beta-catenin gene. *The EMBO Journal*. 18(21):5931-5942.
- Haslam, S.Z., and G. Shyamala. 1981. Relative distribution of estrogen and progesterone receptors among the epithelial, adipose, and connective tissue components of the normal mammary gland. *Endocrinology*. 108(3):825-830.
- Hayes, M.J., Thomas, D., Emmons, A., Giordano, T.J., and C.G. Kleer. 2008. Genetic changes of Wnt pathway genes are common events in metaplastic carcinomas of the breast. *Clinical Cancer Research*. 14(13):4038-4044.
- Heemskerk-Gerritsen, B.A., C.T. Brekelmans, M.B. Menke-Pluymers, A.N. van Geel, M.M. Tilanus-Linthorst, C.C. Bartels, M. Tan, H.E. Meijers-Heijboer, J.G. Klijn, and C. Seynaeve. 2007. Prophylactic mastectomy in BRCA1/2 mutation carriers and women at risk of hereditary breast cancer: long-term experiences at the Rotterdam Family Cancer Clinic. *Annals of surgical oncology*. 14:3335-3344.

- Hennessy, B.T., Gonzalez-Angulo, AM., Stemke-Hale, K., Gilcrease, M.Z., Krishnamurthy, S., Lee, JS., Fridlyand, J., Sahin, A., Agarwal, R., Joy, C., Liu, W., Stivers, D., Baggerly, K., Carey, M., Lluch, A., Monteagudo, C., He, X., Weigman, V., Fan, C., Palazzo, J., Hortobagyi, G.N., Nolden, L.K., Wang, N.J., Valero, V., Gray, J.W., Perou, C.M., and G.B. Mills. 2009. Characterization of a naturally occurring breast cancer subset enriched in epithelial-to-mesenchymal transition and stem cell characteristics. *Cancer Research*. 69(10):4116-4124.
- Hennighausen, L., and G.W. Robinson. 2005. Information networks in the mammary gland. *Nature reviews. Molecular cell biology*. 6:715-725.
- Herschkowitz, J.I., K. Simin, V.J. Weigman, I. Mikaelian, J. Usary, Z. Hu, K.E. Rasmussen, L.P. Jones, S. Assefnia, S. Chandrasekharan, M.G. Backlund, Y. Yin, A.I. Khramtsov, R. Bastein, J. Quackenbush, R.I. Glazer, P.H. Brown, J.E. Green, L. Kopelovich, P.A. Furth, J.P. Palazzo, O.I. Olopade, P.S. Bernard, G.A. Churchill, T. Van Dyke, and C.M. Perou. 2007. Identification of conserved gene expression features between murine mammary carcinoma models and human breast tumors. *Genome biology*. 8:R76.
- Hewitt, S.C., B.J. Deroo, K. Hansen, J. Collins, S. Grissom, C.A. Afshari, and K.S. Korach. 2003. Estrogen receptor-dependent genomic responses in the uterus mirror the biphasic physiological response to estrogen. *Molecular endocrinology*. 17:2070-2083.
- Hewitt, S.C., W. Winuthayanon, and K.S. Korach. 2016. What's new in estrogen receptor action in the female reproductive tract. *Journal of molecular endocrinology*. 56:R55-71.
- Hidalgo, M., F. Amant, A.V. Biankin, E. Budinska, A.T. Byrne, C. Caldas, R.B. Clarke, S. de Jong, J. Jonkers, G.M. Maelandsmo, S. Roman-Roman, J. Seoane, L. Trusolino, and A. Villanueva. 2014. Patient-derived xenograft models: an emerging platform for translational cancer research. *Cancer Discov*. 4:998-1013.
- Hinck, L., and G.B. Silberstein. 2005. Key stages in mammary gland development: the mammary end bud as a motile organ. *Breast cancer research : BCR*. 7:245-251.
- Hnisz, D., B.J. Abraham, T.I. Lee, A. Lau, V. Saint-Andre, A.A. Sigova, H.A. Hoke, and R.A. Young. 2013. Super-enhancers in the control of cell identity and disease. *Cell*. 155:934-947.
- Hoi, C.S., S.E. Lee, S.Y. Lu, D.J. McDermitt, K.M. Osorio, C.M. Piskun, R.M. Peters, R. Paus, and T. Tumber. 2010. Runx1 directly promotes proliferation of hair follicle stem cells and epithelial tumor formation in mouse skin. *Molecular and cellular biology*. 30:2518-2536.
- Holen, I., V. Speirs, B. Morrissey, and K. Blyth. 2017. In vivo models in breast cancer research: progress, challenges and future directions. *Disease models & mechanisms*. 10:359-371.
- Holliday, D.L., and V. Speirs. 2011. Choosing the right cell line for breast cancer research. *Breast cancer research : BCR*. 13:215.
- Holzapfel, B.M., Wagner, F., Thibaudeau, L., Levesque, J.P., and D.W. Huttmacher. 2015. Concise review: humanized models of tumor immunology in the 21st century: convergence of cancer research and tissue engineering. *Stem Cells*. 33(6):1696-1704.
- Hoover, R.N., M. Hyer, R.M. Pfeiffer, E. Adam, B. Bond, A.L. Cheville, T. Colton, P. Hartge, E.E. Hatch, A.L. Herbst, B.Y. Karlan, R. Kaufman, K.L. Noller, J.R. Palmer, S.J. Robboy, R.C. Saal, W. Strohsnitter, L. Titus-Ernstoff,

- and R. Troisi. 2011. Adverse health outcomes in women exposed in utero to diethylstilbestrol. *The New England journal of medicine*. 365:1304-1314.
- Hoshino, K. 1964. Regeneration and growth of quantitatively transplanted mammary glands of normal female mice. *The Anatomical Record*. 150:221-235.
- Huang, A.L., Ostrowski, M.C., Berard, D., and G.L. Hager. 1981. Glucocorticoid regulation of the Ha-MuSV p21 gene conferred by sequences from mouse mammary tumour virus. *Cell*. 27:245-255.
- Huang, G., K. Shigesada, K. Ito, H.J. Wee, T. Yokomizo, and Y. Ito. 2001. Dimerization with PEBP2beta protects RUNX1/AML1 from ubiquitin-proteasome-mediated degradation. *Embo J*. 20:723-733.
- Huang, S.P., Y.H. Lan, T.L. Lu, J.B. Pao, T.Y. Chang, H.Z. Lee, W.H. Yang, C.J. Hsieh, L.M. Chen, L.C. Huang, W.C. Ting, and B.Y. Bao. 2011. Clinical significance of runt-related transcription factor 1 polymorphism in prostate cancer. *BJU Int*. 107:486-492.
- Huang, B., Z. Qu, C.W. Ong, Y.H. Tsang, G. Xiao, D. Shapiro, M. Salto-Tellez, K. Ito, Y. Ito, and L.F. Chen. 2012. RUNX3 acts as a tumor suppressor in breast cancer by targeting estrogen receptor alpha. *Oncogene*. 31:527-534.
- Hwang, K.T., W. Han, J.Y. Bae, S.E. Hwang, H.J. Shin, J.E. Lee, S.W. Kim, H.J. Min, and D.Y. Noh. 2007. Downregulation of the RUNX3 gene by promoter hypermethylation and hemizygous deletion in breast cancer. *J Korean Med Sci*. 22:S24-31.
- Imbert, A., Eelkema, R., Jordan, S., Feiner, H., and P. Cowin. 2001. $\Delta n89B$ -catenin induces precocious development, differentiation, an neoplasia in mammary gland. *The Journal of Cell Biology*. 153(3):555-568.
- Incassati, A., Chandramouli, A., Eelkema, R., and P. Cowin. 2010. Key signaling nodes in mammary gland development and cancer: β -catenin. *Breast Cancer Research*. 12(6):213
- Inic, Z., M. Zegarac, M. Inic, I. Markovic, Z. Kozomara, I. Djuriscic, I. Inic, G. Pupic, and S. Jancic. 2014. Difference between Luminal A and Luminal B Subtypes According to Ki-67, Tumor Size, and Progesterone Receptor Negativity Providing Prognostic Information. *Clinical Medicine Insights. Oncology*. 8:107-111.
- Inman, J.L., C. Robertson, J.D. Mott, and M.J. Bissell. 2015. Mammary gland development: cell fate specification, stem cells and the microenvironment. *Development*. 142:1028-1042.
- Israel, M.A., Chan, H.W., Hourihan, S.A., Rowe, W.P., and M.A. Martin. 1979. Biological activity of polyoma viral DNA in mice and hamsters. *Journal of Virology*. 29:990-996.
- Ito, Y., S.C. Bae, and L.S. Chuang. 2015. The RUNX family: developmental regulators in cancer. *Nature reviews. Cancer*. 15:81-95.
- Jacks, T. 1996. Tumor suppressor gene mutations in mice. *Annual Review of Genetics*. 30:603-636.
- Jatoi, I., Hilsenbeck, S.G., Clark, G.M., and C.K. Osborne. 1999. Significance of axillary lymph node metastasis in primary breast cancer. *Journal of Clinical Oncology*. 17(8):2334-2340.
- Jensen, E.V. 1984. Intracellular localization of estrogen receptors: implications for interaction mechanism. *Lab Invest*. 51(5):487-488.
- Jiang, Y., D. Tong, G. Lou, Y. Zhang, and J. Geng. 2008. Expression of RUNX3 gene, methylation status and clinicopathological significance in breast

- cancer and breast cancer cell lines. *Pathobiology : journal of immunopathology, molecular and cellular biology*. 75:244-251.
- Jonkers, J., and A. Berns. 2002. Conditional mouse models of sporadic cancer. *Nature reviews. Cancer*. 2:251-265.
- Joshi, P.A., H.W. Jackson, A.G. Beristain, M.A. Di Grappa, P.A. Mote, C.L. Clarke, J. Stingl, P.D. Waterhouse, and R. Khokha. 2010. Progesterone induces adult mammary stem cell expansion. *Nature*. 465:803-807.
- Kadota, M., H.H. Yang, B. Gomez, M. Sato, R.J. Clifford, D. Meerzaman, B.K. Dunn, L.M. Wakefield, and M.P. Lee. 2010. Delineating genetic alterations for tumor progression in the MCF10A series of breast cancer cell lines. *PLoS One*. 5:0009201.
- Kaelin, W.G., Jr. 2005. The concept of synthetic lethality in the context of anticancer therapy. *Nature reviews. Cancer*. 5:689-698.
- Kagoshima, H., Shigesada, K., Satake, M., Ito, Y., Miyoshi, H., Ohki, M., Pepling, M., and P. Gergen. 1993. The runt domain identifies a new family of heteromeric transcriptional regulators. *Trends in Genetics*. 9(10):338-341.
- Kamachi, Y., E. Ogawa, M. Asano, S. Ishida, Y. Murakami, M. Satake, Y. Ito, and K. Shigesada. 1990. Purification of a mouse nuclear factor that binds to both the A and B cores of the polyomavirus enhancer. *Journal of Virology*. 64:4808-4819.
- Karn, T., L. Pusztai, U. Holtrich, T. Iwamoto, C.Y. Shiang, M. Schmidt, V. Muller, C. Solbach, R. Gaetje, L. Hanker, A. Ahr, C. Liedtke, E. Ruckhaberle, M. Kaufmann, and A. Rody. 2011. Homogeneous datasets of triple negative breast cancers enable the identification of novel prognostic and predictive signatures. *PLoS One*. 6:29.
- Kendrick, H., J.L. Regan, F.A. Magnay, A. Grigoriadis, C. Mitsopoulos, M. Zvelebil, and M.J. Smalley. 2008. Transcriptome analysis of mammary epithelial subpopulations identifies novel determinants of lineage commitment and cell fate. *BMC genomics*. 9:591.
- Kersten, K., K.E. de Visser, M.H. van Miltenburg, and J. Jonkers. 2017. Genetically engineered mouse models in oncology research and cancer medicine. *EMBO molecular medicine*. 9:137-153.
- Kishida, S., Yamamoto, H., Hino, S, Ikeda, S., Kishida, M., and A. Kikuchi. 1999. DIX domains of Dvl and Axin are necessary for protein interactions and their ability to regulate beta-catenin stability. *Molecular and Cellular Biology*. 19(6):4414-4422.
- Knoblich, J.A. 2010. Asymmetric cell division: recent developments and their implications for tumour biology. *Nature reviews. Molecular cell biology*. 11:849-860.
- Kordon, E.C., and G.H. Smith. 1998. An entire functional mammary gland may comprise the progeny from a single cell. *Development*. 125(10):1921-1930.
- Koren, S., and M. Bentires-Alj. 2015. Breast Tumor Heterogeneity: Source of Fitness, Hurdle for Therapy. *Molecular cell*. 60:537-546.
- Kushner, P.J., D.A. Agard, G.L. Greene, T.S. Scanlan, A.K. Shiau, R.M. Uht, and P. Webb. 2000. Estrogen receptor pathways to AP-1. *The Journal of Steroid Biochemistry and Molecular Biology*. 74:311-317.
- Landis, M.D., Lehmann, B.D., Pietenpol, J.A., and J.C. Chang. 2013. Patient-derived breast tumour xenografts facilitating personalized cancer therapy. *Breast Cancer Research*. 15(1):201.
- Lasfargues, E.Y., and L. Ozzello. 1958. Cultivation of human breast carcinomas. *J Natl Cancer Inst*. 21:1131-1147.

- Levanon, D., Y. Bernstein, V. Negreanu, M.C. Ghazi, I. Bar-Am, R. Aloya, D. Goldenberg, J. Lotem, and Y. Groner. 1996. A large variety of alternatively spliced and differentially expressed mRNAs are encoded by the human acute myeloid leukemia gene AML1. *DNA Cell Biol.* 15:175-185.
- Li, Z., J. Yan, C.J. Matheny, T. Corpora, J. Bravo, A.J. Warren, J.H. Bushweller, and N.A. Speck. 2003. Energetic contribution of residues in the Runx1 Runt domain to DNA binding. *The Journal of biological chemistry.* 278:33088-33096.
- Lim, E., F. Vaillant, D. Wu, N.C. Forrest, B. Pal, A.H. Hart, M.L. Asselin-Labat, D.E. Gyorki, T. Ward, A. Partanen, F. Feleppa, L.I. Huschtscha, H.J. Thorne, kConFab, S.B. Fox, M. Yan, J.D. French, M.A. Brown, G.K. Smyth, J.E. Visvader, and G.J. Lindeman. 2009. Aberrant luminal progenitors as the candidate target population for basal tumor development in BRCA1 mutation carriers. *Nature medicine.* 15:907-913.
- Lin, SY., Xia, W., Wang, J.C., Kwong, K.Y., Spohn, B., Wen, Y., Pestell, R.G., and MC. Hung. 2000. β -catenin, a novel prognostic marker for breast cancer: its roles in cyclin D1 expression and cancer progression. *Proceedings of the National Academy of Sciences of the United States of America.* 97(8):44262-4266.
- Lin, H. 2002. The stem-cell niche theory: lessons from flies. *Nat Rev Genet.* 3:931-940.
- Lin, E.Y., Jones, J.G., Li, P., Zhu, L., Whitney, K.D., Muller, W.J., and J.W. Pollard. 2003. Progression to malignancy in the polyoma middle T oncoprotein mouse breast cancer model provides a reliable model for human diseases. *American Journal of Pathology.* 163(5):2113-2126.
- Liu, B.Y., McDermott, S.P., Khwaje, S.S., and C.M. Alexander. 2004. The transforming activity of Wnt effectors correlates with their ability to induce the accumulation of mammary progenitor cells. *Proceedings of the National Academy of Sciences of the United States of America.* 101(12):4158-4163.
- Liu, Y.N., W.W. Lee, C.Y. Wang, T.H. Chao, Y. Chen, and J.H. Chen. 2005. Regulatory mechanisms controlling human E-cadherin gene expression. *Oncogene.* 24:8277-8290.
- Lloyd-Lewis, B., O.B. Harris, C.J. Watson, and F.M. Davis. 2017. Mammary Stem Cells: Premise, Properties, and Perspectives. *Trends in cell biology.* 27:556-567.
- Lord, C.J., and A. Ashworth. 2008. Targeted therapy for cancer using PARP inhibitors. *Current opinion in pharmacology.* 8:363-369.
- Luche, H., O. Weber, T. Nageswara Rao, C. Blum, and H.J. Fehling. 2007. Faithful activation of an extra-bright red fluorescent protein in "knock-in" Cre-reporter mice ideally suited for lineage tracing studies. *European journal of immunology.* 37:43-53.
- Lydon, J.P., F.J. DeMayo, C.R. Funk, S.K. Mani, A.R. Hughes, C.A. Montgomery, Jr., G. Shyamala, O.M. Conneely, and B.W. O'Malley. 1995. Mice lacking progesterone receptor exhibit pleiotropic reproductive abnormalities. *Genes Dev.* 9:2266-2278.
- Lyons, T.R., P.J. Schedin, and V.F. Borges. 2009. Pregnancy and breast cancer: when they collide. *J Mammary Gland Biol Neoplasia.* 14:87-98.
- Macias, H., and L. Hinck. 2012. Mammary gland development. *Wiley interdisciplinary reviews. Developmental biology.* 1:533-557.
- Malaney, P., S.V. Nicosia, and V. Dave. 2014. One mouse, one patient paradigm: New avatars of personalized cancer therapy. *Cancer letters.* 344:1-12.

- Malhotra, G.K., Zhao, X., Band, H., and V. Band. 2010. Histological, molecular, and functional subtypes of breast cancer. *Cancer Biology & Therapy*. 10(10):955-960.
- Mallepell, S., A. Krust, P. Chambon, and C. Brisken. 2006. Paracrine signaling through the epithelial estrogen receptor alpha is required for proliferation and morphogenesis in the mammary gland. *Proceedings of the National Academy of Sciences of the United States of America*. 103:2196-2201.
- Marouf, C., S. Gohler, M.I. Filho, O. Hajji, K. Hemminki, S. Nadifi, and A. Forsti. 2016. Analysis of functional germline variants in APOBEC3 and driver genes on breast cancer risk in Moroccan study population. *BMC Cancer*. 16:016-2210.
- Masters, J.R.W., Drife, J.O., and J.J. Scarisbrick. 1977. Cyclic variation of DNA synthesis in human breast epithelium. *Journal of the National Cancer Institute*. 58(5):1263-1265.
- McCormack, V.A., and I. dos Santos Silva. 2006. Breast density and parenchymal patterns as markers of breast cancer risk: a meta-analysis. *Cancer epidemiology, biomarkers & prevention: a publication of the American Association for Cancer Research, cosponsored by the American Society of Preventive Oncology*. 15:1159-1169.
- McDonald, L., N. Ferrari, A. Terry, M. Bell, Z.M. Mohammed, C. Orange, A. Jenkins, W.J. Muller, B.A. Gusterson, J.C. Neil, J. Edwards, J.S. Morris, E.R. Cameron, and K. Blyth. 2014. RUNX2 correlates with subtype-specific breast cancer in a human tissue microarray, and ectopic expression of Runx2 perturbs differentiation in the mouse mammary gland. *Disease models & mechanisms*. 7:525-534.
- Medina, D. 1996. The mammary gland: a unique organ for the study of development and tumorigenesis. *J Mammary Gland Biol Neoplasia*. 1:5-19.
- Meier-Abt, F., Milani, E., Roloff, T., Brinkhaus, H., Duss, S., Meyer, D.S., Klebba, I., Balwierz, P.J., van Nimwegen, E., and M. Bentires-Alj. 2013. Parity induces differentiation and reduces Wnt/Notch signaling ratio and proliferation potential of basal stem/progenitor cells isolated from mouse mammary epithelium. *Breast Cancer Research*. 15(2):R36.
- Meyers, S., Downing, J.R., and S.W. Hiebert. 1993. Identification of AML-1 and the (8;21) translocation protein (AML-1/ETO) as sequence-specific DNA-binding proteins: the *runt* homology domain is required for DNA binding and protein-protein interactions. *Molecular and Cellular Biology*. 13(10):6336-6345.
- Michaelson, J.S., and P. Leder. 2001. β -catenin is a downstream effector of Wnt-mediated tumourigenesis in mammary gland. *Oncogene*. 20(37):5093-5099.
- Miyagawa, K., C. Sakakura, S. Nakashima, T. Yoshikawa, S. Kin, Y. Nakase, K. Ito, H. Yamagishi, H. Ida, S. Yazumi, T. Chiba, Y. Ito, and A. Hagiwara. 2006. Down-regulation of RUNX1, RUNX3 and CBFbeta in hepatocellular carcinomas in an early stage of hepatocarcinogenesis. *Anticancer Res*. 26:3633-3643.
- Miyoshi, Y., Nagase, H., Ando, H., Ichii, S., Nakatsura, S., Aoki, T., Miki, Y., Mori, T., and Y. Nakamura. 1992. Somatic mutations of the APC gene in colorectal tumors: mutation cluster region in the APC gene. *Human Molecular Genetics*. 1(4):229-233.
- Miyoshi, Y., Iwao, K., Nagasawa, Y., Aihara, T., Sasaki, Y., Imaoka, S., Murata, M., Shimano, T., and Y. Nakamura. 1998. Activation of the β -catenin gene

- in primary hepatocellular carcinomas by somatic alterations involving exon 3. *Cancer Research*. 58(12):2524-2527.
- Miyoshi, H., M. Ohira, K. Shimizu, K. Mitani, H. Hirai, T. Imai, K. Yokoyama, E. Soeda, and M. Ohki. 1995. Alternative splicing and genomic structure of the AML1 gene involved in acute myeloid leukemia. *Nucleic Acids Res.* 23:2762-2769.
- Miyoshi, K., Shillingford, J.M., Le Provost, F., Gounari, F., Bronson, R., von Boehmer, H., Taketo, M.M., Cardiff, R.D., Henninghausen, L., and K. Khazaie. 2002. Activation of β -catenin signaling in differentiated mammary secretory cells induces transdifferentiation into epidermis and squamous metaplasias. *Proceedings of the National Academy of Sciences of the United States of America*. 99(1):219-224.
- Molyneux, G., F.C. Geyer, F.A. Magnay, A. McCarthy, H. Kendrick, R. Natrajan, A. Mackay, A. Grigoriadis, A. Tutt, A. Ashworth, J.S. Reis-Filho, and M.J. Smalley. 2010. BRCA1 basal-like breast cancers originate from luminal epithelial progenitors and not from basal stem cells. *Cell stem cell*. 7:403-417.
- Mukherjee, A., S.M. Soyak, J. Li, Y. Ying, B. He, F.J. DeMayo, and J.P. Lydon. 2010. Targeting RANKL to a specific subset of murine mammary epithelial cells induces ordered branching morphogenesis and alveologenesis in the absence of progesterone receptor expression. *FASEB journal : official publication of the Federation of American Societies for Experimental Biology*. 24:4408-4419.
- Mulac-Jericevic, B., J.P. Lydon, F.J. DeMayo, and O.M. Conneely. 2003. Defective mammary gland morphogenesis in mice lacking the progesterone receptor B isoform. *Proceedings of the National Academy of Sciences of the United States of America*. 100:9744-9749.
- Muller, W.J., Sinn, E., Pattengale, P.K., Wallace, R., and P. Leder. 1988. Single-step induction of mammary adenocarcinoma in transgenic mice bearing the activated c-neu oncogene. *Cell*. 54(1):105-115.
- Nik-Zainal, S., H. Davies, J. Staaf, M. Ramakrishna, D. Glodzik, X. Zou, I. Martincorena, L.B. Alexandrov, S. Martin, D.C. Wedge, P. Van Loo, Y.S. Ju, M. Smid, A.B. Brinkman, S. Morganella, M.R. Aure, O.C. Lingjaerde, A. Langerod, M. Ringner, S.M. Ahn, S. Boyault, J.E. Brock, A. Broeks, A. Butler, C. Desmedt, L. Dirix, S. Dronov, A. Fatima, J.A. Foekens, M. Gerstung, G.K. Hooijer, S.J. Jang, D.R. Jones, H.Y. Kim, T.A. King, S. Krishnamurthy, H.J. Lee, J.Y. Lee, Y. Li, S. McLaren, A. Menzies, V. Mustonen, S. O'Meara, I. Pauporte, X. Pivot, C.A. Purdie, K. Raine, K. Ramakrishnan, F.G. Rodriguez-Gonzalez, G. Romieu, A.M. Sieuwerts, P.T. Simpson, R. Shepherd, L. Stebbings, O.A. Stefansson, J. Teague, S. Tommasi, I. Treilleux, G.G. Van den Eynden, P. Vermeulen, A. Vincent-Salomon, L. Yates, C. Caldas, L. van't Veer, A. Tutt, S. Knappskog, B.K. Tan, J. Jonkers, A. Borg, N.T. Ueno, C. Sotiriou, A. Viari, P.A. Futreal, P.J. Campbell, P.N. Span, S. Van Laere, S.R. Lakhani, J.E. Eyfjord, A.M. Thompson, E. Birney, H.G. Stunnenberg, M.J. van de Vijver, J.W. Martens, A.L. Borresen-Dale, A.L. Richardson, G. Kong, G. Thomas, and M.R. Stratton. 2016. Landscape of somatic mutations in 560 breast cancer whole-genome sequences. *Nature*. 534:47-54.
- Norum, J.H., K. Andersen, and T. Sorlie. 2014. Lessons learned from the intrinsic subtypes of breast cancer in the quest for precision therapy. *The British journal of surgery*. 101:925-938.

- Novak, A., Guo, C., Yang, W., Nagy, A., and C.G. Lobe. 2000. Z/EG, a double reporter mouse line that expresses enhanced green fluorescent protein upon cre-mediated excision. *Genesis*. 28(3-4):147-155.
- Nowell, P.C. 1976. The clonal evolution of tumor cell populations. *Science*. 194(4260):23-28.
- Nusse, R., and H.E. Varmua. 1982. Many tumors induced by the mouse mammary tumor virus contain a provirus integrated in the same region of the host genome. *Cell*. 31(1):99-109.
- Ogawa, E., M. Maruyama, H. Kagoshima, M. Inuzuka, J. Lu, M. Satake, K. Shigesada, and Y. Ito. 1993. PEBP2/PEA2 represents a family of transcription factors homologous to the products of the Drosophila runt gene and the human AML1 gene. *Proceedings of the National Academy of Sciences of the United States of America*. 90:6859-6863.
- Okuda, T., J. van Deursen, S.W. Hiebert, G. Grosveld, and J.R. Downing. 1996. AML1, the target of multiple chromosomal translocations in human leukemia, is essential for normal fetal liver hematopoiesis. *Cell*. 84:321-330.
- Osato, M., Asou, N., Abdalla, E., Hoshino, K., Yamasaki, H., Okubo, T., Suzushima, H., Takatsuki, K., Kanno, T., Shigesada, K., and Y. Ito. 1999. Biallelic and heterozygous point mutations in the runt domain of the AML1/PEBP2alphaB gene associated with myeloblastic leukemias. *Blood*. 93(6):1817-1824.
- Osborne, C.K., Yochmowitz, M.G., Knight, W.A. 3rd, and W.L. McGuire. 1980. The value of estrogen and progesterone receptors in the treatment of breast cancer. *Cancer*. 46(12 Suppl):2884-2888.
- Owens, T.W., R.L. Rogers, S.A. Best, A. Ledger, A.M. Mooney, A. Ferguson, P. Shore, A. Swarbrick, C.J. Ormandy, P.T. Simpson, J.S. Carroll, J.E. Visvader, and M.J. Naylor. 2014. Runx2 is a novel regulator of mammary epithelial cell fate in development and breast cancer. *Cancer research*. 74:5277-5286.
- Palacios, J., and C. Gamallo. 1998. Mutations in the β -catenin gene (*CTNNB1*) in endometrioid ovarian carcinomas. *Cancer Research*. 58(7):1344-1347.
- Parimi, V., R. Goyal, K. Poropatich, and X.J. Yang. 2014. Neuroendocrine differentiation of prostate cancer: a review. *American Journal of Clinical and Experimental Urology*. 2:273-285.
- Pereira, B., S.F. Chin, O.M. Rueda, H.K. Volland, E. Provenzano, H.A. Bardwell, M. Pugh, L. Jones, R. Russell, S.J. Sammut, D.W. Tsui, B. Liu, S.J. Dawson, J. Abraham, H. Northen, J.F. Peden, A. Mukherjee, G. Turashvili, A.R. Green, S. McKinney, A. Oloumi, S. Shah, N. Rosenfeld, L. Murphy, D.R. Bentley, I.O. Ellis, A. Purushotham, S.E. Pinder, A.L. Borresen-Dale, H.M. Earl, P.D. Pharoah, M.T. Ross, S. Aparicio, and C. Caldas. 2016. The somatic mutation profiles of 2,433 breast cancers refines their genomic and transcriptomic landscapes. *Nature communications*. 7:11479.
- Perou, C.M., T. Sorlie, M.B. Eisen, M. van de Rijn, S.S. Jeffrey, C.A. Rees, J.R. Pollack, D.T. Ross, H. Johnsen, L.A. Akslen, O. Fluge, A. Pergamenschikov, C. Williams, S.X. Zhu, P.E. Lonning, A.L. Borresen-Dale, P.O. Brown, and D. Botstein. 2000. Molecular portraits of human breast tumours. *Nature*. 406:747-752.
- Petersen, O.W., Ronnov-Jessen, L., Howlett, A.R., and M.J. Bissell. 1992. Interaction with basement membrane serves to rapidly distinguish growth and differentiation pattern of normal and malignant human breast

- epithelial cells. *Proceedings of the National Academy of Sciences of the United States of America*. 89(19):9064-9068.
- Plaks, V., A. Brenot, D.A. Lawson, J.R. Linnemann, E.C. Van Kappel, K.C. Wong, F. de Sauvage, O.D. Klein, and Z. Werb. 2013. Lgr5-expressing cells are sufficient and necessary for postnatal mammary gland organogenesis. *Cell reports*. 3:70-78.
- Polakis, P. 1999. The oncogenic activation of β -catenin. *Current Opinion in Genetics and Development*. 9(1):15-21.
- Polakis, P. 2000. Wnt signaling and cancer. *Genes and Development*. 14:1837-1851.
- Prat, A., J.S. Parker, O. Karginova, C. Fan, C. Livasy, J.I. Herschkowitz, X. He, and C.M. Perou. 2010. Phenotypic and molecular characterization of the claudin-low intrinsic subtype of breast cancer. *Breast cancer research : BCR*. 12:R68.
- Rajaram, R.D., D. Buric, M. Caikovski, A. Ayyanan, J. Rougemont, J. Shan, S.J. Vainio, O. Yalcin-Ozuysal, and C. Brisken. 2015. Progesterone and Wnt4 control mammary stem cells via myoepithelial crosstalk. *The EMBO Journal*. 34:641-652.
- Rakha, E.A., J.S. Reis-Filho, F. Baehner, D.J. Dabbs, T. Decker, V. Eusebi, S.B. Fox, S. Ichihara, J. Jacquemier, S.R. Lakhani, J. Palacios, A.L. Richardson, S.J. Schnitt, F.C. Schmitt, P.H. Tan, G.M. Tse, S. Badve, and I.O. Ellis. 2010. Breast cancer prognostic classification in the molecular era: the role of histological grade. *Breast cancer research*. 12:207.
- Ramaswamy, S., K.N. Ross, E.S. Lander, and T.R. Golub. 2003. A molecular signature of metastasis in primary solid tumors. *Nature genetics*. 33:49-54.
- Regan, J.L., H. Kendrick, F.A. Magnay, V. Vafaizadeh, B. Groner, and M.J. Smalley. 2012. c-Kit is required for growth and survival of the cells of origin of Brca1-mutation-associated breast cancer. *Oncogene*. 31:869-883.
- Reya, T., and H. Clevers. 2005. Wnt signalling in stem cells and cancer. *Nature*. 434(7035):843-850.
- Reynolds, B.A., and S. Weiss. 1992. Generation of neurons and astrocytes from isolated cells of the adult mammalian central nervous system. *Science*. 255(5052):1707-1710.
- Richard, E., T. Grellety, V. Velasco, G. MacGrogan, H. Bonnefoi, and R. Iggo. 2016. The mammary ducts create a favourable microenvironment for xenografting of luminal and molecular apocrine breast tumours. *The Journal of pathology*. 240:256-261.
- Riggio, A.I., and K. Blyth. 2017. The enigmatic role of RUNX1 in female-related cancers - current knowledge & future perspectives. *The FEBS journal*. 284:2345-2362.
- Rijsewijk, F., Schuermann, M., Wagenaar, E., Parren, P., Weigel, D., and R. Nusse. 1987. The *Drosophila* homolog of the mouse mammary oncogene *int-1* is identical to the segment polarity gene *wingless*. *Cell*. 50(4):649-657.
- Rios, A.C., N.Y. Fu, J. Cursons, G.J. Lindeman, and J.E. Visvader. 2016. The complexities and caveats of lineage tracing in the mammary gland. *Breast cancer research*. 18:116.
- Rios, A.C., N.Y. Fu, G.J. Lindeman, and J.E. Visvader. 2014. In situ identification of bipotent stem cells in the mammary gland. *Nature*. 506:322-327.

- Rodilla, V., Dasti, A., Huyghe, M., Lafkas, D., Laurent, C., Reyal, F., and S.Fre. 2015. Luminal progenitors restrict their lineage potential during mammary gland development. *PLoS Biology*. 13(2):e1002069.
- Rody, A., T. Karn, C. Liedtke, L. Pusztai, E. Ruckhaeberle, L. Hanker, R. Gaetje, C. Solbach, A. Ahr, D. Metzler, M. Schmidt, V. Muller, U. Holtrich, and M. Kaufmann. 2011. A clinically relevant gene signature in triple negative and basal-like breast cancer. *Breast cancer research*.13(5):R97.
- Roelink, H., Wagenaar, E., Lopes da Silva, S., and R. Nusse. 1990. Wnt-3, a gene activated by proviral insertion in mouse mammary tumours, is homologous to int-1/Wnt-1 and is normally expressed in mouse embryos and adult brain. *Proceedings of the National Academy of Sciences of the United States of America*. 87(12):4519-4523.
- Rooney, N., Riggio, A.I., Mendoza-Villanueva, D., Shore, P., Cameron, E.R., and K. Blyth. 2017. Run genes in breast cancer and the mammary lineage. *Advances in Experimental Medicine and Biology*. 962:353-368.
- Ross, J.S., E.A. Slodkowska, W.F. Symmans, L. Pusztai, P.M. Ravdin, and G.N. Hortobagyi. 2009. The HER-2 receptor and breast cancer: ten years of targeted anti-HER-2 therapy and personalized medicine. *The oncologist*. 14:320-368.
- Roumier, C., V. Eclache, M. Imbert, F. Davi, E. MacIntyre, R. Garand, P. Talmant, P. Lepelley, J.L. Lai, O. Casasnovas, M. Maynadie, F. Mugneret, C. Bilhou-Naberra, F. Valensi, I. Radford, M.J. Mozziconacci, C. Arnoulet, E. Duchayne, N. Dastugue, P. Cornillet, S. Daliphard, F. Garnache, N. Boudjerra, H. Jouault, O. Fenneteau, B. Pedron, R. Berger, G. Flandrin, P. Fenaux, C. Preudhomme, H. Groupe Francais de Cytogenetique, and C. Groupe Francais d'Hematologie. 2003. M0 AML, clinical and biologic features of the disease, including AML1 gene mutations: a report of 59 cases by the Groupe Francais d'Hematologie Cellulaire (GFHC) and the Groupe Francais de Cytogenetique Hematologique (GFCH). *Blood*. 101:1277-1283.
- Russo, J., L.K. Tay, D.R. Ciocca, and I.H. Russo. 1983. Molecular and cellular basis of the mammary gland susceptibility to carcinogenesis. *Environ Health Perspect*. 49:185-199.
- Russo, J., Ao, X., Grill, C., and I.H. Russo. 1999. Pattern of distribution of cells positive for estrogen receptor alpha and progesterone receptor in relation to proliferating cells in the mammary gland. *Breast Cancer Research and Treatment*. 53(3):217-227.
- Russo, J., R. Moral, G.A. Balogh, D. Mailo, and I.H. Russo. 2005. The protective role of pregnancy in breast cancer. *Breast cancer research*. 7:131-142.
- Safe, S., and K. Kim. 2008. Non-classical genomic estrogen receptor (ER)/specificity protein and ER/activating protein-1 signaling pathways. *Journal of molecular endocrinology*. 41:263-275.
- Saji, S., Jensen, E.V., Nilsson, S., Rylander, T., Warner, M., and J.A. Gustafsson. 2000. Estrogen receptors alpha and beta in the rodent mammary gland. *Proceedings of the National Academy of Sciences of the United States of America*. 97(1):337-342.
- Sakakura, C., A. Hagiwara, K. Miyagawa, S. Nakashima, T. Yoshikawa, S. Kin, Y. Nakase, K. Ito, H. Yamagishi, S. Yazumi, T. Chiba, and Y. Ito. 2005. Frequent downregulation of the runt domain transcription factors RUNX1, RUNX3 and their cofactor CBF β in gastric cancer. *International journal of cancer*. 113:221-228.

- Samokhvalov, I.M., N.I. Samokhvalova, and S. Nishikawa. 2007. Cell tracing shows the contribution of the yolk sac to adult haematopoiesis. *Nature*. 446:1056-1061.
- Schroeder, J.A., and D.C. Lee. 1998. Dynamic expression and activation of ERBB receptors in the developing mouse mammary gland. *Cell Growth and Differentiation*. 9(6):451-464.
- Schuijers, J., Junker, J.P., Mokry, M., Hatzis, P., Koo, B.K., Sasselli, V., van der Flier, L.G., Cuppen, E., van Oudenaarden, A., and H. Clevers. 2015. Ascl2 acts as an R-spondin/Wnt-responsive switch to control stemness in intestinal crypts. *Cell Stem Cell*. 16(2):158-170.
- Selbert, S., Bentley, D.J., Melton, D.W., Rannie, D., Lourenco, P., Watson, C.J., and A.R. Clarke. 1998. Efficient BLG-Cre mediated gene deletion in the mammary gland. *Transgenic Research*. 7(5):387-396.
- Sflomos, G., V. Dormoy, T. Metsalu, R. Jeitziner, L. Battista, V. Scabia, W. Raffoul, J.F. Delaloye, A. Treboux, M. Fiche, J. Vilo, A. Ayyanan, and C. Brisken. 2016. A Preclinical Model for ERalpha-Positive Breast Cancer Points to the Epithelial Microenvironment as Determinant of Luminal Phenotype and Hormone Response. *Cancer cell*. 29:407-422.
- Shackleton, M., F. Vaillant, K.J. Simpson, J. Stingl, G.K. Smyth, M.L. Asselin-Labat, L. Wu, G.J. Lindeman, and J.E. Visvader. 2006. Generation of a functional mammary gland from a single stem cell. *Nature*. 439:84-88.
- Shehata, M., A. Teschendorff, G. Sharp, N. Novcic, I.A. Russell, S. Avril, M. Prater, P. Eirew, C. Caldas, C.J. Watson, and J. Stingl. 2012. Phenotypic and functional characterisation of the luminal cell hierarchy of the mammary gland. *Breast cancer research*. 14:R134.
- Shipitsin, M., L.L. Campbell, P. Argani, S. Weremowicz, N. Bloushtain-Qimron, J. Yao, T. Nikolskaya, T. Serebryiskaya, R. Beroukhim, M. Hu, M.K. Halushka, S. Sukumar, L.M. Parker, K.S. Anderson, L.N. Harris, J.E. Garber, A.L. Richardson, S.J. Schnitt, Y. Nikolsky, R.S. Gelman, and K. Polyak. 2007. Molecular definition of breast tumor heterogeneity. *Cancer cell*. 11:259-273.
- Shoker, B.S., Jarvis, C., Clarke, R.B., Anderson, E., Hewlett, J., Davies, M.P.A., Sibson, D.R., and J.P. Sloane. 1999. Estrogen receptor-positive proliferating cells in the normal and precancerous breast. *American Journal of Pathology*. 155(6):1811-1815.
- Shyamala, G., Chou, Y.C., Louie, S.G., Guzman, R.C., Smith, G.H., and S. Nandi. 2002. Cellular expression of estrogen and progesterone receptors in mammary glands: regulation by hormones, development and aging. *The Journal of Steroid Biochemistry and Molecular Biology*. 80(2):137-148.
- Siddharta, M. 2010. The emperor of all maladies: a biography of cancer.
- Sinn, E., Muller, W., Pattengale, P., Tepler, I., Wallace, R., and P. Leder. 1987. Coexpression of MMTV/v-Ha-ras and MMTV/c-myc genes in transgenic mice: synergistic action of oncogenes in vivo. *Cell*. 49(4):465-475.
- Slattery, M.L., A. Lundgreen, J.S. Herrick, B.J. Caan, J.D. Potter, and R.K. Wolff. 2011. Associations between genetic variation in RUNX1, RUNX2, RUNX3, MAPK1 and eIF4E and risk of colon and rectal cancer: additional support for a TGF-beta-signaling pathway. *Carcinogenesis*. 32:318-326.
- Sleeman, K.E., H. Kendrick, D. Robertson, C.M. Isacke, A. Ashworth, and M.J. Smalley. 2007. Dissociation of estrogen receptor expression and in vivo stem cell activity in the mammary gland. *The Journal of cell biology*. 176:19-26.

- Smalley, M.J., Titley, J., and M.J. O'Hare. 1998. Clonal characterization of mouse mammary luminal epithelial and myoepithelial cells separated by fluorescence-activated cell sorting. *In Vitro Cellular and Developmental Biology*. 34(9):711-721.
- Smith, G.H. 1996. Experimental mammary epithelial morphogenesis in an in vivo model: evidence for distinct cellular progenitors of the ductal and lobular phenotype. *Breast Cancer Research and Treatment*. 39(1):21-31.
- Smith, G.H. 2005. Label-retaining epithelial cells in mouse mammary gland divide asymmetrically and retain their template DNA strands. *Development*. 132:681-687.
- Sokol, E.S., S. Sanduja, D.X. Jin, D.H. Miller, R.A. Mathis, and P.B. Gupta. 2015. Perturbation-expression analysis identifies RUNX1 as a regulator of human mammary stem cell differentiation. *PLoS computational biology*. 11:e1004161.
- Sorlie, T., C.M. Perou, R. Tibshirani, T. Aas, S. Geisler, H. Johnsen, T. Hastie, M.B. Eisen, M. van de Rijn, S.S. Jeffrey, T. Thorsen, H. Quist, J.C. Matese, P.O. Brown, D. Botstein, P.E. Lonning, and A.L. Borresen-Dale. 2001. Gene expression patterns of breast carcinomas distinguish tumor subclasses with clinical implications. *Proceedings of the National Academy of Sciences of the United States of America*. 98:10869-10874.
- Sorlie, T., R. Tibshirani, J. Parker, T. Hastie, J.S. Marron, A. Nobel, S. Deng, H. Johnsen, R. Pesich, S. Geisler, J. Demeter, C.M. Perou, P.E. Lonning, P.O. Brown, A.L. Borresen-Dale, and D. Botstein. 2003. Repeated observation of breast tumor subtypes in independent gene expression data sets. *Proceedings of the National Academy of Sciences of the United States of America*. 100:8418-8423.
- Soule, H.D., Vasquez, J., Long, A., Albert, S., and M. Brennan. 1973. A human cell line from a pleural effusion derived from a breast carcinoma. *Journal of the National Cancer Institute*. 51: 1409-1413.
- Spangrude, G.J., Heimfeld, S., and I.L. Weissman. 1988. Purification and characterization of mouse hematopoietic stem cells. *Science*. 241(4861):58-62.
- Spike, B.T., D.D. Engle, J.C. Lin, S.K. Cheung, J. La, and G.M. Wahl. 2012. A mammary stem cell population identified and characterized in late embryogenesis reveals similarities to human breast cancer. *Cell stem cell*. 10:183-197.
- Sree, S.V., E.Y. Ng, R.U. Acharya, and O. Faust. 2011. Breast imaging: A survey. *World journal of clinical oncology*. 2:171-178.
- Stender, J.D., K. Kim, T.H. Charn, B. Komm, K.C. Chang, W.L. Kraus, C. Benner, C.K. Glass, and B.S. Katzenellenbogen. 2010. Genome-wide analysis of estrogen receptor alpha DNA binding and tethering mechanisms identifies Runx1 as a novel tethering factor in receptor-mediated transcriptional activation. *Molecular and cellular biology*. 30:3943-3955.
- Sternlicht, M.D., S.W. Sunnarborg, H. Kouros-Mehr, Y. Yu, D.C. Lee, and Z. Werb. 2005. Mammary ductal morphogenesis requires paracrine activation of stromal EGFR via ADAM17-dependent shedding of epithelial amphiregulin. *Development*. 132:3923-3933.
- Stewart, T.A., Pattengale, P.K., and P. Leder. 1984. Spontaneous mammary adenocarcinomas in transgenic mice that carry and express MTV/myc fusion genes. *Cell*. 38:627-637.
- Stingl, J., and C. Caldas. 2007. Molecular heterogeneity of breast carcinomas and the cancer stem cell hypothesis. *Nature reviews. Cancer*. 7:791-799.

- Stingl, J., P. Eirew, I. Ricketson, M. Shackleton, F. Vaillant, D. Choi, H.I. Li, and C.J. Eaves. 2006. Purification and unique properties of mammary epithelial stem cells. *Nature*. 439:993-997.
- Streuli, C.H., and A.P. Gilmore. 1999. Adhesion-mediated signaling in the regulation of mammary epithelial cell survival. *Journal of Mammary Gland Biology and Neoplasia*. 4(2):183-191.
- Stumpf, W.E., Narbaitz, R., and M. Sar. 1980. Estrogen receptors in the fetal mouse. *Journal of Steroid Biochemistry*. 12:55-64.
- Talmage, D.A., Freund, R., Young, A.T., Dahl, J., Dawe, C.J., and T.L. Benjamin. 1989. Phosphorylation of middle T by pp60 c-src: a switch for binding of phosphatidylinositol 3-kinase and optimal tumorigenesis. *Cell*. 59:55-65.
- Tanaka, T., M. Kurokawa, K. Ueki, K. Tanaka, Y. Imai, K. Mitani, K. Okazaki, N. Sagata, Y. Yazaki, Y. Shibata, T. Kadowaki, and H. Hirai. 1996. The extracellular signal-regulated kinase pathway phosphorylates AML1, an acute myeloid leukemia gene product, and potentially regulates its transactivation ability. *Molecular and cellular biology*. 16:3967-3979.
- Tanos, T., L. Rojo, P. Echeverria, and C. Brisken. 2012. ER and PR signaling nodes during mammary gland development. *Breast cancer research*. 14:210.
- Teissedre, B., Pinderhughes, A., Incassati, A., Hatsell, S.J., Hiremath, M., and P. Cowin. 2009. *PLoS One*. 4(2):e4537.
- Teuliere, J., Faraldo, M.M., Deugnier, MA., Shtuman, M., Ben-Ze'ev, A., Thiery, J.P., and M.A. Glukhova. 2004. Targeted activation of β -catenin signaling in basal mammary epithelial cells affects mammary development and leads to hyperplasia. *Development*. 132(2):267-277.
- Torre, L.A., R.L. Siegel, E.M. Ward, and A. Jemal. 2016. Global Cancer Incidence and Mortality Rates and Trends--An Update. *Cancer epidemiology, biomarkers & prevention: a publication of the American Association for Cancer Research, cosponsored by the American Society of Preventive Oncology*. 25:16-27.
- Torti, D., and L. Trusolino. 2011. Oncogene addiction as a foundational rationale for targeted anti-cancer therapy: promises and perils. *EMBO molecular medicine*. 3:623-636.
- Trejo, C.L., G. Luna, C. Dravis, B.T. Spike, and G.M. Wahl. 2017. Lgr5 is a marker for fetal mammary stem cells, but is not essential for stem cell activity or tumorigenesis. *NPJ breast cancer*. 3:16.
- Yamagata, T, Maki, K., and I. Mitani. 2005. Runx1/AML1 in normal and abnormal hematopoiesis. *International Journal of Hematology*. 82(1):1-8.
- Yamashiro, T., Aberg, T., Levanon, D., Groner, Y., and I. Thesleff. 2002. Expression of Runx1, -2, and -3 during tooth, palate and craniofacial bone development. *Mechanisms of Development*. 119:107-110.
- Yang-Snyder, J., Miller, J.R., Brown, J.D., Lai, C.J., and R.T. Moon. 1996. A frizzled homolog functions in a vertebrate Wnt signaling pathway. *Current Biology*. 6(10):1302-1306.
- Yu, M., A. Bardia, N. Aceto, F. Bersani, M.W. Madden, M.C. Donaldson, R. Desai, H. Zhu, V. Comaills, Z. Zheng, B.S. Wittner, P. Stojanov, E. Brachtel, D. Sgroi, R. Kapur, T. Shioda, D.T. Ting, S. Ramaswamy, G. Getz, A.J. Iafrate, C. Benes, M. Toner, S. Maheswaran, and D.A. Haber. 2014. Cancer therapy. Ex vivo culture of circulating breast tumor cells for individualized testing of drug susceptibility. *Science*. 345:216-220.

- van Bragt, M.P., X. Hu, Y. Xie, and Z. Li. 2014. RUNX1, a transcription factor mutated in breast cancer, controls the fate of ER-positive mammary luminal cells. *Elife*. 21:03881.
- Van Keymeulen, A., M. Fioramonti, A. Centonze, G. Bouvencourt, Y. Achouri, and C. Blanpain. 2017. Lineage-Restricted Mammary Stem Cells Sustain the Development, Homeostasis, and Regeneration of the Estrogen Receptor Positive Lineage. *Cell reports*. 20:1525-1532.
- Van Keymeulen, A., A.S. Rocha, M. Ousset, B. Beck, G. Bouvencourt, J. Rock, N. Sharma, S. Dekoninck, and C. Blanpain. 2011. Distinct stem cells contribute to mammary gland development and maintenance. *Nature*. 479:189-193.
- Veltmaat, J.M., Ramsdell, A.F., and E. Sterneck. 2013. Positional variations in mammary gland development and cancer. *Journal of Mammary Gland Biology and Neoplasia*. 18(2):179-188.
- Veronesi, U., Boyle, P., Goldhirsch, A., Orecchia, R., and G. Viale. 2005. Breast Cancer. *The Lancet*. 365(9472):1727-1741.
- Visvader, J.E. 2009. Keeping abreast of the mammary epithelial hierarchy and breast tumorigenesis. *Genes and Development*. 23:2563-2577.
- Visvader, J.E., and J. Stingl. 2014. Mammary stem cells and the differentiation hierarchy: current status and perspectives. *Genes and Development*. 28:1143-1158.
- Vogelstein, B., and K.W. Kinzler. 1983. The multistep nature of cancer. *Trends in Genetics*. 9(4):138-141.
- Vogelstein, B., and K.W. Kinzler. 2004. Cancer genes and the pathways they control. *Nature Medicine*. 10:789-799.
- Vogelstein, B., N. Papadopoulos, V.E. Velculescu, S. Zhou, L.A. Diaz, Jr., and K.W. Kinzler. 2013. Cancer genome landscapes. *Science*. 339:1546-1558.
- Wang, Q., Stacy, T., Binder, M., Marin-Padilla, M., Sharpe, A.H., and N.A. Speck. 1996. Disruption of the *Cbfa2* gene causes necrosis and hemorrhaging in the central nervous system and blocks definitive hematopoiesis. *Proceedings of the National Academy of Sciences of the United States of America*. 93(8):3444-3449.
- Wang, L., J.S. Brugge, and K.A. Janes. 2011. Intersection of FOXO- and RUNX1-mediated gene expression programs in single breast epithelial cells during morphogenesis and tumor progression. *Proceedings of the National Academy of Sciences of the United States of America*. 108:22.
- Wang, D., C. Cai, X. Dong, Q.C. Yu, X.O. Zhang, L. Yang, and Y.A. Zeng. 2015. Identification of multipotent mammary stem cells by protein C receptor expression. *Nature*. 517:81-84.
- Wang, C., J.R. Christin, M.H. Oktay, and W. Guo. 2017. Lineage-Biased Stem Cells Maintain Estrogen-Receptor-Positive and -Negative Mouse Mammary Luminal Lineages. *Cell reports*. 18:2825-2835.
- Weigelt, B., Peterse, J.L., and L.J. van't Veer. 2005. Breast cancer metastasis: markers and models. *Nature Reviews Cancer*. 5(8):591-602.
- Weinstein, I.B. 2002. Addiction to oncogenes - the Achilles heel of cancer. *Science*. 297(5578):63-64.
- Welm, B.E., S.B. Tepera, T. Venezia, T.A. Graubert, J.M. Rosen, and M.A. Goodell. 2002. Sca-1(pos) cells in the mouse mammary gland represent an enriched progenitor cell population. *Developmental biology*. 245:42-56.
- Whitman, M., Kaplan, D.R., Schaffhausen, B., Cantley, L., and T.M. Roberts. 1985. Association of phosphatidylinositol kinase activity with polyoma middle T competent for transformation. *Nature*. 315:239-242.

- Wiesen, J.F., Young, P., Werb, Z., and G.R. Cunha. 1999. Signaling through the stromal epidermal growth factor receptor is necessary for mammary ductal development. *Development*. 126(2):335-344.
- Wood, L.D., D.W. Parsons, S. Jones, J. Lin, T. Sjoblom, R.J. Leary, D. Shen, S.M. Boca, T. Barber, J. Ptak, N. Silliman, S. Szabo, Z. Dezso, V. Ustyansky, T. Nikolskaya, Y. Nikolsky, R. Karchin, P.A. Wilson, J.S. Kaminker, Z. Zhang, R. Croshaw, J. Willis, D. Dawson, M. Shipitsin, J.K. Willson, S. Sukumar, K. Polyak, B.H. Park, C.L. Pethiyagoda, P.V. Pant, D.G. Ballinger, A.B. Sparks, J. Hartigan, D.R. Smith, E. Suh, N. Papadopoulos, P. Buckhaults, S.D. Markowitz, G. Parmigiani, K.W. Kinzler, V.E. Velculescu, and B. Vogelstein. 2007. The genomic landscapes of human breast and colorectal cancers. *Science*. 318:1108-1113.
- Wodarz, A., and R. Nusse. 1998. Mechanisms of Wnt signaling in development. *Annual Review of Cell and Developmental Biology*. 14:59-88.
- Yamagata, T., K. Maki, and K. Mitani. 2005. Runx1/AML1 in normal and abnormal hematopoiesis. *International journal of hematology*. 82:1-8.
- Yamashiro, T., Aberg, T., Levanon, D., Groner, Y., and I. Thesleff. 2002. Expression of Runx1, -2, and -3 during tooth, palate and craniofacial bone development. *Mechanisms of Development*. 119:S107-110.
- Young, L.J., Medina, D., DeOme, K.B., and C.W. Daniel. 1971. The influence of host and tissue age on life span and growth rate of serially transplanted mouse mammary gland. *Experimental Gerontology*. 6(1):49-56.
- Zeng, Y.A., and R. Nusse. 2010. Wnt proteins are self-renewal factors for mammary stem cells and promote their long-term expansion in culture. *Cell Stem Cell*. 6(6):568-577.